Proceedings of the 18th International Symposium on BioPolymers (ISBP2022)

Edited by
Manfred Zinn, George Guo-Qiang Chen, Richard A. Gross,
Georg M. Guebitz, Sang Yup Lee, Kevin Edward O Connor,
M. Auxiliadora Prieto, Luiziana Ferreira Da Silva, Anthony Sinskey,
Alexander Steinbüchel, Kumar Sudesh, Dieter Jendrossek
and Roger Marti

About Frontiers

Frontiers is more than just an open access publisher of scholarly articles: it is a pioneering approach to the world of academia, radically improving the way scholarly research is managed. The grand vision of Frontiers is a world where all people have an equal opportunity to seek, share and generate knowledge. Frontiers provides immediate and permanent online open access to all its publications, but this alone is not enough to realize our grand goals.

Frontiers journal series

The Frontiers journal series is a multi-tier and interdisciplinary set of open-access, online journals, promising a paradigm shift from the current review, selection and dissemination processes in academic publishing. All Frontiers journals are driven by researchers for researchers; therefore, they constitute a service to the scholarly community. At the same time, the *Frontiers journal series* operates on a revolutionary invention, the tiered publishing system, initially addressing specific communities of scholars, and gradually climbing up to broader public understanding, thus serving the interests of the lay society, too.

Dedication to quality

Each Frontiers article is a landmark of the highest quality, thanks to genuinely collaborative interactions between authors and review editors, who include some of the world's best academicians. Research must be certified by peers before entering a stream of knowledge that may eventually reach the public - and shape society; therefore, Frontiers only applies the most rigorous and unbiased reviews. Frontiers revolutionizes research publishing by freely delivering the most outstanding research, evaluated with no bias from both the academic and social point of view. By applying the most advanced information technologies, Frontiers is catapulting scholarly publishing into a new generation.

What are Frontiers Research Topics?

Frontiers Research Topics are very popular trademarks of the *Frontiers journals series*: they are collections of at least ten articles, all centered on a particular subject. With their unique mix of varied contributions from Original Research to Review Articles, Frontiers Research Topics unify the most influential researchers, the latest key findings and historical advances in a hot research area.

Find out more on how to host your own Frontiers Research Topic or contribute to one as an author by contacting the Frontiers editorial office: frontiersin.org/about/contact

Proceedings of the 18th International Symposium on BioPolymers (ISBP2022)

Topic editors

Manfred Zinn — HES-SO Valais-Wallis, Switzerland

George Guo-Qiang Chen — Tsinghua University, China

Richard A. Gross — Rensselaer Polytechnic Institute, United States

Georg M. Guebitz — University of Natural Resources and Life Sciences Vienna, Austria

Sang Yup Lee — Korea Advanced Institute of Science and Technology (KAIST), Republic of Korea

Kevin Edward O Connor — University College Dublin, Ireland

M. Auxiliadora Prieto — Spanish National Research Council (CSIC), Spain

Luiziana Ferreira Da Silva — University of São Paulo, Brazil

Anthony Sinskey — MIT Dept of Biology, United States

Alexander Steinbüchel — Lodz University of Technology, Poland

Kumar Sudesh — University of Science Malaysia (USM), Malaysia

Dieter Jendrossek — University of Stuttgart, Germany

Roger Marti — Haute école d'ingénierie et d'architecture Fribourg, Institute ChemTech, Switzerland

Table of contents

frontiers | Research Topics

A review on poly(3-hydroxybutyrate-*co*-3-hydroxyhexanoate) [P(3HB-*co*-3HHx)] and genetic modifications that affect its production

Hui Jia Tang, Soon Zher Neoh and Kumar Sudesh*

Ecobiomaterial Research Laboratory, School of Biological Sciences, Universiti Sains Malaysia, Pulau Pinang, Malaysia

Polyhydroxyalkanoates (PHAs) have garnered global attention to replace petroleum-based plastics in certain applications due to their biodegradability and sustainability. Among the different types of PHAs, poly(3-hydroxybutyrate-*co*-3-hydroxyhexanoate) [P(3HB-*co*-3HHx)] copolymer has similar properties to commodity plastics, making them a suitable candidate to replace certain types of single-use plastics, medical devices, and packaging materials. The degradation rate of P(3HB-*co*-3HHx) is faster than the commercial petroleum-based plastics which take a very long time to be degraded, causing harmful pollution to both land and marine ecosystem. The biodegradability of the P(3HB-*co*-3HHx) is also dependent on its 3HHx molar composition which in turn influences the crystallinity of the material. Various metabolic pathways like the common PHA biosynthesis pathway, which involves *phaA, phaB,* and *phaC*, β-oxidation, and fatty acids *de novo* synthesis are used by bacteria to produce PHA from different carbon sources like fatty acids and sugars, respectively. There are various factors affecting the 3HHx molar composition of P(3HB-*co*-3HHx), like PhaCs, the engineering of PhaCs, and the metabolic engineering of strains. It is crucial to control the 3HHx molar composition in the P(3HB-*co*-3HHx) as it will affect its properties and applications in different fields.

KEYWORDS

polyhydroxyalkanoate, poly(3-hydroxybutyrate-*co*-3-hydroxyhexanoate) [P(3HB-*co*-3HHx)], metabolic pathway, PHA synthase, engineering of PhaCs

Introduction

Petroleum-based plastics are used in our daily life due to their characteristics like being cheap, light, resistant to chemicals, and convenient (Loo and Sudesh, 2007). Due to those desirable characteristics, they are applied in many sectors, such as packaging, medical equipment, household utensils, construction, etc. However, it was estimated that more than a million tons of plastic waste are being disposed into land and marine

environment yearly due to improper disposal (Alabi et al., 2019; Masry et al., 2021). When exposed to sunlight and wind, plastic wastes are broken down into microplastics, causing toxic effects on aquatic life and human health (Bajt, 2021).

The use of bio-based plastics as one of the alternatives to replace single-use petroleum-based plastics may be one of the options for solving this issue. There are several potential bio-based plastics, such as polyhydroxyalkanoates (PHAs), polylactides (PLA), polysaccharides, etc. Among the bio-based plastics, PHAs have been reported to have interesting properties like biodegradable, thermoplastic, renewable, and can be tailored to fit various applications attracted both academic and industrial (Sudesh and Iwata, 2008). PHA was first discovered by Lemoigne in *Bacillus megaterium* (Lemoigne, 1926). The timeline of the P(3HB-*co*-3HHx) developments is shown in Figure 1. PHAs are bio-based polymers produced by a wide range of microorganisms under deprived nutrients and excessive carbon sources (Anderson and Dawes, 1990; Fukui and Doi, 1998). They are deposited as intracellular granules and function as energy or carbon reservoir (Anderson and Dawes, 1990; Sudesh et al., 2000). Figure 2 shows the PHA granules in cell cytoplasm synthesized by *Cupriavidus necator* transformant under phase contrast light microscope.

PHAs can be divided into three groups, short-chain-length PHA (SCL-PHA) of 3–5 carbon units, medium-chain-length PHA (MCL-PHA) of 6–14 carbon units, and a mixture of both SCL- and MCL-PHA of 3–14 carbon units (Sudesh et al., 2000). Examples of SCL monomeric units are 3-hydroxybutyrate (3HB) and 3-hydroxyvalerate (3HV), while MCL monomeric units are 3-hydroxyhexanoate (3HHx) and 3-hydroxydodecanoate (3HD) (Sudesh, 2012). Example of the mixture of SCL- and MCL-PHA is poly [(*R*)-3-hydroxybutyrate-*co*-(*R*)-3-hydroxyhexanoate] P(3HB-*co*-3HHx). The monomers incorporated into PHA polymers will affect the thermal and physical properties of the PHAs produced.

Poly(3-hydroxybutyrate) [P(3HB)] homopolymer is brittle, stiff, has high crystallinity, and low elongation at break, causing it to be limited in many applications (Yu, 2007). This drawback of PHA homopolymers can be overcome by copolymerizing P(3HB) with MCL monomers for better properties (Noda et al., 2005). For instance, the incorporation of MCL-PHA monomer like 3HHx into P(3HB) results in P(3HB-*co*-3HHx) copolymer, which has elastomeric properties such as high elasticity, low crystallinity, and high elongation at break. The flexibility of this copolymer can be varied depending on the 3HHx molar compositions (Asrar et al., 2002). P(3HB-*co*-3HHx) with 17 mol% 3HHx molar fraction was also reported to have similar properties as low-density polyethylene (LDPE) (Doi, 1990; Doi et al., 1995).

PHA synthase (PhaC) is the key enzyme in PHA production since it is responsible for catalyzing the polymerization of PHA monomers into PHA polymers. In addition, it also determines the monomer composition integrated into the PHA polymer,

which will impact the properties of the PHA produced. Based on the substrate specificities of PhaC and subunit composition, PhaCs are categorized into four main classes: class I, II, III and IV. Class I, III and IV PhaC prefer SCL-PHA monomer, whereas class II PhaC prefers MCL-PHA monomer. Class I and II PhaCs are single-unit enzymes. Class III consists of two subunits, PhaC and PhaE, while class IV consists of PhaC and PhaR (Rehm, 2003).

This present paper reviews the properties, metabolic pathways of P(3HB-*co*-3HHx) production, factors affecting the 3HHx molar composition in P(3HB-*co*-3HHx) copolymer, and potential applications of P(3HB-*co*-3HHx).

Properties of P(3HB-*co*-3HHx)

P(3HB-*co*-3HHx) copolymer consists of two monomer compositions, which are 3HB and 3HHx. The chemical structure of P(3HB-*co*-3HHx) is shown in Figure 3.

P(3HB) is a homopolymer of SCL monomer unit consisting of four carbon atoms and is the most common type of PHA. It is reported that the properties of P(3HB) are approximately similar to commercial plastics such as polypropylene in terms of tensile strength and Young's Modulus (Sudesh and Iwata, 2008). However, the elongation at break of P(3HB) is 5% which is way lower than polypropylene which is 400% (Sudesh et al., 2000). The melting temperature (T_m) of P(3HB) is approximately 180°C, and the degree of crystallinity is 55–80% (Holmes, 1988). Due to its brittleness, stiffness and high T_m, P(3HB) has poor processability and limits applications.

On the other hand, 3HHx is a MCL monomer unit that consists of six carbon atoms. Since 3HHx has a longer alkyl side chain, it cannot crystallize in the 3HB lattice and hence, avoiding the isodimorphism phenomenon. MCL-PHAs are amorphous in contrast to crystalline SCL-PHAs. MCL-PHAs exhibit elastomeric properties, soft, low T_m, low glass transition temperature (T_g), low tensile strength, and high elongation at break (Yu, 2007; Reddy et al., 2022).

The mixture of SCL- and MCL-PHA has superior thermal and mechanical properties than PHA homopolymers. Compared to SCL-PHA and MCL-PHA, the mixture of SCL- and MCL-PHA results in lower T_m, lower degree of crystallinity, and higher elongation at break (Doi et al., 1995; Kellerhals et al., 2000; Noda et al., 2005).

The flexibility of P(3HB-*co*-3HHx) also depends on 3HHx monomer compositions (Shimamura et al., 1994). As 3HHx monomeric units increase, it becomes more flexible, softer, and has better processability. Hence, its improved properties and processability attract industrial attention for various applications, especially in packaging and single-use plastic.

The physicomechanical properties of P(3HB-*co*-3HHx) with different 3HHx molar fractions have been summarized in Table 1. In general, as the 3HHx molar fraction increases, the
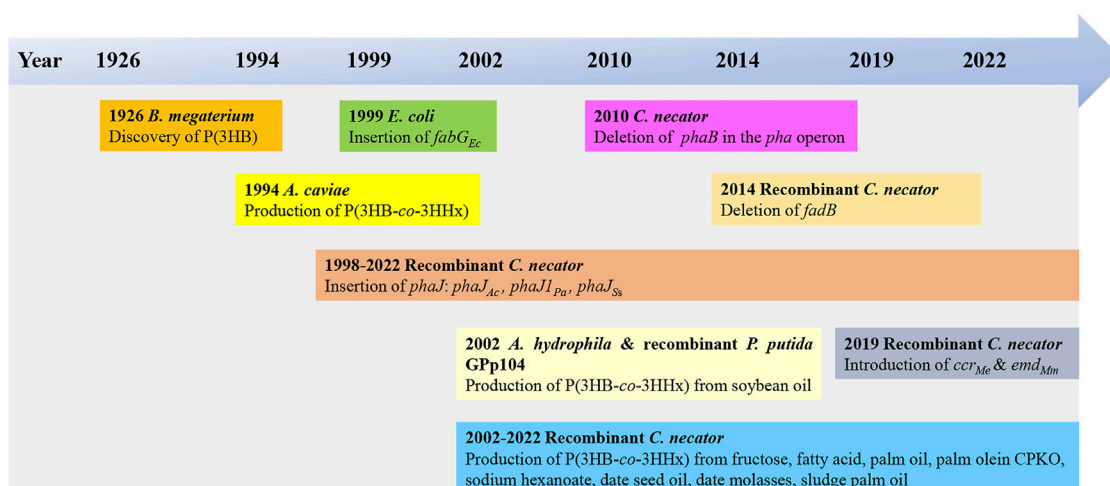
FIGURE 1
Timeline of the P(3HB-*co*-3HHx) developments (Lemoigne, 1926; Shimamura et al., 1994; Fukui et al., 1998; Asrar et al., 2002; Fukui et al., 2002; Tsuge et al., 2004; Loo et al., 2005; Budde, 2010; Wong et al., 2012; Insomphun et al., 2014; Volova et al., 2016; Murugan et al., 2017; Purama et al., 2018; Thinagaran and Sudesh, 2019; Zhang et al., 2019; Tan et al., 2020; Tan et al., 2022)

M_w, T_m, T_g, Young's modulus, and tensile strength decrease, whereas the elongation at break of the copolymer increases.

Biodegradability of P(3HB-*co*-3HHx)

Previous research has established that P(3HB-*co*-3HHx) can be biodegraded in aerobic environments such as seawater, freshwater, soil, and domestic compost (Morse et al., 2011). Under aerobic conditions, P(3HB-*co*-3HHx) is degraded into water and carbon dioxide. On the other hand, anaerobic biodegradation has also been carried out using PHB depolymerase, whereby P(3HB-*co*-3HHx) is degraded into water and methane (Abe and Doi, 1999; Lee and Choi, 1999). P(3HB-*co*-3HHx) takes around six months to be degraded in seawater (KANEKA Corporation, 2019). There are a few factors that affect the biodegradation of PHA copolymers, such as the environment, the microbial community, types of PHA monomer composition, temperature, and humidity.

The rate of PHA degradation increases as the degree of crystallinity decreases (Morse et al., 2011). Morse and co-workers reported that the films made from P(3HB-*co*-3HHx) with 10 mol% of 3HHx had a faster degradation rate than those with 3.8 mol% of 3HHx. Furthermore, Volova and co-workers reported that the biodegradability of P(3HB-*co*-3HHx), a PHA copolymer was faster than P(3HB), a PHA homopolymer (Volova et al., 2017). This is because P(3HB) has higher crystallinity than P(3HB-*co*-3HHx), leading to a lower degradation rate. Moreover, it was reported that the rate of enzymatic degradation of P(3HB-*co*-3HHx) film by P(3HB)

depolymerase gets higher as the 3HHx content increases to 15 mol% (Shimamura et al., 1994). When the 3HHx mol% in the P(3HB-*co*-3HHx) increases, the degree of crystallinity of P(3HB-*co*-3HHx) decreases, thereby increasing the biodegradation rate of the polymer. It is also reported that the degradation rate of the amorphous polymer was faster than that of highly crystalline polymer (Molitoris et al., 1996).

Besides that, Wang and co-workers reported that P(3HB-*co*-3HHx) polymer surface morphology could affect its biodegradation rate. Molitoris and co-workers reported that the degradation was faster on PHA with fissures on its surface than on PHA with a smooth surface (Molitoris et al., 1996). A porous and rough surface tends to have a faster degradation rate as it facilitates the attachment of lipase or bacteria to the film to begin the degradation process (Wang et al., 2004).

Metabolic pathway of P(3HB-*co*-3HHx) production

The most common PHA biosynthesis pathway consists of three genes which are β-ketothiolase (PhaA) coded by *phaA* gene, NADPH-dependent acetoacetyl-CoA reductase (PhaB) coded by *phaB* gene and PhaC coded by *phaC* gene (Anderson and Dawes, 1990). The acetyl-CoA from various pathways like fatty acid β-oxidation, glycolysis, and many more will first be converted to acetoacetyl-CoA by PhaA. The acetoacetyl-CoA will then be reduced to (*R*)-3-hydroxybutyryl-CoA [(*R*)-3HB-CoA] by PhaB and followed by incorporation into PHA by PhaC (Figure 4).
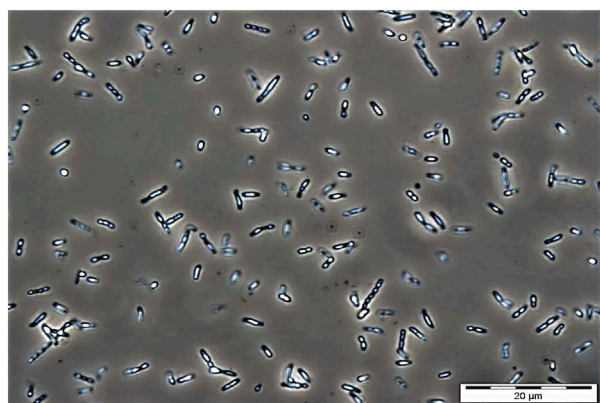
FIGURE 2
Phase contrast microscopic image of PHA granules in *C. necator* mutant Re2058 harboring plasmid pHT1 with *phaC* from *Chromobacterium* sp. USM2 (*phaC$_{Cs}$*) containing P(3HB-*co*-3 mol % 3HHx) copolymer after cultivating in minimal medium at 30°C, 200 rpm for 48 h with 0.54 g/L of urea as nitrogen source and supplemented with crude palm kernel oil (CPKO). Magnification: 1000 ×. The PHA content produced was 60 wt%.
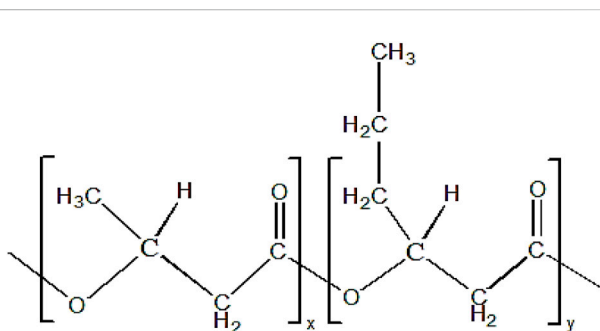
FIGURE 3
Chemical structure of P(3HB-*co*-3HHx). 'x' and 'y' indicate the repeating units of monomer.

When fatty acids are used as carbon sources, fatty acids will be converted to acyl-CoA by acyl-CoA synthetase (FadD). Acyl-CoA will be oxidized to *trans*-enoyl-CoA catalyzed by acyl-CoA dehydrogenase (FadE) followed by hydration into (S)-3-hydroxyacyl-CoA by enoyl-CoA hydratase (FadB). (S)-3-hydroxyacyl-CoA will then be oxidized into 3-ketoacyl-CoA by 3-hydroxyacyl-CoA dehydrogenase (Had). Lastly, 3-ketoacyl-CoA thiolase (FadA) will convert 3-ketoacyl-CoA into acyl-CoA with two carbon atoms lesser, releasing one acetyl-CoA. This acetyl-CoA can be converted to PHA using the previous pathway. Six carbons of (S)-3-hydroxyacyl-CoA or (S)-3-hydroxyhexanoyl-CoA [(S)-3HHx-CoA] will be converted into (R)-3-hydroxyhexanoyl-CoA [(R)-3HHx-CoA] by (R)-specific enoyl-CoA hydratase (PhaJ). (R)-3HHx-CoA will then

be incorporated into P(3HB-*co*-3HHx) by PhaC (Figure 4) (Tsuge, 2002).

Another engineered pathway involving the formation of P(3HB-*co*-3HHx) is the fatty acids *de novo* synthesis pathway, where sugar is used as the sole carbon source. This pathway begins with sugar which will be converted to pyruvate via glycolysis and decarboxylated into acetyl-CoA by pyruvate dehydrogenase. The acetyl-CoA will be converted into acetoacetyl-CoA by PhaA. The acetoacetyl-CoA formed will be reduced to (S)-3-hydroxybutyryl-CoA [(S)-3HB-CoA] by Had followed by conversion to crotonyl-CoA by crotonase (Crt2). Crotonyl-CoA will either be converted to (R)-3HB-CoA by PhaJ or butyryl-CoA. The (R)-3HB-CoA will be incorporated into P(3HB-*co*-3HHx) as 3HB. The crotonyl-CoA will be reduced to butyryl-CoA by crotonyl-CoA reductase (Ccr). The butyryl-CoA will be converted to 3-oxohexanoyl-CoA followed by reduction to (S)-3HHx-CoA by Had. (S)-3HHx-CoA will be converted to 2-hexenoyl-CoA by Crt2 and then hydrated to (R)-3HHx-CoA by PhaJ. (R)-3HHx-CoA will be incorporated into P(3HB-*co*-3HHx) by PhaC as 3HHx (Figure 4) (Zhang et al., 2019).

Factors affecting the 3-hydroxyhexanoate (3HHx) compositions of P(3HB-*co*-3HHx)

PhaCs

One of the main factors affecting the 3HHx molar composition is the PhaC. PhaC is the most important protein in PHA biosynthesis because it determines the type of PHA produced (Sudesh et al., 2000). Hence, many researchers have dedicated their time in search of a good naturally occurring PhaC.

As mentioned above in the introduction, class I, III, and IV PhaCs could only incorporate SCL-PHA monomers, while class II PhaCs could incorporate MCL-PHA. There is also a particular group of class I PhaC that will incorporate both SCL- and MCL-PHA monomers into the PHA polymer produced (Neoh et al., 2022). For example, PhaCs from *A. caviae* (PhaC$_{Ac}$), *Rhodococcus aetherivorans* I24 (PhaC1$_{Ra}$ and PhaC2$_{Ra}$), PhaC from mangrove soil (PhaC$_{BP-M-CPF4}$), *Chromobacterium* sp. USM2 (PhaC$_{Cs}$) and *Pseudomonas* sp. 61–3 (PhaC1$_{Ps}$ and PhaC2$_{Ps}$) (Doi et al., 1995; Fukui and Doi, 1997; Matsusaki et al., 1998; Bhubalan et al., 2010; Budde et al., 2011; Foong et al., 2018).

A. caviae was one of the first bacterial strains to be discovered to produce P(3HB-*co*-3HHx) (Shimamura et al., 1994). PhaC$_{Ac}$ possesses substrate specificity for copolymerizing both 3HB-CoA and 3HHx-CoA into P(3HB-*co*-3HHx) copolymer using alkanoic acids and olive oil (Doi et al., 1995). Heterologous expression of PhaC$_{Ac}$ in *C. necator* mutant, PHB⁻4, and

TABLE 1 The physicomechanical properties of P(3HB-co-3HHx).

3HHx composition (mol%)[a]	T_g (°C)[b]	T_m (°C)[c]	Tensile strength, MPa (Thickness)	Young's modulus, MPa	Elongation at break, %	Molecular weight, Da			Source
						M_n ($\times 10^5$)[d]	M_w ($\times 10^5$)[e]	PDI[f]	
1 ± 0	ND	ND	ND	ND	ND	6.0 ± 0.0	15.3 ± 0.5	2.6 ± 0.1	Tan et al. (2020)*
3 ± 0	ND	ND	ND	ND	ND	4.2 ± 0.2	14.0 ± 0.8	3.3 ± 0.3	Tan et al. (2020)*
3 ± 0	ND	ND	ND	ND	ND	6.5 ± 0.2	17.3 ± 0.5	2.7 ± 0.0	Tan et al. (2020)*
4	−1	164	ND	ND	ND	2.99 ± 0.04	5.47 ± 0.60	1.66	Murugan et al. (2017)*
5	0	151	ND	ND	ND	1.0	1.9	1.9	Doi et al. (1995)
5	−3	125; 143	ND	ND	ND	4.6	15.8	3.3	Loo et al. (2005)
6 ± 0	ND	ND	ND	ND	ND	4.3 ± 0.2	12.7 ± 1.2	2.9 ± 0.1	Tan et al. (2020)*
7	−1	132	ND	ND	ND	1.7	4.5	2.65	Foong et al. (2018)*
7 ± 0	ND	ND	ND	ND	ND	5.9 ± 0.7	18.7 ± 1.7	3.2 ± 0.1	Tan et al. (2020)*
10	−1	127	21 (0.1 mm)	ND	400	1.2	3.04	2.6	Doi et al. (1995)
11 ± 1	ND	ND	ND	ND	ND	2.5 ± 0.1	8.4 ± 1.2	3.3 ± 0.3	Tan et al. (2020)*
11 ± 0	ND	ND	ND	ND	ND	5.9 ± 0.3	18.3 ± 1.9	3.1 ± 0.1	Tan et al. (2020)*
12	ND	170	18.3 ± 1.8 (25–30 μm)	1286.4 ± 90.8	3.6 ± 0.1	0.14	0.44 ± 19	3.10 ± 0.05	Volova et al. (2016)
12	−9	163	ND	ND	ND	2.63 ± 0.16	6.01 ± 0.34	2.30	Murugan et al. (2017)*
13	−9	160	ND	ND	ND	ND	ND	ND	Murugan et al. (2016)*
13 ± 0	ND	ND	ND	ND	ND	2.2 ± 0.2	8.0 ± 0.2	3.6 ± 0.2	Tan et al. (2020)*
14 ± 1	ND	ND	ND	ND	ND	3.3 ± 0.1	7.7 ± 0.4	2.3 ± 0.0	Tan et al. (2020)*
15	0	115	23 (0.1 mm)	ND	760	2.1	7.92	3.7	Doi et al. (1995)
15	−12	156	ND	ND	ND	0.39 ± 0.04	6.85 ± 0.65	1.77	Murugan et al. (2017)*
16	0.9	116.1; 131.5	ND	ND	ND	2.89 ± 0.16	4.45 ± 0.46	1.5 ± 0.1	Thinagaran and Sudesh (2019)*
17	−2	130	ND	ND	ND	6.62	11.92	1.8	Shimamura et al. (1994)
17	−2	120	20 (0.1 mm)	ND	850	5.1	11.22	2.2	Doi et al. (1995)
17	ND	ND	ND	ND	ND	1.05 ± 0.40	2.60 ± 0.52	2.50	Murugan et al. (2017)*
17	−1.6	113.4; 129.5	ND	ND	ND	2.76 ± 0.08	4.37 ± 0.54	1.6 ± 0.1	Thinagaran and Sudesh (2019)*
18	−22	167	ND	ND	ND	2.6	8.6	3.3	Foong et al. (2018)*
18	−0.3	110.6; 125.6	ND	ND	ND	2.40 ± 0.07	3.58 ± 0.09	1.5 ± 0.0	Thinagaran and Sudesh (2019)*
18	ND	ND	ND	ND	ND	3.2 ± 0.2	6.9 ± 0.7	2.2 ± 0.1	Tan et al. (2020)*
19	−4	111	ND	ND	ND	0.4	3.32	8.3	Doi et al. (1995)
19	0	145	ND	ND	ND	ND	ND	ND	Murugan et al. (2016)*
19	ND	ND	ND	ND	ND	1.57 ± 0.00	3.30 ± 0.00	2.10	Murugan et al. (2017)*
19	−1.7	99.6; 113.3	ND	ND	ND	1.84 ± 0.19	2.77 ± 0.31	1.5 ± 0.0	Thinagaran and Sudesh (2019)*

TABLE 1 (*Continued*) The physicomechanical properties of P(3HB-*co*-3HHx).

3HHx composition (mol%)[a]	T_g (°C)[b]	T_m (°C)[c]	Tensile strength, MPa (Thickness)	Young's modulus, MPa	Elongation at break, %	Molecular weight, Da			Source
						M_n (× 10^5)[d]	M_w (× 10^5)[e]	PDI[f]	
20	−4.79	107.72	ND	ND	ND	4.4	7.5	1.7	Purama et al. (2018)*
24	−2.0	109.7	ND	ND	ND	1.81 ± 0.30	2.7 ± 0.42	1.5 ± 0.1	Thinagaran and Sudesh (2019)*
24.6	ND	167	21.6 ± 0.8 (25–30 μm)	1207.5 ± 21.4	4.1 ± 0.1	0.11	0.60	5.42	Volova et al. (2016)
25	−4	52	ND	ND	ND	2.12	7.42	3.5	Doi et al. (1995)
27	−1	120	ND	ND	ND	ND	ND	ND	Murugan et al. (2016)*
28	−2.29	85.33	ND	ND	ND	3.2	5.8	1.8	Purama et al. (2018)*
32	−1	88	8 ± 1	101 ± 6	856 ± 21	2.24 ± 0.20	3.47 ± 0.18	1.55 ± 0.06	Wong et al. (2012)*
43	−4	86	5 ± 1	75 ± 9	481 ± 47	0.72 ± 0.05	1.17 ± 0.06	1.63 ± 0.03	Wong et al. (2012)*
43	ND	176	19.0 ± 0.3 (25–30 μm)	938.0 ± 14.1	5.0 ± 0.1	0.08	0.31	3.88	Volova et al. (2016)
55	ND	171	6.6 ± 0.3 (25– 30 μm)	311.4 ± 21.8	13.6 ± 0.3	0.17	0.70	4.10	Volova et al. (2016)
56	−6	86	1 ± 1	12 ± 2	368 ± 1	0.82 ± 0.06	1.20 ± 0.10	1.45 ± 0.01	Wong et al. (2012)*
60	−11	ND	<1 ± 1	3 ± 1	424 ± 23	1.26 ± 0.03	2.11 ± 0.13	1.75 ± 0.07	Wong et al. (2012)*
65.7	ND	173	7.8 ± 0.7 (25–30 μm)	209.5 ± 17.0	140.6 ± 5.5	0.17	0.68	3.90	Volova et al. (2016)
68	ND	172	7.4 ± 0.7 (25–30 μm)	217.0 ± 11.3	177.0 ± 4.8	0.14	0.72	4.84	Volova et al. (2016)
70	−12	ND	<1 ± 1	<1 ± 0	1075 ± 158	1.37 ± 0.16	2.27 ± 0.2	1.66 ± 0.03	Wong et al. (2012)*

[a]3HHx, 3-hydroxyhexanoate.
[b]T_g, glass transition temperature.
[c]T_m, melting temperature.
[d]M_n, number average molecular weight.
[e]M_w, weight average molecular weight.
[f]PDI, polydispersity index (M_w/M_n); ND, not detected. Asterisk (*) indicates the data are obtained from Ecobiomaterial Laboratory, School of Biological Sciences, Universiti Sains Malaysia, 11800, Pulau Pinang, Malaysia.
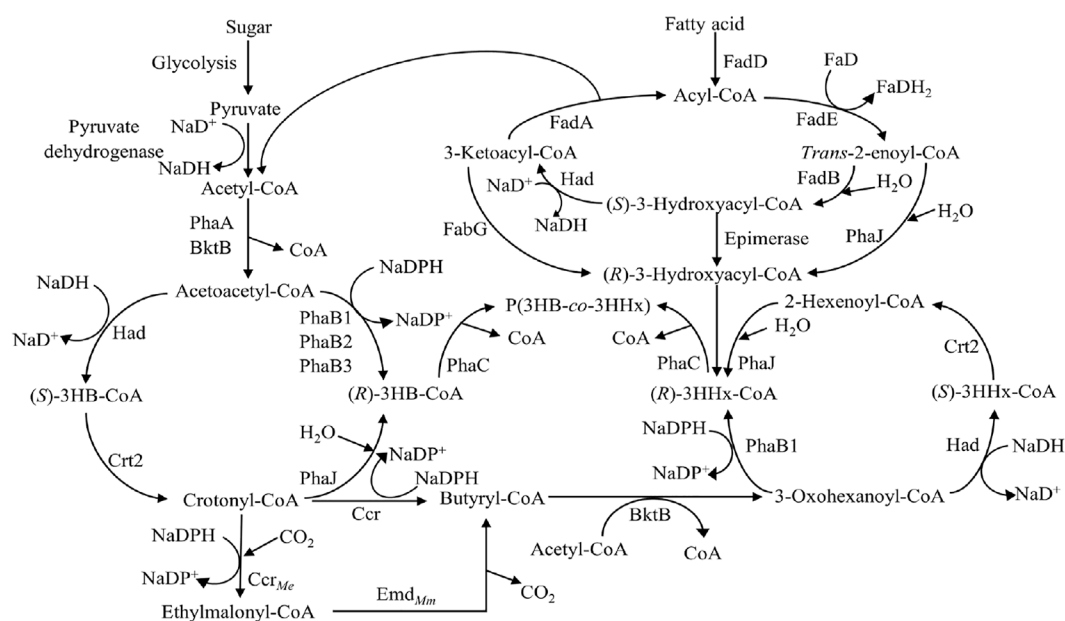
FIGURE 4

Metabolic pathway of P(3HB) and P(3HB-*co*-3HHx) production (Sudesh et al., 2000; Tsuge, 2002; Zhang et al., 2019). Abbreviation: PHA, polyhydroxyalkanoate; PhaA, *β*-ketothiolase; PhaB, NADPH-dependent acetoacetyl-CoA reductase; PhaC, PHA synthase; FadA, 3-ketoacyl-CoA thiolase; FadB, enoyl-CoA hydratase; FadD, acyl-CoA synthetase; FadE, acyl-CoA dehydrogenase; FabG, 3-ketoacyl-CoA reductase; 3HB-CoA, 3-hydroxybutyryl-CoA; 3HHx-CoA, 3-hydroxyhexanoyl-CoA; PhaJ, (*R*)-specific enoyl-CoA hydratase; Had, 3-hydroxyacyl-CoA dehydrogenase; Crt2, crotonase; Ccr, crotonyl-CoA reductase; Ccr_{Me}, crotonyl-CoA carboxylase from *Methylorubrum extorquens*; Emd_{Mm}, ethylmalonyl-CoA decaroboxylase from *Mus musculus*.

Pseudomonas putida GPp104 could produce P(3HB-*co*-3HHx) with a maximum 22 mol% of 3HHx using octanoate and 40 mol % of 3HHx using hexanoate respectively (Fukui & Doi, 1997). The recombinant strain *A. eutrophus* (PHB⁻4/pJRDEE32d13) harboring *phaC_{Ac}* could produce P(3HB-*co*-3HHx) with 4 mol% of 3HHx content using olive oil (Fukui and Doi, 1998). Kahar and co-workers reported that recombinant strain *C. necator* PHB⁻4 harboring pJRDEE32d13 inserted with *phaC_{Ac}* could accumulate P(3HB-*co*-3HHx) with 5 mol% of 3HHx content from soybean oil (Kahar et al., 2004).

Budde and co-workers reported two different PhaCs, PhaC1_{Ra} and PhaC2_{Ra}, in *R. aetherivorans* I24 (Budde et al., 2011). The heterologous expression of PhaC1_{Ra} and PhaC2_{Ra} in recombinant *C. necator* could produce P(3HB-*co*-3HHx). The study showed that recombinant *C. necator* strains, Re2000 and Re 2001, expressing PhaC1_{Ra} and PhaC2_{Ra}, respectively, could produce P(3HB-*co*-3HHx) using hexanoate and octanoate. Re2000 and Re2001 could produce 11.5 mol% of 3HHx and 18.9 mol% of 3HHx from hexanoate, respectively, while producing 6.6 mol% of 3HHx and 10.4 mol% of 3HHx from octanoate, respectively (Budde et al., 2011). This result showed that PhaC2_{Ra} produced P(3HB-*co*-3HHx) with higher 3HHx content than PhaC1_{Ra} from fatty acids.

PhaC_{BP-M-CPF4} was discovered in mangrove soil metagenome at Balik Pulau, Malaysia. It has wide substrate specificity as it can incorporate both SCL-PHA and MCL-PHA. The heterologous expression of PhaC_{BP-M-CPF4} in *C. necator* PHB⁻4 produced P(3HB-*co*-3HHx) with 7 mol% of 3HHx from CPKO and 18 mol% of 3HHx when co-fed with fructose and sodium hexanoate (Foong et al., 2018). Besides *C. necator* PHB⁻4, another *C. necator* PHA-negative mutant strains, H16ΔC, Re2058, and Re2160 harboring *phaC_{BP-M-CPF4}* were reported to be able to produce P(3HB-*co*-3HHx) ranging from 3–18 mol% of 3HHx from CPKO (Tan et al., 2020).

Chromobacterium sp. strain USM2 was discovered in Langkawi, Malaysia (Yong, 2009). It was reported that PhaC_{Cs} heterologous expressed in *C. necator* PHB⁻4 could synthesize P(3HB-*co*-3HHx) copolymer with 4 mol% of 3HHx using CPKO (Bhubalan et al., 2010). In addition, *Pseudomonas* sp. 61–3 isolated from soil possesses two different PhaCs, PhaC1_{Ps} and PhaC2_{Ps}. It could incorporate 3HB and 3HA units of C₄ and C₁₂ when supplemented with sugars and alkanoic acids. The heterologous expression of PhaC1_{Ps} and PhaC2_{Ps} in *P. putida* GPp104 and *C. necator* PHB⁻4 could produce P(3HB-*co*-3HHx) with 3HHx ranging from 1 to 16 mol% from alkanoic acids (Matsusaki et al., 1998).

Based on the above, it is clear that PhaCs can affect the 3HHx molar composition of P(3HB-*co*-3HHx) produced. The difference in 3HHx molar composition is due to the substrate specificity of the PhaC towards 3HHx. Some PhaCs with higher

TABLE 2 Production titers of P(3HB-*co*-3HHx).

Bacterial strains	Carbon sources	PHA content (wt%)	3HHx monomer composition (mol%)	Production scale	References
A. caviae	Olive oil	ND	17	3 L fermenter	Shimamura et al. (1994)
A. caviae	Alkanoic acids and olive oil	27	25	500 ml flask	Doi et al. (1995)
Pseudomonas putida GPp104 harboring *phaC_{Ac}*	Hexanoate	38	40	500 ml flask	Fukui and Doi (1997)
A. eutrophus (PHB⁻4/pJRDEE32d13) harboring *phaC_{Ac}*	Olive oil	76	4	500 ml flask	Fukui and Doi (1998)
P. putida GPp104 harboring *phaC1_{Ps}*	Alkanoic acids	43	16	500 ml flask	Matsusaki et al. (1998)
C. necator PHB⁻4 harboring *phaC-J_{Ac}*	Fructose	39	1.6	500 ml flask	Fukui et al. (2002)
C. necator PHB⁻4 harboring pJRDEE32d13 harboring *phaC_{Ac}*	Soybean oil	71–74	5	10 L fermenter	Kahar et al. (2004)
C. necator strains, Re2001 harboring *phaC2_{Ra}*	Hexanoate	48	18.9	250 ml flask	Budde et al. (2011)
C. necator Re2058/pCB113	Palm oil	73	19	2 L fermenter	Riedel et al. (2012)
C. necator Re2160/pCB113	CPKO	45	68	250 ml flask	Wong et al. (2012)
C. necator Re2058/pCB113	PO	67	27	13 L fermenter	Murugan et al. (2017)
C. necator PHB⁻4 harboring *phaC_{BP-M-CPF4}*	Sodium hexanoate	44	18	250 ml flask	Foong et al. (2018)
C. necator Re2058/pCB113	Date seed oil and date molasses	10	28	250 ml flask	Purama et al. (2018)
C. necator Re2058/pCB113	SPO	33	34	250 ml flask	Thinagaran and Sudesh (2019)
C. necator Re2160/pHT1-*C_{BP-M-CPF4}*	CPKO	63.3	18	250 ml flask	Tan et al. (2020)
C. necator PHB⁻4 harboring *phaC_{Cs}*	CPKO	63	4	250 ml flask	Bhubalan et al. (2010)

CPKO, crude palm kernel oil; PO, palm olein; SPO, sludge palm oil; ND, not detected.

TABLE 3 Commercialized P(3HB-*co*-3HHx), its production strains, carbon sources, the name of company, production scale, and applications.

Production strains	Carbon sources	Company	Scale (ton/year)	Applications	References
A. caviae, recombinant *C. necator*	Natural oils from canola and soy	Danimer Scientific, United States	10,000	Bottles, recyclable paper, and board products	Danimer Scientific, (2022)
Recombinant *C. necator*	Vegetable oils	KANEKA, Japan	5000	Straws, cutlery, shopping bags, makeup container, and packaging materials	KANEKA The Dreamology Company, (2022)
Recombinant *C. necator*	Waste cooking oil	RWDC, Singapore and United States	4000	Cutlery, cups, bags, utensils, food containers, and drinking straws	RWDC Industries, (2022)
Recombinant *C. necator*	Crops and kitchen waste	Bluepha, China	1000	Cutlery, straw, packaging, coating, textiles, polymer films, 3D printing inks, and aquarium water restoration	Bluepha, (2022)

substrate specificity towards 3HHx tend to produce P(3HB-*co*-3HHx) with higher 3HHx, and some PhaCs with lower substrate specificity towards 3HHx will lead to lower 3HHx. This may be due to the substrate entrance channel and the binding pocket of the PhaC where folding of the amino acid forming both substrate entrance channel and binding pocket are better in binding to 3HHx-CoA and hence, incorporating into P(3HB-*co*-3HHx). However, this is yet to be reported as to date, there is no co-crystal structure of (*R*)-3HHx-CoA with PhaC, but there is a co-crystal structure of PhaCs with CoA, which was reported by Chek

and co-workers elucidating how the CoA group is bound to the binding pocket of PhaC_{Cs}-CAT (Chek et al., 2020). The comparison of the production titers of the P(3HB-*co*-3HHx) from different researchers is shown in Table 2.

Engineering of PhaCs

Besides naturally occurring PhaCs, engineering existing PhaCs could also affect the 3HHx molar composition in

P(3HB-*co*-3HHx). *In vitro* evolution system can be used to improve the activity and broaden the substrate specificity of PhaC.

Kichise and co-workers had selected PhaC$_{Ac}$ for *in vitro* evolution as it can produce P(3HB-*co*-3HHx) copolymer from plant oils or alkanoic acid. *In vitro* evolution of PhaC$_{Ac}$ was carried out using error-prone PCR, and as a result, two PhaC$_{Ac}$ mutants (E2-50 and T3-11) were obtained, which had improved 3HHx incorporation. The PhaC$_{Ac}$ mutants (E2-50 and T3-11) in *E. coli* LS5218 could synthesize P(3HB-*co*-3HHx) with higher 3HHx content, which was 18 mol% of 3HHx and 16 mol% of 3HHx, respectively compared to wild-type with 10 mol% of 3HHx using sodium dodecanoate. P(3HB-*co*-3HHx) accumulated was 3-fold higher than the wild-type PhaC$_{Ac}$. It was discovered that E2-50 and T3-11 have the single amino acid substitution of N149S and D171G, respectively (Kichise et al., 2002).

Tsuge and co-workers further studied the synergistic effects of PhaC$_{Ac}$ mutants, N149S and D171G double mutation (NSDG) in *C. necator* PHB⁻4 for PHA production. The NSDG mutant was able to produce P(3HB-*co*-3HHx) with 3HHx as high as 18.1 mol%, which was higher than the wild type with 12.2 mol% using sodium octanoate. Besides sodium octanoate, the NSDG mutant could also produce P(3HB-*co*-3HHx) with 5.2 mol% of 3HHx from soybean oil, which was higher than the wild type with only 3.5 mol% of 3HHx. The NSDG mutant could also produce P(3HB-*co*-3HHx) with 2.90×10^6 Da from sodium octanoate, which is near to ultrahigh molecular weight PHA (UHMW-PHA), and it is suitable for making strong films and fibers (Iwata, 2005; Tsuge et al., 2007). N149S mutation increased the incorporation of 3HA into PHA polymer and the molecular weight of the polymer, whereas D171G mutation increased PHA accumulation. Hence, the synergistic effect of N149S and D171G double mutation on PHA production was higher than predicted (Tsuge et al., 2007).

PhaC$_{Cn}$ belongs to the type I PHA synthase, which shows substrate specificity towards (R)-3HA-CoAs with the acyl chain length of C3–C5. The alanine residue at position 510 may define the substrate specificity and the properties of the enzyme. Tsuge and co-workers found out that the performance of saturation point mutagenesis at position 510 in PhaC$_{Cn}$ using a PCR-based method could drastically impact the substrate specificity and polymerization activity for *in vivo* PHA biosynthesis in *E. coli* and *C. necator* PHB⁻4. The co-expression of the mutant PhaC$_{Cn}$ and PhaJ$_{Ac}$ in *E. coli* LS5218 in the presence of fatty acids could produce P(3HB-*co*-3HHx) with 0.7 mol% 3HHx content, which was higher than that of the wild-type with only 0.2 mol%. Besides *E. coli*, *C. necator* PHB⁻4 harboring mutant PhaC$_{Cn}$ produced P(3HB-*co*-3HHx) with as high as 1.6 mol% 3HHx compared to the wild type of 1.2 mol%. This study also showed that the molecular weight of PHA produced by mutant PhaC$_{Cn}$ was

higher than the wild type (Tsuge et al., 2004). In addition, Chuah and co-workers reported that saturation point mutagenesis at position A479 in PhaC$_{Cs}$ could enhance substrate specificity for 3HHx. A479 in PhaC$_{Cs}$ corresponded to A510 of PhaC$_{Cn}$ and was selected as the site of saturation point mutagenesis. It showed that the A479S mutation could increase 3HHx content to 6.6 mol%, 4-fold higher than the wild-type with only 1.6 mol% 3HHx. Besides that, mutation of A479T and A479G showed a 2.8-fold and 1.6-fold increment of 3HHx compared to wild-type PhaC$_{Cs}$ (Chuah et al., 2013).

Metabolic engineering of PHA-producing strains

Another factor affecting the 3HHx molar composition is metabolic engineering through the genetic modification of microbial strains. It can involve genes from various pathways, including PHA-related and non-PHA-related genes.

Firstly, the deletion of *phaB* in the *pha* operon could affect the 3HHx monomer supply and hence, affect the 3HHx molar composition of the P(3HB-*co*-3HHx) produced. Budde and co-workers reported that the deletion of *phaB* from the genome of *C. necator* could result in the disruption of the 3HB-CoA synthesis pathway (Budde, 2010). Based on Figure 4, PhaB is an important enzyme for supplying (R)-3HB-CoA from acetoacetyl-CoA due to its high catalytic efficiency and expression (Zhang et al., 2019). Budde and co-workers reported that *C. necator* strains Re2058 and Δ*phaB* genes mutant, Re2160, were evaluated for their performances through high cell density P(3HB-*co*-3HHx) production from palm oil. As a result, Re2058 and Re2160 accumulated 17 mol% of 3HHx and 30 mol% of 3HHx, respectively (Budde et al., 2011). Disruption in the 3HB-CoA synthesis pathway leads to lower 3HB-CoA and hence increases the 3HHx molar compositions in the P(3HB-*co*-3HHx) copolymer produced.

Besides that, modification of the acetoacetyl-CoA reduction step in engineered *C. necator* could affect the 3HHx molar composition in P(3HB-*co*-3HHx) from sugars. Zhang and co-workers managed to produce P(3HB-*co*-3HHx) with 22 mol% of 3HHx content from glucose using *C. necator* strain NSDG-GG harboring *phaJ4a* with Δ*phaB1* because deletion of *phaB1* affected the flux for (R)-3HB-CoA and (R)-3HHx-CoA formation. They introduced *had* and *crt2* into the *phaB* locus in the *pha* operon to increase the 3HHx monomer composition without significantly affecting PHA synthesis. Based on Figure 4, acetyl-CoA can be converted to 2-hexenoyl-CoA via fatty acid *de novo* synthesis pathway. In that pathway, acetoacetyl-CoA will be converted to crotonyl-CoA by Had and Crt2. At this stage, crotonyl-CoA will be hydrated to (R)-3HB-CoA by PhaJ, or crotonyl-CoA will be reduced to butyryl-CoA by Ccr, respectively. Butyryl-CoA will then be converted to 2-

hexenoyl-CoA to produce (R)-3HHx-CoA. Zhang and co-workers have further enhanced the fatty acid de novo synthesis pathway by adding crotonyl-CoA carboxylase from *Methylorubrum extorquens* (Ccr$_{Me}$) and ethylmalonyl-CoA decarboxylase from *Mus musculus* (Emd$_{Mm}$) (Zhang et al., 2019). Both Ccr$_{Me}$ and Emd$_{Mm}$ create an alternative pathway towards the formation of butyryl-CoA, which will eventually be converted to (R)-3HHx-CoA and hence, increasing the 3HHx molar composition in the P(3HB-co-3HHx) copolymer produced (Figure 4).

In addition, the deletion of FadB will disrupt (R)-3HB-CoA synthesis, leading to the formation of (R)-3HHx-CoA by PhaJ. Insomphun and co-workers reported that the disruption of *fadB1* in engineered *C. necator* harboring *phaJ* could enhance the (R)-3HHx-CoA supply from 6-carbons *trans*-2-enoyl-CoA (2-hexenoyl-CoA) catalyzed by PhaJ and increase the copolymerization of (R)-3HHx-CoA in P(3HB-co-3HHx) copolymer. It was shown that 3HHx monomer composition was increased by around 1–1.5 mol% (Insomphun et al., 2014). Originally, *trans*-2-enoyl-CoA formed will be converted to (S)-3-hydroxyacyl-CoA or (R)-3-hydroxyacyl-CoA by FadB and PhaJ, respectively. When *trans*-2-enoyl-CoA is catalyzed by FadB, it is converted to (S)-3-hydroxyacyl-CoA, which will lead to the formation of acyl-CoA and acetyl-CoA, and eventually, the acetyl-CoA formed will be converted to (R)-3HB-CoA. (R)-3HB-CoA will then be incorporated into P(3HB-co-3HHx) as 3HB, hence might lower the 3HHx molar composition in P(3HB-co-3HHx). When FadB is deleted, there will be no formation of (S)-3-hydroxyacyl-CoA, hence favoring the hydration of 2-hexenoyl-CoA to form (R)-3HHx-CoA (Figure 4). This will increase the ratio of (R)-3HHx-CoA to (R)-3HB-CoA, leading to higher 3HHx molar composition.

Besides that, the fatty acid β-oxidation pathway could be modified to increase 3HHx molar composition by inserting 3-ketoacyl-CoA reductase of *E. coli* (FabG$_{Ec}$). Taguchi and co-workers co-expressed *phaC$_{Ac}$* and *fabG$_{Ec}$* in *E. coli,* and as a result, the 3HHx molar composition of P(3HB-co-3HHx) increased from 0 to 14 mol%. Besides that, they also co-expressed a class II PhaC, PhaC from *Pseudomonas* sp. 61–3, which is known to have substrate specificity towards MCL-PHA monomer with *fabG$_{Ec}$*, resulting in an increase of 3HHx from 0 to 12 mol% (Figure 4) (Taguchi et al., 1999). This is probably due to the ability of FabG$_{Ec}$ to catalyze the conversion of 6-carbons of 3-ketoacyl-CoA to (R)-3HHx-CoA which will then be incorporated into P(3HB-co-3HHx) by PhaC.

Furthermore, the overexpression of PhaJ using plasmid could enhance 3HHx monomer composition in P(3HB-co-3HHx). Kawashima and co-workers reported that insertion of *phaJ$_{Ac}$* with *phaC$_{NSDG}$* in *C. necator* strain could produce 10.5 mol% of 3HHx, which is 6.6-fold higher than the *C. necator* strain harboring *phaC$_{NSDG}$* only (Kawashima et al., 2015). Tan and co-workers also co-expressed *phaJ1* from *Pseudomonas aeruginosa* with *phaC$_{BP-M-CPF4}$* in *C. necator* transformants

which could produce 3HHx as high as 14 mol%, which is higher than *C. necator* transformants harboring *phaC$_{BP-M-CPF4}$* with only 6 mol% (Tan et al., 2020). PhaJ is involved in fatty acid β-oxidation, whereby it creates an alternative pathway for supplying (R)-3HHx-CoAs to be incorporated into P(3HB-co-3HHx), hence increasing the 3HHx molar composition. It catalyzes the hydration of (R)-2-hexenoyl-CoA from fatty acid β-oxidation and hydrates them to (R)-3HHx-CoA (Figure 4) (Fukui et al., 1998). This showed that the expression of PhaJ could lead to more (R)-3HHx-CoA production by enhancing the channeling pathway from fatty acid β-oxidation and hence, increasing 3HHx mol% in P(3HB-co-3HHx). Besides that, expression of PhaJ from *Streptomyces* sp. CFMR7 (PhaJ$_{Ss}$) was reported to increase the 3HHx molar composition from 4 mol% and 7 mol% to 12 mol% and 18 mol% using palm oil and crude palm oil, respectively (Tan et al., 2022).

Applications of P(3HB-co-3HHx)

P(3HB-co-3HHx) has been extensively utilized in making straws, shopping bags, cutlery, containers, food packaging, coffee capsules, fishery items, biomedicine and adhesive due to its biodegradability and lack of toxicity (Qiu et al., 2021). Table 3 shows P(3HB-co-3HHx) production strains, carbon sources, the name of the company, the production scale, and their applications.

KANEKA Corporation has collaborated with Seven-Eleven Japan Corporation and THE NORTH FACE cafes to use straws made of P(3HB-co-3HHx) in the cafe area. Cutlery made from P(3HB-co-3HHx) by KANEKA Corporation is also available at FamilyMart convenience stores to promote the utilization of environmental-friendly materials (KANEKA Corporation, 2021a). Moreover, ITO EN Corporation has used the telescopic straws of "Oi Ocha Tea," made of P(3HB-co-3HHx) and sold in Japan's supermarkets (KANEKA Corporation, 2021b). Furthermore, JALUX corporation adopted shopping bags made of P(3HB-co-3HHx) in the BLUE SKY stores at Japan's airports (KANEKA Corporation, 2021c).

Besides that, KANEKA has collaborated with Shiseido Company to use P(3HB-co-3HHx) copolymer as cosmetics packaging material. For example, the case of AquaGel Lip Palette is made of biodegradable P(3HB-co-3HHx), and this product has been sold since the 2020s (KANEKA Corporation, 2020). P(3HB-co-3HHx) is also applied in compostable capsules. Capsul' in Pro, a manufacturer, has launched a Zero Impact capsule where the capsule is made of 100% biobased P(3HB-co-3HHx) derived from plant oils (Magazine, 2021). It provides an oxygen barrier to protect the flavor and aroma of coffee for 12 months. However, this capsule is still under development and has not been published.

Due to its biocompatibility and bioresorbable, the P(3HB-co-3HHx) copolymer is also suitable to be used as a scaffold for

tissue engineering (Chang et al., 2014). It can be biocompatible with various cell types: smooth muscle cells, fibroblasts, osteoblasts and bone marrow cells (Qu et al., 2006a; Yang et al., 2011; Yu et al., 2012). To test *in vitro* biocompatibilities, rabbit bone marrow cells were injected into P(3HB-*co*-3HHx) 3D scaffolds, and it was discovered that P(3HB-*co*-3HHx) performed best in terms of bone marrow cell attachment and proliferation (Chen and Wu, 2005). Scaffolds provide physical support and an artificial extracellular matrix (ECM) that promotes cell adhesion, proliferation and differentiation (Bryant and Anseth, 2003). Zhao and co-workers reported that P(3HB-*co*-3HHx) composite scaffolds produced *via* the 3D printing technique could improve their bioactive and osteogenic characteristics by enhancing the regeneration of bone in the defected calvarium of rats (Zhao et al., 2014). Ang and co-workers reported that blending of P(3HB-*co*-3HHx) with silk fibroin (SF) could improve the proliferation and osteogenic differentiation of human umbilical cord-derived mesenchymal stem cells (hUC-MSCs), which is a potential biomaterial for bone tissue engineering (Ang et al., 2020). Besides that, due to its elasticity, the P(3HB-*co*-3HHx) biomaterial could resist systemic pressure and support cell growth, making it a potential tissue-engineered blood vessel (Qu et al., 2006b). It is a potential biomaterial to replace synthetic blood vessels during surgeries and reduce the risk of infection.

In addition, P(3HB-*co*-3HHx) can be utilized as a drug delivery system in cancer treatment due to its biodegradability and nontoxicity. A combination of P(3HB-*co*-3HHx) with folic acid and loaded with etoposide could improve the medication delivery to tumors (Chang et al., 2014). Another application is P(3HB-*co*-3HHx) nanoparticles filled with an insulin phospholipid complex to make a form of insulin that has a long-acting release to treat diabetes. Peng and co-workers have made a thermosensitive hydrogel filled with P(3HB-*co*-3HHx) nanoparticles that can be injected and broken down through biological processes (Peng et al., 2013). This allows insulin to be released slowly and steadily. Due to the long-term basal insulin release by this combination of nanoparticle and hydrogel, which might reduce the frequency of injections of patients, this may assist not just the elderly with diabetes but also patients from other age groups.

Conclusion

In conclusion, P(3HB-*co*-3HHx) copolymer is a type of PHA capable of replacing petroleum-based plastics in different applications like single-used plastics, medical devices, and packaging due to its similar properties and biodegradability. It has a superior biodegradation rate compared to petroleum-based plastics, hence leaving no or little pollution. P(3HB-*co*-3HHx) can be produced by PHA-producing microorganisms through

various pathways like the PHA biosynthesis pathway involving *phaA*, *phaB*, and *phaC*, β-oxidation, and fatty acids *de novo* synthesis dependent on the carbon source fed during cultivation. However, the properties of P(3HB-*co*-3HHx) are dependent on its 3HHx molar composition. Hence, it is necessary to control the 3HHx molar composition of the P(3HB-*co*-3HHx) produced by using different PhaCs, engineering of PhaCs, and metabolic engineering of bacteria for P(3HB-*co*-3HHx) to be applied. With more knowledge and information regarding PhaCs and the metabolic pathway on PHA biosynthesis, P(3HB-*co*-3HHx) with the desired 3HHx molar composition can be produced, making them more suitable for their respective applications.

Author contributions

HJT drafted, wrote, reviewed the manuscript, and designed the figures. SZN wrote and reviewed the manuscript. KS reviewed and approved the final manuscript.

Funding

Acknowledgments

Conflict of interest

The authors declare that the research was conducted in the absence of any commercial or financial relationships that could be construed as a potential conflict of interest.

Publisher's note

All claims expressed in this article are solely those of the authors and do not necessarily represent those of their affiliated organizations, or those of the publisher, the editors and the reviewers. Any product that may be evaluated in this article, or claim that may be made by its manufacturer, is not guaranteed or endorsed by the publisher.

References

Abe, H., and Doi, Y. (1999). Structural effects on enzymatic degradabilities for poly[(R)-3-hydroxybutyric acid] and its copolymers. *Int. J. Biol. Macromol.* 25, 185–192. doi:10.1016/s0141-8130(99)00033-1

Alabi, O. A., Ologbonjaye, K. I., Awosolu, O., and Alalade, O. E. (2019). Public and environmental health effects of plastic wastes disposal: A review. *J. Toxicol. Risk Assess.* 5, 1–13. doi:10.23937/2572-4061.1510021

Anderson, A. J., and Dawes, E. A. (1990). Occurrence, metabolism, metabolic role, and industrial uses of bacterial polyhydroxyalkanoates. *Microbiol. Rev.* 54, 450–472. doi:10.1128/mr.54.4.450-472.1990

Ang, S. L., Sivashankari, R., Shaharuddin, B., Chuah, J. A., Tsuge, T., Abe, H., et al. (2020). Potential applications of polyhydroxyalkanoates as a biomaterial for the aging population. *Polym. Degrad. Stab.* 181, 109371. doi:10.1016/j.polymdegradstab.2020.109371

Asrar, J, Valentin, H. E., Berger, P. A., Tran, M., Padgette, S. R., and Garbow, J. R. (2002). Biosynthesis and properties of poly(3-hydroxybutyrate-co-3-hydroxyhexanoate) polymers. *Biomacromolecules* 3, 1006–1012. doi:10.1021/bm025543a

Bajt, O. (2021). From plastics to microplastics and organisms. *FEBS Open Bio* 11, 954–966. doi:10.1002/2211-5463.13120

Bhubalan, K., Kam, Y. C., Yong, K. H., and Sudesh, K. (2010). Cloning and expression of the PHA synthase gene from a locally isolated *Chromobacterium* sp. *Malays. J. Microbiol.* 6, 81–90. doi:10.21161/mjm.21809

Bluepha (2022). Bluepha® for the blue planet. Available at: https://www.bluepha.bio/(Accessed October 14, 2022).

Bryant, S. J., and Anseth, K. S. (2003). Controlling the spatial distribution of ECM components in degradable PEG hydrogels for tissue engineering cartilage. *J. Biomed. Mat. Res.* 64, 70–79. doi:10.1002/jbm.a.10319

Budde, C. F. (2010). *Production of polyhydroxyalkanoate copolymers from plant oil.* Cambridge (MA): Massachusetts Institute of Technology. [Doctoral dissertation].

Budde, C. F., Riedel, S. L., Willis, L. B., Rha, C., and Sinskey, A. J. (2011). Production of poly(3-hydroxybutyrate-co-3-hydroxyhexanoae) from plant oil by engineered *Ralstonia eutropha* strains. *Appl. Environ. Microbiol.* 77, 2847–2854. doi:10.1128/AEM.02429-10

Chang, H. M., Wang, Z. H., Luo, H. N., Xu, M., Ren, X. Y., Zheng, G. X., et al. (2014). Poly(3-hydroxybutyrate-co-3-hydroxyhexanoate)-based scaffolds for tissue engineering. *Braz. J. Med. Biol. Res.* 47, 533–539. doi:10.1590/1414-431X20143930

Chek, M. F., Kim, S. Y., Mori, T., Tan, H. T., Sudesh, K., and Hakoshima, T. (2020). Asymmetric open-closed dimer mechanism of polyhydroxyalkanoate synthase PhaC. *Iscience* 23, 101084. doi:10.1016/j.isci.2020.101084

Chen, G. Q., and Wu, Q. (2005). The application of polyhydroxyalkanoates as tissue engineering materials. *Biomaterials* 26, 6565–6578. doi:10.1016/j.biomaterials.2005.04.036

Chuah, J. A., Tomizawa, S., Yamada, M., Tsuge, T., Doi, Y., Sudesh, K., et al. (2013). Characterization of site-specific mutations in a short-chain-length/medium-chain-length polyhydroxyalkanoate synthase: *In vivo* and *in vitro* studies of enzymatic activity and substrate specificity. *Appl. Environ. Microbiol.* 79, 3813–3821. doi:10.1128/AEM.00564-13

Danimer Scientific (2022). The future of plastics is here. Available at: https://danimerscientific.com/(Accessed October 14, 2022).

Doi, Y., Kitamura, S., and Abe, H. (1995). Microbial synthesis and characterization of poly(3-hydroxybutyrate-co-3-hydroxyhexanoate). *Macromolecules* 28, 4822–4828. doi:10.1021/ma00118a007

Doi, Y. (1990). *Microbial polyesters.* New York: VCH Publishers.

Foong, C. P., Lakshmanan, M., Abe, H., Taylor, T. D., Foong, S. Y., and Sudesh, K. (2018). A novel and wide substrate specific polyhydroxyalkanoate (PHA) synthase from uncluturable bacteria found in mangrove soil. *J. Polym. Res.* 25, 23. doi:10.1007/s10965-017-1403-4

Fukui, T., Abe, H., and Doi, Y. (2002). Engineering of *Ralstonia eutropha* for production of poly(3-hydroxybutyrate-co-3-hydroxyhexanoate) from fructose and solid-state properties of the copolymer. *Biomacromolecules* 3, 618–624. doi:10.1021/bm0255084

Fukui, T., and Doi, Y. (1997). Cloning and analysis of the poly (3-hydroxybutyrate-co-3-hydroxyhexanoate) biosynthesis genes of *Aeromonas caviae*. *J. Bacteriol.* 179, 4821–4830. doi:10.1128/jb.179.15.4821-4830.1997

Fukui, T., and Doi, Y. (1998). Efficient production of polyhydroxyalkanoates from plant oils by *Alcaligenes eutrophus* and its recombinant strain. *Appl. Microbiol. Biotechnol.* 49, 333–336. doi:10.1007/s002530051178

Fukui, T., Shiomi, N., and Doi, Y. (1998). Expression and characterization of (R)-specific enoyl coenzyme A hydratase involved in polyhydroxyalkanoate biosynthesis by *Aeromonas caviae*. *J. Bacteriol.* 180, 667–673. doi:10.1128/jb.180.3.667-673.1998

Holmes, P. (1988). "Biologically produced (R)-3-hydroxy-alkanoate polymers and copolymers," in *Developments in crystalline polymers*. Editor C. D. Basset (New York: Springer), 1.

Insomphun, C., Mifune, J., Orita, I., Numata, K., Nakamura, S., and Fukui, T. (2014). Modification of β-oxidation pathway in *Ralstonia eutropha* for production of poly(3-hydroxybutyrate-co-3-hydroxyhexanoate) from soybean oil. *J. Biosci. Bioeng.* 117, 184–190. doi:10.1016/j.jbiosc.2013.07.016

Iwata, T. (2005). Strong fibers and films of microbial polyesters. *Macromol. Biosci.* 5, 689–701. doi:10.1002/mabi.200500066

Kahar, P., Tsuge, T., Taguchi, K., and Doi, Y. (2004). High yield production of polyhydroxyalkanoates from soybean oil by *Ralstonia eutropha* and its recombinant strain. *Polym. Degrad. Stab.* 83, 79–86. doi:10.1016/S0141-3910(03)00227-1

KANEKA Corporation (2021a). KANEKA Biodegradable Polymer Green Planet™ is adopted in shopping bags for JALUX. Available at: https://www.kaneka.co.jp/en/topics/news/2021/ennr2106141.html (Accessed June 21, 2022).

KANEKA Corporation (2020). KANEKA Biodegradable Polymer PHBH™ used in Shiseido's cosmetics packages. Available at: https://www.kaneka.co.jp/en/topics/news/2020/ennr2008061.html (Accessed June 21, 2022).

KANEKA Corporation (2021b). Spoons made from KANEKA biodegradable polymer green Planet™ are adopted in FamilyMart. Available at: https://www.kaneka.co.jp/en/topics/news/2021/ennr2106221.html (Accessed June 21, 2022).

KANEKA Corporation (2019). Target area expanded for seven café straws made from KANEKA biodegradable polymer PHBH™. Available at: https://www.kaneka.co.jp/en/topics/information/in20191031/(Accessed June 21, 2022).

KANEKA Corporation (2021c). Use of KANEKA Biodegradable Polymer Green Planet™ expands to ITO EN's tea beverages following vegetable juices. Available at: https://www.kaneka.co.jp/en/topics/news/2021/ennr2109211.html (Accessed June 21, 2022).

KANEKA The Dreamology Company (2022). Kaneka. Available at: https://www.kaneka.be/(Accessed October 14, 2022).

Kawashima, Y., Orita, I., Nakamura, S., and Fukui, T. (2015). Compositional regulation of poly(3-hydroxybutyrate-co-3-hydroxyhexanoate) by replacement of granule-associated protein in *Ralstonia eutropha*. *Microb. Cell. Fact.* 14, 187–212. doi:10.1186/s12934-015-0380-8

Kellerhals, M. B., Kessler, B., Witholt, B., Tchouboukov, A., and Brandl, H. (2000). Renewable long-chain fatty acids for production of biodegradable medium-chain-length polyhydroxyalkanoates (mcl-PHAs) at laboratory and pilot plant scales. *Macromolecules* 33, 4690–4698. doi:10.1021/ma000655k

Kichise, T., Taguchi, S., and Doi, Y. (2002). Enhanced accumulation and changed monomer composition in polyhydroxyalkanoate (PHA) copolyester by *in vitro* evolution of *Aeromonas caviae* PHA synthase. *Appl. Environ. Microbiol.* 68, 2411–2419. doi:10.1128/AEM.68.5.2411-2419.2002

Lee, S. Y., and Choi, J. I. (1999). Production and degradation of polyhydroxyalkanoates in waste environment. *Waste Manag.* 19, 133–139. doi:10.1016/S0956-053X(99)00005-7

Lemoigne, M. (1926). Products of dehydration and of polymerization of β-hydroxybutyric acid. *Bull. Soc. Chim. Biol.* 8, 770

Loo, C., and Sudesh, K. (2007). Polyhydroxyalkanoates: Bio-based microbial plastics and their properties. *Malays. Polym. J.* 2, 31–57.

Loo, C. Y., Lee, W. H., Tsuge, T., Doi, Y., and Sudesh, K. (2005). Biosynthesis and characterization of poly(3-hydroxybutyrate-co-3-hydroxyhexanoate) from palm oil products in a *Wautersia eutropha* mutant. *Biotechnol. Lett.* 27, 1405–1410. doi:10.1007/s10529-005-0690-8

Magazine, B. (2021). Capsul'in Pro launches world's first certified home compostable coffee capsule. Available at: https://www.bioplasticsmagazine.com/en/news/meldungen/20210310-Capsul-in-Pro-launches-world-s-first-certified-home-compostable-coffee-capsule.php (Accessed May 30, 2022).

Masry, M., Rossignol, S., Gardette, J. L., Therias, S., Bussière, P. O., and Wong-Wah-Chung, P. (2021). Characteristics, fate, and impact of marine plastic debris exposed to sunlight: A review. *Mar. Pollut. Bull.* 171, 112701. doi:10.1016/j.marpolbul.2021.112701

Matsusaki, H., Manji, S., Taguchi, K., Kato, M., Fukui, T., and Doi, Y. (1998). Cloning and molecular analysis of the poly(3-hydroxybutyrate) and poly(3-hydroxybutyrate-co-3-hydroxyalkanoate) biosynthesis genes in *Pseudomonas* sp. strain 61-3. *J. Bacteriol.* 180, 6459–6467. doi:10.1128/JB.180.24.6459-6467.1998

Molitoris, H. P., Moss, S. T., Koning, D., and Jendrossek, D. (1996). Scanning electron microscopy of polyhydroxyalkanoate degradation by bacteria. *Appl. Microbiol. Biotechnol.* 46, 570–579. doi:10.1007/s002530050863

Morse, M. C., Liao, Q., Criddle, C. S., and Frank, C. W. (2011). Anaerobic biodegradation of the microbial copolymer poly(3-hydroxybutyrate-co-3-

hydroxyhexanoate): Effects of comonomer content, processing history, and semi-crystalline morphology. *Polymer* 52, 547–556. doi:10.1016/j.polymer.2010.11.024

Murugan, P., Chhajer, P., Kosugi, A., Arai, T., Brigham, C. J., and Sudesh, K. (2016). Production of P(3HB-*co*-3HHx) with controlled compositions by recombinant *Cupriavidus necator* Re2058/pCB113 from renewable resources. *Clean. Soil Air Water* 44, 1234–1241. doi:10.1002/clen.201500714

Murugan, P., Gan, C. Y., and Sudesh, K. (2017). Biosynthesis of P(3HB-*co*-3HHx) with improved molecular weights from a mixture of palm olein and fructose by *Cupriavidus necator* Re2018/pCB113. *Int. J. Biol. Macromol.* 102, 1112–1119. doi:10.1016/j.ijbiomac.2017.05.006

Neoh, S. Z., Chek, M. F., Tan, H. T., Linares-Pastén, J. A., Nandakumar, A., Hakoshima, T., et al. (2022). Polyhydroxyalkanoate synthase (PhaC): The key enzyme for biopolyester synthesis. *Curr. Res. Biotechnol.* 4, 87–101. doi:10.1016/j.crbiot.2022.01.002

Noda, I., Green, P. R., Satkowski, M. M., and Schechtman, L. A. (2005). Preparation and properties of a novel class of polyhydroxyalkanoate copolymers. *Biomacromolecules* 6, 580–586. doi:10.1021/bm049472m

Peng, Q., Sun, X., Gong, T., Wu, C. Y., Zhang, T., Tan, J., et al. (2013). Injectable and biodegradable thermosensitive hydrogels loaded with PHBHHx nanoparticles for the sustained and controlled release of insulin. *Acta Biomater.* 9, 5063–5069. doi:10.1016/j.actbio.2012.09.034

Purama, R. K., Al-Sabahi, J. N., and Sudesh, K. (2018). Evaluation of date seed oil and date molasses as novel carbon sources for the production of poly(3Hydroxybutyrate-*co*-3Hydroxyhexanoate) by *Cupriavidus necator* H16 Re2058/pCB113. *Industrial Crops Prod.* 119, 83–92. doi:10.1016/j.indcrop.2018.04.013

Qiu, Y., Fu, J., Sun, B., and Ma, X. (2021). Sustainable nanocomposite films based on SiO2 and biodegradable poly(3-hydroxybutyrate-*co*-3-hydroxybutyrate) (PHBH) for food packaging. *e-Polymers* 21, 072–081. doi:10.1515/epoly-2021-0009

Qu, X. H., Wu, Q., Liang, J., Zou, B., and Chen, G. Q. (2006a). Effect of 3-hydroxyhexanoate content in poly(3-hydroxybutyrate-*co*-3-hydroxyhexanoate) on *in vitro* growth and differentiation of smooth muscle cells. *Biomaterials* 27, 2944–2950. doi:10.1016/j.biomaterials.2006.01.013

Qu, X. H., Wu, Q., Zhang, K. Y., and Chen, G. Q. (2006b). *In vivo* studies of poly(3-hydroxybutyrate-*co*-3-hydroxyhexanoate) based polymers: Biodegradation and tissue reactions. *Biomaterials* 27, 3540–3548. doi:10.1016/j.biomaterials.2006.02.015

Reddy, V. U. N., Ramanaiah, S. V., Reddy, M. V., and Chang, Y. C. (2022). Review of the developments of bacterial medium-chain-length polyhydroxyalkanoates (mcl-PHAs). *Bioengineering* 9, 225. doi:10.3390/bioengineering9050225

Rehm, B. H. (2003). Polyester synthases: Natural catalysts for plastics. *Biochem. J.* 376, 15–33. doi:10.1042/BJ20031254

Riedel, S. L., Bader, J., Brigham, C. J., Budde, C. F., Yusof, Z. A. M., Rha, C., et al. (2012). Production of poly(3-hydroxybutyrate-*co*-3-hydroxyhexanoate) by *Ralstonia eutropha* in high cell density palm oil fermentations. *Biotechnol. Bioeng.* 109, 74–83. doi:10.1002/bit.23283

RWDC Industries (2022). We believe it is our duty as stewards of the planet to use our talents, energy and time to leave a legacy of a sustainable future. Available at: https://www.rwdc-industries.com/(Accessed October 14, 2022).

Shimamura, E., Kasuya, K., Kobayashi, G., Shiotani, T., Shima, Y., and Doi, Y. (1994). Physical properties and biodegradability of microbial poly(3-hydroxybutyrate-*co*-3-hydroxyhexanoate). *Macromolecules* 27, 878–880. doi:10.1021/ma00081a041

Sudesh, K., Abe, H., and Doi, Y. (2000). Synthesis, structure and properties of polyhydroxyalkanoates: Biological polyesters. *Prog. Polym. Sci.* 25, 1503–1555. doi:10.1016/S0079-6700(00)00035-6

Sudesh, K., and Iwata, T. (2008). Sustainability of biobased and biodegradable plastics. *Clean. Soil Air Water* 36, 433–442. doi:10.1002/clen.200700183

Sudesh, K. (2012). *Polyhydroxyalkanoates from palm oil: Biodegradable plastics*. Berlin Heidelberg: Springer-Verlag.

Taguchi, K., Aoyagi, Y., Matsusaki, H., Fukui, T., and Doi, Y. (1999). Co-expression of 3-ketoacyl-ACP reductase and polyhydroxyalkanoate synthase

genes induces PHA production in *Escherichia coli* HB101 strain. *FEMS Microbiol. Lett.* 176, 183–190. doi:10.1111/j.1574-6968.1999.tb13660.x

Tan, H. T., Chek, M. F., Lakshmanan, M., Foong, C. P., Hakoshima, T., and Sudesh, K. (2020). Evaluation of BP-M-CPF4 polyhydroxyalkanoate (PHA) synthase on the production of poly(3-hydroxybutyrate-*co*-3-hydroxyhexanoate) from plant oil using *Cupriavidus necator* transformants. *Int. J. Biol. Macromol.* 159, 250–257. doi:10.1016/j.ijbiomac.2020.05.064

Tan, H. T., Chek, M. F., Miyahara, Y., Kim, S. Y., Tsuge, T., Hakoshima, T., et al. (2022). Characterization of an (*R*)-specific enoyl-CoA hydratase from *Streptomyces* sp. strain CFMR 7: A metabolic tool for enhancing the production of poly(3-hydroxybutyrate-*co*-3-hydroxyhexanoate). *J. Biosci. Bioeng.* S1389-1723 (22), 288–294. doi:10.1016/j.jbiosc.2022.07.005

Thinagaran, L., and Sudesh, K. (2019). Evaluation of sludge palm oil as feedstock and development of efficient method for its utilization to produce polyhydroxyalkanoate. *Waste Biomass Valor.* 10, 709–720. doi:10.1007/s12649-017-0078-8

Tsuge, T. (2002). Metabolic improvements and use of inexpensive carbon sources in microbial production of polyhydroxyalkanoates. *J. Biosci. Bioeng.* 94, 579–584. doi:10.1016/s1389-1723(02)80198-0

Tsuge, T., Saito, Y., Narike, M., Muneta, K., Normi, Y. M., Kikkawa, Y., et al. (2004). Mutation effects of a conserved alanine (Ala510) in Type I polyhydroxyalkanoate synthase from *Ralstonia eutropha* on polyester biosynthesis. *Macromol. Biosci.* 4, 963–970. doi:10.1002/mabi.200400075

Tsuge, T., Watanabe, S., Shimada, D., Abe, H., Doi, Y., and Taguchi, S. (2007). Combination of N149S and D171G mutations in *Aeromonas caviae* polyhydroxyalkanoate synthase and impact on polyhydroxyalkanoate biosynthesis. *FEMS Microbiol. Lett.* 277, 217–222. doi:10.1111/j.1574-6968.2007.00958.x

Volova, T. G., Prudnikova, S. V., Vinogradova, O. N., Syrvacheva, D. A., and Shishatskaya, E. I. (2017). Microbial degradation of polyhydroxyalkanoates with different chemical compositions and their biodegradability. *Microb. Ecol.* 73, 353–367. doi:10.1007/s00248-016-0852-3

Volova, T. G., Syrvacheva, D. A., Zhila, N. O., and Sukovatiy, A. G. (2016). Synthesis of P(3HB-*co*-3HHx) copolymers containing high molar fraction of 3-hydroxyhexanoate monomer by *Cupriavidus eutrophus* B10646. *J. Chem. Technol. Biotechnol.* 91, 416–425. doi:10.1002/jctb.4592

Wang, Y. W., Mo, W., Yao, H., Wu, Q., Chen, J., and Chen, G. Q. (2004). Biodegradation studies of poly(3-hydroxybutyrate-*co*-3-hydroxyhexanoate). *Polym. Degrad. Stab.* 85, 815–821. doi:10.1016/j.polymdegradstab.2004.02.010

Wong, Y. M., Brigham, C. J., Rha, C., Sinskey, A. J., and Sudesh, K. (2012). Biosynthesis and characterization of polyhydroxyalkanoate containing high 3-hydroxyhexanoate monomer fraction from crude palm kernel oil by recombinant *Cupriavidus necator*. *Bioresour. Technol.* 121, 320–327. doi:10.1016/j.biortech.2012.07.015

Yang, H. X., Sun, M., Zhang, Y., and Zhou, P. (2011). Degradable PHBHHx modified by the silk fibroin for the applications of cardiovascular tissue engineering. *ISRN Mater. Sci.* 2011, 1–11. doi:10.5402/2011/389872

Yong, K. H. (2009). Biosynthesis and characterization of polyhydroxyalkanoates by a locally isolated *Chromobacterium* sp. USM2. Georgetown: Universiti Sains Malaysia. [MSc. thesis].

Yu, B. Y., Chen, P. Y., Sun, Y. M., Lee, Y. T., and Young, T. H. (2012). Response of human mesenchymal stem cells (hMSCs) to the topographic variation of poly(3-hydroxybutyrate-*co*-3-hydroxyhexanoate) (PHBHHx) films. *J. Biomaterials Sci. Polym. Ed.* 23, 1–26. doi:10.1163/092050610X541386

Yu, J. (2007). "Microbial production of bioplastics from renewable resources," in *Bioprocessing for value-added products from renewable resources: New Technologies and Applications*. Editor S. T. Yang (Amsterdam: Elsevier), 585

Zhang, M., Kurita, S., Orita, I., Nakamura, S., and Fukui, T. (2019). Modification of acetoacetyl-CoA reduction step in *Ralstonia eutropha* for biosynthesis of poly(3-hydroxybutyrate-*co*-3-hydroxyhexanoate) from structurally unrelated compounds. *Microb. Cell. Fact.* 18, 147–212. doi:10.1186/s12934-019-1197-7

Zhao, S., Zhu, M., Zhang, J., Zhang, Y., Liu, Z., Zhu, Y., et al. (2014). Three dimensionally printed mesoporous bioactive glass and poly(3-hydroxybutyrate-*co*-3-hydroxyhexanoate) composite scaffolds for bone regeneration. *J. Mat. Chem. B* 2, 6106–6118. doi:10.1039/c4tb00838c

Physicochemical studies of novel sugar fatty acid esters based on (*R*)-3-hydroxylated acids derived from bacterial polyhydroxyalkanoates and their potential environmental impact

Wojciech Snoch[1], Ewelina Jarek[1], Dusan Milivojevic[2], Jasmina Nikodinovic-Runic[2] and Maciej Guzik[1]*

[1]Jerzy Haber Institute of Catalysis, Surface Chemistry Polish Academy of Sciences, Kraków, Poland, [2]Institute of Molecular Genetics and Genetic Engineering, University of Belgrade, Belgrade, Serbia

Sugar fatty acids esters are popular compounds widely used in both the nutritional, cosmetic and pharmaceutical industries due to their amphiphilic structure and consequent ability to reduce the surface tension of solutions. Furthermore, an important aspect in the implementation of any additives and formulations is their environmental impact. The properties of the esters depend on the type of sugar used and the hydrophobic component. In this work, selected physicochemical properties of new sugar esters based on lactose, glucose and galactose and hydroxy acids derived from bacterial polyhydroxyalkanoates are shown for the first time. Values for critical aggregation concentration, surface activity and pH make it possible that these esters could compete with other commercially used esters of similar chemical structure. The investigated compounds showed moderate emulsion stabilization abilities presented on the example of water-oil systems containing squalene and body oil. Their potential environmental impact appears to be low, as the esters are not toxic to *Caenorhabditis elegans* even at concentrations much higher than the critical aggregation concentration.

KEYWORDS

polyhydroxyalkanoates (PHA), sugar esters, cosmetic industry, *Caenorhabditis elegans*, environmental impact, surface activity

Introduction

The demand for various emulsion systems and lubricants for skin care and protection is increasing every year (Farias et al., 2021). It became even more significant in recent years due to the fight against the COVID-19 pandemic–when the frequency of disinfection has become an inseparable part of everyone's life (Masen, 2020; Patruno et al., 2020; Dini and Laneri, 2021). Therefore, the pharmaceutical and cosmetic industries are constantly working on perfect water-oil (W/O) systems that are less irritating to skin, are more stable in temperature and time, and are even capable of delivering bioactive compounds (Fabbron-Appas et al., 2021). At the same time, the impact of these systems on the environment is not without significance. Emulsions used in the industry should have physical and chemical parameters allowing them to be easily decomposed to not harm living organisms (Dini and Laneri, 2021; Tang et al., 2022). In order to meet these requirements a perfect combination of the oil phase and the emulsion stabilizer

FIGURE 1
Scheme of the research and it's workflow.
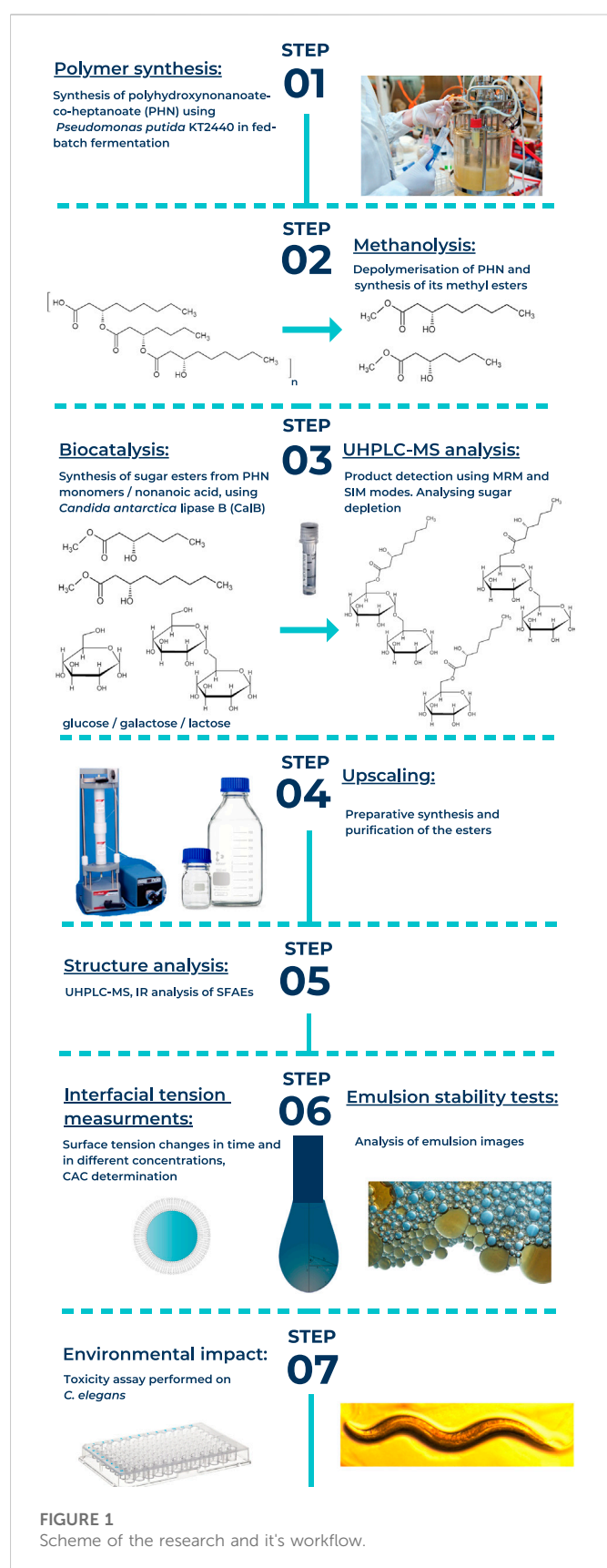
needs to be sought. Sugar fatty acid esters (SFAE) seem to be fair candidates for supporting such W/O systems. Their chemical structure and physicochemical properties, provide numerous applications in the pharmaceutical, cosmetic and food industries, including dietary

supplements (Kumar, 2005; Łopaciuk and Łoboda, 2013; Blanc, 2015). The foremost important feature these chemicals offer in the formulation of products (i.e. creams, gels, foams, *etc.*) are their ability to decrease interfacial tension and to stabilize emulsions. Sometimes they are even accompanied by antimicrobial characteristics (Hill and Rhode, 1999; Van Kempen et al., 2013; Lucarini et al., 2016; Shao et al., 2018). These surfactant features can be manipulated either by the number of–OH groups within a sugar component, the length or modification of an aliphatic chain, which together can be described by hydrophilic-lipophilic balance (HLB) values (Sharma and Sarangdevot, 2012; Lémery et al., 2015; Pe et al., 2017). The hydrophobic component may be branched, include unsaturated bonds, additional hydroxylic groups or other desirable functionalities (van Kempen et al., 2014; Zhou et al., 2014; Riecan et al., 2022). Worth mentioning is a fact that global surfactant market size was 39,901 million USD in 2019 and is projected to grow to 52,417 million USD by 2025 (Tortilla et al., 2019).

Having the above in mind, our attention was drawn by a family of bacterial polyesters, namely polyhydroxyalkanoates (PHAs), as a source of easily modifiable hydroxyacids, used here as the hydrophobic component of SFAEs. Polyhydroxyalkanoates are synthesized by bacteria in response to environmental stress from various carbon sources and so far around 150 different building blocks are incorporated in their structure (Steinbüchel and Steinbüchel, 1995). The PHA monomers, namely (*R*)-3-hydroxylated fatty acids, are promising components for SFAEs synthesis with intrinsic antimicrobial and anticancer potential (Snoch et al., 2019; Snoch et al., 2021). Their structure–a hydroxyl group at the 3rd position–allows for further modifications by decorating the molecule with the desired functionality (i.e. *via* an ether or an ester bond). Moreover, these sugar esters can be synthesized with an aid of biocatalysis, using enzymes such as lipases or esterases (Ansorge-Schumacher and Thum, 2013; Khan and Rathod, 2015; Pappalardo et al., 2017; Staroń et al., 2018), enabling preparation of true green additives. We have followed this path and employed biocatalysis in synthesis of our novel esters. However, little is known about their physicochemical characteristics.

This work describes surface activity of biotically synthesized sugar esters in comparison with their aliphatic counterparts (Figure 1). Their hydrophobic part was originated from bacterial poly–(*R*)–3–hydroxynonanoate–co–heptanoate (PHN). Firstly, we provide data on critical aggregation concentration (CAC), the point, conventionally chosen, where an increase of the surfactant concentration does not lead to a significant further reduction of the surface tension (Garofalakis et al., 2000) of the investigated compounds. Additionally, we performed simple tests of their emulsifying abilities with popular ingredients in cosmetic industry as skincare oil and squalene. Next, determination of emulsion stabilizing properties of these systems enabled us to verify industrial potential application of the SFAE as emulsifier. Finally, performing toxicity assay on *Caenorhabditis elegans* provided prognosis about the final key issue: potential environmental impact of the investigated stabilizers (Place, 2020; Ali and El-Ashry, 2021; Lanzerstorfer et al., 2021).

Materials and methods

Sugar esters used in this study

Sugar esters of aliphatic nonanoic acid along with a mixture of (*R*)-3-hydroxylated nonanoic acid and heptanoic acids (mPHN, derived from PHN) of glucose, galactose and lactose were obtained and characterized as

TABLE 1 Composition of enzymatically obtained sugar esters used in this work.

Compound name[a]	Type of mono/diester	Amount of mono/diester (%)	Mean molar mass (g mol^{-1})
C9-glu	c9	75.8	370.57
	c9c9	24.2	
C9-gal	c9	91.0	352.68
	c9c9	9.0	
C9-lac	c9	89.4	497.31
	c9c9	10.6	
mPHN-glu	c9	20.0	406.98
	c9c9	09.8	
	c7	16.3	
	c7c7	32.9	
	c9c7	21.0	
mPHN-gal	c9	20.5	401.61
	c9c9	27.0	
	c7	25.6	
	c7c7	15.0	
	c9c7	11.9	
mPHN-lac	c9	24.6	584.22
	c9c9	18.9	
	c7	06.3	
	c7c7	21.5	
	c9c7	28.8	

a) C9-glu: a mixture of mono and diesters of glucose nonanoate, C9-gal: a mixture of mono and diesters of galactose nonanoate, C9-lac: a mixture of mono and diesters of lactose non-aoate, mPHN-glu: a mixture of PHN monomers originated glucose mono and diesters, mPHN-gal: a mixture of PHN monomers originated from galactose mono and diesters, mPHN-lac: a mixture of PHN monomers originated lactose mono and diesters.

- c9-monoester containing one nine carbon atom chain
- c7-monoester containing one seven carbon atom chain
- c9c9-diester containing two nine carbon atom chains
- c7c7-diester containing two seven carbon atom chains
- c9c7-diester containing one nine and one seven carbon atom chain

described in our previous works. In search of effective anticancer agents—novel sugar esters based on polyhydroxyalkanoate Monomers (Snoch et al., 2021). The composition of new synthesized compounds is presented in Table 1, the yields and their purity are presented in Supplementary Table S1.

Determination of surface activity of synthesized compounds

The surface tension has been measured for different batches of synthetized compounds by using pendant drop shape analysis method by two apparatus. First apparatus: a home-made experimental set-up described in detail in (Para et al., 2006), with experimental error equals to 2 mN/m, was used. The Young–Laplace capillary equation was fitted to the digitally recorded drop image. Measured surface tension value corresponds to the value of the best fit (note: it is as the only

unknown parameter in this equation). The dynamic surface tension measurements were performed every 5 s. Measured equilibrium surface tension corresponded to the obtained steady-state time after adsorption, which was depended on surfactant concentration. The studied solutions of surfactant were mixtures of sugars mono and diesters, which can differ by number of hydrophobic hydrocarbon chains. As a consequence, the kinetic curves for different drops of the same solution did not often overlap. That is why the experimental values for one solution are the mean values from all the recorder dynamic curves. As second apparatus a commercial tensiometer (PAT–1M, Sinterface, Berlin, Germany), with experimental error of 0.2 mN/m, was used. (Kairaliyeva et al., 2017). The PAT-1M apparatus allows for an accurate control of the droplet area (or its volume) by a syringe pump, driven by a feedback loop software based on the drop imaging. The dynamic interfacial tension *versus* time on a freshly formed drop is measured during the ageing of the interface while keeping the drop volume constant (11 μL). The equilibrium interfacial

tensions are obtained from these data at long period of time. The greatest experimental error is mainly connected with small differences in composition from batch to batch so we present all experimental points and determined the critical aggregation concentration (CAC). All surface tension measurements were performed at 295 K. For all the experiments, ultrapure water—produced from the Millipore Direct-Q ® 5UV purification system (18 MΩ cm⁻¹), was used. Its surface tension measurement provides a value of 72.5 ± 0.2 mN/m, stable for at least 2 hours at 20°C meaning negligible amount of surface-active impurities.

Determination of hydrophilic- lipophilic balance

Hydrophilic-Lipophilic Balance was determined according Griffin method by using following equation (Griffin W.C., 1954)

$$HLB = 20 \ x \ \frac{hydrophilic \ group \ molecular \ weight}{total \ surfactant \ molecular \ weight} \qquad (1)$$

Emulsion stability

The ability of the SFAE to stabilize water–oil (W/O) systems was estimated by measuring time of phase separation in each performed emulsion. The experiment was conducted under following protocol: 5 g of each SFAE solutions were prepared as water phase and mixed with 0.5 g of oil phase: squalane or popular commercially available skincare oil- Bambino® respectively. Concentrations of the SFAE in solutions were: 0.5 × CAC, 1.0 × CAC 1.5 × CAC respectively. The skincare oil consisted of: glycine soya oil, paraffinum liquidum, parfum, ethyl linolate, ethyl oleate, tocopherol, propylene glycol, propyl galate, citric acid, BHA, according to the manufacturer label in the unknown proportions. The mixtures were mixed in shaker at 25 C for 20 min and mixed vigorously with Vortex for another 1 min to ensure the phases were mixed sufficiently (An et al., 2019; Li and Xiang, 2019).

Caenorgabditis elegans toxicity assay

Potential environmental impact of the investigated compounds was tested by treating *Caenorhabditis elegans* according to following protocol adapted from WormBook (Stiernagle, 2006) and (Djapovic et al., 2021). Briefly, synchronized worms (L4 stage) were suspended in a medium containing 95% M9 buffer (3.0 g of KH_2PO_4, 6.0 g of Na_2HPO_4, 5.0 g of NaCl, and 1 mL of 1 mol L⁻¹ $MgSO_4 \times 7 \ H_2O$ in 1 L of water), 5% LB broth (10 g L⁻¹ tryptone, 5 g L⁻¹ yeast extract, and 10 g L⁻¹NaCl), and 10 µg mL⁻¹ of cholesterol. The experiment was carried out in 96-well flat-bottomed microtiter plates (Sarstedt, Nümbrecht, Germany) in the final volume of 100 µL per well. Suspension of nematodes (25 µL containing 25–35 nematodes) was transferred to the wells of a 96-well microtiter plate, where 50 µL of the medium was previously added. Next, 25 µL of a solvent control (DMSO) or 25 µL of a concentrated solution was added to the test wells. The examined esters were dissolved in DMSO to obtain stock solutions than added to the wells with worms. The final concentrations of the compounds were 2.0, 1.5, 1.0, 0.5, 0.25 and 0.125 mg mL⁻¹. The final

concentration of DMSO in each well was 1% (v/v) Subsequently, the plates were incubated at 25 C for 2 days. The fraction of dead worms was determined after 48 h by counting the number of dead worms and the total number of worms in each well, using a stereomicroscope (SMZ143-N2GG, Motic, Wetzlar, Germany). As a negative control experiment, nematodes were exposed to the medium containing 1% (v/v) DMSO.

Results

After preparative synthesis, purification and drying the obtained SFAE were analyzed using UHPLC-MS (QQQ) in both selected ionic mass (SIM) and multiple reaction monitoring (MRM) modes. The obtained peaks from ESI+, i.e. (M + Na)⁺ adducts, were integrated so their peak areas enabled us to calculate fractions of mono and diesters. Mean molar masses of SFAE mixtures were calculated as well. The obtained results are presented below in Table 1.

Instead of the critical micelle concentration (CMC), we decided to use the more general term—critical aggregation concentration (CAC)—because the LC-MS analysis shows that the synthesised compounds are in fact mixtures of mono and diesters with different percentage compositions (See Table 1) and undefined stereochemistry of the resulting esters. As the concentration of the surfactants tested increases, the surface tension does not transition sharply to a constant value, as is the case with pure mono-component surfactant solutions, but gradually changes marginally (Supplementary Figure S1). We used as CAC values the concentration at which the slopes of the curves connecting the experimental points significantly change shape and the surface tension for subsequent concentrations does not differ significantly (dashed lines in Figure 2). Despite the large scatter in the data obtained especially for the galactose derivatives, the experimental results of the solutions of the different batches, obtained on the two apparatus, coincide, and the trend in the differences in surface activity between the simple esters and mPHN derivatives is the same (Figure 2). The lactose derivatives are the most surface active, followed by galactose and the least glucose, as evidenced by the increasing values of the critical aggregation concentration (Table 2). A comparison of the aliphatic sugar esters and the corresponding mPHN derivatives shows that the mPHN derivatives are more surface active (Figure 3). In our case the quality of the anomers (α or β) in the tested solutions was not determined. Nevertheless, literature data indicate that the stereochemistry of the sugar derivatives can affect the surface tension. For example, *ß* anomers are more effective surfactants than α anomers, and differences in surface tension can be as high as 8 mN m⁻¹. This is a result of differences in the ability to form intermolecular hydrogen bonds with other ester molecules and the surrounding water molecules (Nilsson et al., 1998). As a consequence, the sugar moieties' hydrophilicity, surface activity and solubility are altered, which can result in the presence of relatively large aggregates in solution, but too fine (below 300 nm) to cause visible turbidity in solutions (Nilsson and So, 1998; Larsson et al., 2019). Clearly, this is an issue that will require additional research in the future.

The pH of the solutions tested for simple sugar derivatives and mPHN-lac ranged from 5.2 to 6.8, which is characteristic of aqueous solutions in contact with carbon dioxide. Only in the case of mPHN-glu and mPHN-gal were the solutions slightly acidic (pH = 4.0 ± 0.2),
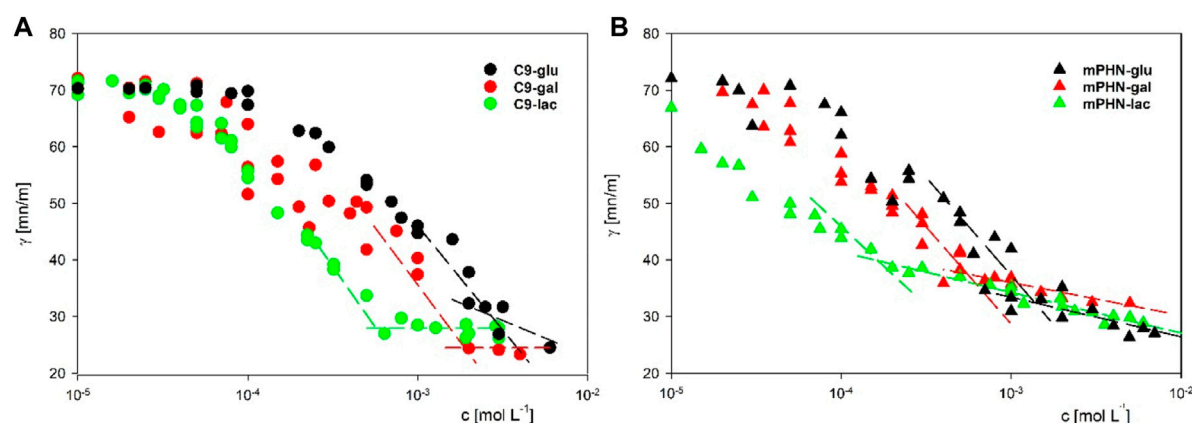
FIGURE 2
The surface tension dependency on surfactants concentration **(A)** C9-glu black circles; C9-gal red circles; C9-lac green circles **(B)** mPHN-glu black triangles; mPHN-gal red triangles; mPHN-lac green triangles. The intersection of the lines indicates the concentration at which the slope of the surface tension isotherms changes significantly, which is conventionally taken as CAC.

so surface tension measurements were carried out for these solutions (C = 1 mmol L^{-1}) in the presence of 0.1 mol L^{-1} NaCl. Increasing the ionic strength did not result in significant changes in surface tension (e.g. from 34.8 mN m^{-1} in H$_2$0 to 33.1 mN m^{-1} in 0.1 mol L^{-1} NaCl for mPHN-gal and from 34.5 mN m^{-1} in H$_2$0 to 32.6 in 0.1 mol L^{-1} NaCl), which are within the experimental limit of the apparatus error (2 mN m^{-1}). This may indicate that surface-active ionic compounds are absent from the solution. In contrast, measurements in 0.1 mol L^{-1} NaOH solution resulted in a significant increase in surface tension (e.g. for mPHN-gal it increased to a value of 42 mN m^{-1} and for mPHN-gal to 58.6 mN m^{-1}). This may be due to the different susceptibility to hydrolysis - the released organic acids dissociate in an alkaline environment and, as ionic surfactants, show much lower surface activity. In addition, the different degree of hydrolysis may be due to the different content of α and ß anomers.

Both glucose and galactose esters CAC values were much lower than the referenced CMC glucose monooctanoate (10.5 mmol L^{-1}) and higher than glucose monodecanoate (0.71–1.5 mmol L^{-1}) (Lee et al., 2018), which directly correlates with the chain length of the hydrophobic component of SFAE. Interestingly, C9-lac and mPHN-gal ester mixtures are somewhat identical to the commercial sucrose monodecanoate (SM-1000), the CMC of which was 0.56 mmol L^{-1}. In general CACs of the mPHN derived esters obtained are higher than their counterparts in the literature, giving slightly lower interfacial tension values. The difference was observed for mPHN-lac which CAC is much lower than sucrose and lactose caprate (c10), laurate (c12) and even oleate (c18). Although mPHN-lac can be compare to Tween 80 (γ = 0.01 mmol L^{-1}, 38 mN m^{-1}). (Lee et al., 2018) (Lucarini et al., 2018) (Ye et al., 2016). All the synthesized based SFAE have their measured surface tension at the similar level (varying for the lowest of γ = 25.2–23.5 mN m^{-1} for C9-gal to the highest of γ = 32–28 mN m^{-1} for mPHN-lac, without any visible trend, Table 2). The HLB indexes calculated are lower for mono carbohydrates in both groups when compared to lactose esters. However, when hydrophobic component is considered, the HLB indexes are larger by 1–3 units for the aliphatic SFAEs. All the HLB values were in range of the referenced compounds (Table 2) regardless of whether the calculations took into account the content of mono- or diesters.

On the basis of the obtained interfacial tension profiles, it was possible to draw equilibrium concentrations curves, thus to determine aggregation concentrations (Figures 2A,B). The curves for different concentrations, but with a similar profile and little difference in values, are indicative of aggregation or micelle formation. They also provide indirect information on how the presence of mono- and diesters of c7 and c9 chains affects the ability to reduce surface tension. It is noticeable that the shape of each curve is depended on the sugar component (glucose and galactose vs. lactose esters, Figures 2A,B). In both cases the slopes of lactose esters were steeper than in these of glucose and galactose esters mixtures, which may be related to the difference in the size of the hydrophilic sugar heads. (Gaudin et al., 2019). Moreover, the slope of the curve for the mPHN-lac mixture was steeper than C9-lac (containing 89.4% monoester, 10.6% diesters), which may be related to the higher ratio of diesters in the mPHN-lac mixture (containing 30.8% of the total monoesters of c9 and c7 and 69.2% of the total of c9c9, c7c7, c9c7 diesters).

Taking into account the composition of the tested mixtures and contribution of diesters, we would expect lower ranges of CAC concentrations. Similar to those presented in Table 2 e.g. sucrose oleate. As can be seen, the presence of additional c9 or c7 chains in the hydrophobic component does not translate directly into properties comparable to twice as long aliphatic chains of other esters. It can be partially explained by the catalytic action of the lipase, which decorates a sugar moiety by attaching hydrophobic components on the opposite sides of the carbohydrate. There is also uncertainty when it comes to decorating sugars with (R)–3–hydroxylated fatty acids by the action of lipase, whether the final structure of the resultant SFAE is as described above for the aliphatic appendixes or it reassembles this of rhamnolipids (sugar + (R) –3-hydroxylated fatty acid + (R)–3-hydroxylated fatty acid). Moreover, the mere presence of hydroxyl group of monomers can also influence the branching of the entire molecule and disrupt the hydrophobicity of a carbon chain. (Hollenbach et al., 2020). Therefore, more detailed studies are needed in order to elucidated the final structure of the produced esters and also their behaviour on the molecular scale.

TABLE 2 Physicochemical properties of the synthetized sugar esters and reference compounds.

Compounds used in this study								
Compound name	CAC	Surface tension γ	HLB griffin for each SFAE component					pH
	(mmol L−1)	(mN m−1)	c9	c7	c9c9	c7c7	c9c7	
C9-glu	2.7	31.5–24.5	11.25	–	7.83	–	–	5.39
C9-gal	2	25.2–23.5	11.25	–	7.83	–	–	5.33
C9-lac	0.56	29.2–25.8	14.2	–	11	–	–	6.29
mPHN-glu	1.4	35–26	11.72	12.79	8.7	9.81	9.22	3.92
mPHN-gal	0.56	37–32	11.72	12.79	8.7	9.81	9.22	4.12
mPHN-lac	0.016	39–28.5	14.41	15.27	11.49	12.57	12.01	6.8

Referenced compounds				
Compound name	CMC/CAC	Surface tension γ	HLB Griffin	References
	(mmol L-1)	(mN m-1)		
octyl- B-D- glucoside	21.2	31	12.32	Gaudin et al. (2019)
nonyl- B-D- glucoside	6.9	29.6	11.7	
Glucose monooctanoate (c8)	10.15	26.37	11.76	Zhang et al. (2015)
Glucose monodecanoate (c10)	0.71	30.49	10.77	
Glucose monodecanoate (c10)	1.5	25.5	10.77	Hollenbach et al. (2020)
Lactose caprate (c10)	2.5	40.6	14.8	Lee et al. (2018); Lucarini et al. (2018)
Lactose laurate (c12)	0.55	40.4	14.1	
Sucrose Laurate (c12)	1.2	19.7	8.19	Ye et al. (2016)
Sucrose oleate (c18)	0.0345	29.6	10.1	
Tween 80	0.01	38	15	
α-D-Glucose laurate (c12)	0.13	41.2	3.8	Garofalakis et al. (2000)
α-D-Maltose laurate (c12)	0.12	35.9	4.5	
Lactose tetradecanoate (c14)	0.041	38.6	4.3	
Sucrose monooctanoate (c8) SM- 800 ®	6	28.7	15.8	
Sucrose monooctanoate (c10) SM- 1000 ®	0.57	32.9	–	
Sucrose monooctanoate (c12) SM- 1200 ®	0.29	33.5	–	

Emulsion stability

Basing on a series of 5-min films and images taken up to 48 h of water/oil systems containing different concentrations of the tested SFAEs, it was not possible to measure the thickness of the emulsion layer and thus determine the stability index of the emulsion (Supplementary Figure S2). This was due to the short lifetime of the emulsion. However, depending on the type of ester, its concentration, and the composition of the oil phase, emulsion systems formed and maintained from several minutes to 1 hour (Table 3.). Emulsions containing squalene were less stable. W/O control systems containing no esters blurred after only a few minutes. On the other hand, systems containing SFAEs based on body care oil turned out to be more durable, as they had a diverse composition and contained co-surfactants such as alcohols. Furthermore, in most cases, differences in the durability and consistency of emulsions can be observed. They depend

on the concentration of SFAEs in aqueous solutions. The higher the SFAE concentration, the more stable and homogeneous the system was. Systems containing C9-glu and C9-gal proved to be the most stable. The least stable system contained C9-lac. Emulsions based on mPHN-glu and mPHN-gal esters proved to be less stable than those originated from nonanoic acid. In contrast, the emulsions containing mPHN-lac exhibited a higher persistence than mPHN-glu, mPHN-gal and C9-lac. The maximum lifetime of the investigated homogeneous emulsion systems (Table 3 emulsion quality assessment 3, Supplementary Figure S2) was 60 min. These were systems containing a commercial baby care oil. However, some remaining emulsions were visible and even more stable: 180 min for mPHN-glu, mPHN-gal and mPHN-lac to 1440 min for C9-glu, C9-gal, C9-lac. In W/O systems that contained squalane, after 60 min, the quality rating were 2 or 1, respectively. These lifetimes are definitely too short to make them competitive against other surfactants used in the industry, such
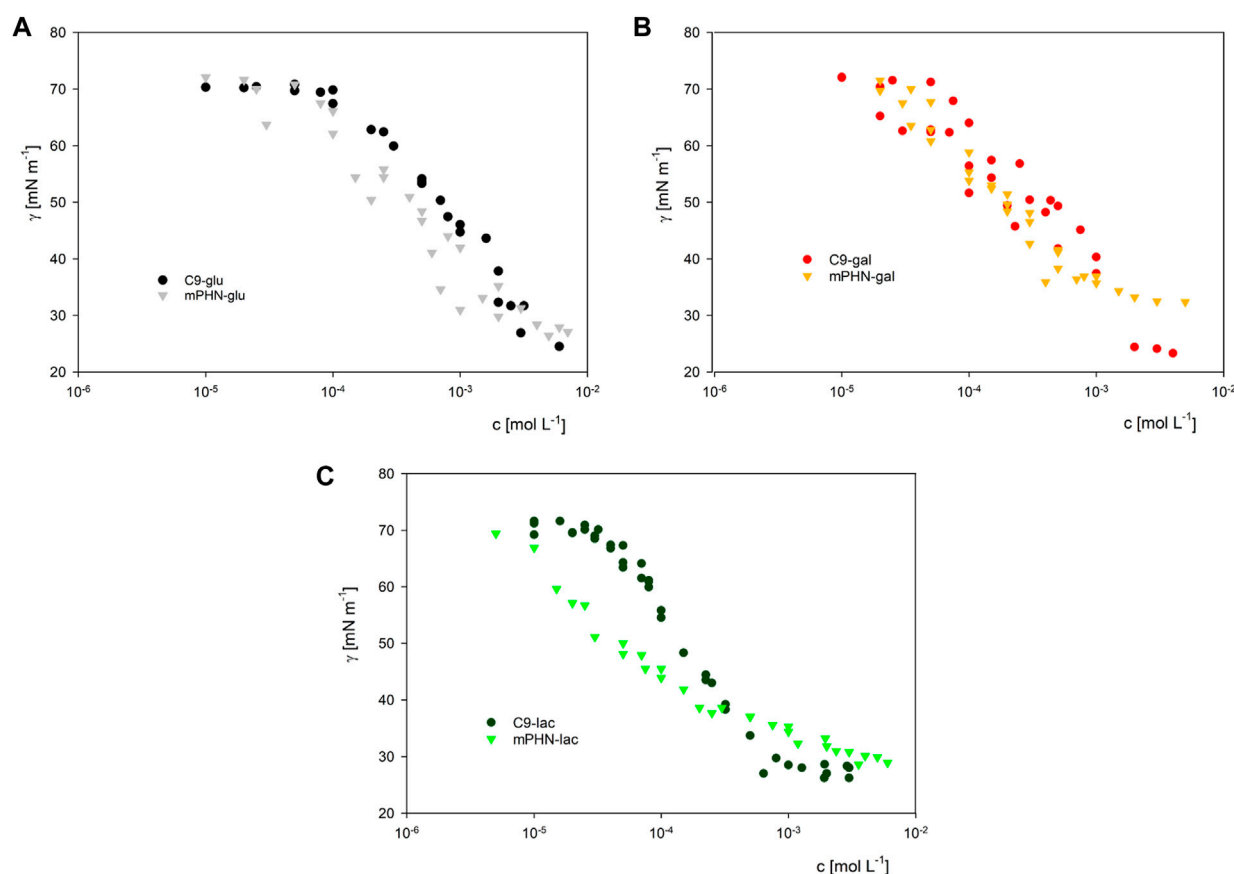
FIGURE 3
The comparison of surface activity of biocatalytically synthesized mPHN sugar esters with their aliphatic counterparts. Respectively for glucose (Panel A), galactose (Panel B) and lactose (Panel C) derivatives.

as Tween 80, Triton-X, Span 20, Span 60, polyethylene glycol (PEG). However, noteworthy is that commercially available products very often contain combinations of various surfactants e.g. Tween 80- polyoxoethylene sorbitan monooleate or Triton X-100-consisted of PEG and p-tert-octylphenol. Usually investigated W/O systems are based on combinations of two or more different ionic and/or nonionic surfactants and other co-surfactants i.e. alcohols and fatty acids, that make together the emulsions even more stable and extend their lifetime. (Watanabe et al., 2018). (Li and Friberg, 1982; McClements and Jafari, 2018). This approach should be investigated with our biocatalytically synthetized SFAE.

Although the expected lifetime of a commercially acceptable emulsion should be counted in days up to 1 month, the prepared here W/O systems did not perform well more than 24 h. We can explain this either by poor stabilizing properties of the SFAEs or their too-low concentrations used in preparation W/O systems, as well as lack of other co-surfactants. The calculated concentrations of the investigated surfactants present in the emulsions were between 0.001% and 1.0% m/v respectively (from 0.5 to 1.5 x CAC) while usually used concentrations of surfactants from the literature are between 0.1% and 5.0% m/v (Feng et al., 2022) but rarely calculated on their CAC or CMC values. That makes our system difficult to compare. Moreover, literature mentions several different techniques used for emulsion preparation i.e. shaking, ultrasound mixing, microwave pulsing, (Taha et al., 2020; Hyde et al., 2021), magnetic mixing, high pressure homogenization (Li and Xiang, 2019), and syringe mixing (Koursari et al., 2020). In recent years, even use of solid stabilizing

particles (Pickering emulsions) became more popular. Nanomaterials derived from natural sources are an interesting alternative or supplementary for this application. (Velásquez-Cock et al., 2021). In order to compare our surfactants for their feasibility in applications other than described below (drug delivery purposes), studies should be conducted in greater concentrations and with other additives.

The ideal W/O system used in the cosmetic or pharmaceutical industry should arise from natural sources, and also should be able to form stable and durable emulsions. Emulsions need to be stable enough to be stored at room temperature. Most importantly, they should be biodegradable and biocompatible. When it comes to drug delivery systems, their life time longer than 48–72 h is not advisable either. Another crucial factor is emulsion bioaccessibility. That means easy absorption by the epithelial surfaces, passing through cell membranes but not damaging them. (Production of green surfactants: Market prospects | Elsevier Enhanced Reader) The micelles protecting the structure of the drug from enzymes and/or pH changes should be able to release it gradually to the tissues. (Felzenszwalb et al., 2019). The micelle-building components ought to be easily degraded or removed from the body and easily decomposed in the environment. (Tovar-Sanchez et al., 2020) (Hunt, 2017) (Fagan and Portman, 2014). Undoubtedly, the studied SFAEs show some emulsion-stabilizing properties, but in order to give these W/O systems the desired longer lifespan, further optimization of SFAEs concentration, oil phase composition, mixing methods and addition of co-surfactants is required.

TABLE 3 Emulsion stability of two exemplary water/oil systems in time. Numbers-colors and their intensity is a scale referring to the intensity of a particular emulsion. Exemplary photos of the formed emulsions Supplementary Figure S2. a) Control- W/O systems with no SFAE addition b) squalene as oil phase with SFAEs as stabilizers c) baby care oil as an oil phase with SFAEs as stabilizers.

A

time [min]	Squalane	Olive
0	3	3
1	1	3
5	0	2
30	0	1
60	0	0
180	0	0
1440	0	0

B

N x CMC / time [min]	Control	C9-glu 0.5×CAC	C9-glu 1.0×CAC	C9-glu 1.5×CAC	C9-gal 0.5×CAC	C9-gal 1.0×CAC	C9-gal 1.5×CAC	C9-lac 0.5×CAC	C9-lac 1.0×CAC	C9-lac 1.5×CAC	mPHN-glu 0.5×CAC	mPHN-glu 1.0×CAC	mPHN-glu 1.5×CAC	mPHN-gal 0.5×CAC	mPHN-gal 1.0×CAC	mPHN-gal 1.5×CAC	mPHN-lac 0.5×CAC	mPHN-lac 1.0×CAC	mPHN-lac 1.5×CAC
0	3	3	3	3	3	3	3	1	1	1	3	3	3	3	3	3	3	3	3
1	1	3	3	3	3	3	3	1	1	1	2	3	3	3	3	3	3	3	3
5	0	1	2	2	2	3	2	1	1	1	2	3	3	2	3	3	2	3	3
30	0	1	2	2	2	2	2	0	0	0	1	2	2	1	2	2	1	2	2
60	0	0	1	2	2	2	2	0	0	0	0	1	1	0	1	1	0	1	1
180	0	0	1	1	1	1	1	0	0	0	0	1	1	0	1	1	0	1	1
1440	0	0	0	0	0	0	1	0	0	0	0	0	0	0	0	0	0	0	0

C

N x CMC / time [min]	Control	C9-glu 0.5×CAC	C9-glu 1.0×CAC	C9-glu 1.5×CAC	C9-gal 0.5×CAC	C9-gal 1.0×CAC	C9-gal 1.5×CAC	C9-lac 0.5×CAC	C9-lac 1.0×CAC	C9-lac 1.5×CAC	mPHN-glu 0.5×CAC	mPHN-glu 1.0×CAC	mPHN-glu 1.5×CAC	mPHN-gal 0.5×CAC	mPHN-gal 1.0×CAC	mPHN-gal 1.5×CAC	mPHN-lac 0.5×CAC	mPHN-lac 1.0×CAC	mPHN-lac 1.5×CAC
0	3	4	4	4	4	4	4	3	4	3	3	3	3	3	4	4	3	4	4
1	3	3	3	3	4	4	3	3	3	3	2	3	2	3	3	4	3	3	4
5	2	3	3	3	4	4	3	3	3	3	2	3	2	3	3	3	3	3	3
30	1	3	3	3	3	3	3	2	2	2	2	3	1	3	3	3	3	3	3
60	0	3	3	3	3	3	3	2	3	2	2	2	1	3	3	3	3	3	3
180	0	2	2	2	1	2	2	2	2	1	2	2	1	1	1	2	1	1	2
1440	0	1	2	2	2	2	2	2	2	1	0	0	0	0	1	1	0	1	1

(McCartney et al., 2019). The emulsion stabilizing properties of the investigated SFAE may not be spectacular, nevertheless sometimes desired if there is a need of administration of a less stable formulation to a patient prepared minutes prior injection/topical application. The used SFAE were already shown to exhibit anticancer properties, which increase their possibility to be applied in the medical industry (Tuvia et al., 2014).

Environmental impact of sugar fatty acid esters

Caenorhabditis elegans is a multicellular, non-parasitic model organism that is a valuable research object for testing the effects of various industrial chemicals such as anti-cancer drugs and antibiotics (Judy et al., 2019; Wittkowski et al., 2019). Every year, mankind supplies a huge amount of industrial wastewater and with it–surfactants (Production of green surfactants: Market prospects | Elsevier Enhanced Reader; Akbari et al., 2018; Felzenszwalb et al., 2019; Tovar-Sanchez et al., 2020). Therefore, there is a need for continuous monitoring of their impact on organisms living in soil and groundwaters (Ebele et al., 2017; Rathi et al., 2021). The usefulness of nematodes representatives is manifested in a fast life cycle, easy multiplication and obtaining a large number of individuals in subsequent generations, the possibility of long–term storage of larvae and eggs in laboratory conditions. They do not require continuous breeding, and the procedure for synchronizing the life cycles of individuals in a population is simple. In addition, *Caenorhabditis elegans* feed on an easily available source of food–bacteria *E. coli*. The most important from the human point of view, is the presence of simple organ systems: nervous (nerve ring), blood, protonfridial, gonads, and the ability to assess not only the size of the population under the microscope, but also the ability to actively move individuals in the population. Therefore, nematodes can be indirect

FIGURE 4
Toxicity of the sugar esters against *Caenorhabditis elegans* after 48 h exposure.
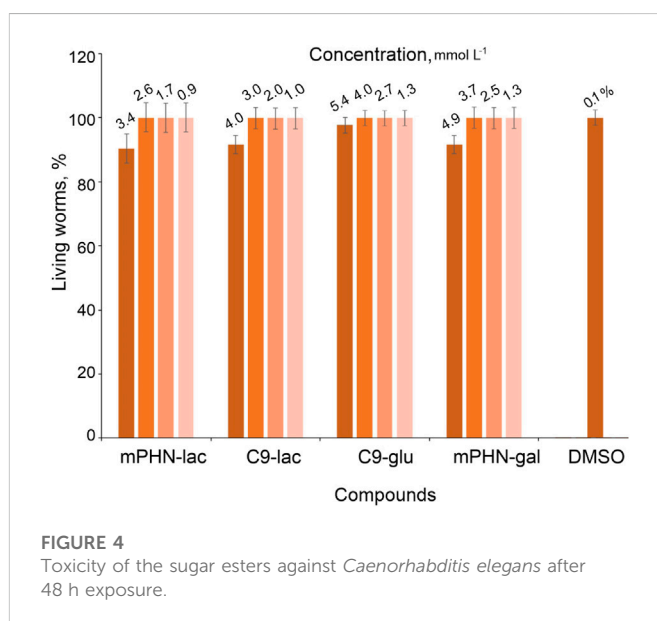
bioindicators of the influence of the tested substances on the natural environment (Fagan and Portman, 2014; Hunt, 2017). Having the above in mind, toxicity of the tested sugar esters against *Caenorhabditis elegans* was assessed by observing the nematodes under a microscope after 48 h of exposure. Based on the mobility of *Caenorhabditis elegans* their viability was assessed. Actively moving organisms were considered living, non-moving organisms were considered dead, and barely moving organisms were considered alive as well (having in mind, that the compounds could have a negative effect on worms) (Figure 4).

Observations of the nematodes allowed us to conclude that the obtained SFAEs do not pose a major threat to *Caenorhabditis elegans* at the given time of exposure. Only the highest concentrations

(2.0 mg ml^{-1}) of the mixtures reduced nematodes populations up to 15% but 1.5 mg ml^{-1} was already not effective. The concentrations of the esters per the well ranged from 0.0625 to 2.0 mg ml^{-1} which correspond to their molar concentrations of: C9-glu 0.186.14–5.69 mmol L^{-1}; C9-gal 0.162–5.312 mmol L^{-1}; C9-lac 0.125–4.0 mmol L^{-1}; mPHN-glu 0.142–4.544 mmol L^{-1}; mPHN-gal 0.148–4.744 mmol L^{-1}; mPHN-lac 0.119–3.816 mmol L^{-1}, respectively. We have previously reported that SFAE esters based on nonanoic acid and PHN monomers show anticancer potential. The reported consternations (IC$_{50}$) of these compounds that were found to be effective against certain cancer lines (In Search of Effective Anticancer Agents—Novel Sugar Esters Based on Polyhydroxyalkanoate Monomers-W. Snoch et al., 2021. pdf) are at the levels of being non-toxic to *Caenorhabditis elegans*. For example, the effective IC$_{50}$ for Du145 and HTB140 cell lines after 24 h exposures to all tested SFAE were below 0.25 mg ml^{-1} (i.e. IC$_{50}$ range respectively 0.09–1.5 mmol L^{-1}for cancer cells and 0.5–2.5 mmol L^{-1}, respectively for reference healthy cells).

Sugar esters belong to the group of non-ionic surfactants. The presence of a hydrophobic fatty acid tail and a hydrophilic sugar head give them an amphiphilic character. The chemical structure itself does not, in general, pose a direct threat to the entire organism of nematode. However, this amphiphilicity and the ability of compounds to lower the surface tension of solutions may permeabilize cell membranes (Tuvia et al., 2014; McCartney et al., 2019). On the other hand, the presence of long carbon chains (such as c18 steric acid) increases the solubility of individual compounds in water (e.g. in industrial wastewaters) (Vinarov et al., 2018). All this together causes the entry of undesirable substances from the environment into the cells, an increase in the concentration of H$^+$ ions, free oxygen radicals, herbicides, pesticides or salts (which can cause an osmotic shock), which in turn may direct the cells to the apoptotic pathway (Shao et al., 2018; Cavanagh et al., 2019; Appah et al., 2020; Liu et al., 2021; Martins-Gomes et al., 2022). In addition, the hydrophobic components of the SFAE tested do not exceed 9 carbon atoms, which may be another advantage compared to other commonly used esters based on acids with a chain length of c12, c16 or c18 (e.g. Span 20, Span 80, PEG 20– Sorbitan monolaurate (SPEG), Tween 20, Tween 80). Since increasing the chain length of the hydrophobic component also increases the toxicity of SFAE (Bunchongprasert and Shao, 2020). For comparison, the toxicity of other structurally similar allose-based esters to *Caenorhabditis elegans* with various carbon chain lengths n = 2, 4, 6, 8 was in the between 0.2 and 1.0 mmol L^{-1} (Sakoguchi et al., 2019).

In addition, every cosmetic or drug carrier potentially used in the industry must be thoroughly tested in terms of toxicology, before it goes to preclinical research (the smallest, largest harmful dose, and chronic administration of the compound), at every possible stage, not only cellular, but also more complex living organisms (Dent et al., 2018; Bopp et al., 2019). The highest tested levels of the SFAE (2.0 mg ml^{-1} around 6.0 mmol L^{-1}) that reduced *Caenorhabditis elegans* populations ~15% were near to CMC values. At the same time, the range of surfactants concentrations used in the water phase, to design model emulsion systems, were 0.5–10-fold CAC. Information obtained about minor negative effects of the esters on tested nematode in this concentration range opens the possibility for further application trials. However, it should be remembered that the SFAE molecules building micelles have a different concentration and organization than those dispersed in the buffers in which the *Caenorhabditis elegans* were used. They may behave differently and

show a different level of toxicity, therefore more detailed investigation is foreseen for the future (Khamkar, 2011; Kaur et al., 2016; Rusanov, 2018; Bunchongprasert and Shao, 2020).

Conclusion

The physicochemical properties of the obtained sugar esters were characterized which enabled their application potential evaluation. The obtained CAC and surface tension values correspond to compounds with a similar structure from the literature (such as SM-800, lactose caprate, or glucose monodecanoate). Also, the ability to create water–oil systems based on popular cosmetic ingredients, such as squalene and the commercial skincare oil confirmed application potential of the tested esters. However, the process of forming and testing these emulsions should be further optimized. It would be necessary to test a series of different oil components, as well as co-surfactants, in order to compare their emulsion stability indexes, size of the micelles formed and their behaviour.

In future prospective, it is worthy to focus on assessing the toxicity of not only the compounds themselves, but entire SFAEs based stable emulsion systems. Extending these experiments to such aspects as influence the of SFAE on increasing the vulnerability of *Caenorhabditis elegans* for these emulsion systems and repeat it in unfavourable water and soil conditions (presence of pesticides, inorganic salts, low pH, osmotically active substances). Even assessing susceptibility to opportunistic organisms would be valuable. From pharmaceutical and medical points of view, a key step is to answer questions about the mechanisms of the esters interaction with cells and/or model organisms, including the permeabilization of cells and intracellular membranes, and the ability to reversibly modulate endothelial electrical resistance (TEER), would be of great value. (Lucarini et al., 2018) Nematodes should be examined in more detail in terms of the impact of SFAE, and emulsion systems stabilized by them, on their internal organs, such as the endocrine and nervous systems, and also the ability to reproduce. (Ebele et al., 2017; Alfhili et al., 2018)

Data availability statement

The original contributions presented in the study are included in the article/Supplementary Material, further inquiries can be directed to the corresponding author.

Author contributions

WS—synthesis of PHN polymer, production of its monomers, synthesis, purification, determination of all SFAE in the analytical (UHPLC-MS) and preparative quantity, carrying out some of the toxicity experiments on *Caenorhabditis elegans*, surface tensions measurements, pH, emulsion stability measurements, coordination of the team's work, preparation a draft of the manuscript, applying corrections, editing Figure 1, Figure 4 and all tables. EJ—Infrared spectra confirming structures of the SFAE, measurements of surface tensions, emulsion stability measurements, edition and understanding of surface tension results and determination of equilibrium tensions, kinetics, CAC, Figure 2 and Figure 3, writing a part of the discussion. DM—major toxicity experiments performed on *Caenorhabditis elegans*

JNR—content consultation, editing Figure 4, introducing corrections to the manuscript, editing a part of the discussion. MG—setting up the research topic, introducing corrections to the manuscript, coordination of the team's work, communication in the team. All authors have approved for the publication.

Funding

Acknowledgments

Conflict of interest

The authors declare that the research was conducted in the absence of any commercial or financial relationships that could be construed as a potential conflict of interest.

Publisher's note

All claims expressed in this article are solely those of the authors and do not necessarily represent those of their affiliated organizations, or those of the publisher, the editors and the reviewers. Any product that may be evaluated in this article, or claim that may be made by its manufacturer, is not guaranteed or endorsed by the publisher.

Supplementary material

The Supplementary Material for this article can be found online at: https://www.frontiersin.org/articles/10.3389/fbioe.2023.1112053/full#supplementary-material

References

Akbari, S., Abdurahman, N. H., Yunus, R. M., Fayaz, F., and Alara, O. R. (2018). Biosurfactants—a new frontier for social and environmental safety: A mini review. *Biotechnol. Res. Innov.* 2, 81–90. doi:10.1016/j.biori.2018.09.001

Alfhili, M. A., Yoon, D. S., Faten, T. A., Francis, J. A., Cha, D. S., Zhang, B., et al. (2018). Non-ionic surfactants antagonize toxicity of potential phenolic endocrine-disrupting chemicals, including triclosan, in *C. elegans*. *Mol. Cells* 41, 1052–1060. doi:10.14348/molcells.2018.0378

Ali, A., and El-Ashry, R. (2021). Potential effect of the nematicide oxamyl and surfactant combinations on root-knot nematode *Meloidogyne incognita* infecting tomato plants. *Egypt. Acad. J. Biol. Sci. F. Toxicol. Pest Control* 13, 159–176. doi:10.21608/eajbsf.2021.153353

An, D., Zhang, X., Liang, F., Xian, M., Feng, D., and Ye, Z. (2019). Synthesis, surface properties of glucosyl esters from renewable materials for use as biosurfactants. *Colloids Surfaces A Physicochem. Eng. Asp.* 577, 257–264. doi:10.1016/j.colsurfa.2019.05.079

Ansorge-Schumacher, M. B., and Thum, O. (2013). Immobilised lipases in the cosmetics industry. *Chem. Soc. Rev.* 42, 6475–6490. doi:10.1039/c3cs35484a

Appah, S., Jia, W., Ou, M., Wang, P., and Asante, E. A. (2020). Analysis of potential impaction and phytotoxicity of surfactant-plant surface interaction in pesticide application. *Crop Prot.* 127, 104961. doi:10.1016/j.cropro.2019.104961

Blanc, L. (2015). What drives EU exports of pharmaceuticals? Available at: http://www.efpia.eu/uploads/Modules/Documents/the-pharmaceutical-industry-in-a-global-economy-_-what-drives-eu-exports-of-pharmaceuticals-overseas-2.pdf%5Cnhttps://www.coleurope.eu/sites/default/files/research-paper/beer31.pdf.

Bopp, S. K., Kienzler, A., Richarz, A. N., van der Linden, S. C., Paini, A., Parissis, N., et al. (2019). Regulatory assessment and risk management of chemical mixtures: Challenges and ways forward. *Crit. Rev. Toxicol.* 49, 174–189. doi:10.1080/10408444.2019.1579169

Bunchongprasert, K., and Shao, J. (2020). Effect of fatty acid ester structure on cytotoxicity of self-emulsified nanoemulsion and transport of nanoemulsion droplets. *Colloids Surfaces B Biointerfaces* 194, 111220. doi:10.1016/j.colsurfb.2020.111220

Cavanagh, R. J., Smith, P. A., and Stolnik, S. (2019). Exposure to a nonionic surfactant induces a response akin to heat-shock apoptosis in intestinal epithelial cells: Implications for excipients safety. *Mol. Pharm.* 16, 618–631. doi:10.1021/acs.molpharmaceut.8b00934

Dent, M., Amaral, R. T., Da Silva, P. A., Ansell, J., Boisleve, F., Hatao, M., et al. (2018). Principles underpinning the use of new methodologies in the risk assessment of cosmetic ingredients. *Comput. Toxicol.* 7, 20–26. doi:10.1016/j.comtox.2018.06.001

Dini, I., and Laneri, S. (2021). The new challenge of green cosmetics: Natural food ingredients for cosmetic formulations. *Molecules* 26, 3921. doi:10.3390/molecules26133921

Djapovic, M., Milivojevic, D., Ilic-Tomic, T., Lješević, M., Nikolaivits, E., Topakas, E., et al. (2021). Synthesis and characterization of polyethylene terephthalate (PET) precursors and potential degradation products: Toxicity study and application in discovery of novel PETases. *Chemosphere* 275, 130005. doi:10.1016/j.chemosphere.2021.130005

Ebele, A. J., Abou-Elwafa Abdallah, M., and Harrad, S. (2017). Pharmaceuticals and personal care products (PPCPs) in the freshwater aquatic environment. *Emerg. Contam.* 3, 1–16. doi:10.1016/j.emcon.2016.12.004

Fabbron-Appas, C. T., Pandey, P., Parekh, H. S., Sales, C. C., Duque, M. D., Andréo-Filho, N., et al. (2021). Impact of different emollient esters on body emulsions: Sensory, physicochemical, and biometrological characterization. *J. Sens. Stud.* 36. doi:10.1111/joss.12660

Fagan, K. A., and Portman, D. S. (2014). Sexual modulation of neural circuits and behavior in *C. elegans*. *Semin. Cell Dev. Biol.* 33, 3–9. doi:10.1016/j.semcdb.2014.06.007

Farias, C. B. B., Almeida, F. C. G., Silva, I. A., Souza, T. C., Meira, H. M., and Soares da Silva, R. de C. F. (2021). Production of green surfactants: Market prospects. *Electron. J. Biotechnol.* 51, 28–39. doi:10.1016/j.ejbt.2021.02.002

Felzenszwalb, I., Fernandes, A. da S., Brito, L. B., Oliveira, G. A. R., Silva, P. A. S., Arcanjo, M. E., et al. (2019). Toxicological evaluation of nail polish waste discarded in the environment. *Environ. Sci. Pollut. Res.* 26, 27590–27603. doi:10.1007/s11356-018-1880-y

Feng, J., Valkova, Z., Lin, E. E., Nourafkan, E., Wang, T., Tcholakova, S., et al. (2022). Minimum surfactant concentration required for inducing self-shaping of oil droplets and competitive adsorption effects. *Soft Mat.* 18, 6729–6738. doi:10.1039/d1sm01326b

Garofalakis, G., Murray, B. S., and Sarney, D. B. (2000). Surface activity and critical aggregation concentration of pure sugar esters with different sugar headgroups. *J. Colloid Interface Sci.* 229, 391–398. doi:10.1006/jcis.2000.7035

Gaudin, T., Lu, H., Fayet, G., Berthauld-Drelich, A., Rotureau, P., Pourceau, G., et al. (2019). Impact of the chemical structure on amphiphilic properties of sugar-based surfactants: A literature overview. *Adv. Colloid Interface Sci.* 270, 87–100. doi:10.1016/j.cis.2019.06.003

Griffin, W. C. (1954). Calculation of HLB values of non-ionic surfactants. *J. Soc. Cosmet. Chem.* 1, 311–326. doi:10.1002/jps.2600581203

Hill, K., and Rhode, O. (1999). Sugar-based surfactants for consumer products and technical applications. *Lipid - Fett* 101, 25–33. doi:10.1002/(SICI)1521-4133(19991)101:1<25::AID-LIPI25>3.0.CO;2-N

Hollenbach, R., Völp, A. R., Höfert, L., Rudat, J., Ochsenreither, K., Willenbacher, N., et al. (2020). Interfacial and foaming properties of tailor-made glycolipids—influence of the hydrophilic head group and functional groups in the hydrophobic tail. *Molecules* 25, 3797. doi:10.3390/molecules25173797

Hunt, P. R. (2017). The *Caenorhabditis elegans* model in toxicity testing. *J. Appl. Toxicol.* 37, 50–59. doi:10.1002/jat.3357

Hyde, A., Saiuchi, K., Sonobe, S., Shibata, Y., Asakuma, Y., and Phan, C. (2021). Influence of microwave pulsing patterns on oil/water interfacial behavior. *Colloids Surf. A Physicochem Eng. Asp.* 631, 127660. doi:10.1016/j.colsurfa.2021.127660

Judy, J. D., Williams, M., Gregg, A., Oliver, D., Kumar, A., Kookana, R., et al. (2019). Microplastics in municipal mixed-waste organic outputs induce minimal short to long-term toxicity in key terrestrial biota. *Environ. Pollut.* 252, 522–531. doi:10.1016/j.envpol.2019.05.027

Kairaliyeva, T., Aksenenko, E. V., Mucic, N., Makievski, A. V., Fainerman, V. B., and Miller, R. (2017). Surface tension and adsorption studies by drop profile analysis tensiometry. *J. Surfactants Deterg.* 20, 1225–1241. doi:10.1007/s11743-017-2016-y

Kaur, P., Garg, T., Rath, G., Murthy, R. S. R., and Goyal, A. K. (2016). Surfactant-based drug delivery systems for treating drug-resistant lung cancer. *Drug Deliv.* 23, 717–728. doi:10.3109/10717544.2014.935530

Khamkar, G. S. (2011). Self Micro Emulsifying Drug Delivery System (SMEED) o/w microemulsion for BCS class II drugs: An approach to enhance an oral bioavailability. *Int. J. Pharm. Pharm. Sci.* 3, 1–3.

Khan, N. R., and Rathod, V. K. (2015). Enzyme catalyzed synthesis of cosmetic esters and its intensification: A review. *Process Biochem.* 50, 1793–1806. doi:10.1016/j.procbio.2015.07.014

Koursari, N., Johnson, P., Parsa, M., Schneider, M., Trybala, A., and Starova, V. M. (2020). Modelling of foamed emulsion drainage. *Colloids Surf. A Physicochem. Eng. Asp.* 600, 124915. doi:10.1016/j.colsurfa.2020.124915

Kumar, S. (2005). Exploratory analysis of global cosmetic industry: Major players, technology and market trends. *Technovation* 25, 1263–1272. doi:10.1016/j.technovation.2004.07.003

Lanzerstorfer, P., Sandner, G., Pitsch, J., Mascher, B., Aumiller, T., and Weghuber, J. (2021). Acute, reproductive, and developmental toxicity of essential oils assessed with alternative *in vitro* and *in vivo* systems. *Arch. Toxicol.* 95, 673–691. doi:10.1007/s00204-020-02945-6

Larsson, J., Sanchez-Fernandez, A., Mahmoudi, N., Barnsley, L. C., Wahlgren, M., Nylander, T., et al. (2019). Effect of the anomeric configuration on the micellization of hexadecylmaltoside surfactants. *Langmuir* 35, 13904–13914. doi:10.1021/acs.langmuir.9b01960

Lee, S.-M., Wagh, A., Sandhu, G., and Walsh, M. K. (2018). Emulsification properties of lactose fatty acid esters. *Food Nutr. Sci.* 09, 1341–1357. doi:10.4236/fns.2018.912096

Lémery, E., Briançon, S., Chevalier, Y., Bordes, C., Oddos, T., Gohier, A., et al. (2015). Skin toxicity of surfactants: Structure/toxicity relationships. *Colloids Surfaces A Physicochem. Eng. Asp.* 469, 166–179. doi:10.1016/j.colsurfa.2015.01.019

Li, G.-Z., and Friberg, S. E. (1982). Surfactant/cosurfactant association and emulsion stability. *J. Am. Oil Chem. Soc.* 59, 569–572. doi:10.1007/BF02636326

Li, Y., and Xiang, D. (2019). Stability of oil-in-water emulsions performed by ultrasound power or high-pressure homogenization. *PLoS One* 14, 02131899–e213214. doi:10.1371/journal.pone.0213189

Liu, B., Fan, Y., Li, H., Zhao, W., Luo, S., Wang, H., et al. (2021). Control the entire journey of pesticide application on superhydrophobic plant surface by dynamic covalent trimeric surfactant coacervation. *Adv. Funct. Mat.* 31, 2006606. doi:10.1002/adfm.202006606

Łopaciuk, A., and Łoboda, M. (2013). "Global beauty industry trends in the 21st century," in Knowl. Manag. Innov. Knowl. Learn., Zadar, Croatia, 19-21 June 2013, 1079–1087.

Lucarini, S., Fagioli, L., Campana, R., Cole, H., Duranti, A., Baffone, W., et al. (2016). Unsaturated fatty acids lactose esters: Cytotoxicity, permeability enhancement and antimicrobial activity. *Eur. J. Pharm. Biopharm.* 107, 88–96. doi:10.1016/j.ejpb.2016.06.022

Lucarini, S., Fagioli, L., Cavanagh, R., Liang, W., Perinelli, D. R., Campana, M., et al. (2018). Synthesis, structure–activity relationships and *in vitro* toxicity profile of lactose-based fatty acid monoesters as possible drug permeability enhancers. *Pharmaceutics* 10, 81–18. doi:10.3390/pharmaceutics10030081

Martins-Gomes, C., Silva, T. L., Andreani, T., and Silva, A. M. (2022). Glyphosate vs. Glyphosate-based herbicides exposure: A review on their toxicity. *J. Xenobiotics* 12, 21–40. doi:10.3390/jox12010003

Masen, M. (2020). Evaluating lubricant performance to reduce COVID-19 PPE-related skin injury. *PLoS One* 15 (9), e0239363. doi:10.1371/journal.pone.0239363

McCartney, F., Rosa, M., and Brayden, D. J. (2019). Evaluation of sucrose laurate as an intestinal permeation enhancer for macromolecules: *Ex vivo* and *in vivo* studies. *Pharmaceutics* 11, 565. doi:10.3390/pharmaceutics11110565

McClements, D. J., and Jafari, S. M. (2018). Improving emulsion formation, stability and performance using mixed emulsifiers: A review. *Adv. Colloid Interface Sci.* 251, 55–79. doi:10.1016/j.cis.2017.12.001

Nilsson, F., and So, O. (1998). Physical - chemical properties of C 9 G 1 and C 10 G 1 - alkylglucosides. *Phase Diagrams Aggreg. Size/Struct.* 7463, 4050–4058.

Nilsson, F., Söderman, O., and Johansson, I. (1998). Four different C8G1 alkylglucosides. Anomeric effects and the influence of straight vs branched hydrocarbon chains. *J. Colloid Interface Sci.* 203, 131–139. doi:10.1006/jcis.1998.5487

Pappalardo, V. M., Boeriu, C. G., Zaccheria, F., and Ravasio, N. (2017). Synthesis and characterization of arabinose-palmitic acid esters by enzymatic esterification. *Mol. Catal.* 433, 383–390. doi:10.1016/j.mcat.2017.02.029

Para, G., Jarek, E., and Warszynski, P. (2006). The Hofmeister series effect in adsorption of cationic surfactants-theoretical description and experimental results. *Adv. Colloid Interface Sci.* 122, 39–55. doi:10.1016/j.cis.2006.06.017

Patruno, C., Fabbrocini, G., Stingeni, L., and Napolitano, M. (2020). The role of occupational dermatology in the COVID-19 outbreak. *Contact Dermat.* 83, 174–175. doi:10.1111/cod.13568

Pe, B., Anankanbil, S., and Guo, Z. (2017). Synthesis of sugar fatty acid esters and their industrial utilizations. *Fat. Acids* 2017, 329–354. doi:10.1016/B978-0-12-809521-8.00010-6

Place, M. (2020). *In vivo* eco-toxicological assessment of some cationic and amphoteric surfactants in transgenic *Caenorhabditis elegans* CICÎRMA Marius 1,2*. POMERAI David 3 25, 19–32.

Rathi, B. S., Kumar, P. S., and Vo, D. V. N. (2021). Critical review on hazardous pollutants in water environment: Occurrence, monitoring, fate, removal technologies and risk assessment. *Sci. Total Environ.* 797, 149134. doi:10.1016/j.scitotenv.2021.149134

Riecan, M., Paluchova, V., Lopes, M., Brejchova, K., and Kuda, O. (2022). Branched and linear fatty acid esters of hydroxy fatty acids (FAHFA) relevant to human health. *Pharmacol. Ther.* 231, 107972. doi:10.1016/j.pharmthera.2021.107972

Rusanov, A. I. (2018). Theory of surfactant diffusion in micellar systems with variable aggregation numbers. *Colloids Surfaces A Physicochem. Eng. Asp.* 551, 158–164. doi:10.1016/j.colsurfa.2018.04.065

Sakoguchi, H., Shintani, T., Ishiyama, H., Yanagita, R. C., Kawanami, Y., and Sato, M. (2019). Nematocidal activity of 6-O-octanoyl- and 6-O-octyl-D-allose against larvae of *C. elegans. Biosci. Biotechnol. Biochem.* 83, 2194–2197. doi:10.1080/09168451.2019.1648206

Shao, S., Shi, Y., Wu, Y., Bian, L., and Zhu, Y. (2018). Lipase-Catalyzed synthesis of sucrose monolaurate and its antibacterial property and mode of action. *Molecules* 23 (5), 1118. doi:10.3390/molecules23051118

Sharma, S., and Sarangdevot, K. (2012). Nanoemulsions for cosmetics. *IJARPB* 2, 408–415.

Snoch, W., Wnuk, D., Witko, T., Staroń, J., Bojarski, A. J., Jarek, E., et al. (2021). In Search of effective anticancer agents—novel sugar esters based on polyhydroxyalkanoate monomers. *Int. J. Mol. Sci.* 22 (13), 7238. doi:10.3390/ijms22137238

Snoch, W., Stępień, K., Prajsnar, J., Staroń, J., Szaleniec, M., and Guzik, M. (2019). Influence of chemical modifications of polyhydroxyalkanoate-derived fatty acids on their antimicrobial properties. *Catalysts* 9, 510. doi:10.3390/catal9060510

Staroń, J., Dąbrowski, J. M., Cichoń, E., and Guzik, M. (2018). Lactose esters: Synthesis and biotechnological applications. *Crit. Rev. Biotechnol.* 38, 245–258. doi:10.1080/07388551.2017.1332571

Steinbüchel, A., and Steinbüchel, A. (1995). Diversity of bacterial polyhydroxyalkanoic acids. *FEMS Microbiol. Lett.* 128, 219–228. doi:10.1016/0378-1097(95)00125-O

Stiernagle, T. (2006). Maintenance of *Caenorhabditis elegans. WormBook* 2006, 1–11. doi:10.1895/wormbook.1.101.1

Tang, L., Zhang, Y., Li, C., Zhou, Z., Nie, X., Chen, Y., et al. (2022). Biological stability of water-based cutting fluids: Progress and application. *Chin. J. Mech. Eng.* 35, 3. doi:10.1186/s10033-021-00667-z

Taha, A., Ahmed, E., Ismaiel, A., Ashokkumar, M., Xua, X., Pana, S., et al. (2020). Ultrasonic emulsification: An overview on the preparation of different emulsifiers-stabilized emulsions. *Trends Food Sci. Technol.* 105, 363–377. doi:10.1016/j.tifs.2020.09.024

Tortilla, G., Market, C., Chips, T., Size, M., Distribution, B., Forecasts, S., et al. (2019). Report coverage & deliverables key companies & market share insights. 1–6.

Tovar-Sanchez, A., Sparaventi, E., Gaudron, A., and Rodriguez-Romero, A. (2020). A new approach for the determination of sunscreen levels in seawater by ultraviolet absorption spectrophotometry. *PLoS One* 15, e0243591. doi:10.1371/journal.pone.0243591

Tuvia, S., Pelled, D., Marom, K., Salama, P., Levin-Arama, M., Karmeli, I., et al. (2014). A novel suspension formulation enhances intestinal absorption of macromolecules via transient and reversible transport mechanisms. *Pharm. Res.* 31, 2010–2021. doi:10.1007/s11095-014-1303-9

van Kempen, S. E. H. J., Schols, H. A., van der Linden, E., and Sagis, L. M. C. (2014). Effect of variations in the fatty acid chain on functional properties of oligofructose fatty acid esters. *Food Hydrocoll.* 40, 22–29. doi:10.1016/j.foodhyd.2014.01.031

Van Kempen, S. E. H. J., Schols, H. A., Van Der Linden, E., and Sagis, L. M. C. (2013). The effect of diesters and lauric acid on rheological properties of air/water interfaces stabilized by oligofructose lauric acid monoesters. *J. Agric. Food Chem.* 61, 7829–7837. doi:10.1021/jf4018355

Velásquez-Cock, J., Serpa, A. M., Gomez-Hoyos, C., Ganan, P., Romero-Saez, M., Velez, L. M., et al. (2021). Influence of a non-ionic surfactant in the microstructure and rheology of a pickering emulsion stabilized by cellulose nanofibrils. *Polymers* 13 (21), 3625. doi:10.3390/polym13213625

Vinarov, Z., Katev, V., Radeva, D., Tcholakova, S., and Denkov, N. D. (2018). Micellar solubilization of poorly water-soluble drugs: Effect of surfactant and solubilizate molecular structure. *Drug Dev. Ind. Pharm.* 44, 677–686. doi:10.1080/03639045.2017.1408642

Watanabe, T., Kawai, T., and Nonomura, Y. (2018). Effects of fatty acid addition to oil-in-water emulsions stabilized with sucrose fatty acid ester. *J. Oleo. Sci.* 67 (3), 307–313. doi:10.5650/jos.ess17097

Wittkowski, P., Marx-Stoelting, P., Violet, N., Fetz, V., Schwarz, F., Oelgeschläger, M., et al. (2019). *Caenorhabditis elegans* as a promising alternative model for environmental chemical mixture effect assessment - a comparative study. *Environ. Sci. Technol.* 53, 12725–12733. doi:10.1021/acs.est.9b03266

Ye, R., Hayes, D. G., Burton, R., Liu, A., Harte, F. M., and Wang, Y. (2016). Solvent-free lipase-catalyzed synthesis of technical-grade sugar esters and evaluation of their physicochemical and bioactive properties. *Catalysts* 6, 78. doi:10.3390/catal6060078

Zhang, X., Wei, W., Cao, X., and Feng, F. (2015). Characterization of enzymatically prepared sugar medium-chain fatty acid monoesters. *J. Sci. Food Agric.* 95, 1631–1637. doi:10.1002/jsfa.6863

Zhou, Z. H., Zhang, Q., Liu, Y., Wang, H. Z., Cai, H. Y., Zhang, F., et al. (2014). Effect of fatty acids on interfacial tensions of novel sulfobetaines solutions. *Energy Fuels* 28, 1020–1027. doi:10.1021/ef402416j

Exploring Class I polyhydroxyalkanoate synthases with broad substrate specificity for polymerization of structurally diverse monomer units

Ramamoorthi M Sivashankari[1], Maierwufu Mierzati[1], Yuki Miyahara[1], Shoji Mizuno[1], Christopher T. Nomura[2], Seiichi Taguchi[3], Hideki Abe[4] and Takeharu Tsuge[1]*

[1]Department of Materials Science and Engineering, Tokyo Institute of Technology, Yokohama, Japan, [2]Department of Biological Sciences, College of Science, University of Idaho, Moscow, ID, United States, [3]Graduate School of Science, Technology and Innovation, Kobe University, Kobe, Japan, [4]Bioplastic Research Team, RIKEN Center for Sustainable Resource Science, Wako, Japan

Polyhydroxyalkanoate (PHA) synthases (PhaCs) are key enzymes in PHA polymerization. PhaCs with broad substrate specificity are attractive for synthesizing structurally diverse PHAs. In the PHA family, 3-hydroxybutyrate (3HB)-based copolymers are industrially produced using Class I PhaCs and can be used as practical biodegradable thermoplastics. However, Class I PhaCs with broad substrate specificities are scarce, prompting our search for novel PhaCs. In this study, four new PhaCs from the bacteria *Ferrimonas marina*, *Plesiomonas shigelloides*, *Shewanella pealeana*, and *Vibrio metschnikovii* were selected *via* a homology search against the GenBank database, using the amino acid sequence of *Aeromonas caviae* PHA synthase (PhaC$_{Ac}$), a Class I enzyme with a wide range of substrate specificities, as a template. The four PhaCs were characterized in terms of their polymerization ability and substrate specificity, using *Escherichia coli* as a host for PHA production. All the new PhaCs were able to synthesize P(3HB) in *E. coli* with a high molecular weight, surpassing PhaC$_{Ac}$. The substrate specificity of PhaCs was evaluated by synthesizing 3HB-based copolymers with 3-hydroxyhexanoate, 3-hydroxy-4-methylvalerate, 3-hydroxy-2-methylbutyrate, and 3-hydroxypivalate monomers. Interestingly, PhaC from *P. shigelloides* (PhaC$_{Ps}$) exhibited relatively broad substrate specificity. PhaC$_{Ps}$ was further engineered through site-directed mutagenesis, and the variant resulted in an enzyme with improved polymerization ability and substrate specificity.

KEYWORDS

PHA synthases, broad substrate specificities, molecular weight, blast, copolymer

Introduction

The bacterial polyesters polyhydroxyalkanoates (PHAs) are considered excellent bio-based plastics and have been demonstrated to be biodegradable in various environments such as compost, soil, freshwater, and marine water (Suzuki et al., 2021). A myriad of microorganisms can synthesize PHA as an intracellular carbon and energy reserve under stressful conditions (Anderson and Dawes, 1990). Poly[(R)-3-hydroxybutyrate], P(3HB), is a

major member of the PHA family and has been extensively studied since its discovery in 1926 (Lenz and Marchessault, 2005). Despite these merits, it is still challenging for PHA to compete with petroleum-based plastics because of the inherent flaws in P(3HB). The poor material properties of P(3HB) (Lehrle and Williams, 1994) such as its high crystallinity and narrow processing temperature window have greatly hampered the entry of this polymer into the commercial world. Fortunately, 3HB-based copolymers (Tsuge et al., 2005; Mizuno et al., 2010; Mierzati et al., 2020; Furutate et al., 2021) have been proven to overcome the material property limitations of P(3HB) to a certain extent, and have been used as a remedy for problems related to plastics (Sivashankari and Tsuge, 2021).

PHA synthases are key enzymes involved in PHA polymerization (Sudesh et al., 2000). Based on the substrate specificities and subunit compositions of PHA synthases, they are categorized into four classes (Rehm, 2003). Class I and II PHA synthases are homodimers of the PhaC subunits. Class I PHA synthases, represented by the *Ralstonia eutropha* enzyme, mainly polymerize short chain length (scl)-monomers (C3-C5), whereas Class II PHA synthases, represented by the *Pseudomonas aeruginosa* and *Pseudomonas putida* enzymes, polymerize medium chain length (mcl)-monomers (C6-C14). Class III PHA synthases such as *Allochromatium vinosum* and *Synechocystis* sp. PCC 6803 consists of two heterosubunits (PhaC and PhaE). Class IV PHA synthases, represented by *Bacillus megaterium* and *Bacillus cereus*, are similar to Class III PHA synthases and possess two subunits (PhaC and PhaR). Similar to Class I synthases, Class III and IV PHA synthases preferentially polymerize scl-monomers (C3-C5).

PhaCs with broad substrate specificities are attractive biocatalysts for PHA synthesis because they can naturally copolymerize different monomers to produce polymers with desirable physical properties. PhaC from *Aeromonas caviae* (PhaC$_{Ac}$) can naturally synthesize poly(3HB-*co*-3-hydroxyhexanoate) [P(3HB-*co*-3HHx)] from vegetable oils and fatty acids (Kobayashi et al., 1994; Shimamura et al., 1994; Doi et al., 1995; Tsuge et al., 2007a; Tsuge, 2016), distinguishing it from other Class I PhaCs because it exhibits polymerization activities toward 3HB monomers and mcl 3HHx monomers (Kobayashi et al., 1994). Therefore, PhaC$_{Ac}$ is a marketable biocatalyst to produce P(3HB-*co*-3HHx) copolymers. The potential of PhaC$_{Ac}$ has been fortified through evolutionary engineering with the development of the PhaC$_{Ac}$NSDG variant (Tsuge et al., 2007b). The PhaC$_{Ac}$NSDG variant has amino acid substitutions of asparagine 149 by serine (N149S) and aspartate 171 by glycine (D171G) and was shown to have the ability to synthesize the P(3HB-*co*-3HHx) copolymer with an enhanced 3HHx fraction compared to the wild-type enzyme, as well as recognize and incorporate other monomer units, such as 3-hydroxy-4-methylvalerate (3H4MV) (Tanadchangsaeng et al., 2009) and 3-hydroxy-2-methylbutyrate (3H2MB) (Watanabe et al., 2015). In addition, the molecular weight of P(3HB) synthesized by PhaC$_{Ac}$NSDG was higher than that of the wild-type enzyme (Tsuge et al., 2007b). These properties of PhaC$_{Ac}$NSDG variant are desirable for the development of PHA as an industrial biomaterial, making it a promising biocatalyst.

The partial crystal structures for several PhaCs have been solved (Wittenborn et al., 2016; Chek et al., 2017; Kim et al., 2017; Chek et al., 2020). The differences in the catalytic properties of these enzymes can be possibly due to their different structures (Chek et al., 2019). Although the crystal structure of PhaC$_{Ac}$ has not yet been solved, a basic understanding of the enzymatic capability of PhaC$_{Ac}$ could be elucidated using *in silico* homology modeling (Harada et al., 2021). Additionally, the use of structural information, namely the comparison of the amino acid residues that constitute the substrate-binding pocket of PhaCs, led to the generation of further engineered PhaC$_{Ac}$s (Harada et al., 2021).

PhaC$_{Ac}$ and its PhaC$_{Ac}$NSDG variant are biocatalysts that produce PHA polymers with desirable material properties; however, the number of other naturally occurring PhaCs with broad substrate specificities are limited, hindering the development and commercial mass production of desirable PHAs. Thus, it is necessary to identify other novel PhaCs with broad substrate specificities to enable industrial-scale production of PHA copolymers to completely replace petroleum-based plastics. PhaCs, which can synthesize high-molecular-weight PHA, is essential to produce PHA as practical materials. The currently available PhaC$_{Ac}$ is highly sensitive to ethanol (Hiroe et al., 2015), which is a metabolite of some bacteria, including *Escherichia coli,* and functions as a chain transfer agent to terminate polymerization reactions (Tsuge, 2016), resulting in the synthesis of relatively low-molecular-weight PHA when using *E. coli* as a production host. These low-molecular-weight PHA polymers have less desirable physical properties than their high-molecular-weight counterparts. Despite the unique ability of PhaC$_{Ac}$ to polymerize various monomers, the relatively low molecular weight of PHA produced in recombinant *E. coli* using this enzyme has room for improvement.

In this study, to explore novel PhaCs with high polymerization ability and broad substrate specificity, four new PhaCs were identified by a bioinformatics approach using the PhaC$_{Ac}$ amino acid sequence as a template for a basic local alignment search tool (BLAST) and included PhaCs from the bacteria *Ferrimonas marina, Plesiomonas shigelloides*, *Shewanella pealeana*, and *Vibrio metschnikovii*. PhaC proteins were individually expressed in *E. coli* LSBJ to synthesize P(3HB) and 3HB-based copolymers containing 3HHx, 3H4MV, 3H2MB, and 3-hydroxypivalate (3HPi) units. Furthermore, the effects of mutagenesis on polymerization activity and substrate specificity in the highest-performing PhaC enzyme were investigated.

Materials and methods

Bioinformatic analysis

A BLAST-protein (BLASTP) search was performed against the protein sub-sections of the National Center for Biotechnology Information (NCBI) and DNA Data Bank of Japan (DDBJ) databases using the PhaC$_{Ac}$ amino sequence as a template (Accession No. BAA21815) (Altschul et al., 1990). PhaCs with more than 85% similarity index and an identity index of 50%–60% in the BLASTP search were targeted as potential PhaCs with broad substrate specificities. Among the various PhaCs from different organisms that satisfied the criteria in the BLASTP search, four PhaCs were selected based on the diversity of the N-terminal region for further evaluation. Phylogenetic analyses

were performed using the maximum likelihood method in MEGA11 (Tamura et al., 2021) and the protein sequences were aligned using ClustalW. This analysis involved six amino acid sequences: PhaC$_{Ac}$, four newly selected PhaCs from BLASTP, and PhaC from *Ralstonia eutropha* (WP_011615085) as an outgroup.

Bacterial strain and plasmid

Four PhaC amino acid sequences were chosen based on the BLASTP search results. These *phaC* genes were chemically synthesized with optimized codon usage in *E. coli* by Eurofins Genomics Co. Ltd. (Tokyo, Japan) for plasmid construction and evaluation. *E. coli* LSBJ, a *fadB fadJ* double-deletion strain of *E. coli* LS5218 [*fadR601*, *atoC* (Con)] (Tappel et al., 2012a), was used as the host strain for PHA biosynthesis. This strain is an ideal host for non-native PHA production because of its ability to take up a wide variety of substrates to be incorporated into PHA homo- and copolymers, and bench-level scale-up methodologies available for overall production (Tappel et al., 2012b; Levine et al., 2016; Pinto et al., 2016; Fadzil et al., 2018; Furutate et al., 2021; Scheel et al., 2021). A broad-host-range plasmid pBBR1MCS-2 (Kovach et al., 1995) harboring the genes encoding the PhaCs to be evaluated, the *lac* promoter region, the (*R*)-specific enoyl-CoA hydratase gene from *A. caviae* (*phaJ$_{Ac}$*), the 3-ketothiolase gene (*phaA*) from *Ralstonia eutropha* H16, and the acetoacetyl-CoA reductase gene (*phaB*) from *R. eutropha* H16, termed pBBR1-phaCsAB$_{Re}$J$_{Ac}$, was used for the expression of PhaCs (Supplementary Figure S1). For *phaAB* expression, the *R. eutropha pha* promoter and terminator regions were located upstream and downstream of their genes, respectively. To enhance the supply of 3HHx, 3H4MV, and 3H2MB monomers, the plasmid pTTQ-PCT (Furutate et al., 2017) containing the propionyl-CoA transferase (PCT) gene from *Megasphaera elsdenii* (*pct*) (Taguchi et al., 2008) was introduced into the *E. coli* LSBJ strain (Supplementary Figure S1).

Cell culture conditions

Initially, recombinant *E. coli* LSBJ was incubated overnight at 37°C with reciprocal shaking (160 rpm) in a 50 mL baffle flask containing 20 mL of lysogeny broth (LB) medium as a seed culture. The LB medium contained 10 g/L Bacto-tryptone (Difco Laboratories, Detroit, MI, United States), 5 g/L Bacto-yeast extract (Difco Laboratories), and 10 g/L NaCl. For plasmid maintenance throughout the initial incubation period, 50 mg/L of kanamycin and 50 mg/L of carbenicillin were added.

Inoculations for PHA production were started with 5 mL of seed culture added to 500 mL shake flasks containing 95 mL of modified M9 medium (Furutate et al., 2021) (final volume:100 mL and 5% inoculum). The modified M9 medium comprised of 17.1 g/L Na$_2$HPO$_4$·12H$_2$O, 3 g/L KH$_2$PO$_4$, 0.5 g/L NaCl, 2 mL of 1 M MgSO$_4$·7H$_2$O, 0.1 mL of 1 M CaCl$_2$, and 2.5 g/L Bacto-yeast extract. For plasmid maintenance during PHA production, 50 mg/L of kanamycin and 50 mg/L of carbenicillin were added. Additionally, 1 mM isopropyl-β-D-thiogalactopyranoside (IPTG) was used to induce *phaJ and pct* gene expression. The P(3HB) homopolymer was synthesized from 20 g/L glucose, which was

added at the beginning of the culture at 30°C for 72 h. For the synthesis of 3HB-based copolymers, the total incubation time was set to 76 h, in which an initial step for 4 h at 30°C with reciprocal shaking (130 rpm) was performed before the addition of IPTG, precursors, and glucose, and further cultured for 72 h. Hexanoic acid, 4-methylvaleric acid, *trans*-2-methylbut-2-enoic acid (tiglic acid), and 2,2-dimethyl-3-hydroxypropionic acid (3-hydroxypivalic acid), which had previously been converted to their respective sodium salts, were used as precursors for the 3HHx, 3H4MV, 3H2MB, and 3HPi units, respectively (Füchtenbusch et al., 1998; Tanadchangsaeng et al., 2009; Watanabe et al., 2015). These precursors are known to inhibit cell growth, and a high concentration of glucose can repress *phaJ* and *pct* genes, otherwise induced by IPTG. Thus, lower concentrations of glucose and the precursors were added intermittently to the culture medium (at 4, 28, and 52 h). A total of 7.5 g/L glucose (2.5 g/L each time) and 0.6 g/L precursors (0.2 g/L each time) were added throughout the main incubation period. Finally, cells were harvested by centrifugation and lyophilized for further analysis. The relationship between the precursors used and biosynthesized polymers is shown in Figure 1.

Site-directed mutagenesis

To construct mutated *phaC$_{Ps}$*, a substitution (N175G) was introduced into the gene by overlap extension PCR (Supplementary Figure S2) (Warrens et al., 1997). The primers for amino acid substitution were designed and chemically synthesized as follows:5′-GGCGGCCGCTCTAGAACTAGTGGATCCCGGGGCAA-3′ and 5′- CACTAAGTTTTGACCGCCGTTCTCCAAGGT-3′ for an amplification of the 1.4-kb fragment, 5′-GCGCTTGGAGGCCGG CACCG-3′ and 5′- GTGACCTTGGAGAACGGCGGTCAAAAC TTA-3′ for an amplification of the 2.3-kb fragment. The underlined sequence in the primer indicates the codon used to replace Asn175 (AAT) with Gly (GGC). The resulting plasmid carrying the mutated gene was introduced into *E. coli* LSBJ along with pTTQ-PCT for PHA biosynthesis analysis.

Analysis of PHA

The dry cell weight was gravimetrically measured after centrifuging the culture medium at 6,000 × *g* for 10 min at room temperature three times (once for collecting the cells, discarding the medium, and twice to wash away the remaining salts with water) and lyophilized for approximately 3 days.

PHA content, PHA yield, and 3HA monomer composition were determined by gas chromatography (GC) using a Shimadzu GC-2014s instrument (Shimadzu, Kyoto, Japan) with a flame ionization detector. Lyophilized cells were methanolyzed to convert PHA into 3HA-methyl ester constituents in the presence of 15% sulfuric acid for GC analysis. The methanolysis reaction was carried out at 100°C for 140 min, except for 3H2MB- and 3HPi-containing polymers, for which the reaction time was set to 8 h to increase the reaction yield. The methanolyzed samples were allowed to cool to room temperature, and 1 mL of deionized water was added to separate the polar components from the non-polar components. The non-
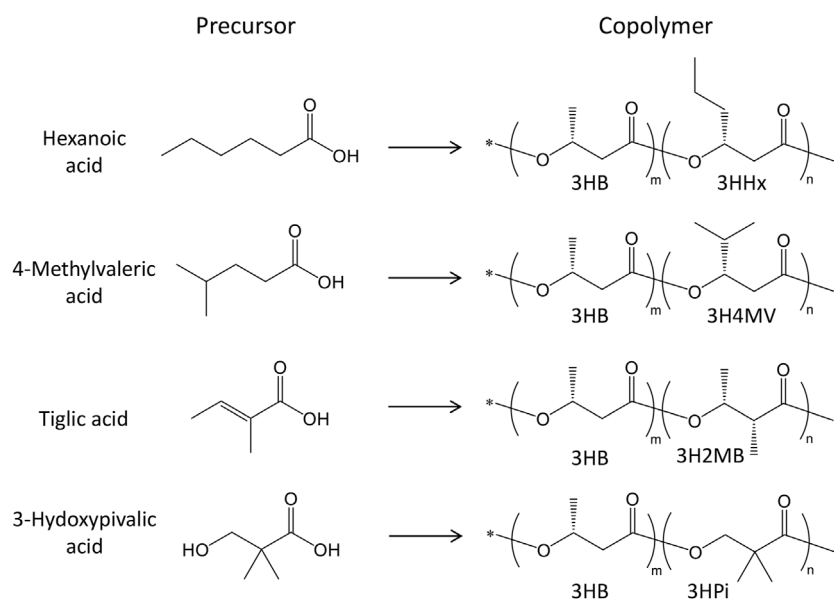
FIGURE 1
Chemical structure of PHA copolymers and precursors.

polar fraction containing 3HA-methyl ester was filtered, and an equal volume of chloroform solution containing 0.1% (w/v) methyl-n-octanoate as an internal standard was added to prepare the final sample for GC analysis. The samples were injected through the GC capillary column InertCap 1 (30 m × 0.25 mm, GL Science, Tokyo, Japan). The column temperature was initially set at 90°C for 2 min, increased to 110°C at a rate of 5°C/min, and then increased to 280°C at a rate of 20°C/min. The signal peak areas obtained were calculated for the total PHA content and 3HA monomer composition.

The molecular weight of P(3HB) synthesized using various PhaC enzymes was determined by gel permeation chromatography (GPC) using a Shimadzu Nexera GPC system with an RI-504 refractive index detector (Shodex, Tokyo, Japan) equipped with two KF-406 LHQ joint-columns (at 40°C, Shodex, Tokyo, Japan). Chloroform was used as the mobile phase at a flow rate of 0.3 mL/min. The sample concentration and injection volume were set at 1 mg/mL and 10 μL, respectively. Polystyrene standards with low polydispersity were also analyzed as reference standards to construct a calibration curve.

Results and discussion

Identification of new PhaC enzymes using BLAST

A BLASTP search was performed against the protein sub-sections of the NCBI and DDBJ databases using the amino acid sequence of $PhaC_{Ac}$, the first enzyme characterized by the natural copolymerization of 3HB and 3HHx monomers to PHA copolymers. Four PhaCs from the bacteria *Ferrimonas marina* (Katsuta et al., 2005), *Plesiomonas shigelloides* (Ferguson and

Henderson 1947; Janda et al., 2016), *Shewanella pealeana* (Leonardo et al., 1999), and *Vibrio metschnikovii* (Lee et al., 1978) were selected for further evaluation, because of the diversity of the N-terminal region such as positions 149 and 171 in $PhaC_{Ac}$. These PhaCs were identified as Class I PHA synthases, which have a high potential for synthesizing scl-mcl PHA copolymers in a manner similar to $PhaC_{Ac}$, based on their homology. Although these bacteria were discovered long ago, their ability to produce PHA has not yet been studied.

A comparison with the amino acid sequence of $PhaC_{Ac}$ revealed that the four PhaC enzymes identified in this study shared 85%–91% similarity and approximately 55% identity with $PhaC_{Ac}$ (Table 1). Multiple sequence alignment of PhaCs is shown in Figure 2. All new PhaCs have a PhaC box sequence at the active site, which is typically described as G-X-C-X-G-G (where X is an arbitrary amino acid), and cysteine (Cys^{319} in $PhaC_{Ac}$) is the active center (Nambu et al., 2020). In $PhaC_{Ac}$, the active sites Cys^{319}, Asp^{475}, and His^{503} have been proposed to form a catalytic triad (Tsuge et al., 2007a), which are all conserved in the newly identified PhaC enzymes. In contrast, PhaC from *P. shigelloides* has a primary sequence of approximately 30 amino acid residues greater than that of others and exhibits relatively low sequence homology in the C-terminal region. The phylogenetic tree shown in Figure 3 indicates that PhaC from *F. marina* is closely related to $PhaC_{Ac}$, whereas PhaC enzymes from *S. pealeana* and *V. metchniskovii* are evolutionarily distinct. PhaC from *P. shigelloides* is neither closely related nor evolutionarily distant from $PhaC_{Ac}$. To the best of our knowledge, no study has explored PhaC enzymes isolated from these bacteria for PHA production. Thus, genes encoding the four PhaC enzymes were chemically synthesized with optimized codon usage in *E. coli*. The DNA sequences are included in Supplementary Information.

TABLE 1 Four PhaCs characterized in this study.

PhaC from	Abbreviation	Accession	Protein size (amino acids)	Homology to PhaC$_{Ac}$	
				Identity	Similarity
Ferrimonas marina	PhaC$_{Fm}$	WP_067661665	592	58% (341/585)	91% (534/585)
Plesiomonas shigelloides	PhaC$_{Ps}$	WP_116546999	623	54% (324/595)	86% (512/595)
Shewanella pealeana	PhaC$_{Sp}$	WP_012154995	584	53% (303/564)	88% (499/564)
Vibrio metschnikovii	PhaC$_{Vm}$	WP_154168902	590	52% (306/580)	85% (494/580)

PhaC$_{Ac}$: PhaC from *Aeromonas caviae* (Accession BAA21815) with a protein size of 594 aa.

FIGURE 2
Multiple sequence alignment of PHA synthases (PhaCs) from *Aeromonas caviae*, *Ferrimonas marina*, *Plesiomonas shigelloides*, *Shewanella pealeana*, and *Vibrio metschnikovii*. The active site residues of PhaC$_{Ac}$, cysteine (C^{319}), aspartic acid (D^{475}), and histidine (H^{503}) are highlighted in blue. For the PhaC$_{Ac}$NSDG variant, the positions of two amino acid substitutions (N^{149} replaced with S and D^{171} replaced with G) are highlighted in orange.

FIGURE 3
A phylogenetic tree of PhaCs rooted by outgroup (PhaC from *Ralstonia eutrophus*, WP_011615085). Sequences were aligned using ClustalW, and the phylogenetic tree was generated using MEGA11 software. PhaCs from *Aeromonas caviae* (BAA21815), *Ferrimonas marina* (WP_067661665), *Plesiomonas shigelloides* (WP_116546999), *Shewanella pealeana* (WP_012154995), and *Vibrio metschnikovii* (WP_154168902) were used. Bootstrap values (expressed as percentages of 1,000 replications) are shown at the branch points. Scale bar = 0.2 substitution per amino acid position.
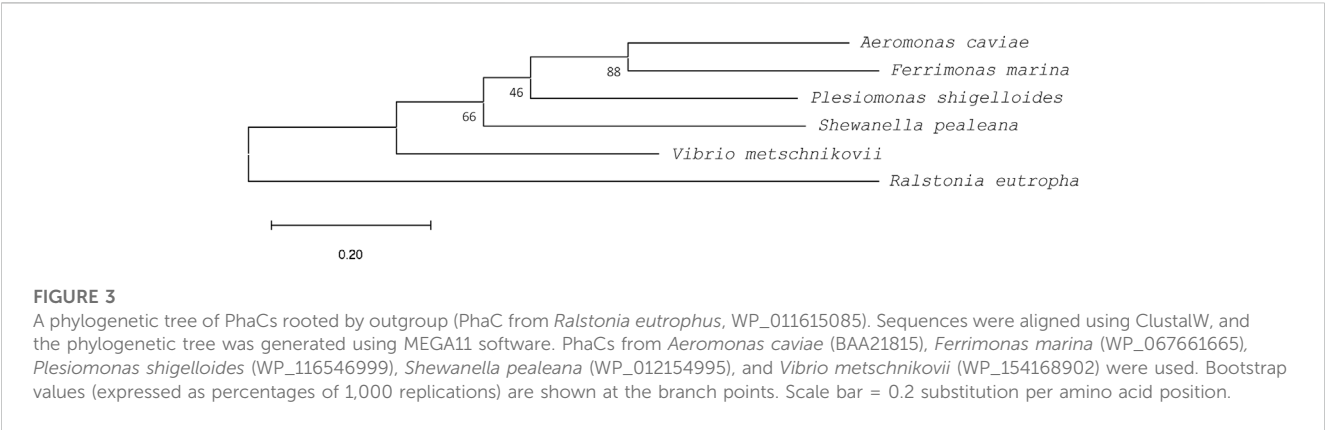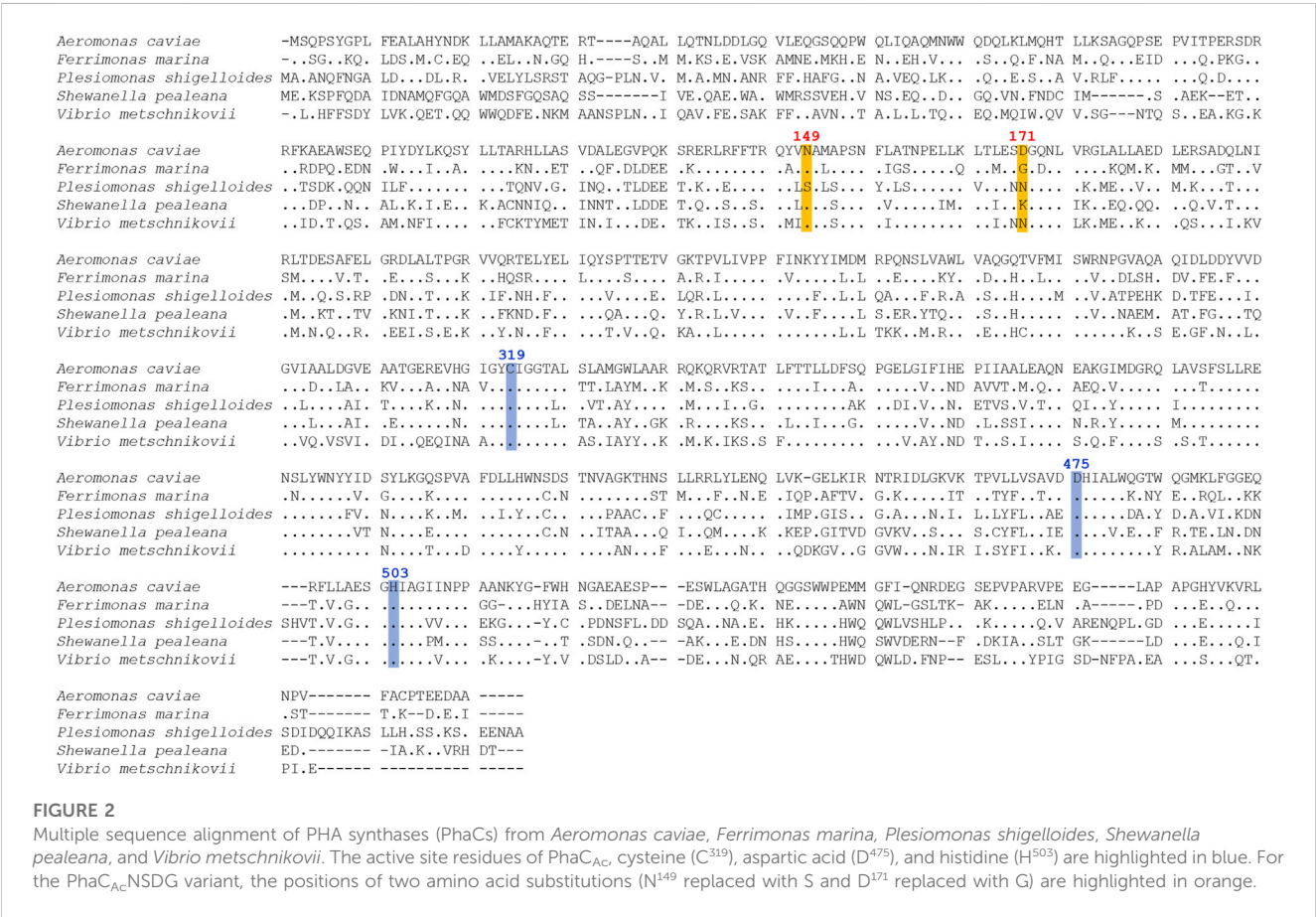
TABLE 2 Biosynthesis of P(3HB) from glucose by *E. coli* LSBJ expressing various PhaCs.

PhaC	Dry cell wt. (g/L)	P(3HB) content (wt%)	P(3HB) yield (g/L)	Molecular weight	
				M_w ($\times 10^5$)	PDI
A. caviae	2.66 ± 0.02	39.8 ± 1.4	1.06 ± 0.04	8.5 ± 0.4	2.58 ± 0.36
A. caviae NSDG variant	3.83 ± 0.04	60.1 ± 4.3	2.30 ± 0.15	13.2 ± 0.5	2.45 ± 0.17
F. marina	2.77 ± 0.04	42.3 ± 1.1	1.17 ± 0.04	24.0 ± 3.0	1.39 ± 0.12
P. shigelloides	3.31 ± 0.02	54.2 ± 1.0	1.80 ± 0.03	34.4 ± 2.7	1.46 ± 0.13
P. shigelloides NG variant	3.59 ± 0.07	63.5 ± 1.4	2.28 ± 0.07	31.8 ± 5.9	1.37 ± 0.04
S. pealeana	2.39 ± 0.02	38.4 ± 5.0	0.92 ± 0.13	22.6 ± 1.6	1.54 ± 0.25
V. metschnikovii	3.08 ± 0.10	49.0 ± 2.2	1.51 ± 0.12	19.7 ± 1.5	2.62 ± 0.10

E. coli LSBJ harboring pBBR1-phaCsAB$_{Re}$J$_{Ac}$ was incubated in the modified M9 medium containing 20 g/L glucose as a carbon source. The values of dry cell weight, PHA content, and molecular weight were the averages of three independent experiments. P(3HB): poly(3-hydroxybutyrate). The NSDG variant of *A. caviae* PhaC had a double mutation of N149S and D171G. The NG variant of *P. shigelloides* PhaC had a single mutation of N175G. PDI is polydispersity index (M_w/M_n).

P(3HB) synthesis in recombinant *E. coli* expressing PhaC enzymes

The biosynthesis of P(3HB) from 20 g/L glucose using one of the four PhaC enzymes is summarized in Table 2. P(3HB) accumulation ranging from 38.4 wt% to 54.2 wt% was achieved using the new PhaC enzymes, which was comparable to PhaC$_{Ac}$ and its variant PhaC$_{Ac}$NSDG. Thus, all newly identified PhaC enzymes showed great potential as biocatalysts for P(3HB) production. However, PhaCs from *P. shigelloides* (PhaC$_{Ps}$) showed the highest P(3HB) accumulation among the wild-type PhaCs tested.

The molecular weight is a crucial aspect in determining the suitability of a material for various commercial uses (Sudesh et al., 2000). The weight-average molecular weight (M_w) is more closely related to material properties than the number-average molecular weight (M_n). For PHA, ultrahigh molecular weight polymers can form strong fibers (Tsuge, 2016), thus meeting the requirements for practical use. In addition, a low polydispersity index (PDI) (Tsuge, 2016) also plays a significant role in determining the suitability of PHA for specific applications. However, not all PhaC enzymes can synthesize PHAs with high M_w and low PDI. In this study, PhaC$_{Ps}$ synthesized P(3HB) with an ultrahigh M_w, which exceeded 3×10^6, with a relatively low PDI below 1.5 (Table 2). Moreover, the other two identified PhaC enzymes from *F. marina* and *S. pealeana* could also synthesize P(3HB) with M_w of approximately 2×10^6 with PDIs ranging from 1.3 to 1.5. PhaC$_{Vm}$ from *V. metschnikovii* proved to be an exception, with PDI >2.5. The currently available PhaC$_{Ac}$ is highly sensitive to ethanol (Hiroe et al., 2015), which is a metabolite of some bacteria, including *E. coli,* and functions as a chain transfer agent to terminate polymerization reactions (Tsuge, 2016), resulting in the synthesis of relatively low-molecular-weight PHA. The new PhaCs reported in this study may be less sensitive toward ethanol, thereby producing PHA with high M_w and low PDI. These new PhaC enzymes, especially PhaC$_{Ps}$, exhibited superior M_w and PDI

values compared with PhaC$_{Ac}$ and its NSDG variant, which could benefit PHA processing and material properties.

PHA copolymer synthesis by recombinant *E. coli* expressing PhaC enzymes

The new PhaC enzymes were evaluated for their substrate specificities alongside PhaC$_{Ac}$ and its NSDG variant for incorporating 3HHx, 3H4MV, 3H2MB, and 3HPi monomers. Biosynthesis was performed using four precursors (hexanoic acid, 4-methylvaleric acid, tiglic acid, and 3-hydroxypivalic acid) in the presence of glucose (Figure 1). These precursors are toxic to cells, thus inhibiting cell growth and subsequently lowering PHA accumulation in bacteria. As PHA production is associated with cell growth (Sudesh et al., 2000), it is imperative to eliminate or reduce the risk of toxicity induced by such precursors. Therefore, the precursors were introduced into the culture medium after 4 h, once substantial cell growth was achieved, mainly for better tolerance (Furutate et al., 2021). Meanwhile, a high glucose concentration can cause catabolic repression of *phaJ* and *pct* genes induced by IPTG (Furutate et al., 2021); thus, the glucose concentration was maintained at a minimum to promote cell growth only. Glucose and its precursors were intermittently added to allow for better uptake of the second monomer, with no or fewer unanticipated effects on the cells. The details of the biosynthesis results are summarized in Tables 3–6.

All PhaCs, except PhaC from *S. pealeana* (PhaC$_{Sp}$), were able to incorporate all targeted monomers (3HHx, 3H4MV, 3H2MB, and 3HPi). PhaC$_{Sp}$ copolymerized 3HB with 3HHx or 3HPi, but not 3H4MV or 3H2MB. The number of PhaC enzymes with broad substrate specificity is scarce; thus, the new PhaC enzymes reported in this study are highly intriguing for future studies. Furthermore, PHAs containing α-carbon methylated units are potentially attractive bio-based materials (Füchtenbusch et al., 1998; Furutate et al., 2021); thus, PhaCs with the ability to polymerize 3H2MB and 3HPi are of great interest. PhaC$_{Ps}$ demonstrated superior performance in the

TABLE 3 Biosynthesis of P (3HB-*co*-3HHx) by *E. coli* LSBJ expressing various PhaCs from glucose and hexanoic acid.

PhaC	Dry cell wt. (g/L)	PHA content (wt%)	PHA yield (g/L)	PHA composition (mol%)	
				3HB	3HHx
A. caviae	1.93 ± 0.04	16.9 ± 0.8	0.30 ± 0.01	86.7 ± 0.8	13.3 ± 0.8
A. caviae NSDG variant	2.12 ± 0.02	25.2 ± 1.3	0.51 ± 0.03	78.2 ± 1.4	21.8 ± 1.4
F. marina	1.92 ± 0.03	23.6 ± 1.2	0.45 ± 0.02	90.5 ± 1.0	9.5 ± 1.0
P. shigelloides	1.78 ± 0.04	19.1 ± 0.3	0.34 ± 0.01	89.1 ± 1.2	10.9 ± 1.2
P. shigelloides NG variant	1.80 ± 0.05	11.9 ± 0.7	0.21 ± 0.12	90.0 ± 0.2	10.0 ± 0.2
S. pealeana	1.68 ± 0.06	12.2 ± 0.5	0.20 ± 0.01	89.5 ± 0.5	10.5 ± 0.5
V. metschnikovii	1.82 ± 0.01	18.7 ± 0.9	0.34 ± 0.02	96.0 ± 0.2	4.0 ± 0.2

E. coli LSBJ harboring pBBR1-phaCsAB$_{Re}$J$_{Ac}$ and pTTQ-PCT was incubated in the modified M9 containing 7.5 g/L glucose (2.5 g/L × 3 times) and 0.6 g/L hexanoic acid (0.2 g/L × 3 times), which were added at 4, 28, and 52 h. The values of dry cell weight, PHA content, and PHA composition were the averages of three independent experiments. The NSDG variant of *A. caviae* PhaC had a double mutation of N149S and D171G. The NG variant of *P. shigelloides* PhaC had a single mutation of N175G. 3HB: 3-hydroxybutyrate; 3HHx: 3-hydroxyhexanoate.

TABLE 4 Biosynthesis of P (3HB-*co*-3H4MV) by *E. coli* LSBJ expressing various PhaCs from glucose and 4-methylvaleric acid.

PhaC	Dry cell wt. (g/L)	PHA content (wt%)	PHA yield (g/L)	PHA composition (mol%)	
				3HB	3H4MV
A. caviae	1.66 ± 0.04	17.8 ± 1.2	0.30 ± 0.03	95.4 ± 0.3	4.6 ± 0.3
A. caviae NSDG variant	1.68 ± 0.01	18.0 ± 1.4	0.30 ± 0.02	93.7 ± 0.5	6.3 ± 0.5
F. marina	1.92 ± 0.02	27.0 ± 2.9	0.52 ± 0.06	98.5 ± 0.1	1.5 ± 0.1
P. shigelloides	1.78 ± 0.03	20.9 ± 0.8	0.37 ± 0.01	97.5 ± 0.2	2.5 ± 0.2
P. shigelloides NG variant	1.86 ± 0.01	16.6 ± 4.9	0.31 ± 0.10	96.3 ± 0.1	3.7 ± 0.1
S. pealeana	1.69 ± 0.01	18.4 ± 1.2	0.31 ± 0.02	100	ND
V. metschnikovii	1.85 ± 0.02	20.7 ± 2.1	0.38 ± 0.04	98.1 ± 0.4	1.9 ± 0.4

E. coli LSBJ harboring pBBR1-phaCsAB$_{Re}$J$_{Ac}$ and pTTQ-PCT was incubated in the modified M9 containing 7.5 g/L glucose (2.5 g/L × 3 times) and 0.6 g/L 4-methylvaleric acid (0.2 g/L × 3 times), which were added at 4, 28, and 52 h. The values of dry cell weight, PHA content, and PHA composition were the averages of three independent experiments. The NSDG variant of *A. caviae* PhaC had a double mutation of N149S and D171G. The NG variant of *P. shigelloides* PhaC had a single mutation of N175G. 3HB: 3-hydroxybutyrate; 3H4MV: 3-hydroxy-4-methylvalerate.

polymerization of 3HPi to PhaC$_{Ac}$. Additionally, all PhaC$_{Ps}$-expressing strains showed higher PHA content than PhaC$_{Ac}$-expressing strains. Therefore, the potential of PhaC$_{Ps}$ was further explored using site-directed mutagenesis.

Generation and evaluation of PhaC$_{Ps}$NG variant

In vitro evolution of PhaC is a powerful approach for enhancing the productivity and quality of PHA (Kichise et al., 2002; Taguchi and Doi, 2004). For instance, PhaC$_{Ac}$NSDG, a variant of PhaC$_{Ac}$, exhibits enhanced performance (such as

production yield and substrate specificity) compared to that of the wild-type enzyme (Tsuge et al., 2007b). In addition, various studies have proven the efficacy of PhaC engineering in PHA production towards the formation of super biocatalysts for tailor-made PHAs (Taguchi and Doi, 2004; Nomura and Taguchi, 2007). Therefore, PhaC$_{Ps}$, which exhibited the best performance among the new PhaCs, were selected for site-directed mutagenesis to study their potential positive effects on PHA production. Considering that the double mutation of PhaC$_{Ac}$NSDG, amino acid substitutions of N149S and D171G drastically enhanced the performance of the enzyme (Tsuge et al., 2007b; Harada et al., 2021), similar efforts were adopted to generate a PhaC$_{Ps}$ variant. According to the alignment

TABLE 5 Biosynthesis of P (3HB-*co*-3H2MB) by *E. coli* LSBJ expressing various PhaCs from glucose and tiglic acid.

PhaC	Dry cell wt. (g/L)	PHA cont. (wt%)	PHA yield (g/L)	PHA composition (mol%)	
				3HB	3H2MB
A. caviae	2.02 ± 0.04	23.1 ± 0.6	0.47 ± 0.02	95.7 ± 0.1	4.3 ± 0.1
A. caviae NSDG variant	2.33 ± 0.03	29.5 ± 2.6	0.69 ± 0.06	95.1 ± 0.2	4.9 ± 0.2
F. marina	2.30 ± 0.08	31.9 ± 1.2	0.74 ± 0.05	99.3 ± 0.0	0.7 ± 0.0
P. shigelloides	2.21 ± 0.08	29.5 ± 2.6	0.76 ± 0.05	97.9 ± 0.2	2.1 ± 0.2
P. shigelloides NG variant	2.24 ± 0.03	30.0 ± 1.2	0.67 ± 0.03	94.6 ± 0.1	5.4 ± 0.1
S. pealeana	1.88 ± 0.06	20.3 ± 0.3	0.38 ± 0.01	100	ND
V. metschnikovii	2.31 ± 0.03	30.4 ± 2.7	0.72 ± 0.01	99.5 ± 0.0	0.5 ± 0.0

E. coli LSBJ harboring pBBR1-phaCsAB$_{Re}$J$_{Ac}$ and pTTQ-PCT was cultured in the modified M9 medium containing 7.5 g/L glucose (2.5 g/L × 3 times) and 0.6 g/L tiglic acid (0.2 g/L × 3 times), which were added at 4, 28, and 52 h. The values of dry cell weight, PHA content, and PHA composition were the averages of three independent experiments. The NSDG variant of *A. caviae* PhaC had a double mutation of N149S and D171G. The NG variant of *P. shigelloides* PhaC had a single mutation of N175G. 3HB: 3-hydroxybutyrate; 3H2MB: 3-hydroxy-2-methylbutyrate.

TABLE 6 Biosynthesis of P (3HB-*co*-3HPi) by *E. coli* LSBJ expressing various PhaCs from glucose and 3-hydoxypivalic acid.

PhaC	Dry cell wt. (g/L)	PHA cont. (wt%)	PHA yield (g/L)	PHA composition (mol%)	
				3HB	3HPi
A. caviae	2.01 ± 0.03	16.3 ± 1.4	0.33 ± 0.03	94.2 ± 0.6	5.8 ± 0.6
A. caviae NSDG variant	2.07 ± 005	19.4 ± 1.2	0.40 ± 0.03	79.9 ± 1.1	20.1 ± 1.1
F. marina	2.22 ± 0.04	23.1 ± 0.3	0.51 ± 0.01	97.5 ± 0.6	2.5 ± 0.6
P. shigelloides	1.98 ± 0.05	16.7 ± 1.3	0.33 ± 0.03	89.8 ± 0.4	10.1 ± 0.4
P. shigelloides NG variant	1.91 ± 0.22	15.0 ± 2.7	0.29 ± 0.06	88.4 ± 0.5	11.6 ± 0.5
S. pealeana	1.80 ± 0.08	9.7 ± 0.1	0.17 ± 0.01	97.9 ± 0.4	2.1 ± 0.4
V. metschnikovii	2.15 ± 0.03	24.2 ± 0.9	0.52 ± 0.02	97.2 ± 0.2	2.8 ± 0.2

E. coli LSBJ harboring pBBR1-phaCsAB$_{Re}$J$_{Ac}$ and pTTQ-PCT was incubated in the modified M9 medium containing 7.5 g/L glucose (2.5 g/L × 3 times) + 0.6 g/L 3-hydroxypivalic acid (0.2 g/L × 3 times), which were added at 4, 28, and 52 h. The values of dry cell weight, PHA content, and PHA composition were the averages of three independent experiments. The NSDG variant of *A. caviae* PhaC had a double mutation of N149S and D171G. The NG variant of *P. shigelloides* PhaC had a single mutation of N175G. 3HB: 3-hydroxybutyrate; 3HPi: 3-hydroxypivalate.

(Figure 2), PhaC$_{Ps}$ naturally contain a serine residue at the corresponding position of 149 in PhaC$_{Ac}$NSDG. Thus, a single amino acid substitution was performed in PhaC$_{Ps}$ in which asparagine 175 was changed to glycine (N175G). The resultant variant was termed PhaC$_{Ps}$NG, and its PHA production ability was examined.

Interestingly, PhaC$_{Ps}$NG showed enhanced P(3HB) synthesis, while maintaining a high molecular weight (Table 2). PhaC$_{Ps}$NG exhibited enhanced activity for the incorporation of the *α*-methylated monomer 3H2MB compared with the parent enzyme and PhaC$_{Ac}$NSDG (Table 5). This indicates the potential of PhaC$_{Ps}$NG to surpass the currently best-performing enzyme (PhaC$_{Ac}$NSDG) for the

incorporation of the 3H2MB monomer. Moreover, PhaC$_{Ps}$NG was shown to have a better ability to incorporate 3H4MV and 3HPi than the parent enzyme but less so than PhaC$_{Ac}$NSDG (Table 4 and Table 6). Finally, PhaC$_{Ps}$NG exhibited an almost similar level of 3HHx incorporation as the parent enzyme, which was inferior to PhaC$_{Ac}$NSDG (Table 3).

Conclusion

In conclusion, four Class I PhaC enzymes from different bacteria were identified using BLASTP and were characterized for PHA production. To the best of our knowledge, this is the

first report to characterize PhaC enzymes from *F. marina*, *P. shigelloides*, *S. pealeana*, and *V. metschnikovii*. These PhaCs exhibited a relatively high potential for polymerizing P(3HB) in recombinant *E. coli*. PhaC enzymes identified in this study, with the exception of PhaC$_{Sp}$ from *S. pealeana,* were able to incorporate all the targeted monomers, namely 3HHx, 3H4MV, α-carbon methylated 3H2MB, and α-carbon dimethylated 3HPi. Among the four new PhaCs, PhaC$_{Ps}$ from *P. shigelloides* displayed the best performance; thus, we attempted to further improve their attributes through protein engineering. The resultant variant PhaC$_{Ps}$NG exhibited superior capability in polymerizing the 3H2MB monomer compared to PhaC$_{Ac}$ and its NSDG variant. Furthermore, PhaC$_{Ps}$NG showed the enhanced synthesis of P(3HB) with ultrahigh molecular weight and low PDI. Finally, these newly identified PhaC enzymes show great versatility, suggesting their potential as workhorse enzymes for the industrial-scale production of 3HB-based copolymers.

Data availability statement

The datasets presented in this study can be found in online repositories. The names of the repository/repositories and accession number(s) can be found in the article/Supplementary Material.

Author contributions

RS, MM, YM, SM, CN, ST, HA, and TT jointly conceived the study. RS, MM, YM, and SM performed the experiments. RS wrote the manuscript in consultation with CN, ST, HA, and TT. All authors read and approved the final manuscript.

Conflict of interest

The authors declare that the research was conducted in the absence of any commercial or financial relationships that could be construed as a potential conflict of interest.

Publisher's note

All claims expressed in this article are solely those of the authors and do not necessarily represent those of their affiliated organizations, or those of the publisher, the editors and the reviewers. Any product that may be evaluated in this article, or claim that may be made by its manufacturer, is not guaranteed or endorsed by the publisher.

Supplementary material

The Supplementary Material for this article can be found online at: https://www.frontiersin.org/articles/10.3389/fbioe.2023.1114946/full#supplementary-material

References

Altschul, S. F., Gish, W., Miller, W., Myers, E. W., and Lipman, D. J. (1990). Basic local alignment search tool. *J. Mol. Biol.* 215, 403–410. doi:10.1016/S0022-2836(05)80360-2

Anderson, A. J., and Dawes, E. (1990). Occurrence, metabolism, metabolic role, and industrial uses of bacterial polyhydroxyalkanoates. *Microbiol. Rev.* 54, 450–472. doi:10.1128/mr.54.4.450-472.1990

Chek, M. F., Hiroe, A., Hakoshima, T., Sudesh, K., and Taguchi, S. (2019). PHA synthase (PhaC): Interpreting the functions of bioplastic-producing enzyme from a structural perspective. *Appl. Microbiol. Biotechnol.* 103, 1131–1141. doi:10.1007/s00253-018-9538-8

Chek, M. F., Kim, S. Y., Mori, T., Arsad, H., Samian, M. R., Sudesh, K., et al. (2017). Structure of polyhydroxyalkanoate (PHA) synthase PhaC from *Chromobacterium* sp. USM2, producing biodegradable plastics. *Sci. Rep.* 7, 5312. doi:10.1038/s41598-017-05509-4

Chek, M. F., Kim, S. Y., Mori, T., Tan, H. T., Sudesh, K., and Hakoshima, T. (2020). Asymmetric open-closed dimer mechanism of polyhydroxyalkanoate synthase PhaC. *iScience* 23, 101084. doi:10.1016/j.isci.2020.101084

Doi, Y., Kitamura, S., and Abe, H. (1995). Microbial synthesis and characterization of poly(3-hydroxybutyrate-*co*-3-hydroxyhexanoate). *Macromolecules* 28, 4822–4828. doi:10.1021/ma00118a007

Fadzil, F. I. M., Mizuno, S., Hiroe, A., Nomura, C. T., and Tsuge, T. (2018). Low carbon concentration feeding improves medium-chain-length polyhydroxyalkanoate production in *Escherichia coli* strains with defective β-oxidation. *Front. Bioeng. Biotechnol.* 6, 178. doi:10.3389/fbioe.2018.00178

Ferguson, W. W., and Henderson, N. D. (1947). Description of strain C27: A motile organism with the major antigen of *Shigella sonnei* phase I. *J. Bacteriol. Res.* 54, 179–181. doi:10.1128/jb.54.2.179-181.1947

Füchtenbusch, B., Fabritius, D., Wältermann, M., and Steinbüchel, A. (1998). Biosynthesis of novel copolyesters containing 3-hydroxypivalic acid by *Rhodococcus ruber* NCIMB 40126 and related bacteria. *FEMS Microbiol. Lett.* 159, 85–92. doi:10.1111/j.1574-6968.1998.tb12845.x

Furutate, S., Kamoi, J., Nomura, C. T., Taguchi, S., Abe, H., and Tsuge, T. (2021). Superior thermal stability and fast crystallization behavior of a novel, biodegradable α-methylated bacterial polyester. *NPG Asia Mater* 13, 31. doi:10.1038/s41427-021-00296-x

Furutate, S., Nakazaki, H., Maejima, K., Hiroe, A., Abe, H., and Tsuge, T. (2017). Biosynthesis and characterization of novel polyhydroxyalkanoate copolymers consisting of 3-hydroxy-2-methylbutyrate and 3-hydroxyhexanoate. *J. Polym. Res.* 24, 221. doi:10.1007/s10965-017-1392-3

Harada, K., Kobayashi, S., Oshima, K., Yoshida, S., Tsuge, T., and Sato, S. (2021). Engineering of *Aeromonas caviae* polyhydroxyalkanoate synthase through site-directed mutagenesis for enhanced polymerization of the 3-hydroxyhexanoate unit. *Front. Bioeng. Biotechnol.* 9, 627082. doi:10.3389/fbioe.2021.627082

Hiroe, A., Shiraishi, M., Mizuno, K., and Tsuge, T. (2015). Behavior of different polyhydroxyalkanoate synthases in response to the ethanol level in *Escherichia coli* cultures. *Polym. J.* 47, 767–770. doi:10.1038/pj.2015.53

Janda, J. M., Abbott, S. L., and McIver, C. J. (2016). *Plesiomonas shigelloides* revisited. *Clin. Microbiol. Rev.* 29, 349–374. doi:10.1128/CMR.00103-15

Katsuta, A., Adachi, K., Matsuda, S., Shizuri, Y., and Kasai, H. (2005). *Ferrimonas marina* sp. nov. *Int. J. Syst. Evol. Microbiol.* 55, 1851–1855. doi:10.1099/ijs.0.63689-0

Kichise, T., Taguchi, S., and Doi, Y. (2002). Enhanced accumulation and changed monomer composition in polyhydroxyalkanoate (PHA) copolyester by *in vitro*

evolution of Aeromonas caviae PHA synthase. *Appl. Environ. Microbiol.* 68, 2411–2419. doi:10.1128/AEM.68.5.2411-2419.2002

Kim, J., Kim, Y. J., Choi, S. Y., Lee, S. Y., and Kim, K. J. (2017). Crystal structure of *Ralstonia eutropha* polyhydroxyalkanoate synthase C-terminal domain and reaction mechanisms. *Biotechnol. J.* 12, 1600648. doi:10.1002/biot.201600648

Kobayashi, G., Shiotani, T., Shima, Y., and Doi, Y. (1994). "Biosynthesis and characterization of poly(3-hydroxybutyrate-*co*-3-hydroxyhexanoate) from oils and fats by *Aeromonas* sp. OL-338 and *Aeromonas* sp. FA-440," in *Biodegradable plastics and polymers*. Editors Y. Doi and K. Fukuda (Amsterdam: Elsevier), 410–416. doi:10.1016/b978-0-444-81708-2.50044-0

Kovach, M. E., Elzer, P. H., Hill, D. S., Robertson, G. T., Farris, M. A., Roop, R. M., et al. (1995). Four new derivatives of the broad-host-range cloning vector pBBR1MCS, carrying different antibiotic-resistance cassettes. *Gene* 166, 175–176. doi:10.1016/0378-1119(95)00584-1

Lee, J. V., Donovan, T. J., and Furniss, A. L. (1978). Characterization, taxonomy, and emended description of Vibrio metschnikovii. *Vibrio metschnikovii Int. J. Syst. Evol. Microbiol.* 28, 99–111. doi:10.1099/00207713-28-1-99

Lehrle, R., and Williams, R. J. (1994). Thermal degradation of bacterial poly(hydroxybutyric acid): Mechanisms from the dependence of pyrolysis yields on sample thickness. *Macromolecules* 27, 3782–3789. doi:10.1021/ma00092a017

Lenz, R. W., and Marchessault, R. H. (2005). Bacterial polyesters: Biosynthesis, biodegradable plastics and biotechnology. *Biomacromolecules* 6, 1–8. doi:10.1021/bm049700c

Leonardo, M. R., Moser, D. P., Barbieri, E., Brantner, C. A., MacGregor, B. J., Paster, B. J., et al. (1999). *Shewanella pealeana* sp. nov., a member of the microbial community associated with the accessory nidamental gland of the squid *Loligo pealei. Int. J. Syst. Evol. Microbiol.* 49, 1341–1351. doi:10.1099/00207713-49-4-1341

Levine, A. C., Heberlig, G. W., and Nomura, C. T. (2016). Use of thiol-ene click chemistry to modify mechanical and thermal properties of polyhydroxyalkanoates (PHAs). *Int. J. Biol. Macromol.* 83, 358–365. doi:10.1016/j.ijbiomac.2015.11.048

Mierzati, M., Mizuno, S., and Tsuge, T. (2020). Biosynthesis and characterization of poly(3-hydroxybutyrate-*co*-2-hydroxyalkanoate) with different comonomer fractions. *Polym. Degrad. Stabil.* 178, 109193. doi:10.1016/j.polymdegradstab.2020.109193

Mizuno, K., Ohta, A., Hyakutake, M., Ichinomiya, Y., and Tsuge, T. (2010). Isolation of polyhydroxyalkanoate-producing bacteria from a polluted soil and characterization of the isolated strain *Bacillus cereus* YB-4. *Polym. Degrad. Stabil.* 95, 1335–1339. doi:10.1016/j.polymdegradstab.2010.01.033

Nambu, Y., Ishii-Hyakutake, M., Harada, K., Mizuno, S., and Tsuge, T. (2020). Expanded amino acid sequence of the PhaC box in the active center of polyhydroxyalkanoate synthases. *FEBS Lett.* 594, 710–716. doi:10.1002/1873-3468.13651

Nomura, C. T., and Taguchi, S. (2007). PHA synthase engineering toward superbiocatalysts for custom-made biopolymers. *Appl. Microbiol. Biotechnol.* 73, 969–979. doi:10.1007/s00253-006-0566-4

Pinto, A., Ciesla, J., Palucci, A., Sutliff, B., and Nomura, C. T. (2016). Chemically intractable no more: *In vivo* incorporation of "click"-ready fatty acids into poly-[(R)-3-hydroxyalkanoates in *Escherichia coli. ACS Macro. Lett.* 5, 215–219. doi:10.1021/acsmacrolett.5b00823

Rehm, B. H. (2003). Polyester synthases: Natural catalysts for plastics. *Biochem. J.* 376, 15–33. doi:10.1042/bj20031254

Scheel, R. A., Ho, T., Kageyama, Y., Masisak, J., McKenney, S., Lundgren, B. R., et al. (2021). Optimizing a fed-batch high-density fermentation process for medium-chain-length poly(3-hydroxyalkanoates) in *Escherichia coli*. 9, 134. *Front. Bioeng. Biotechnol.* 9, 618259. doi:10.3389/fbioe.2021.618259

Shimamura, E., Kasuya, K., Kobayashi, G., Shiotani, T., Shima, Y., and Doi, Y. (1994). Physical properties and biodegradability of microbial poly(3-hydroxybutyrate-*co*-3-hydroxyhexanoate). *Macromolecules* 27, 878–880. doi:10.1021/ma00081a041

Sivashankari, R., and Tsuge, T. (2021). "Development of polyhydroxyalkanoate (PHA) and its copolymers as a possible "cure" for the plastic pollution," in Environmental and Microbial Biotechnology *book series*. Editor R. Prasad (Singapore: Springer), 59–79. doi:10.1007/978-981-15-5499-5_3

Sudesh, K., Abe, H., and Doi, Y. (2000). Synthesis, structure and properties of polyhydroxyalkanoates: Biological polyesters. *Prog. Polym. Sci.* 25, 1503–1555. doi:10.1016/S0079-6700(00)00035-6

Suzuki, M., Tachibana, Y., and Kasuya, K. I. (2021). Biodegradability of poly(3-hydroxyalkanoate) and poly(ε-caprolactone) via biological carbon cycles in marine environments. *Polym. J.* 53, 47–66. doi:10.1038/s41428-020-00396-5

Taguchi, S., and Doi, Y. (2004). Evolution of polyhydroxyalkanoate (PHA) production system by "enzyme evolution": Successful case studies of directed evolution. *Macromol. Biosci.* 4, 145–156. doi:10.1002/mabi.200300111

Taguchi, S., Yamada, M., Matsumoto, K. I., Tajima, K., Satoh, Y., Munekataet, M., et al. (2008). A microbial factory for lactate-based polyesters using a lactate-polymerizing enzyme. *Proc. Natl. Acad. Sci. U.S.A.* 105, 17323–17327. doi:10.1073/pnas.0805653105

Tamura, K., Stecher, G., and Kumar, S. (2021). Mega 11: Molecular evolutionary genetics analysis version 11. *Mol. Biol. Evol.* 38, 3022–3027. doi:10.1093/molbev/msab120

Tanadchangsaeng, N., Kitagawa, A., Yamamoto, T., Abe, H., and Tsuge, T. (2009). Identification, biosynthesis, and characterization of polyhydroxyalkanoate copolymer consisting of 3-hydroxybutyrate and 3-hydroxy-4-methylvalerate. *Biomacromolecules* 10 2866-10, 2866–2874. doi:10.1021/bm900696c

Tappel, R. C., Kucharski, J. M., Mastroianni, J. M., Stipanovic, A. J., and Nomura, C. T. (2012b). Biosynthesis of poly[(*R*)-3-hydroxyalkanoate] copolymers with controlled repeating unit compositions and physical properties. *Biomacromolecules* 13, 2964–2972. doi:10.1021/bm301043t

Tappel, R. C., Wang, Q., and Nomura, C. T. (2012a). Precise control of repeating unit composition in biodegradable poly(3-hydroxyalkanoate) polymers synthesized by *Escherichia coli. Escherichia coli J. Biosci. Bioeng.* 113, 480–486. doi:10.1016/j.jbiosc.2011.12.004

Tsuge, T. (2016). Fundamental factors determining the molecular weight of polyhydroxyalkanoate during biosynthesis. *Polym. J.* 48, 1051–1057. doi:10.1038/pj.2016.78

Tsuge, T., Watanabe, S., Sato, S., Hiraishi, T., Abe, H., Doi, Y., et al. (2007a). Variation in copolymer composition and molecular weight of polyhydroxyalkanoate generated by saturation mutagenesis of *Aeromonas caviae* PHA synthase. *Macromol. Biosci.* 7, 846–854. doi:10.1002/mabi.200700023

Tsuge, T., Watanabe, S., Shimada, D., Abe, H., Doi, Y., and Taguchi, S. (2007b). Combination of N149S and D171G mutations in *Aeromonas caviae* polyhydroxyalkanoate synthase and impact on polyhydroxyalkanoate biosynthesis. *FEMS Microbiol. Lett.* 277, 217–222. doi:10.1111/j.1574-6968.2007.00958.x

Tsuge, T., Yano, K., Imazu, S. I., Numata, K., Kikkawa, Y., Abe, H., et al. (2005). Biosynthesis of polyhydroxyalkanoate (PHA) copolymer from fructose using wild-type and laboratory evolved PHA synthases. *Macromol. Biosci.* 5, 112–117. doi:10.1002/mabi.200400152

Warrens, A. N., Jones, M., and Lechler, R. I. (1997). Splicing by overlap extension by PCR using asymmetric amplification: An improved technique for the generation of hybrid proteins of immunological interest. *Gene* 186, 29–35. doi:10.1016/S0378-1119(96)00674-9

Watanabe, Y., Ishizuka, K., Furutate, S., Abe, H., and Tsuge, T. (2015). Biosynthesis and characterization of novel poly(3-hydroxybutyrate-*co*-3-hydroxy-2-methylbutyrate): Thermal behavior associated with α-carbon methylation. *RSC Adv.* 5, 58679–58685. doi:10.1039/C5RA08003G

Wittenborn, E. C., Jost, M., Wei, Y., Stubbe, J., and Drennan, C. L. (2016). Structure of the catalytic domain of the class I polyhydroxybutyrate synthase from *Cupriavidus necator. J. Biol. Chem.* 291, 25264–25277. doi:10.1074/jbc.M116.756833

Acetobacteraceae as exopolysaccharide producers: Current state of knowledge and further perspectives

Julia Wünsche and Jochen Schmid ⓘD *

Institute for Molecular Microbiology and Biotechnology, University of Münster, Münster, Germany

Exopolysaccharides formation against harmful biotic and abiotic environmental influences is common among bacteria. By using renewable resources as a substrate, exopolysaccharides represent a sustainable alternative to fossil-based polymers as rheological modifiers in food, cosmetics, and pharmaceutical applications. The family of *Acetobacteraceae,* traditionally associated with fermented food products, has demonstrated their ability to produce a wide range of structural and functional different polymers with interesting physicochemical properties. Several strains are well known for their production of homopolysaccharides of high industrial importance, such as levan and bacterial cellulose. Moreover, some *Acetobacteraceae* are able to form acetan-like heteropolysaccharides with a high structural resemblance to xanthan. This mini review summarizes the current knowledge and recent trends in both homo- and heteropolysaccharide production by *Acetobacteraceae*.

KEYWORDS

bacterial exopolysaccharides, *Acetobacteraceae*, acetan-like biopolymers, bacterial cellulose, levan, xanthan-like biopolymers

1 Introduction

The biosynthesis of carbohydrate polymers is a common characteristic of both prokaryotic and eukaryotic organisms. Extracellularly secreted glycosides are classified as exopolysaccharides (EPS). Major functions include the protection against environmental influences such as desiccation, osmotic stress, phagocytosis, or antibiotics. Furthermore, intercellular interactions like cell recognition and surface adhesion are also promoted (Suresh Kumar et al., 2007; Corbett et al., 2010; Moradali and Rehm, 2020). EPS are known for their high diversity in terms of physicochemical and rheological properties (Hundschell and Wagemans, 2019).

EPS are either classified as homopolysaccharides or heteropolysaccharides based on their general chemical complexity. Although homopolysaccharides consist per definition of only one kind of monomer, the linkage pattern usually varies a lot resulting in branched (e.g. glycogen) and unbranched (e.g. cellulose) polymer structures. Heteropolysaccharides, on the other hand tend to have highly complex structures as they are composed of at least two different sugar moieties. Additionally, polymers can be further decorated with organic and inorganic moieties such as acetyl, pyruvyl, glyceryl, succinyl, and sulphate constituents (Sutherland, 1990; Freitas et al., 2011; Nwodo et al., 2012). Along with the conformation of

glycosidic linkages, a vast amount of potential structures emerge, giving rise to a wide range of physicochemical properties (Freitas et al., 2011).

Those variable material properties in combination with a high natural water-binding capacity are one of the main reasons for the broad commercial potential of EPS, representing an alternative to replace petrochemical polymers in current applications (Kamaruddin et al., 2021). However, only a rather limited number of microbial EPS can be regarded as industrially established, e.g. hyaluronan, xanthan, pullulan, dextran and gellan gum (Sutherland, 1998; Heinze et al., 2006; Osmałek et al., 2014; Singhsa et al., 2018; Schilling et al., 2020; Meliawati et al., 2022). Low titers and yields, as well as expensive downstream processing, result in high production costs and consequently impede the industrial establishment of new strains and polymers. Thus, EPS are up to now mainly used in high-value niche products in cosmetics, food, and pharmacy (More et al., 2021). This applies in particular to the Gram-negative *Acetobacteraceae* which are mainly known for the production of fermented food products like vinegar, kefir, or acetic acid production but have also demonstrated their ability to produce structurally different EPS with interesting physicochemical properties (La China et al., 2018).

This mini review aims to summarize the knowledge of homopolysaccharides and heteropolysaccharides production in *Acetobacteraceae* with regard to the current state of strain development, bioprocess optimization, and knowledge of rheological properties to evaluate the *status quo* and provide a further outlook on this particular group of promising biopolymers. Since the phylogenetic classification of *Acetobacteraceae* is not finalized and currently consists of 47 genera in April 2022, the classification of the original publication is used in this article (Parr et al., 2014).

2 Homopolysaccharide production in *Acetobacteraceae*

2.1 Levan

Acetobacteraceae are known for their production of high-value homopolysaccharides such as levan. Levan synthesis is widespread within the family of *Acetobacteraceae* and was reported for numerous organisms including the genera *Neoasaia*, *Kozakia*, and *Gluconobacter* (Kornmann et al., 2003; Hermann et al., 2015; Hövels et al., 2020; Anguluri et al., 2022). Its formation is catalyzed by an extracellular enzyme named levansucrase (LS, EC 2.4.1.10). By cleaving sucrose, LSs are capable of polymerizing the emerging D-fructose monomers to β-(2,6) linked polyfructans (Öner et al., 2016; Xu et al., 2019). Meanwhile, D-glucose as a sacrificial substrate is metabolized and used for bacterial growth resulting in a theoretical maximum levan yield of 0.5 g_{Lev}/g_{Suc}. Based on the evaluation of phylogenetic clades in *Acetobacteraceae*, two types of LS with different ecological relationship could be distinguished, differing in yield and molecular weight (Jakob et al., 2019). Levan is currently highly requested as a stabilizer, emulsifier, and flavor enhancing agent in food applications (Öner et al., 2016).

Up to now, investigations on levan production by *Acetobacteraceae* focused mainly on the characterization of wild-type strains which might be explained by the large number of levan-producing strains in this particular family as well as high titers already obtained under non-optimized cultivation conditions (Table 1). Comparatively low titers of 6.3 g L^{-1} and 7.3 g L^{-1} were reported for cultivations in shake flask experiments for *Gluconobacter cerinus* DSM 9533 and *Neoasaia chiangmaiensis* NBRC 101099, respectively. Slightly higher titers of 7.8 g L^{-1} were obtained under identical conditions for *Kozakia baliensis* DSM 14400 (Jakob et al., 2012). However, for all strains carbon yields remained at a low level of approximately 0.1 g_{Lev}/g_{Suc}. Anguluri et al. (2022) reported a final titer of 35.0 g L^{-1} for the same *Neoasaia chiangmaiensis* strain after increasing the final sucrose concentration up to 250 g L^{-1}. Despite increased product titers, in both studies carbon yields of only 0.10 and 0.14 g_{Lev}/g_{Suc} were achieved, respectively. For *Gluconacetobacter diazotrophicus* PA1 5 a decent titer of 24.8 g L^{-1} was obtained showing similar carbon yields (0.16 g_{Lev}/g_{Suc}). Significantly higher yields of 0.33 and 0.38 g_{Lev}/g_{Suc} were observed for the species *Acetobacter xylinum* NCIM 2526 and *Gluconobacter frateurii* TMW 2.767, respectively (Jakob et al., 2012; Semjonovs et al., 2016). Recently, *Tanticharoenia sakaeratensis* TBRC 22 was identified as a promising alternative production strain with a final levan titer of 24.7 g L^{-1} using 200 g L^{-1} sucrose as the initial substrate concentration (Aramsangtienchai et al., 2020). By plasmid-based overexpression of the native LS gene *sacB* in *Gluconobacter japonicus* LMG 2417, LS activity could be successfully increased 2.5-fold compared to the wild-type strain, resulting in higher space-time yields and titers (Hövels et al., 2020). In general, in-depth investigations on bioprocess optimization approaches for levan production in *Acetobacteraceae* seem to be rare and mainly limited to the identification of the best media compositions so far as extensively reviewed by Öner et al. (2016).

Levan formation is controlled by LS as the only enzyme in the biosynthesis process (Schmid, 2018). Depending on the available fructosyl acceptor molecule, the enzyme catalyzes hydrolysis, transfructosylation (in the presence of small oligosaccharides) and polymerization (in the presence of a increasing fructan chain) (Li et al., 2015). In consequence, defined process conditions are essential to push the reaction equilibrium towards levan formation while avoiding product degradation. Several studies in Gram-positive and Gram-negative bacteria demonstrated the importance of the right temperature settings during cultivation and the influence of metal ions, which need to be carefully determined for each LS respectively (Park et al., 2003; Rairakhwada et al., 2010; Tian et al., 2011; Belghith et al., 2012). Moreover, the optimal length of the fermentation process has to be carefully evaluated since the equilibrium naturally tends towards hydrolysis with the depletion of sucrose as the substrate during the cultivation (Chambert et al., 1974; Hernandez et al., 1995). In a recent study of Anguluri et al. (2022), the authors could show that a longer process time of 96 h resulted in a significant product decrease for *Kozakia baliensis* DSM 14400 in comparison to 48 h of cultivation. In contrast, 96 h of fermentation increased yields for *Neoasaia chiangmaiensis* NBRC 101099 by 32 %, thus underlining the need for further strain-specific bioprocess optimization approaches.

TABLE 1 Overview of homopolysaccharides producing *Acetobacteraceae*.

EPS	Strain	Titer [g·L^{-1}]	Yield [g$_{EPS}$/g$_{Sub}$]	Cultivation conditions in the selected study [g·L^{-1}]	Reference
Levan	*Gluconobacter cerinus* DSM 9533	6.3	0.08	20 sodium gluconate, 3 yeast extract, 2 peptone, 3 glycerol, 10 mannitol, 80 sucrose, pH 6.0	Jakob et al., 2012
				50 mL cultivation volume in shake flasks, 30°C, 24 h, 180 U min^{-1}	
Levan	*Neoasaia chiangmaiensis* NBRC 101099	7.3	0.09	20 sodium gluconate, 3 yeast extract, 2 peptone, 3 glycerol, 10 mannitol, 80 sucrose, pH 6.0	Jakob et al., 2012
				50 mL cultivation volume in shake flasks, 30°C, 24 h, 180 U min^{-1}	
		35.0	0.14	250 sucrose, 0.5 yeast extract, 0.5 polypeptone, 0.73 Na$_2$HPO$_4$, 0.115 citric acid, 0.05 MgSO$_4$ (%, *w/v*)	Anguluri et al., 2022
				40 mL cultivation volume in shake flasks, 30°C, 140–200 rpm	
Levan	*Kozakia baliensis* DSM 14400	7.8	0.10	20 sodium gluconate, 3 yeast extract, 2 peptone, 3 glycerol, 10 mannitol, 80 sucrose, pH 6.0	Jakob et al. (2012)
				50 mL cultivation volume in shake flasks, 30°C, 24 h, 180 U min^{-1}	
Levan	*Gluconobacter cerinus* DSM 9533	56.7	0.23	250 sucrose, 0.5 yeast extract, 0.5 polypeptone, 0.73 Na$_2$HPO$_4$, 0.115 citric acid, 0.05 MgSO4 (%, *w/v*)	Anguluri et al. (2022)
				40 mL cultivation volume in shake flasks, 30°C, 140–200 rpm	
Levan	*Gluconobacter frateurii* TMW 2.676	30.0	0.38	20 sodium gluconate, 3 yeast extract, 2 peptone, 3 glycerol, 10 mannitol, 80 sucrose, pH 6.0	Jakob et al. (2012)
				50 mL cultivation volume in shake flasks, 30°C, 24 h, 180 U min^{-1}	
Levan	*Tanticharoenia sakaeratensis* TBRC22	24.7	0.25	5 peptone, 5 NaCl, 1.5 meat extract, 1.5 yeast extract, 200 sucrose	Aramsangtienchai et al. (2020)
				5% bacterial culture, 37°C, 60 h, 180 rpm	
Levan	*Gluconacetobacter diazotrophicus* PA1 5	24.8	0.17	LGIM media with 150 sucrose, supplemented either with 3 (NH$_4$)$_2$SO$_4$ or 1.5 tryptone/yeast extract	Stephan et al. (1991), Molinari and Boiardi (2013)
				1.5 L working volume fermentation, 30°C, 15–20 L h^{-1}, pH 6.0	
Levan	*Acetobacter xylinum* NCIM 2526	13.2	0.33	40 sucrose, 20 bacteriological peptone, 1.0 (NH$_4$)$_2$SO$_4$, 1.0 KH$_2$PO$_4$, 1.0 MgSO$_4$·7H$_2$O	Srikanth et al. (2015)
				28°C, 60 h	
BC	*Gluconacetobacter sp.* RKY5	5.52	0.37	15.0 glycerol, 8.0 yeast extract, 3.0 KH$_2$PO$_4$, 3.0 acetic acid	Kim et al. (2007)
				1 L working volume in a rotary biofilm conductor, 30°C, 96 h, 15–35 rpm	
BC	*Gluconacetobacter intermedius* SNT-1	12.6	0.63	20 glucose, 5 yeast extract, 5 polypeptone, 2.75 Na$_2$HPO$_4$, 1.15 citric acid monohydrate, pH 6.0	Tyagi and Suresh (2016)
				Static conditions, 30°C, 120 h	
BC	*Gluconacetobacter xylinus* PTCC 1734	1.8	0.03	Hestrin-Schramm, Yamanaka or Zhou media with either date syrup, glucose, mannitol, sucrose, or (food-grade) sucrose	Mohammadkazemi et al., (2015)
				28°C, 168 h, 150 rpm	
		1.9	0.01	20 carbon source (glycerol, sucrose, mannitol, fructose), 5 peptone, 5 yeast extract, 2.7 Na$_2$HPO$_4$, 1.15 citric acid	Jalili Tabaii and Emtiazi, (2015)
				30 mL working volume, static cultivation, 28°C, 480 h, pH 6.0	
BC	*Gluconacetobacter xylinus* ATCC 23770	10.8	n.a.	Cotton-based waste textiles, 2.5 D-mannitol, 0.5 yeast extract, 0.3 peptone, pH 5.0 (%, *w/v*)	Hong et al., 2012
		8.3	0.66	12 wheat straw hydrolysate, 0.3 peptone, 0.5 yeast extract (%, *w/v*)	Chen et al., (2013)
				Static cultivation, 30 °C, 168 h	

TABLE 1 (*Continued*) Overview of homopolysaccharides producing *Acetobacteraceae*.

EPS	Strain	Titer [g·L⁻¹]	Yield [g_EPS/g_Sub]	Cultivation conditions in the selected study [g·L⁻¹]	Reference
BC	*Gluconacetobacter xylinus* NRRL B-42	10.0	0.5	2.0 glycerol/cane molasses, 0.5 peptone, 0.5 yeast extract, 0.27 disodium phosphate, 0.115 citric acid (%, *w/v*), pH 6.0	Vazquez et al. (2013)
				Static cultivation, 5:1 (volume flask: volume media), 28°C, 336 h, pH 5.0	
BC	*Komagataeibacter medellinensis*	3.3	0.17	1/2/3 carbon source (glucose, sucrose, fructose), 0.5 yeast extract, 0.5 peptone, 0.5 Na₂HPO₄, 0.267 citric acid (%, *w/v*)	Molina-Ramírez et al. (2017)
				100 mL working volume, static cultivation, 192 h, pH 6.0	

2.2 Bacterial cellulose

In addition, *Acetobacteraceae* are associated with the biosynthesis of β-(1,4) linked polyglucans which are referred to as bacterial cellulose (BC). Due to the absence of hemicellulose and lignin as present in its eukaryotic plant counterpart, BC is known to be of extremely high purity. Moreover, due to the lack of required energy-intensive downstream processing which is essential for plant-derived cellulose, BC typically demonstrates a low amount of inorganic impurities (Klemm et al., 2011). In applications, BC is valued for its high crystallinity and superior mechanical strength (Nakayama et al., 2004; Castro et al., 2011; Ul-Islam et al., 2012). All of these properties are highly desired in current product development and makes BC an excellent biocompatible material for pharmaceutical products. High potential is reported for wound dressing materials, drug delivery systems and packing materials (Czaja et al., 2006; Abeer et al., 2014; El-Gendi et al., 2023). In order to address this trend, current research focus on *in situ* (optimization during fermentation) and *ex situ* (optimization of existing microfibers) BC properties modifications (Stumpf et al., 2018; Cazón and Vázquez, 2021). Addition of 30% (*v/v*) aloe vera gel for instant resulted in significantly increased mechanical strength and water absorption capacity (Saibuatong and Phisalaphong, 2010).

Traditionally, BC is generated in the air-liquid interface in static fermentation processes. By accumulation on the surface, a gelatinous layer around bacterial cells is formed (Cannon and Anderson, 1991; Jonas and Farah, 1998). In consequence, maximum yields positively correlate to the surface area (Masaoka et al., 1993). However, this leads to several practical problems during production, e.g. insufficient oxygen supply and long lasting fermentations, or a barely separable mixture of biomass and polymer (Shoda and Sugano, 2005; Hsieh et al., 2016). Especially when it comes to industrial scale-up, these issues limit the economic feasibility. Production in large scale are therefore conducted in modified horizontal lift, gas lift, rotary discs and membrane bioreactors (Shi et al., 2014). Titers of 6.2 g L⁻¹ BC were achieved by using a rotary biofilm conductor with eight discs (Kim et al., 2007). However, it has to be mentioned that the optimal static process conditions are often not met completely in those set-ups.

In order to reduce manufacturing costs, optimization approaches focus nowadays more on the establishment of low-cost media and the investigation of alternative raw materials in order to replace glucose, fructose or glycerol as established substrates (Jalili Tabaii and Emtiazi, 2015; Mohammadkazemi et al., 2015;

Molina-Ramírez et al., 2017; Revin et al., 2018; Saleh et al., 2021; El-Gendi et al., 2022). Tyagi and Suresh achieved remarkable titers of 12.6 g L⁻¹ for BC with *Gluconaceteobacter intermedius* SNT1 on sugarcane molasses (Tyagi and Suresh, 2016). Numerous further publications indicate the high potential of this approach, including the redirection of waste streams and by-products of chemical processes (Hong et al., 2012; Chen et al., 2013; Vazquez et al., 2013; Barshan et al., 2019). In addition, BC can also be produced in submerge cultivation systems through agitated or aerated bioreactors with respectable titers between 15 and 20 g L⁻¹ BC (Kouda et al., 1998). However, the occurrence of unintended cellulose-deficient mutants and therefore a decline in product titers have been reported in several studies (Vandamme et al., 1998; Jung et al., 2005; Matsutani et al., 2015). Moreover, higher oxygen supply during cultivation was demonstrated to alter BC morphology towards granule and pellet formation, thus affecting material properties (Singhsa et al., 2018). Recent trends also focus on the impact of additives and co-cultivations in order to optimize both BC titers and rheological properties. Positive effects were demonstrated for pullulan, whose supplementation resulted in improved mechanical polymer properties and 4.4-fold increased BC yield (Hu et al., 2022).

Contrarily to the previously discussed levan-type polyfructans, BC biosynthesis and polymerization is more complex as it is organized in a cellulase synthase operon consisting of at least four different genes (Römling and Galperin, 2015). Several studies aimed to increase and optimize BC production on a molecular level. In order to enable metabolization of sucrose as a cheaper carbon source, a recombinant sucrose synthase was successfully expressed in *Acetobacter xylinum* BRP 2001. By this, final titers on glucose as carbon source could be doubled to 8 g L⁻¹ (Nakai et al., 1999). Furthermore, 28-fold increased BC formation was demonstrated for *Acetobacter xylinus* ITZ3 after the successful genomic integration of the β-galactosidase *lacZ*, thus adding lactose to the group of potential substrates (Battad-Bernardo et al., 2004). Heterologous expression studies might present one way to overcome the prominent issue of long lasting cultivation by *Komagataeibacter* spp. Imai et al. (2014) demonstrated BC production *via* the much faster growing *Escherichia coli* by heterologous expression of the cellulase synthase complex subunits *cesAB* as well as the cyclic-di-GMP diguanylate cylase *dgc* of *Gluconacetobacter xylinus* (Imai et al., 2014). Recently, for the first time, a CRISPR-Cas tool was successfully applied in *Komagataeibacter* spp. The study of Huang et al. (2020), used a
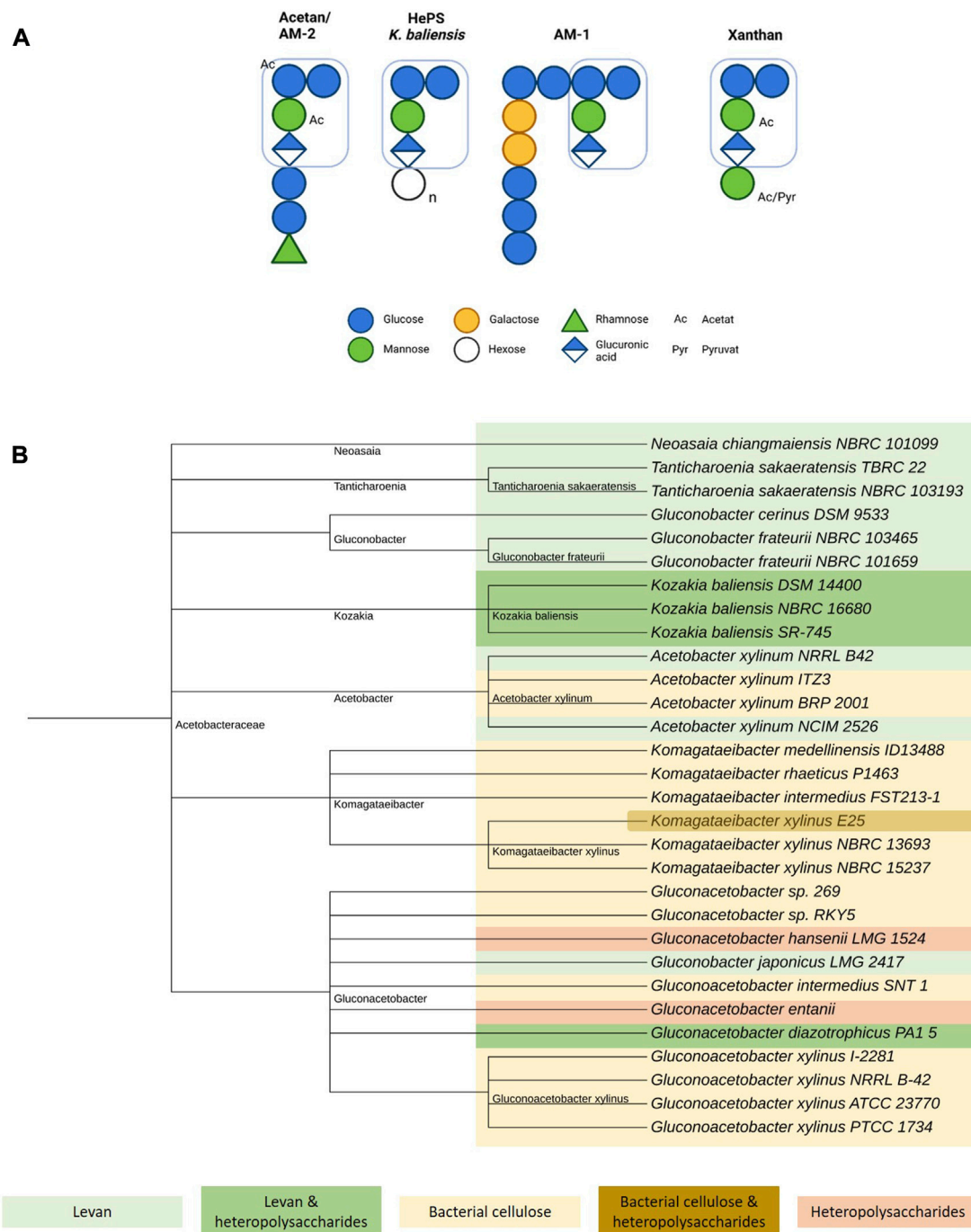
FIGURE 1
Overview of acetan-like heteropolysaccharide production in *Acetobacteraceae*. **(A)** Schematic comparison of selected acetan-like heteropolysaccharides produced by *Acetobacteraceae* including acetan, a yet unnamed heteropolysaccharide by *Kozakia baliensis*, AM-1, and xanthan (Jansson et al., 1975; Tayama et al., 1985, 1986; Edwards et al., 1999; Brandt et al., 2018). The xanthan-like core structure is marked for all polymers. Figure created with BioRender.com. **(B)** Taxonomy tree of EPS-producing *Acetobacteraceae*. Levan producing strains are marked in light green, levan and acetan-like heteropolysaccharides producing strains in dark green, bacterial cellulose producing strains in yellow, bacterial cellulose and acetan-like heteropolysaccharide producing strains in brown and only acetan-like heteropolysaccharide producing strains in light red. Figure created with iTOL (Letunic and Bork, 2021).

CRISPRi-based approach to downregulate *galU*, which controls the metabolic flux between the BC synthesis and the pentose phosphate pathway. By minimizing the expression level of *galU*, BC of higher crystallinity was obtained, although enhanced material porosity as an severe adverse effect was documented as well (Huang et al., 2020).

3 Heteropolysaccharide production in *Acetobacteraceae*

The formation of heteropolysaccharides within the family of *Acetobacteraceae* has been investigated in several publications

(Brandt et al., 2016; Škraban et al., 2018; Rath et al., 2022). Interestingly, many if not all of the yet elucidated heteropolysaccharides in this family are structural related to acetan, whose production was first described in *Acetobacter xylinum* (Figure 1). Acetan consists of a molar subunit ratio of 4 : 1 : 1 : 1 (glucose, mannose, glucuronic acid, rhamnose). In addition to the cellulose-like backbone with a trisaccharide branching sidechain at every other glucose monomer, the first two monomers of the side chain, identified as mannose and glucuronic acid, are identical in sequence and linkage pattern to the core structure of xanthan gum (Jansson et al., 1975; Couso et al., 1987). However, the further side chain composition and acetyl- and pyruvation pattern differs, giving rise to variety of structures and different rheological properties (Tayama et al., 1986; Brandt et al., 2018; Rath et al., 2022). This resemblance is also displayed by a high degree of homology between the heteropolysaccharides encoding genomic regions in *Acetobacteraceae* and the xanthan biosynthesis cluster of *Xanthomonas campestris* (Becker et al., 1998). Genetic alignments demonstrated a strong homology for *aceA* of *Acetobacter xylinum* and *gumD* from *Xanthomonas campestris*, both of these so-called priming glycosyltransferases in heteropolysaccharides synthesis initiating the assembly of the repeating unit at an undecaprenyl-pyrophosphate lipid anchor (Griffin et al., 1994; Schmid and Sieber, 2015). Moreover, a more recent study of Brandt et al. (2016) compared and confirmed homologies in the underlying heteropolysaccharides biosynthesis clusters of *Kozakia baliensis* DSM 14400 and NBRC 16680, *Gluconacetobacter diazotrophicus* PA1 5, *Komagataeibacter xylinus* E25 and *Xanthomonas campestris* ATCC 33913. Although all of the examined clusters showed high structural similarities, variations in numbers and size of the predicted genes and clusters were revealed, explaining the strain-dependent differences in the resulting polymer structures.

Xanthan gum is highly requested in industrial applications as a viscosifier due to its pseudoplastic behavior, high salt tolerance and thermostability amongst others properties (Chaturvedi et al., 2021). Similar beneficial rheological characteristics have also been described for the structure-related heteropolysaccharides of *Acetobacteraceae*, although studies in this field are rather limited. Already in 1989, the first rheological characterization of acetan was performed (Morris et al., 1989). Moreover, rheological behavior investigations of heteropolysaccharides produced by *Kozakia baliensis* confirmed pseudoplastic behavior and high viscosity (Brandt et al., 2018). Although the first results appear to be promising, further in-depth rheological studies are absolutely required in consideration of the rather insufficient data situation.

With regard to strain cultivation, respectable titers for heteropolysaccharides production in *Acetobacteraceae* wild-type strains have been reported. A titer of 5.4 g L^{-1} acetan was obtained under controlled cultivation for *Gluconoacetobacter entanii* (Velasco-Bedrán and López-Isunza, 2007). Significantly higher titers of 11.3 g L^{-1} gluconacetan were achieved for *Gluconoacetobacter xylinus* I-2281, likewise under controlled fermentation conditions in bioreactors and using fructose as the main carbon source (Kornmann et al., 2003). In a recent study based on an systematic optimization by use of experimental design, the putative gluconacetan titer for *Gluconoacetobacter* sp. could be even increased to 25.4 g L^{-1} although the parallel formation of second ribose-containing

heteropolysaccharides could not be completely precluded (Rath et al., 2022). By using glycerol as the carbon source, the authors aimed to minimize the formation and accumulation of undesirable oxidized compounds such as gluconates, which affect the pH of the fermentation broth and contaminate the final polymer. The oxidation of sugar and alcohols within the respiratory chain mechanism in the outer membrane is a characteristic feature of *Acetobacteraceae* (Adachi and Yakushi, 2016). As the formation of numerous (by-) products is a main issue for *Acetobacteraceae*, the right choice of carbon source and cultivation conditions are critical for EPS production and should be investigated further. Moreover, cultivation of *Gluconacetobacter hansenii* LMG 1524 in a media consisting of glycerol as the main carbon source and ammonium sulphate as the corresponding nitrogen source resulted in a maximum titer of 1.22 g L^{-1}, in comparison to other examined carbon and nitrogen sources variations (Valepyn et al., 2012). This once more underlines the importance of strain-dependent bioprocess optimization as the authors were also able to demonstrate that lower temperatures at 25°C and a slightly decreased pH value of 5.0 favored EPS over cell biomass production. Cultivation in the presence of two initial carbon sources (glucose and fructose) and 200 mg L^{-1} of magnesium resulted in a titer of 3.9 g L^{-1} for *Kozakia baliensis* NBRC 16680 in shake flasks (Brandt et al., 2018). Additional magnesium has previously been shown to positively affect heteropolysaccharides production in *Pseudomonadaceae* (Vargas-García et al., 2001). However, in the previously mentioned study of Brandt, significantly increased EPS production in *Kozakia baliensis* due to the presence of magnesium could not be confirmed.

4 Conclusion and further perspectives

The increasing demand for healthier and more sustainable products as driven by the customers, offers a unique chance to increase the replacement of petrol-based compounds and chemicals in a broad range of applications. Hugh potential can be assumed for EPS which possess the required material properties for usage in food, cosmetic and pharmaceutical applications. This applies especially to EPS produced by *Acetobacteraceae*, whose homopolysaccharides levan and BC have shown promising material properties. Due to their structural resemblance to xanthan, acetan-like heteropolysaccharides are also highly interesting.

However, for industrial scale-up processes and in order to enhance economic feasible production, future research must address the need for higher titers and carbon yields as well as utilization of second-generation feed stocks to produce both homopolysaccharides and heteropolysaccharides. In addition, investigation and improvement of rheological polymer properties *via* genetic engineering or fine-tuned formulations are also highly desired to promote future application development for acetan-like polymers.

Author contributions

JW: Literature research, conceptualization, visualization, writing–original draft, writing–review and editing; JS: Conceptualization, writing–review and editing, funding acquisition.

Funding

Acknowledgments

Conflict of interest

The authors declare that the research was conducted in the absence of any commercial or financial relationships that could be construed as a potential conflict of interest.

Publisher's note

All claims expressed in this article are solely those of the authors and do not necessarily represent those of their affiliated organizations, or those of the publisher, the editors and the reviewers. Any product that may be evaluated in this article, or claim that may be made by its manufacturer, is not guaranteed or endorsed by the publisher.

References

Abeer, M. M., Mohd Amin, M. C. I., and Martin, C. (2014). A review of bacterial cellulose-based drug delivery systems: Their biochemistry, current approaches and future prospects. *J. Pharm. Pharmacol.* 66, 1047–1061. doi:10.1111/jphp.12234

Adachi, O., and Yakushi, T. (2016). "Membrane-bound dehydrogenases of acetic acid bacteria," in *Acetic acid bacteria*. Editors K. Matsushita, H. Toyama, N. Tonouchi, and A. Okamoto-Kainuma (Tokyo: Springer Japan), 273–297. doi:10.1007/978-4-431-55933-7_13

Anguluri, K., La China, S., Brugnoli, M., De Vero, L., Pulvirenti, A., Cassanelli, S., et al. (2022). Candidate acetic acid bacteria strains for levan production. *Polymers* 14, 2000. doi:10.3390/polym14102000

Aramsangtienchai, P., Kongmon, T., Pechroj, S., and Srisook, K. (2020). Enhanced production and immunomodulatory activity of levan from the acetic acid bacterium, *Tanticharoenia sakaeratensis*. *Int. J. Biol. Macromol.* 163, 574–581. doi:10.1016/j.ijbiomac.2020.07.001

Barshan, S., Rezazadeh-Bari, M., Almasi, H., and Amiri, S. (2019). Optimization and characterization of bacterial cellulose produced by *Komagatacibacter xylinus* PTCC 1734 using vinasse as a cheap cultivation medium. *Int. J. Biol. Macromol.* 136, 1188–1195. doi:10.1016/j.ijbiomac.2019.06.192

Battad-Bernardo, E., McCrindle, S. L., Couperwhite, I., and Neilan, B. A. (2004). Insertion of an *E. coli lacZ* gene in *Acetobacter xylinus* for the production of cellulose in whey. *FEMS Microbiol. Lett.* 231, 253–260. doi:10.1016/S0378-1097(04)00007-2

Becker, A., Katzen, F., Pühler, A., and Ielpi, L. (1998). Xanthan gum biosynthesis and application: A biochemical/genetic perspective. *Appl. Microbiol. Biotechnol.* 50, 145–152. doi:10.1007/s002530051269

Belghith, K. S., Dahech, I., Belghith, H., and Mejdoub, H. (2012). Microbial production of levansucrase for synthesis of fructooligosaccharides and levan. *Int. J. Biol. Macromol.* 50, 451–458. doi:10.1016/j.ijbiomac.2011.12.033

Brandt, J. U., Jakob, F., Behr, J., Geissler, A. J., and Vogel, R. F. (2016). Dissection of exopolysaccharide biosynthesis in *Kozakia baliensis*. *Microb. Cell Fact.* 15, 170. doi:10.1186/s12934-016-0572-x

Brandt, J. U., Jakob, F., Wefers, D., Bunzel, M., and Vogel, R. F. (2018). Characterization of an acetan-like heteropolysaccharide produced by *Kozakia baliensis* NBRC 16680. *Int. J. Biol. Macromol.* 106, 248–257. doi:10.1016/j.ijbiomac.2017.08.022

Cannon, R. E., and Anderson, S. M. (1991). Biogenesis of bacterial cellulose. *Crit. Rev. Microbiol.* 17, 435–447. doi:10.3109/10408419109115207

Castro, C., Zuluaga, R., Putaux, J.-L., Caro, G., Mondragon, I., and Gañán, P. (2011). Structural characterization of bacterial cellulose produced by *Gluconacetobacter swingsii* sp. from Colombian agroindustrial wastes. *Carbohydr. Polym.* 84, 96–102. doi:10.1016/j.carbpol.2010.12.072

Cazón, P., and Vázquez, M. (2021). Improving bacterial cellulose films by ex-situ and in-situ modifications: A review. *Food Hydrocoll.* 113, 106514. doi:10.1016/j.foodhyd.2020.106514

Chambert, R., Treboul, G., and Dedonder, R. (1974). Kinetic studies of levansucrase of *Bacillus subtilis*. *Eur. J. Biochem.* 41, 285–300. doi:10.1111/j.1432-1033.1974.tb03269.x

Chaturvedi, S., Kulshrestha, S., Bhardwaj, K., and Jangir, R. (2021). "A review on properties and applications of xanthan gum,". *Microbial polymers*. Editors A. Vaishnav and D. K. Choudhary (Singapore: Springer Singapore), 87–107. doi:10.1007/978-981-16-0045-6_4

Chen, L., Hong, F., Yang, X., and Han, S. (2013). Biotransformation of wheat straw to bacterial cellulose and its mechanism. *Bioresour. Technol.* 135, 464–468. doi:10.1016/j.biortech.2012.10.029

Corbett, D., Hudson, T., and Roberts, I. S. (2010). "Bacterial polysaccharide capsules," in *Prokaryotic cell wall compounds*. Editors H. König, H. Claus, and A. Varma (Berlin, Heidelberg: Springer Berlin Heidelberg), 111–132. doi:10.1007/978-3-642-05062-6_3

Couso, R. O., Ielpi, L., and Dankert, M. A. (1987). A xanthan-gum-like polysaccharide from *Acetobacter xylinum*. *Microbiology* 133, 2123–2135. doi:10.1099/00221287-133-8-2123

Czaja, W., Krystynowicz, A., Bielecki, S., and Brownjr, R. (2006). Microbial cellulose—The natural power to heal wounds. *Biomaterials* 27, 145–151. doi:10.1016/j.biomaterials.2005.07.035

Edwards, K. J., Jay, A. J., Colquhoun, I. J., Morris, V. J., Gasson, M. J., and Griffin, A. M. (1999). Generation of a novel polysaccharide by inactivation of the *aceP* gene from the acetan biosynthetic pathway in *Acetobacter xylinum*. *Microbiology* 145, 1499–1506. doi:10.1099/13500872-145-6-1499

El-Gendi, H., Salama, A., El-Fakharany, E. M., and Saleh, A. K. (2023). Optimization of bacterial cellulose production from prickly pear peels and its *ex situ* impregnation with fruit byproducts for antimicrobial and strawberry packaging applications. *Carbohydr. Polym.* 302, 120383. doi:10.1016/j.carbpol.2022.120383

El-Gendi, H., Taha, T. H., Ray, J. B., and Saleh, A. K. (2022). Recent advances in bacterial cellulose: A low-cost effective production media, optimization strategies and applications. *Cellulose* 29, 7495–7533. doi:10.1007/s10570-022-04697-1

Freitas, F., Alves, V. D., and Reis, M. A. M. (2011). Advances in bacterial exopolysaccharides: From production to biotechnological applications. *Trends Biotechnol.* 29, 388–398. doi:10.1016/j.tibtech.2011.03.008

Griffin, A. M., Morris, V. J., and Gasson, M. J. (1994). Genetic analysis of the acetan biosynthetic pathway in *Acetobacter xylinum*. *Int. J. Biol. Macromol.* 16, 287–289. doi:10.1016/0141-8130(94)90057-4

Heinze, T., Liebert, T., Heublein, B., and Hornig, S. (2006). "Functional polymers based on dextran," in Polysaccharides II *advances in polymer science*. Editor D. Klemm (Germany: Springer Berlin Heidelberg), 199–291. doi:10.1007/12_100

Hermann, M., Petermeier, H., and Vogel, R. F. (2015). Development of novel sourdoughs with *in situ* formed exopolysaccharides from acetic acid bacteria. *Eur. Food Res. Technol.* 241, 185–197. doi:10.1007/s00217-015-2444-8

Hernandez, L., Arrieta, J., Menendez, C., Vazquez, R., Coego, A., Suarez, V., et al. (1995). Isolation and enzymic properties of levansucrase secreted by *Acetobacter diazotrophicus* SRT4, a bacterium associated with sugar cane. *Biochem. J.* 309, 113–118. doi:10.1042/bj3090113

Hong, F., Guo, X., Zhang, S., Han, S., Yang, G., and Jönsson, L. J. (2012). Bacterial cellulose production from cotton-based waste textiles: Enzymatic saccharification enhanced by ionic liquid pretreatment. *Bioresour. Technol.* 104, 503–508. doi:10.1016/j.biortech.2011.11.028

Hövels, M., Kosciow, K., Kniewel, J., Jakob, F., and Deppenmeier, U. (2020). High yield production of levan-type fructans by *Gluconobacter japonicus* LMG 1417. *Int. J. Biol. Macromol.* 164, 295–303. doi:10.1016/j.ijbiomac.2020.07.105

Hsieh, J.-T., Wang, M.-J., Lai, J.-T., and Liu, H.-S. (2016). A novel static cultivation of bacterial cellulose production by intermittent feeding strategy. *J. Taiwan Inst. Chem. Eng.* 63, 46–51. doi:10.1016/j.jtice.2016.03.020

Hu, H., Catchmark, J. M., and Demirci, A. (2022). Effects of pullulan additive and co-culture of *Aureobasidium pullulans* on bacterial cellulose produced by. *Komagataeibacter Hansen*. Bioprocess Biosyst. Eng. 45, 573–587. doi:10.1007/s00449-021-02680-x

Huang, L., Liu, Q., Sun, X., Li, X., Liu, M., Jia, S., et al. (2020). Tailoring bacterial cellulose structure through CRISPR interference-mediated downregulation of *galU* in *Komagataeibacter xylinus* CGMCC 2955. *Biotechnol. Bioeng.* 117, 2165–2176. doi:10.1002/bit.27351

Hundschell, C. S., and Wagemans, A. M. (2019). Rheology of common uncharged exopolysaccharides for food applications. *Curr. Opin. Food Sci.* 27, 1–7. doi:10.1016/j.cofs.2019.02.011

Imai, T., Sun, S., Horikawa, Y., Wada, M., and Sugiyama, J. (2014). Functional reconstitution of cellulose synthase in *Escherichia coli. Biomacromolecules* 15, 4206–4213. doi:10.1021/bm501217g

Jakob, F., Quintero, Y., Musacchio, A., Estrada-de los Santos, P., Hernández, L., and Vogel, R. F. (2019). Acetic acid bacteria encode two levansucrase types of different ecological relationship. *Environ. Microbiol.* 21, 4151–4165. doi:10.1111/1462-2920.14768

Jakob, F., Steger, S., and Vogel, R. F. (2012). Influence of novel fructans produced by selected acetic acid bacteria on the volume and texture of wheat breads. *Eur. Food Res. Technol.* 234, 493–499. doi:10.1007/s00217-011-1658-7

Jalili Tabaii, M., and Emtiazi, G. (2015). Comparison of bacterial cellulose production among different strains and fermented media. *Appl. Food Biotechnol.* 3. doi:10.22037/afb.v3i1.10582

Jansson, P., Kenne, L., and Lindberg, B. (1975). Structure of the extracellular polysaccharide from *Xanthomonas campestris. Carbohydr. Res.* 45, 275–282. doi:10.1016/S0008-6215(00)85885-1

Jonas, R., and Farah, L. F. (1998). Production and application of microbial cellulose. *Polym. Degrad. Stab.* 59, 101–106. doi:10.1016/S0141-3910(97)00197-3

Jung, J. Y., Park, J. K., and Chang, H. N. (2005). Bacterial cellulose production by *Gluconacetobacter hansenii* in an agitated culture without living non-cellulose producing cells. *Enzyme Microb. Technol.* 37, 347–354. doi:10.1016/j.enzmictec.2005.02.019

Kamaruddin, I., Dirpan, A., and Bastian, F. (2021). The novel trend of bacterial cellulose as biodegradable and oxygen scavenging films for food packaging application: An integrative review. *IOP Conf. Ser. Earth Environ. Sci.* 807, 022066. doi:10.1088/1755-1315/807/2/022066

Kim, Y.-J., Kim, J.-N., Wee, Y.-J., Park, D.-H., and Ryu, H.-W. (2007). Bacterial cellulose production by *Gluconacetobacter* sp. PKY5 in a rotary biofilm contactor. *Appl. Biochem. Biotechnol.* 137–140, 529–537. doi:10.1007/s12010-007-9077-8

Klemm, D., Kramer, F., Moritz, S., Lindström, T., Ankerfors, M., Gray, D., et al. (2011). Nanocelluloses: A new family of nature-based materials. *Angew. Chem. Int. Ed.* 50, 5438–5466. doi:10.1002/anie.201001273

Kornmann, H., Duboc, P., Marison, I., and von Stockar, U. (2003). Influence of nutritional factors on the nature, yield, and composition of exopolysaccharides produced by *Gluconacetobacter xylinus* I-2281. *Appl. Environ. Microbiol.* 69, 6091–6098. doi:10.1128/AEM.69.10.6091-6098.2003

Kouda, T., Naritomi, T., Yano, H., and Yoshinaga, F. (1998). Inhibitory effect of carbon dioxide on bacterial cellulose production by *Acetobacter* in agitated culture. *J. Ferment. Bioeng.* 85, 318–321. doi:10.1016/S0922-338X(97)85682-6

La China, S., Zanichelli, G., De Vero, L., and Gullo, M. (2018). Oxidative fermentations and exopolysaccharides production by acetic acid bacteria: A mini review. *Biotechnol. Lett.* 40, 1289–1302. doi:10.1007/s10529-018-2591-7

Letunic, I., and Bork, P. (2021). Interactive tree of life (iTOL) v5: An online tool for phylogenetic tree display and annotation. *Nucleic Acids Res.* 49, W293–W296. doi:10.1093/nar/gkab301

Li, W., Yu, S., Zhang, T., Jiang, B., and Mu, W. (2015). Recent novel applications of levansucrases. *Appl. Microbiol. Biotechnol.* 99, 6959–6969. doi:10.1007/s00253-015-6797-5

Masaoka, S., Ohe, T., and Sakota, N. (1993). Production of cellulose from glucose by *Acetobacter xylinum. J. Ferment. Bioeng.* 75, 18–22. doi:10.1016/0922-338X(93)90171-4

Matsutani, M., Ito, K., Azuma, Y., Ogino, H., Shirai, M., Yakushi, T., et al. (2015). Adaptive mutation related to cellulose producibility in *Komagataeibacter medellinensis* (*Gluconacetobacter xylinus*) NBRC 3288. *Appl. Microbiol. Biotechnol.* 99, 7229–7240. doi:10.1007/s00253-015-6598-x

Meliawati, M., Gansbiller, M., and Schmid, J. (2022). "Hyaluronic acid (hyaluronan)," in Microbial Production of high-value products *microbiology monographs*. Editors B. H. A. Rehm and D. Wibowo (Cham: Springer International Publishing), 159–184. doi:10.1007/978-3-031-06600-9_7

Mohammadkazemi, F., Azin, M., and Ashori, A. (2015). Production of bacterial cellulose using different carbon sources and culture media. *Carbohydr. Polym.* 117, 518–523. doi:10.1016/j.carbpol.2014.10.008

Molina-Ramírez, C., Castro, M., Osorio, M., Torres-Taborda, M., Gómez, B., Zuluaga, R., et al. (2017). Effect of different carbon sources on bacterial nanocellulose production and structure using the low pH resistant strain *komagataeibacter medellinensis. Materials* 10, 639. doi:10.3390/ma10060639

Molinari, M. L., and Boiardi, J. L. (2013). Levans production by *Gluconacetobacter diazotrophicus. Electron. J. Biotechnol.* 16. doi:10.2225/vol16-issue3-fulltext-9

Moradali, M. F., and Rehm, B. H. A. (2020). Bacterial biopolymers: From pathogenesis to advanced materials. *Nat. Rev. Microbiol.* 18, 195–210. doi:10.1038/s41579-019-0313-3

More, V. S., Ebinesar, A., Prakruthi, A., Praveen, P., Fasim, A., Rao, A., et al. (2021). "Isolation and purification of microbial exopolysaccharides and their industrial application," in *Microbial polymers*. Editors A. Vaishnav and D. K. Choudhary (Singapore: Springer Singapore), 69–86. doi:10.1007/978-981-16-0045-6_3

Morris, V. J., Brownsey, G. J., Cairns, P., Chilvers, G. R., and Miles, M. J. (1989). Molecular origins of acetan solution properties. *Int. J. Biol. Macromol.* 11, 326–328. doi:10.1016/0141-8130(89)90002-0

Nakai, T., Tonouchi, N., Konishi, T., Kojima, Y., Tsuchida, T., Yoshinaga, F., et al. (1999). Enhancement of cellulose production by expression of sucrose synthase in *Acetobacter xylinum. Proc. Natl. Acad. Sci. U.S.A.* 96, 14–18. doi:10.1073/pnas.96.1.14

Nakayama, A., Kakugo, A., Gong, J. P., Osada, Y., Takai, M., Erata, T., et al. (2004). High mechanical strength double-network hydrogel with bacterial cellulose. *Adv. Funct. Mat.* 14, 1124–1128. doi:10.1002/adfm.200305197

Nwodo, U., Green, E., and Okoh, A. (2012). Bacterial exopolysaccharides: Functionality and prospects. *IJMS* 13, 14002–14015. doi:10.3390/ijms131114002

Öner, E. T., Hernández, L., and Combie, J. (2016). Review of Levan polysaccharide: From a century of past experiences to future prospects. *Biotechnol. Adv.* 34, 827–844. doi:10.1016/j.biotechadv.2016.05.002

Osmałek, T., Froelich, A., and Tasarek, S. (2014). Application of gellan gum in pharmacy and medicine. *Int. J. Pharm.* 466, 328–340. doi:10.1016/j.ijpharm.2014.03.038

Park, H.-E., Park, N. H., Kim, M.-J., Lee, T. H., Lee, H. G., Yang, J.-Y., et al. (2003). Enzymatic synthesis of fructosyl oligosaccharides by levansucrase from *Microbacterium laevaniformans* ATCC 15953. *Enzyme Microb. Technol.* 32, 820–827. doi:10.1016/S0141-0229(03)00062-0

Parr, C. S., Wilson, N., Leary, P., Schulz, K., Lans, K., Walley, L., et al. (2014). The encyclopedia of life v2: Providing global access to knowledge about life on earth. *BDJ* 2, e1079. doi:10.3897/BDJ.2.e1079

Rairakhwada, D., Seo, J.-W., Seo, M., Kwon, O., Rhee, S.-K., and Kim, C. H. (2010). Gene cloning, characterization, and heterologous expression of levansucrase from *Bacillus amyloliquefaciens. J. Ind. Microbiol. Biotechnol.* 37, 195–204. doi:10.1007/s10295-009-0664-2

Rath, T., Rühmann, B., Schmid, J., and Sieber, V. (2022). Systematic optimization of exopolysaccharide production by *Gluconacetobacter* sp. and use of (crude) glycerol as carbon source. *Carbohydr. Polym.* 276, 118769. doi:10.1016/j.carbpol.2021.118769

Revin, V., Liyaskina, E., Nazarkina, M., Bogatyreva, A., and Shchankin, M. (2018). Cost-effective production of bacterial cellulose using acidic food industry by-products. *Braz. J. Microbiol.* 49, 151–159. doi:10.1016/j.bjm.2017.12.012

Römling, U., and Galperin, M. Y. (2015). Bacterial cellulose biosynthesis: Diversity of operons, subunits, products, and functions. *Trends Microbiol.* 23, 545–557. doi:10.1016/j.tim.2015.05.005

Saibuatong, O., and Phisalaphong, M. (2010). Novo aloe vera–bacterial cellulose composite film from biosynthesis. *Carbohydr. Polym.* 79, 455–460. doi:10.1016/j.carbpol.2009.08.039

Saleh, A. K., El-Gendi, H., Ray, J. B., and Taha, T. H. (2021). A low-cost effective media from starch kitchen waste for bacterial cellulose production and its application as simultaneous absorbance for methylene blue dye removal. *Biomass Conv. bioref.* doi:10.1007/s13399-021-01973-1

Schilling, C., Badri, A., Sieber, V., Koffas, M., and Schmid, J. (2020). Metabolic engineering for production of functional polysaccharides. *Curr. Opin. Biotechnol.* 66, 44–51. doi:10.1016/j.copbio.2020.06.010

Schmid, J. (2018). Recent insights in microbial exopolysaccharide biosynthesis and engineering strategies. *Curr. Opin. Biotechnol.* 53, 130–136. doi:10.1016/j.copbio.2018.01.005

Schmid, J., and Sieber, V. (2015). Enzymatic transformations involved in the biosynthesis of microbial exo-polysaccharides based on the assembly of repeat units. *ChemBioChem* 16, 1141–1147. doi:10.1002/cbic.201500035

Semjonovs, P., Shakirova, L., Treimane, R., Shvirksts, K., Auzina, L., Cleenwerck, I., et al. (2016). Production of extracellular fructans by *Gluconobacter nephelii* P1464. *Lett. Appl. Microbiol.* 62, 145–152. doi:10.1111/lam.12521

Shi, Z., Zhang, Y., Phillips, G. O., and Yang, G. (2014). Utilization of bacterial cellulose in food. *Food Hydrocoll.* 35, 539–545. doi:10.1016/j.foodhyd.2013.07.012

Shoda, M., and Sugano, Y. (2005). Recent advances in bacterial cellulose production. *Biotechnol. Bioprocess Eng.* 10, 1–8. doi:10.1007/BF02931175

Singhsa, P., Narain, R., and Manuspiya, H. (2018). Physical structure variations of bacterial cellulose produced by different *Komagataeibacter xylinus* strains and carbon sources in static and agitated conditions. *Cellulose* 25, 1571–1581. doi:10.1007/s10570-018-1699-1

Škraban, J., Cleenwerck, I., Vandamme, P., Fanedl, L., and Trček, J. (2018). Genome sequences and description of novel exopolysaccharides producing species *Komagataeibacter pomaceti* sp. nov. and reclassification of *Komagataeibacter kombuchae* (Dutta and Gachhui 2007). *Syst. Appl. Microbiol.* 41, 581–592. doi:10.1016/j.syapm.2018.08.006

Srikanth, R., Siddartha, G., Sundhar Reddy, C. H. S. S., Harish, B. S., Janaki Ramaiah, M., and Uppuluri, K. B. (2015). Antioxidant and anti-inflammatory levan produced from *Acetobacter xylinum* NCIM2526 and its statistical optimization. *Carbohydr. Polym.* 123, 8–16. doi:10.1016/j.carbpol.2014.12.079

Stephan, M. P., Oliveira, M., Teixeira, K. R. S., Martinez-Drets, G., and Döbereiner, J. (1991). Physiology and dinitrogen fixation of *Acetobacter diazotrophicus*. *FEMS Microbiol. Lett.* 77, 67–72. doi:10.1111/j.1574-6968.1991.tb04323.x

Stumpf, T. R., Yang, X., Zhang, J., and Cao, X. (2018). *In situ* and *ex situ* modifications of bacterial cellulose for applications in tissue engineering. *Mater. Sci. Eng. C* 82, 372–383. doi:10.1016/j.msec.2016.11.121

Suresh Kumar, A., Mody, K., and Jha, B. (2007). Bacterial exopolysaccharides – A perception. *J. Basic Microbiol.* 47, 103–117. doi:10.1002/jobm.200610203

Sutherland, I. W. (1990). *Biotechnology of microbial exopolysaccharides*. 1st ed. Cambridge: Cambridge University Press. doi:10.1017/CBO9780511525384

Sutherland, I. W. (1998). Novel and established applications of microbial polysaccharides. *Trends Biotechnol.* 16, 41–46. doi:10.1016/S0167-7799(97)01139-6

Tayama, K., Minakami, H., Entani, E., Fujiyama, S., and Masai, H. (1985). Structure of an acidic polysaccharide from *acetobacter* sp. NBI 1022. *Agric. Biol. Chem.* 49, 959–966. doi:10.1080/00021369.1985.10866836

Tayama, K., Minakami, H., Fujiyama, S., Masai, H., and Misaki, A. (1986). Structure of an acidic polysaccharide elaborated by *acetobacter* sp. NBI 1005. *Agric. Biol. Chem.* 50, 1271–1278. doi:10.1080/00021369.1986.10867547

Tian, F., Inthanavong, L., and Karboune, S. (2011). Purification and characterization of levansucrases from *Bacillus amyloliquefaciens* in intra- and extracellular forms useful for the synthesis of levan and fructooligosaccharides. *Biosci. Biotechnol. Biochem.* 75, 1929–1938. doi:10.1271/bbb.110315

Tyagi, N., and Suresh, S. (2016). Production of cellulose from sugarcane molasses using *Gluconacetobacter intermedius* SNT-1: Optimization & characterization. *J. Clean. Prod.* 112, 71–80. doi:10.1016/j.jclepro.2015.07.054

Ul-Islam, M., Khan, T., and Park, J. K. (2012). Water holding and release properties of bacterial cellulose obtained by *in situ* and *ex situ* modification. *Carbohydr. Polym.* 88, 596–603. doi:10.1016/j.carbpol.2012.01.006

Valepyn, E., Berezina, N., and Paquot, M. (2012). Optimization of production and preliminary characterization of new exopolysaccharides from *Gluconacetobacter hansenii* LMG1524. *AiM* 02, 488–496. doi:10.4236/aim.2012.24062

Vandamme, E. J., De Baets, S., Vanbaelen, A., Joris, K., and De Wulf, P. (1998). Improved production of bacterial cellulose and its application potential. *Polym. Degrad. Stab.* 59, 93–99. doi:10.1016/S0141-3910(97)00185-7

Vargas-García, M. C., López, M. J., Elorrieta, M. A., Suárez, F., and Moreno, J. (2001). Influence of nutritional and environmental factors on polysaccharide production by *Azotobacter vinelandii* cultured on 4-hydroxybenzoic acid. *J. Ind. Microbiol. Biotech.* 27, 5–10. doi:10.1038/sj.jim.7000152

Vazquez, A., Foresti, M. L., Cerrutti, P., and Galvagno, M. (2013). Bacterial cellulose from simple and low cost production media by *Gluconacetobacter xylinus*. *J. Polym. Environ.* 21, 545–554. doi:10.1007/s10924-012-0541-3

Velasco-Bedrán, H., and López-Isunza, F. (2007). The unified metabolism of *Gluconacetobacter entanii* in continuous and batch processes. *Process Biochem.* 42, 1180–1190. doi:10.1016/j.procbio.2007.05.017

Xu, W., Ni, D., Zhang, W., Guang, C., Zhang, T., and Mu, W. (2019). Recent advances in levansucrase and inulosucrase: Evolution, characteristics, and application. *Crit. Rev. Food Sci. Nutr.* 59, 3630–3647. doi:10.1080/10408398.2018.1506421

Check for updates

*CORRESPONDENCE
Sebastian L. Riedel,
✉ riedel@tu-berlin.de,
✉ sebastian.riedel@bht-berlin.de

†These authors have contributed equally
to this work and share first authorship

Tailoring the HHx monomer content of P(HB-*co*-HHx) by flexible substrate compositions: scale-up from deep-well-plates to laboratory bioreactor cultivations

Lara Santolin[1†], Isabel Thiele[1†], Peter Neubauer[1] and Sebastian L. Riedel[1,2]*

[1]Technische Universität Berlin, Institute of Biotechnology, Chair of Bioprocess Engineering, Berlin, Germany, [2]Berliner Hochschule für Technik, Department VIII – Mechanical Engineering, Event Technology and Process Engineering, Laboratory of Environmental and Bioprocess Engineering, Berlin, Germany

The enhanced material properties exhibited by the microbially synthetized polyhydroxyalkanoate (PHA) copolymer poly(hydroxybutyrate-*co*-hydroxyhexanoate) [P(HB-*co*-HHx)] evidence that this naturally biodegrading biopolymer could replace various functionalities of established petrochemical plastics. In fact, the thermal processability, toughness and degradation rate of P(HB-*co*-HHx) can be tuned by modulating its HHx molar content enabling to manufacture polymers à-la-carte. We have developed a simple batch strategy to precisely control the HHx content of P(HB-*co*-HHx) to obtain tailor-made PHAs with defined properties. By adjusting the ratio of fructose to canola oil as substrates for the cultivation of recombinant *Ralstonia eutropha* Re2058/pCB113, the molar fraction of HHx in P(HB-*co*-HHx) could be adjusted within a range of 2–17 mol% without compromising polymer yields. The chosen strategy proved to be robust from the mL-scale in deep-well-plates to 1-L batch bioreactor cultivations.

1 Introduction

From the poles to the deep ocean basins, plastic pollution has reached every remote corner of our planet. While marine and freshwater ecosystems are threatened by up to 23 million tons of plastics entering the oceans each year, the petrochemical plastics industry is thriving and plastic production could reach over 600 million tons produced by 2030 (Borelle et al., 2020; MacLeod et al., 2021). To counter this threat, legislations must be enacted to curb plastic waste generation and promote the transition to more environmentally friendly yet competitive materials (Gutschmann et al., 2022a).

A key role in this group is played by polyhydroxyalkanoates (PHAs), microbially produced bioplastics that are stored by various microorganisms from various carbon sources as energy and carbon storage compounds. The most common type of PHA is the homopolymer polyhydroxybutyrate (PHB) that was shown to degrade in various environments to CO_2 and water (Narancic and O'Connor, 2019). However, this thermoplastic is very crystalline and has a

high melting point (175°C) which is close to its degradation temperature, making the processing window too small and limiting its practical application (Noda et al., 2005). To be of a real value as replacement for commodity plastics, copolymerization of HB units with longer chain length monomers is often targeted, which reduces the melting temperature and weakens the crystalline structure by steric hindrance (Grigore et al., 2019). Poly(hydroxybutyrate-co-hydroxyhexanoate) (P(HB-co-HHx)) is one of such copolymers and, while biodegradability of PHAs in each environment is strongly affected by the monomer composition and post-processing, this copolymer also shows full biodegradability in soil and seawater (Narancic and O'Connor, 2019; Riedel and Brigham, 2020; Amasawa et al., 2021). Many efforts have been made to genetically modify the PHA operon of the model organism for PHA production, *Ralstonia eutropha,* in order to produce P(HB-co-HHx) from related carbon sources, where HHx precursors are generated from intermediates of the ß-oxidation of fatty acids, like palm oil (Budde, et al., 2011b; Riedel et al., 2014), as well as from unrelated carbon sources such as sucrose and CO_2 (Arikawa et al., 2017; Tanaka et al., 2021). The strain *R. eutropha* Re2058/pCB113 was engineered with an heterologous PHA synthase (phaC2 from *Rhodococcus aethivorans*) and an enoyl-coA hydratase (phaJ1 from *Pseudomonas aeruginosa*) to accumulate P(HB-co-HHx) when fed with raw materials containing fatty acids (Budde, et al., 2011a; Riedel et al., 2012; Saad et al., 2021; Gutschmann et al., 2022b), whereas it accumulates only PHB when fed with sugars (Santolin et al., 2021). The utilization of oily substrates by the strain is realized via the natural secretion of lipases that mediate the hydrolysis of the triacylglycerols forming natural emulsions that may also be stabilized by extracellular polysaccharides (Gutschmann et al., 2021). The great interest reported on P(HB-co-HHx) relates with the possibility of tailoring the physiochemical properties of this bioplastic targeting specific applications by adjusting the HHx molar fraction of the copolymer (Selli et al., 2022).

In the current study we report a very simple batch strategy that enabled to precisely control the HHx molar content in tailor-made P(HB-co-HHx) copolymers employing varying mixtures of fructose and canola oil with a fixed final carbon content for better comparison. An upscale of the method from the mL- to the L-scale starting in deep-well-plates and moving on to shake flasks and finally to lab-scale bioreactors proves the robustness of our approach.

2 Materials and methods

2.1 Bacterial strain

All experiments were conducted with the engineered *R. eutropha* strain Re2058/pCB113 that produces the copolymer P(HB-co-HHx) when grown on oleaginous feedstocks (Budde, et al., 2011b). The strain was stored in 20% (v v^{-1}) glycerol at −80°C.

2.2 Seed train

Tryptic soy broth (TSB) media, agar plates and mineral salt media (MSM) compositions have been described previously (Gutschmann et al., 2019). *Ralstonia eutropha* Re2058/

pCB113 was streaked from a cryoculture on a TSB agar plate and incubated for 3–4 days at 30°C. A single colony from the plate was used to inoculate 10 mL TSB using a 125-mL Ultra Yield Flask (Thomson Instrument Company, United States), equipped with an AirOtop membrane (Thomson Instrument Company, United States). TSB was always supplemented with 10 μg mL^{-1} gentamycin sulfate and 200 μg mL^{-1} kanamycin sulfate. The preculture was incubated at 30°C and 200 rpm shaking speed for approximately 17 h or until an OD_{600} of 5 was reached. The main cultures in MSM were inoculated to an initial OD_{600} of 0.05. Fructose or canola oil (Edeka Zentrale AG and Co. KG, Germany) were used as carbon sources and urea was used as the sole nitrogen source in the MSM. The explicit amounts are described in the text. All chemicals were purchased from Carl Roth GmbH and Co. KG (Germany) unless stated otherwise.

2.3 Calculation of C/N ratio

Specific carbon and nitrogen concentrations (g L^{-1}) and carbon-to-nitrogen ratios [C/N (g g^{-1})] were used for all experiments. See Supplementary Material for calculations.

2.4 Deep-well-plate cultivations

24-deep-well-plates with square shape wells and a maximum volume of 11 mL (Duetz-MTPS, Adolf Kühner AG, Switzerland) were used in this study. To ensure identical cultivation conditions for the deep-well-plate replicates, 50 mL of each media with each chosen fructose to canola oil ratio was prepared and inoculated from TSB overnight cultures (see above), and then 3 mL of culture was transferred into each of the wells. To obtain a defined and comparable canola oil concentration in the different wells, the medium was pre-emulsified with gum arabic (GA) before sterilization using an adapted method from Budde et al. (2011a): each medium was prepared by mixing the phosphate buffer, water and K_2SO_4 with the desired amount of canola oil and adding GA to a final concentration 0.3% (w v^{-1}). The mixture was homogenized with an Ultra-Turrax T25 (IKA-Werke GmbH and Co. KG, Germany) for 1 min at 8,000 rpm. After emulsifying the oil, the media was autoclaved, and the remaining media components were added from sterile stocks. GA was chosen as the emulsifier as it has been shown not to support growth of *R. eutropha* (see Supplementary Figure S1). Plates were incubated for 72 h at 30°C and 225 rpm in an orbital shaker with 50 mm amplitude. Culture volume and incubation conditions were chosen according to manufacturer's instructions to ensure sufficient oxygen supply. Biological triplicates were performed for each condition.

2.4.1 Evaluation of suitable C/N ratio
In the first series of experiments, growth at four different carbon concentrations: 0.5%, 1%, 1.5%, and 2% (w v^{-1}) of fructose and total carbon equivalent concentrations of canola oil: 0.25%, 0.5%, 0.75%, and 1% (w v^{-1}) was evaluated with a fixed amount of 0.744 g L^{-1} urea as nitrogen source, resulting in C/N ratios of about 5, 11, 17, and 22 (g g^{-1}). For increased C/N ratios of about 22, 45, 68, and 90 (g g^{-1}), the same carbon concentrations were tested with 0.186 g L^{-1} urea.

2.4.2 Evaluation of different fructose to canola oil mixtures

A regular distribution of different ratios of canola oil to fructose as well as each sole carbon source were tested to determine their effect on cell growth and PHA accumulation and composition. Seven different mixtures of fructose and canola oil, namely, 1:0, 5:1, 2:1, 1:1, 0.5:1, 0.2:1, and 0:1 [carbon ratio fructose to canola oil (g g^{-1})], all yielding a final carbon content of 5 g L^{-1} were used in combination with 0.46 g L^{-1} urea to reach the selected C/N ratio of 22 (g g^{-1}).

2.5 Shake flask cultivations

Four different mixtures of fructose and canola oil were selected from the deep-well-plate cultivations and upscaled to 100 mL cultures, applying the exact same cultivation strategy at this scale. Cultivations were performed in 500-mL DURAN baffled flasks (DWK Life Science GmbH, Germany) sealed with AirOtop membranes to ensure sufficient oxygen supply. These cultivations, performed in biological triplicates, were incubated at 30°C and 200 rpm in an orbital shaker (50 mm amplitude) for 72 h and sampling was performed every 24 h. The cultivations were then repeated doubling the amount of carbon content available to 10 g L^{-1} but maintaining the C/N ratio by also doubling the urea concentration to 0.92 g L^{-1}.

2.6 Bioreactor cultivations

P(HB-*co*-HHx) production with fructose and canola oil mixtures was upscaled to 1-L bioreactors using six Multifors2 parallel benchtop bioreactors with two six-blade Rushton impellers (Infors AG, Switzerland). The cultivation temperature was kept constant at 30°C and the pH was maintained at 6.8 ± 0.1 using 1 M H$_3$PO$_4$ and 2 M NaOH for pH control. The initial stirring speed was set to 200 rpm, whereas the initial flow rate was set to 0.05 vvm. Via an automatized cascade, aeration was increased up to 0.5 vvm and later stirring was increased up to 1,500 rpm in order to prevent DO values from dropping below 40%. Foam was mechanically broken as described previously (Riedel et al., 2012). Six different mixtures of fructose and canola oil, all yielding a final carbon content of 10 g L^{-1} and a C/N ratio of 22 (g g^{-1}) were used to produce sufficient amounts of P(HB-*co*-HHx) copolymers with varying HHx monomer content for polymer characterization.

2.7 Analytical methods

For quantification, the entire 3 mL culture was taken from the deep-well-plates at the end of the cultivations, while for cultivations in shake flasks and bioreactors, 5 mL samples were taken at each sampling point. For cell dry weight (CDW) determination the samples were collected in pre-weighed 15-mL tubes and centrifuged for 15 min and 4°C at 8,000 ×g. The pellets were washed with 3.5 mL cold deionized (DI) water and 1.5 mL cold hexane to remove residual oil and then resuspended again in 2 mL DI water, frozen at −80°C and dried for 48 h by lyophilization (Gamma 1–20, Martin Christ Gefriertrocknungsanlagen GmbH, Germany).

The PHA content and composition of the dried cells were determined using a methanolysis protocol and gas chromatography as previously described (Bartels et al., 2020). Residual cell dry weight (RCDW) was defined as CDW minus PHA content in g L^{-1}.

During bioreactor cultivations, fructose and NH$_3$ concentrations were measured from the supernatant of centrifuged samples. For fructose measurement, 750 μL of supernatant was washed twice by mixing with 750 μL of cold hexane in a 2-mL Eppendorf tube and shaking for 15 min in an overhead shaker (Rotator Drive STR4, StuartScientific, Cole-Parmer, Germany). Centrifugation was performed at 8,000 × g for 2 min and the bottom phase was collected. The washed supernatant was then filtered through an 0.2 μm PES syringe filter and fructose concentration determined via HPLC-RID. Chromatography was performed with 20 μL injection volume at 80°C for 62 min on an Agilent Hi-Plex Ca column. The eluent was DI H$_2$O with an 0.6 mL min^{-1} flux. Unfiltered and unwashed supernatant was measured using the Cedex Bio HT Analyzer (Cedex Bio HT Analyzer, Roche Diagnostics International AG, Switzerland) to determine NH$_3$ consumption.

2.8 Determination of molecular weight characteristics of the produced PHA

Molecular weight distribution of the PHA polymers was determined by size exclusion chromatography (SEC) from CDW samples as described previously (Thiele et al., 2021).

3 Results

3.1 Determination of a suitable C/N ratio in deep-well-plate cultivations

The choice of a suitable C/N ratio is crucial for matching the monomer composition of P(HB-*co*-HHx) to the substrate mixture supplied as, with excess carbon sources, only the preferred substrate will be used so that the effects of different mixing ratios will be negligible. Different C/N ratios, in the range of 5–90 (g g^{-1}) were investigated in deep-well-plates with a working volume of 3 mL and the results are shown in Figure 1.

Increasing final biomass and PHA content values were observed with increasing C/N ratios from 5 to 22 (Figures 1A, B). For fructose, no increase in these values was observed when the C/N ratio was further increased above 22 (Figure 1C), indicating that the added fructose was not consumed. In the case of canola oil (Figure 1D), a stagnation of the achieved biomass was only observed above a C/N ratio of 68 (g g^{-1}). PHA values showed, that cells growing on fructose accumulated only up to about 50 wt% of PHA, while cells growing on canola oil were able to accumulate up to 80 wt% of PHA, which explains why, with canola oil, more carbon source was consumed and final biomass values increased with increasing C/N ratios above 22 (g g^{-1}). As expected, the final CDW values were about four times higher in the first series of experiments (Figures 1A, B), where the added urea concentration was four times higher than in the second series of experiments (Figures 1C, D), with the same C/N ratio.

For the following experiments with fructose and canola oil mixtures, a C/N ratio of 22 (g g^{-1}) was chosen, as both carbon
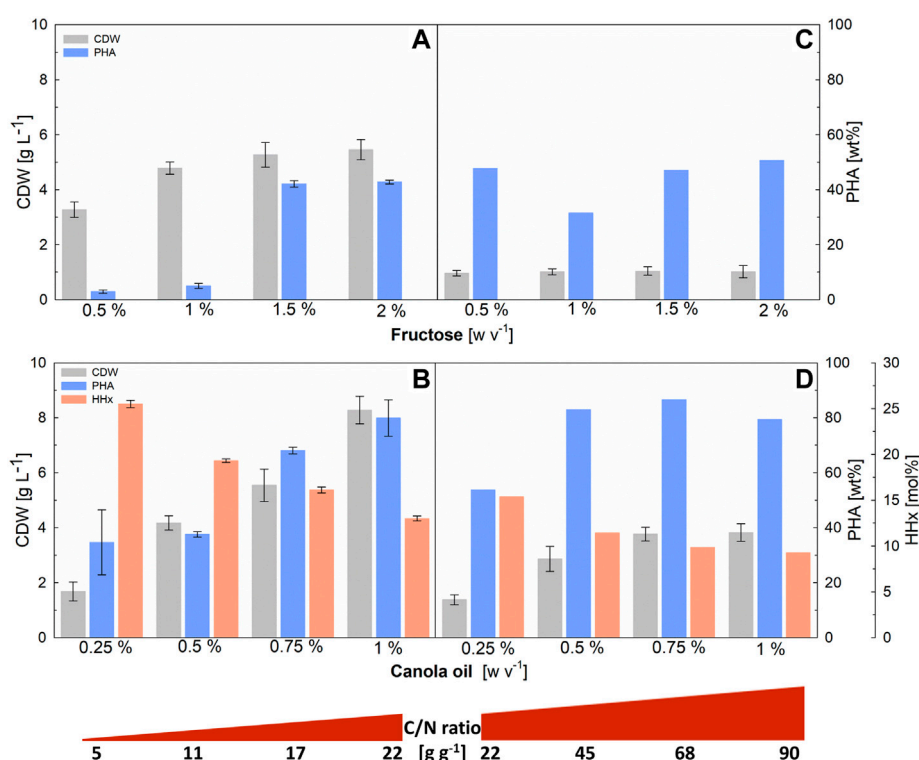
FIGURE 1
Evaluation of C/N ratios in 3-mL deep-well-plates for *R. eutropha* Re2058/pCB113 cultivations using fructose or canola oil as carbon source and urea as nitrogen source. Cell dry weight (CDW; g L^{-1}), PHA content of CDW (PHA; wt%) and HHx content of PHA (HHx; mol%) achieved after 72 h of cultivation with different C/N ratios (g g^{-1}) are shown. Left graphs show the results of low C/N ratios achieved with 0.744 g L^{-1} urea and different (w v^{-1}) concentrations of fructose **(A)** and total-carbon-equivalent canola oil concentrations **(B)**. Right graphs show the results of high C/N ratios obtained with the same fructose **(C)** and canola oil **(D)** concentrations and 0.186 g L^{-1} urea. CDW error bars indicate standard deviation from biological triplicates. PHA and HHx error bars represent standard deviation from duplicate measurements of pulled samples [in **(C,D)** the scarce amount of sample was only sufficient for a single measurement].

sources were to be completely consumed in order to determine the effects of different mixture ratios on the HHx content.

3.2 Evaluation of the impact of different mixtures of fructose and canola oil on the P(HB-*co*-HHx) composition in deep-well-plate cultivations

Seven fructose and canola oil mixtures, all with a total carbon content of 5 g L^{-1}, were used to test the effect of varying substrate ratios on the molar compositions of P(HB-*co*-HHx) in 24-deep-well-plates with a working volume of 3-mL (see Figure 2). Depending on the amount of canola oil, the HHx content increased linearly from 0 mol% when no oleaginous feedstock was available to 16 mol% with canola oil as the sole carbon source (see Supplementary Figure S2 for linear correlation). Comparable final biomass values over 4 g L^{-1} with 65–90 wt% PHA were observed with all mixtures except when fructose was supplied as the sole carbon source. With a maximum accumulation of 57 wt% PHA, the final biomass values of pure fructose cultures showed the lowest CDW accumulation.

3.3 Upscaling and optimization of mixed substrate cultivations to shake flask scale

Four of the previously tested mixtures, namely, 5:1, 1:1, 0.5:1, and 0:1 [carbon ratio fructose to canola oil (g g^{-1})], were scaled up, following the same cultivation strategy (C/N ratio and total carbon content), to 100 mL working volume in shake flask cultivations. When utilizing the same final carbon content as in deep-well-plates cultivations (5 g L^{-1}), comparable biomass values were obtained (see Supplementary Figure S3). Nevertheless, in the three mixtures with the higher canola oil contents, a decrease in the PHA content between 48–72 h was observed showing also an increased HHx content at the end of the cultivation in comparison with the previous deep-well-plate experiments. To avoid premature degradation of the PHA granules and to achieve higher final yields, it was decided to double the used carbon content to 10 g L^{-1} while maintaining the C/N ratio of 22 (g g^{-1}) (see Figure 3). With this approach, comparable results were achieved in terms of PHA content and composition as with the deep-well-plate cultivations, while the final biomass yield was approximately doubled (see Table 1).
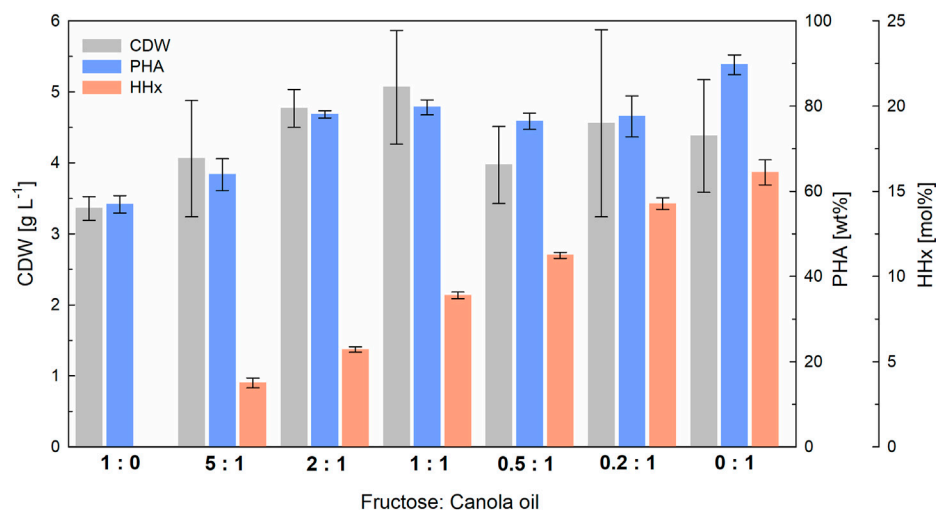
FIGURE 2
Impact of different fructose to canola oil mixture ratios on the composition of P(HB-*co*-HHx) in 3-mL deep-well-plate cultivations with *R. eutropha* Re2058/pCB113 using urea as nitrogen source. Cell dry weight (CDW; g L^{-1}), PHA content of CDW (wt%) and HHx content of PHA (mol%) achieved after 72 h with different mixtures with a final carbon content of 5 g L^{-1} and a C/N ratio of 22 g g^{-1} are displayed. The carbon ratio (g g^{-1}) of fructose to canola oil is indicated for each mixture. CDW error bars indicate standard deviation from biological triplicates. PHA and HHx error bars represent standard deviation from duplicate measurements of pulled samples.

3.4 Upscaling the production of molar-specific P(HB-*co*-HHx) to 1-L bioreactor cultivations

To demonstrate the scalability of our approach, 1-L bioreactor cultivations were carried out transferring the cultivation strategy from shake-flask cultivations (constant C/N ratio and total carbon content). Again, a linear correlation was found between the amount of canola oil and fructose used and the HHx content obtained (see Supplementary Figure S2). With final biomass values between 9–13 g L^{-1} and PHA contents between 60–88 wt%, the final yields were slightly better than in the previous shake flask cultures (Figure 4). The data showed that fructose was not consumed at least during the first 24 h of cultivation, suggesting that canola oil was consumed first, and the cells later switched to fructose as the non-preferred carbon source (Figure 5). In the three cultures with the highest fructose ratios, residual fructose concentrations were measured between 3–5 g L^{-1}, indicating that the cells would have reached slightly higher PHA contents with slightly lower HHx molar contents if the cultivations had been operated for a longer period. In these three cultures nitrogen depletion also set in later than in cultures with higher canola oil ratios (see Supplementary Figure S4).

3.5 Comparison between deep-well-plate-, shake flask- and bioreactor-scale

When comparing the final CDW values at all scales investigated, a slight increase in biomass yields was observed when moving from deep-well-plates to shake flasks and from shake flasks to bioreactor cultivations (see Table 1). Accordingly, when twice the total amount of carbon was added in the second shake flask run, the final CDWs approximately doubled. Within each scale, biomass values were

comparable throughout all mixtures, whereby the values were slightly higher with higher canola oil contents. PHA values were comparable at all scales, with a general increase in polymer accumulation (from 60%–90%) measured with increasing canola oil contents. A linear correlation between the canola oil content in each mixture and the final HHx molar content was observed at all scales (see Supplementary Figure S2) showing that it was possible to tailor P(HB-*co*-HHx) by only applying different fructose and canola oil mixtures. When higher polymer yields were obtained (shake flask with 10 g L^{-1} CC vs. shake flask with 5 g L^{-1} CC and bioreactor vs. shake flask with 10 g L^{-1} CC), slightly lower molar HHx contents were observed.

3.6 Characterization of P(HB-*co*-HHx) copolymers

Molecular weight characteristics of the produced copolymers after 72 h of cultivation in shake flask and bioreactor scale were determined by size exclusion chromatography. A decrease of the molecular weight with increasing scale was noticeable, whereas no marked decrease in M_w was observed with increasing HHx contents (Table 2). Only the shake flask cultivations containing 5 g L^{-1} carbon as substrate showed a slight decrease in the M_w of about 10% with increasing HHx molar fraction. When the final carbon content was doubled from 5–10 g L^{-1} in shake flask cultivations, a clear decrease in the final M_w, up 35% was observed. In bioreactor cultivations, where higher PHA contents per CDW were reached compared to shake flask cultivations, the lowest molecular weights around 3.5×10^5 Da were obtained. The polydispersity index Đ, around 2.5, was comparable along the scales. During bioreactor cultivations no clear decrease in the M_w was observed over time (see Supplementary Table S1).
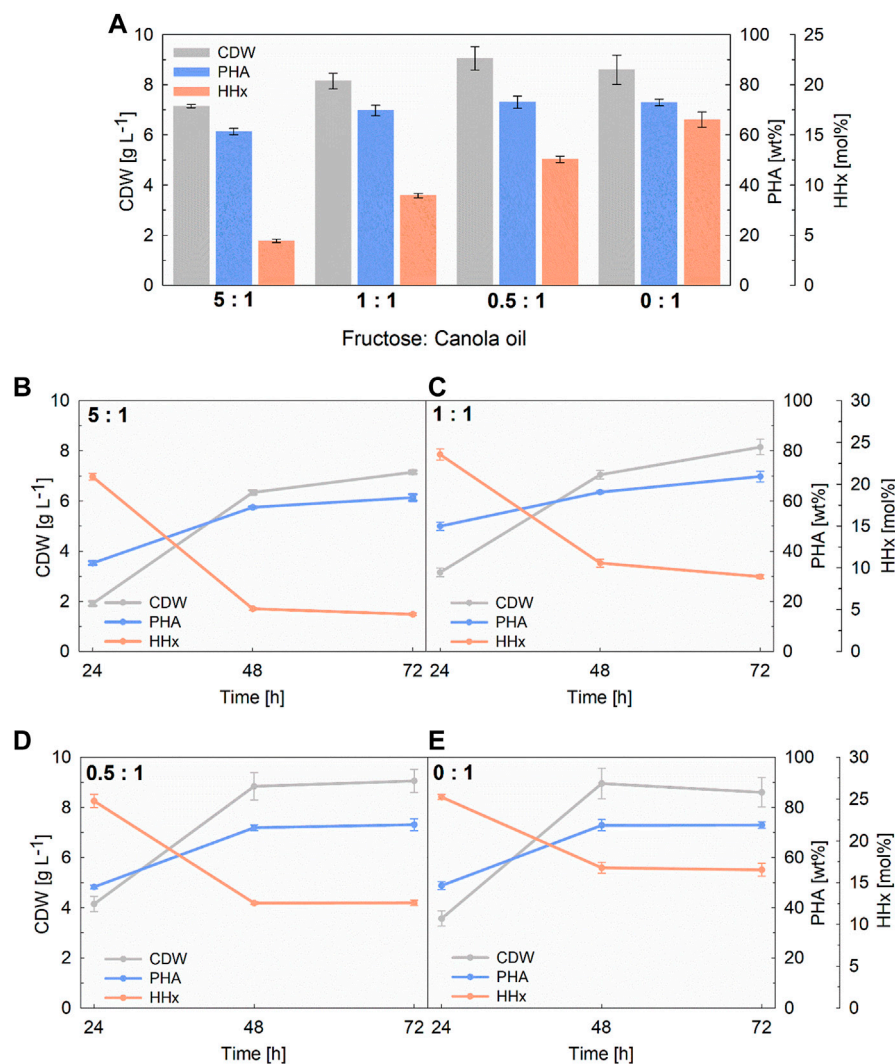
FIGURE 3
100-mL shake flask cultivations with *R. eutropha* Re2058/pCB113 using fructose and canola oil mixtures as carbon source and urea as nitrogen source. Final yields of cell dry weight (CDW; g L^{-1}), PHA content of CDW (PHA; wt%) and HHx content of PHA (HHx; mol%) after 72 h are shown in **(A)** as well as values every 24 h for each cultivation with 5: 1 **(B)**, 1: 1 **(C)**, 0.5: 1 **(D)**, and 0: 1 **(E)** fructose to canola oil ratio. All cultivations had a final carbon content of 10 g L^{-1} with a C/N ratio of 22 g g^{-1}. The carbon ratio of fructose to canola oil (g g^{-1}) is indicated for each mixture. Error bars indicate standard deviation from biological triplicates.

4 Discussion

We have developed a simple and robust batch strategy to control the molar HHx content in P(HB-*co*-HHx) from the 3-mL deep-well-plate to 1-L bioreactor scale. Since *R. eutropha* Re2058/ pCB113 produces the copolymer only when grown on oleaginous feedstocks but not when using sugars (Budde et al., 2011b), mixtures of fructose and canola oil were chosen to tune the monomer composition of P(HB-*co*-HHx). While most published studies to date vary the concentration of one substrate while using a fixed concentration of the respective sugar or oleaginous feedstock (Murugan et al., 2016; Murugan et al., 2017; Purama et al., 2018), we orientated our studies on consistently using the same total carbon content and C/N ratio for all mixtures, achieving comparable CDWs and PHA contents with all mixtures that were reproducible along all

scales (7–13 g L^{-1} CDW and 60–88 wt% PHA respectively). The strategy succeeded in tuning HHx monomer contents from 2–17 mol%, showing a linear correlation, validated at all scales, with the canola oil content in each mixture.

It has been shown that carbon sources containing a higher abundance of MCFAs (medium-chain fatty acids, 6–12 carbons) lead to a higher incorporation of HHx precursors than using plant oils holding LCFAs (long-chain fatty acids, 13–21 carbons) like canola oil as used in this study (Mifune et al., 2008; Budde et al., 2011a). Per fatty acid, only one molecule of 3HHx-CoA can be formed, thus shorter fatty acids lead to a lower ratio of 3HB-CoA to 3HHx-CoA as fewer acetyl-CoA molecules are released from β-oxidation (Riedel et al., 2014). Date seed oil with 19.1% C12:0 (lauric acid) or crude palm kernel oil (CPKO) containing 3% C8:0, 3% C10:0%, and 48% C12:0 produced P(HB-*co*-HHx) with 39 and 44 mol% HHx, respectively (Murugan

TABLE 1 Comparison of biomass, PHA content and composition obtained among all studied scales with *R. eutropha* Re2058/pCB113 using mixtures of fructose and canola oil as carbon source and urea as nitrogen source with an applied C/N ratio of 22 g g-1. For deep-well-plate cultivations, CDW measurements represent means from triplicate cultivations and PHA and HHx measurements represent means from duplicate measurements of pulled samples. For shake flask cultivations, measurements represent means of triplicate cultivations. ± are indicating standard deviation.
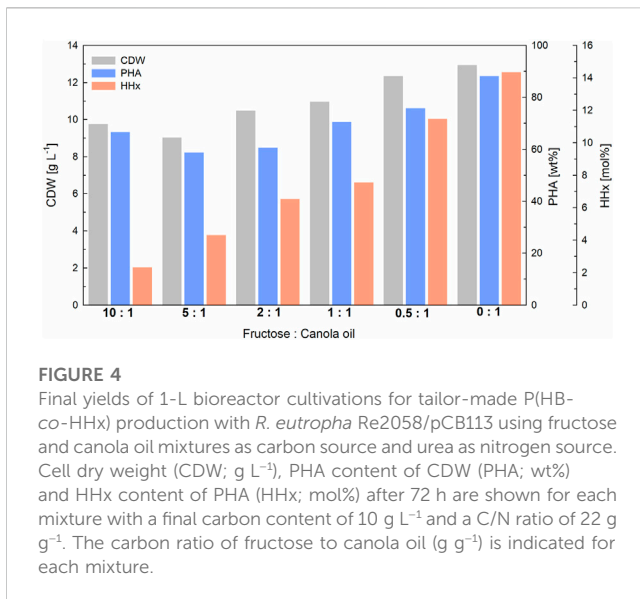
Fructose: Canola oil [g g^{-1}]	Scale	Total carbon [g L^{-1}]	CDW [g L^{-1}]	PHA [wt%]	HHx [mol%]
1: 0	3-mL deep-well-plate	5	3.4 ± 0.2	56.9 ± 2.0	0.0
10: 1	1-L bioreactor	10	9.7	66.5	2.3
5: 1	3-mL deep-well-plate	5	4.1 ± 0.8	63.9 ± 3.7	3.7 ± 0.3
	100-mL shake flask	5	3.9 ± 0.3	57.3 ± 4.7	4.1 ± 0.5
	100-mL shake flask	10	7.1 ± 0.1	61.3 ± 1.3	4.4 ± 0.2
	1-L bioreactor	10	9.0	58.6	4.3
2: 1	3-mL deep-well-plate	5	4.8 ± 0.3	78.1 ± 0.9	5.7 ± 0.2
	1-L bioreactor	10	10.5	60.4	6.5
1: 1	3-mL deep-well-plate	5	5.1 ± 0.8	79.7 ± 1.8	8.9 ± 0.2
	100-mL shake flask	5	4.6 ± 0.4	63.6 ± 2.5	9.2 ± 0.2
	100-mL shake flask	10	8.1 ± 0.3	69.7 ± 2.1	8.9 ± 0.2
	1-L bioreactor	10	10.9	70.4	7.5
0.5: 1	3-mL deep-well-plate	5	4.0 ± 0.5	76.4 ± 1.9	11.2 ± 0.2
	100-mL shake flask	5	4.7 ± 0.2	65.3 ± 3.0	14.6 ± 0.2
	100-mL shake flask	10	9.0 ± 0.5	73.1 ± 2.4	12.6 ± 0.3
	1-L bioreactor	10	12.3	75.7	11.4
0.2: 1	3-mL deep-well-plate	5	4.6 ± 1.3	77.6 ± 4.8	14.3 ± 0.7
0: 1	3-mL deep-well-plate	5	4.4 ± 0.8	89.7 ± 2.3	16.1 ± 0.7
	100-mL shake flask	5	4.0 ± 0.3	66.5 ± 2.6	21.9 ± 1.4
	100-mL shake flask	10	8.6 ± 0.6	72.9 ± 1.3	16.5 ± 0.8
	1-L bioreactor	10	12.9	88.0	14.3

et al., 2016; Purama et al., 2018). Using CPKO in combination with oil palm tree trunk sap in shake flask cultivations, Murugan et al. obtained from 31 up to 68 wt% of PHA at 4.2–7.1 g L^{-1} CDW, and comparatively higher HHx molar ratios from 14–27 mol% (Murugan et al., 2016). In a follow up study, three substrate mixtures of palm olein and fructose were chosen, to obtain P(HB-*co*-HHx) with lowered HHx contents from 4–15 mol% in bioreactor cultivations (Murugan et al., 2017). Here, the effect of increasing the sugar to oil ratio to effectively lower the HHx fraction was proved as palm tree trunk sap, containing only 17% fructose of the total sugars with a large fraction of glucose, was replaced by pure fructose. *Ralstonia eutropha* is only able to metabolize fructose and no glucose (Sichwart et al., 2011). Further, date molasses, containing over 50% fructose, and date seed oil mixtures were also used in bioreactor cultivations reaching varying CDW concentrations from 1.7–6.9 g L^{-1} CDW, up to 49 wt% of PHA and broader HHx molar ratios from 2–28 mol% (Purama et al., 2018).

All abovementioned studies, even if they achieved lower biomass yields due to the use of less urea as nitrogen source (about half of this study) and less comparability along the tested mixtures, are based on the same principle and prove that it is plausible to extend our strategy to other feedstocks. Another different approach to control the HHx

fraction of P(HB-*co*-HHx) on a molecular level was presented by controlling the expression of the *phaJ* gene of *R. eutropha*, involved in the generation of HHx precursors, showing that copolymers with HHx molar contents ranging from 2.8–10.7 mol% could be obtained (Miyahara et al., 2021). Arikawa et al. recently reported the tailored production of P(HB-*co*-HHx) with HHx contents up to 36 mol% by the deletion of the ß-ketothiolase gene together with the overexpression of the (R)-specific enoyl-Coa hydratase and PhaC synthase (Arikawa and Sato, 2022).
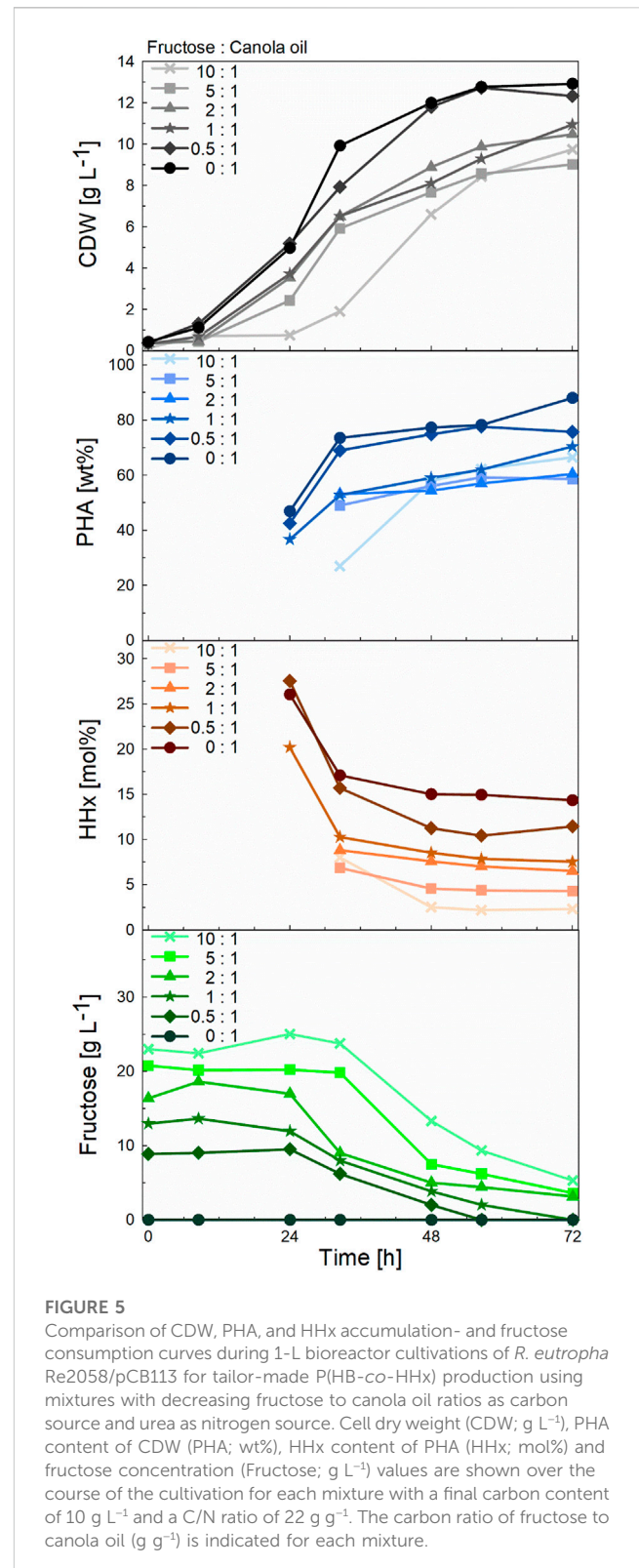
As in the studies mentioned above, an increase in the molar HHx content was observed in mixtures with increasing oleaginous substrate concentrations. Furthermore, in accordance with the literature (Budde et al., 2011a; Riedel et al., 2015), a decrease in the HHx content was measured over the course of the cultivation. Whether growing on a pure oleaginous feedstock or in combination with fructose, during the growth phase less HB precursors will be formed in comparison to the production phase as acetyl-coA flows into the TCA cycle and less HB precursors are formed. In this context, it is reported that high intracellular CoA concentrations inhibit PhaA, leading to a slower rate of HB-CoA synthesis (Oeding and Schlegel, 1973).

FIGURE 4
Final yields of 1-L bioreactor cultivations for tailor-made P(HB-*co*-HHx) production with *R. eutropha* Re2058/pCB113 using fructose and canola oil mixtures as carbon source and urea as nitrogen source. Cell dry weight (CDW; g L^{-1}), PHA content of CDW (PHA; wt%) and HHx content of PHA (HHx; mol%) after 72 h are shown for each mixture with a final carbon content of 10 g L^{-1} and a C/N ratio of 22 g g^{-1}. The carbon ratio of fructose to canola oil (g g^{-1}) is indicated for each mixture.

When PHA storage is triggered by nutrient limitation or stress conditions, more HB precursors will be incorporated into the polymer, gradually levelling off the relative concentration of HHx monomers. Additionally, oil is preferred over sugars which contributes to the higher contents of HHx at the beginning of the cultivation when this substrate is being consumed. Monitoring of the fructose concentration in the medium showed that fructose was not consumed at least in the first 24 h of cultivation, which was also observed in other studies (Murugan et al., 2017). The fact that no dissolved oxygen peak (or dropping of the stirring cascade) was observed around the timepoint when the strain started to consume fructose (data not shown) as the second preferred carbon source suggests a smooth transition from one substrate to the other with the strain presumably being able to assimilate both canola oil and fructose simultaneously.

In general, a higher PHA content of up to 88 wt% was obtained when the carbon source was of oleaginous origin, whereas only about 60 wt% PHA could be obtained with fructose alone as substrate. This is due to the fact that the utilization of fructose in this strain is less efficient than the utilization of oleaginous feedstocks. After the conversion of fructose to two pyruvate molecules via the Entner-Doudoroff pathway, one molecule of CO_2 is released for the conversion to each acetyl-CoA by the pyruvate-dehydrogenase while no carbon in the form of CO_2 is lost in the ß-oxidation of oils. In addition, the strain Re2058/pCB113 was engineered to utilize plant oils efficiently, boosting the synthesis of HHx monomers (Budde et al., 2011b).

When higher polymer yields were obtained (shake flasks with 5 g L^{-1} carbon content vs. shake flasks with 10 g L^{-1} carbon content and shake flasks with 10 g L^{-1} carbon content vs. bioreactor cultivations), slightly lower molar HHx contents were observed. This could be due to the degradation of the HB-rich polymer ends after 48 h in the first case, which was observed when only half of carbon was applied, presumably due to depletion of the carbon sources. In the second case, a faster growth in the bioreactor in comparison to the shake flasks supported by a better overall physiological state (pH- and O$_2$-control) may have

FIGURE 5
Comparison of CDW, PHA, and HHx accumulation- and fructose consumption curves during 1-L bioreactor cultivations of *R. eutropha* Re2058/pCB113 for tailor-made P(HB-*co*-HHx) production using mixtures with decreasing fructose to canola oil ratios as carbon source and urea as nitrogen source. Cell dry weight (CDW; g L^{-1}), PHA content of CDW (PHA; wt%), HHx content of PHA (HHx; mol%) and fructose concentration (Fructose; g L^{-1}) values are shown over the course of the cultivation for each mixture with a final carbon content of 10 g L^{-1} and a C/N ratio of 22 g g^{-1}. The carbon ratio of fructose to canola oil (g g^{-1}) is indicated for each mixture.

enabled the cells to further consume the fructose present in the media, leading to more HB-monomers being incorporated to the polymer chain, thus decreasing the final HHx content.

During cultivations in the bioreactor, CDW values were obtained that were higher than the theoretical yield, which

TABLE 2 Molecular weight characterization of samples after 72 h of 100-mL shake flask and 1-L bioreactor cultivations with R. eutropha Re2058/pCB113 using mixtures of fructose and canola oil and urea as nitrogen source with an applied C/N ratio of 22 g g-1. Mw = weight-average molecular weight, Mn = number-average molecular weight, Đ = polydispersity index. Measurements represent means from duplicate measurements. ± are indicating minimum and maximum values.

Fructose: Canola oil [g g^{-1}]	Scale	Total carbon [g L^{-1}]	$M_w \times 10^5$ [Da]	$M_n \times 10^5$ [Da]	Đ [-]
10: 1	1-L bioreactor	10	3.51	1.42	2.47
5: 1	100-mL shake flask	5	6.2 ± 0.1	2.5 ± 0.3	2.5 ± 0.2
	100-mL shake flask	10	4.0 ± 0.3	1.6 ± 0.2	2.5 ± 0.2
	1-L bioreactor	10	4.0 ± 0.1	1.6 ± 0.1	2.4 ± 0.0
2: 1	1-L bioreactor	10	3.2 ± 0.0	1.3 ± 0.0	2.4 ± 0.0
1: 1	100-mL shake flask	5	6.1 ± 0.1	2.8 ± 0.1	2.2 ± 0.0
	100-mL shake flask	10	4.8 ± 0.7	1.8 ± 0.1	2.6 ± 0.3
	1-L bioreactor	10	3.5 ± 0.0	1.5 ± 0.0	2.3 ± 0.0
0.5: 1	100-mL shake flask	5	5.8 ± 0.1	2.7 ± 0.1	2.2 ± 0.0
	100-mL shake flask	10	4.8 ± 0.3	2.2 ± 0.3	2.2 ± 0.2
	1-L bioreactor	10	3.6 ± 0.1	1.7 ± 0.1	2.2 ± 0.1
0: 1	100-mL shake flask	5	5.6 ± 0.1	2.5 ± 0.3	2.5 ± 0.2
	100-mL shake flask	10	4.2 ± 0.8	1.6 ± 0.9	2.1 ± 0.1
	1-L bioreactor	10	3.4 ± 0.1	1.5 ± 0.0	2.3 ± 0.0

can be explained by evaporation during sterilization of the media and thereby a concentration of the carbon sources, as well as by a slight misestimation of the carbon content of canola oil (Table 1).

In this study, no significant change in the molecular weight with different HHx fractions was observed when the carbon source concentration was 10 g L^{-1}. In the shake flask cultivation, where a lower substrate concentration of 5 g L^{-1} was used (Supplementary Figure S3), a decrease of the molecular weight of the copolymer with increasing HHx fraction was observed, contradicting the results obtained by Murugan et al. (2017) who obtained an increasing M_w. Purama et al. (2018) reported an overall decreasing trend of molecular weights between 8.3 and 5.8 × 10^5 Da with increasing HHx fractions between 5 and 28 mol%. Additionally, they observed a narrower polydispersity index of 1.7 compared to our study, which was around 2.17–2.61. Generally, the bulkier HHx is assumed to reduce the synthase turnover rate leading to lower molecular weights (Murugan et al., 2017). Moreover, when the substrate concentration was doubled, the glycerol concentration from oil cleavage by secreted lipases of *R. eutropha* also increased. Glycerol reportedly acts as a chain terminator and could thus be the cause of the lower molecular weight observed during these cultivations (Ashby et al., 2012).

5 Conclusion

The simple and robust approach presented in this study using mixtures of fructose and canola oil can be used to produce P(HB-*co*-HHx) with precisely controlled compositions. The strategy, which allows the HHx content to be adjusted between 2–17 mol%, proved to be scalable from the mL-scale in deep-well-plates to the L-scale in bioreactors. At all scales, high PHA contents of over 60 wt% were obtained with comparable molecular weight properties. However, to increase the overall yields of tailor-made P(HB-*co*-HHx), a fed-batch process needs to be developed for the different substrate mixtures.

Data availability statement

The raw data supporting the conclusion of this article will be made available by the authors, without undue reservation.

Author contributions

SR, IT, and LS contributed to the conception and design of the study. IT and LS carried out the experiments and analysis of the data. IT and LS prepared the first draft of the manuscript. SR and PN were responsible for the project administration and funding acquisition. All authors contributed to the manuscript revision, read, and approved the submitted version.

Funding

Acknowledgments

Conflict of interest

The authors declare that the research was conducted in the absence of any commercial or financial relationships that could be construed as a potential conflict of interest.

Publisher's note

All claims expressed in this article are solely those of the authors and do not necessarily represent those of their affiliated organizations, or those of the publisher, the editors and the reviewers. Any product that may be evaluated in this article, or claim that may be made by its manufacturer, is not guaranteed or endorsed by the publisher.

Supplementary material

The Supplementary Material for this article can be found online at: https://www.frontiersin.org/articles/10.3389/fbioe.2023.1081072/full#supplementary-material

References

Amasawa, E., Yamanishi, T., Nakatani, J., Hirao, M., and Sato, S. (2021). Climate change implications of bio-based and marine-biodegradable plastic: Evidence from poly (3-hydroxybutyrate-*co*-3-hydroxyhexanoate). *Environ. Sci. Technol.* 55 (5), 3380–3388. doi:10.1021/acs.est.0c06612

Arikawa, H., Matsumoto, K., and Fujiki, T. (2017). Polyhydroxyalkanoate production from sucrose by *Cupriavidus necator* strains harboring csc genes from *Escherichia coli* W. *Appl. Microbiol. Biotechnol.* 101 (20), 7497–7507. doi:10.1007/s00253-017-8470-7

Arikawa, H., and Sato, S. (2022). Impact of various ß-ketothiolase genes on PHBHHx production in *Cupriavidus necator* H16 derivatives. *Appl. Microbiol. Biotechnol.* 106, 3021–3032. doi:10.1007/s00253-022-11928-9

Ashby, R. D., Solaiman, D. K. Y., Strahan, G. D., Zhu, C., Tappel, R. C., and Nomura, C. T. (2012). Glycerine and levulinic acid: Renewable co-substrates for the fermentative synthesis of short-chain poly(hydroxyalkanoate) biopolymers. *Bioresour. Technol.* 118, 272–280. doi:10.1016/j.biortech.2012.05.092

Bartels, M., Gutschmann, B., Widmer, T., Grimm, T., Neubauer, P., and Riedel, S. L. (2020). Recovery of the PHA copolymer P(HB-*co*-HHx) with non-halogenated solvents: Influences on molecular weight and HHx-content. *Front. Bioeng. Biotechnol.* 8, 944. doi:10.3389/fbioe.2020.00944

Borelle, S. B., Ringma, J., Law, K. L., Monnahan, C. C., Lebreton, L., McGivern, A., et al. (2020). Predicted growth in plastic waste exceeds efforts to mitigate plastic pollution. *Science* 369 (6510), 1515–1518. doi:10.1126/SCIENCE.ABA3656

Budde, C. F., Riedel, S. L., Hübner, F., Risch, S., Popović, M. K., Rha, C., et al. (2011a). Growth and polyhydroxybutyrate production by *Ralstonia eutropha* in emulsified plant oil medium. *Appl. Microbiol. Biotechnol.* 89 (5), 1611–1619. doi:10.1007/s00253-011-3102-0

Budde, C. F., Riedel, S. L., Willis, L. B., Rha, C., and Sinskey, A. J. (2011b). Production of poly (3-hydroxybutyrate-*co*-3-hydroxyhexanoate) from plant oil by engineered *Ralstonia eutropha* strains. *Appl. Environ. Microbiol.* 77 (9), 2847–2854. doi:10.1128/AEM.02429-10

Grigore, M. E., Grigorescu, R. M., Iancu, L., Ion, R. M., Zaharia, C., and Andrei, E. R. (2019). Methods of synthesis, properties and biomedical applications of polyhydroxyalkanoates: A review. *J. Biomater. Sci. Polym. Ed.* 30 (9), 695–712. doi:10.1080/09205063.2019.1605866

Gutschmann, B., Bock, M. C. E., Jahns, S., Neubauer, P., Brigham, C. J., and Riedel, S. L. (2021). Untargeted metabolomics analysis of *Ralstonia eutropha* during plant oil cultivations reveals the presence of a fucose salvage pathway. *Sci. Rep.* 11 (14267), 14267. doi:10.1038/s41598-021-93720-9

Gutschmann, B., Huang, B., Santolin, L., Thiele, I., Neubauer, P., and Riedel, S. L. (2022a). Native feedstock options for the polyhydroxyalkanoate industry in europe: A review. *Microbiol. Res.* 264 (127177), 127177. doi:10.1016/j.micres.2022.127177

Gutschmann, B., Maldonado Simões, M., Schiewe, T., Schröter, E. S., Münzberg, M., Neubauer, P., et al. (2022b). Continuous feeding strategy for polyhydroxyalkanoate production from solid waste animal fat at laboratory- and pilot-scale. *Microb. Biotechnol.* 00, 295–306. doi:10.1111/1751-7915.14104

Gutschmann, B., Schiewe, T., Weiske, M. T. H., Neubauer, P., Hass, R., and Riedel, S. L. (2019). In-line monitoring of polyhydroxyalkanoate (PHA) production during high-cell-density plant oil cultivations using photon density wave spectroscopy. *Bioengineering* 6 (3), 85. doi:10.3390/bioengineering6030085

MacLeod, M., Arp, H. P. H., Tekman, M. B., and Jahnke, A. (2021). The global threat from plastic pollution. *Science* 373 (6550), 61–65. doi:10.1126/science.abg5433

Mifune, J., Nakamura, S., and Fukui, T. (2008). Targeted engineering of *Cupriavidus necator* chromosome for biosynthesis of poly(3-hydroxybutyrate-*co*-3-hydroxyhexanoate) from vegetable oil. *Can. J. Chem.* 86 (6), 621–627. doi:10.1139/V08-047

Miyahara, Y., Hiroe, A., Sato, S., Tsuge, T., and Taguchi, S. (2021). "Microbial polyhydroxyalkanoates (PHAs): From synthetic Biology to industrialization," in *Biopolymers for biomedical and biotechnological applications*. Editors B. Rehm and M. F. Moradali (Wiley Online Library, Wiley-WCH, Weinheim), 231–264. doi:10.1002/9783527818310.ch8

Murugan, P., Chhajer, P., Kosugi, A., Arai, T., Brigham, C. J., and Sudesh, K. (2016). Production of P(3HB-*co*-3HHx) with controlled compositions by recombinant *Cupriavidus necator* Re2058/pCB113 from renewable resources. *Clean. (Weinh)* 44 (9), 1234–1241. doi:10.1002/clen.201500714

Murugan, P., Gan, C. Y., and Sudesh, K. (2017). Biosynthesis of P(3HB-*co*-3HHx) with improved molecular weights from a mixture of palm olein and fructose by *Cupriavidus necator* Re2058/pCB113. *Int. J. Biol. Macromol.* 102, 1112–1119. doi:10.1016/j.ijbiomac.2017.05.006

Narancic, T., and O'Connor, K. E. (2019). Plastic waste as a global challenge: Are biodegradable plastics the answer to the plastic waste problem? *Microbiology* 165 (2), 129–137. doi:10.1099/mic.0.000749

Noda, I., Green, P. R., Satkowski, M. M., and Schechtman, L. A. (2005). Preparation and properties of a novel class of polyhydroxyalkanoate copolymers. *Biomacromolecules* 6 (2), 580–586. doi:10.1021/bm049472m

Oeding, V., and Schlegel, H. G. (1973). β-Ketothiolase from *Hydrogenomonas eutropha* H16 and its significance in the regulation of poly-β-hydroxybutyrate metabolism. *Biochem.* 134 (1), 239–248. doi:10.1042/bj1340239

Purama, R. K., Al-Sabahi, J. N., and Sudesh, K. (2018). Evaluation of date seed oil and date molasses as novel carbon sources for the production of poly(3Hydroxybutyrate-*co*-3Hydroxyhexanoate) by *Cupriavidus necator* Re2058/pCB113. *Ind. Crops Prod.* 119, 83–92. doi:10.1016/j.indcrop.2018.04.013

Riedel, S. L., Bader, J., Brigham, C. J., Budde, C. F., Yusof, Z. A. M., Rha, C., et al. (2012). Production of poly(3-hydroxybutyrate-*co*-3-hydroxyhexanoate) by *Ralstonia eutropha* in high cell density palm oil fermentations. *Biotechnol. Bioeng.* 109 (1), 74–83. doi:10.1002/bit.23283

Riedel, S. L., and Brigham, C. J. (2020). "Inexpensive and waste raw materials for PHA production," in *The handbook of polyhydroxyalkanoates*. Editor M. Koller (CRC Press Taylor and Francis Group, CRC Press, Boca Raton), 203–221. doi:10.1201/9780429296611-10

Riedel, S. L., Jahns, S., Koenig, S., Bock, M. C. E., Brigham, C. J., Bader, J., et al. (2015). Polyhydroxyalkanoates production with *Ralstonia eutropha* from low quality waste animal fats. *J. Biotechnol.* 214, 119–127. doi:10.1016/j.jbiotec.2015.09.002

Riedel, S. L., Lu, J., Stahl, U., and Brigham, C. J. (2014). Lipid and fatty acid metabolism in *Ralstonia eutropha*: Relevance for the biotechnological production of value-added products. *Appl. Microbiol. Biotechnol.* 98 (4), 1469–1483. doi:10.1007/s00253-013-5430-8

Saad, V., Gutschmann, B., Grimm, T., Widmer, T., Neubauer, P., and Riedel, S. L. (2021). Low-quality animal by-product streams for the production of PHA-biopolymers: Fats, fat/protein-emulsions and materials with high ash content as low-cost feedstocks. *Biotechnol. Lett.* 43 (3), 579–587. doi:10.1007/s10529-020-03065-y

Santolin, L., Waldburger, S., Neubauer, P., and Riedel, S. L. (2021). Substrate-flexible two-stage fed-batch cultivations for the production of the PHA copolymer P(HB-*co*-HHx) with *Cupriavidus necator* Re2058/pCB113. *Front. Bioeng. Biotechnol.* 9, 623890–623912. doi:10.3389/fbioe.2021.623890

Selli, F., Hufenus, R., Gooneie, A., Halis, U., and Perret, E. (2022). Structure – property relationship in melt-spun poly(hydroxybutyrate-*co*-3-hexanoate) monofilaments. *Polymers* 14, 200–217. doi:10.3390/polym14010200

Sichwart, S., Hetzler, S., Bröker, D., and Steinbüchel, A. (2011). Extension of the substrate utilization range of *Ralstonia eutropha* strain H16 by metabolic engineering to include mannose and glucose. *Appl. Environ. Microbiol.* 77 (4), 1325–1334. doi:10.1128/AEM.01977-10

Tanaka, K., Yoshida, K., Orita, I., and Fukui, T. (2021). Biosynthesis of poly(3-hydroxybutyrate-*co*-3-hydroxyhexanoate) from CO_2 by a recombinant *Cupriavidus necator*. *Bioengineering* 8 (11), 179–210. doi:10.3390/bioengineering8110179

Thiele, I., Rose, J. H., Gutschmann, B., Tofaily, S., Schöttel, J., and Berlin, T. U. (2021). Scale-up of the downstream process for polyhydroxyalkanoate copolymer P(HB-*co*-HHx): Extraction with nonhalogenated solvents. *J. Sib. Fed. Univ. Biol.* 14 (4), 454–464. doi:10.17516/1997-1389-0364

Enzybiotic-mediated antimicrobial functionalization of polyhydroxyalkanoates

Francisco G. Blanco[1,2], Roberto Vázquez[3†],
Ana M. Hernández-Arriaga[1,2], Pedro García[3]* and
M. Auxiliadora Prieto[1,2]*

[1]Polymer Biotechnology Group, Microbial and Plant Biotechnology Department, Margarita Salas Center for Biological Research (CIB−CSIC), Madrid, Spain, [2]Interdisciplinary Platform of Sustainable Plastics towards a Circular Economy, Spanish National Research Council (SusPlast-CSIC), Madrid, Spain, [3]Protein Engineering Against Antibiotic Resistance Group, Microbial and Plant Biotechnology Department, Margarita Salas Center for Biological Research (CIB-CSIC), Madrid, Spain

Polymeric nanoparticles (NPs) present some ideal properties as biomedical nanocarriers for targeted drug delivery such as enhanced translocation through body barriers. Biopolymers, such as polyhydroxyalkanoates (PHAs) are gaining attention as nanocarrier biomaterials due to their inherent biocompatibility, biodegradability, and ability to be vehiculized through hydrophobic media, such as the lung surfactant (LS). Upon colonization of the lung alveoli, below the LS layer, *Streptococcus pneumoniae*, causes community-acquired pneumonia, a severe respiratory condition. In this work, we convert PHA NPs into an antimicrobial material by the immobilization of an enzybiotic, an antimicrobial enzyme, via a minimal PHA affinity tag. We first produced the fusion protein M711, comprising the minimized PHA affinity tag, MinP, and the enzybiotic Cpl-711, which specifically targets *S. pneumoniae*. Then, a PHA nanoparticulate suspension with adequate physicochemical properties for pulmonary delivery was formulated, and NPs were decorated with M711. Finally, we assessed the antipneumococcal activity of the nanosystem against planktonic and biofilm forms of *S. pneumoniae*. The resulting system displayed sustained antimicrobial activity against both, free and sessile cells, confirming that tag-mediated immobilization of enzybiotics on PHAs is a promising platform for bioactive antimicrobial functionalization.

KEYWORDS

polyhydroxyalkanoates, antimicrobial nanoparticles, antimicrobial materials, enzybiotics, drug delivery

1 Introduction

Nanocarriers, or colloidal systems for therapeutic applications, play a prominent role in current biomedical research. Their most common formulation is nanoparticulate suspensions, which, due to their nano size, effectively cross different body barriers, depending on their chemical nature (Jia et al., 2020). Ideally, these biomedical nanocarriers should be biocompatible, biodegradable, with optimal bioavailability, and display sustained bioactivity over time (Li and Loh, 2017). Polymers are materials of interest in the biomedical field due to the design flexibility based on their diversity in chemical nature, synthesis methods, and functionalization approaches (Banik et al., 2016). Although initial research focused on using chemically synthesized polymers such as poly

(ε-caprolactone) or polylactic-*co*-glycolic acid (Cabeza et al., 2017; Amararathna et al., 2022), biopolymers have recently gained interest due to their inherent biocompatibility, biodegradability, and potentially sustainable production processes (Blanco et al., 2021).

Among them, polyhydroxyalkanoates (PHAs), or bacterial polyesters, have been studied for biomedical applications. They are polymers of 3-hydroxyalkanoic acids bearing a wide range of substituents, being the most common aliphatic groups (Mezzina et al., 2021). This confers the resulting polymers a relatively high hydrophobicity, which is advantageous for their vehiculization through challenging body barriers, such as the lung surfactant (Guagliardo et al., 2018; Cañadas et al., 2021). PHAs are naturally synthesized by bacteria as carbon reservoirs in the form of cytoplasmic granules (Kniewel et al., 2019). These granules are covered by a layer of granule-associated proteins (GAPs), mainly synthases, depolymerases, and phasins. The latter are surfactant proteins that coat the hydrophobic polymer, providing a compatible interface with the hydrophilic cytoplasm (Maestro and Sanz, 2017). Their surface-active properties have been extensively studied due to their ability to interact at hydrophilic-hydrophobic interfaces such as the air-water interface, the polymer-buffer interface, with bacterial lipid extracts, or with lung surfactant models (Tarazona et al., 2019a; Mato et al., 2019). These proteins, or their engineered versions, have been used as affinity tags towards PHA-based materials. For instance, a small peptide of 48 amino acids, MinP, was designed based on the binding moiety of phasin PhaF from *Pseudomonas putida*. MinP maintains the global binding capability of the whole protein (Mato et al., 2020). Phasin-mediated immobilization has been demonstrated both *in vivo*, where the PHA synthesis, protein production, and binding to the polymer take place simultaneously within the cytoplasm of the bacterial host; and *in vitro*, where proteins are immobilized onto previously formulated materials (Moldes et al., 2004; Bello-Gil et al., 2018; Mato et al., 2020). The *in vitro* approach is more suitable to ensure endotoxin removal from both the polymer and the protein when targeting biomedical applications (Dinjaski and Prieto, 2015), as well as to tightly control protein load. This approach becomes particularly challenging when the molecule to immobilize is an enzyme, which calls for orientated attachment to maintain its bioactivity. Some approaches based on other GAPs such as protein fusion with synthases and depolymerases have been developed for biomedical applications (Lee et al., 2005; Gonzalez-Miro et al., 2019). However, despite the advantages that phasin system provides, it has been scarcely applied to formulate antimicrobial materials: only one study has previously focused on phasin-mediated immobilization of antimicrobials on PHA by using phasin PhaP from *Cupriavidus necator* to immobilize an antimicrobial peptide onto a PHA polymer for wound healing (Xue et al., 2018).

Regarding antimicrobial applications, the rise of antibiotic resistance is one of the major challenges Global Health is facing in the next decades (Murray et al., 2022). This has fueled the development of new antimicrobial strategies to bypass antibiotic resistance (Rojo et al., 2022). One of such new approaches are "enzybiotics" or enzymatic antimicrobials. These antibacterial proteins are usually phage endolysins, peptidoglycan-degrading enzymes that, when exogenously applied against bacteria, produce a fast bacterial death due to cell wall disruption and subsequent osmotic shock (Murray et al., 2021). They present several advantages over antibiotics: i) activity against antibiotic-resistant strains and biofilms; ii) spontaneous resistance is less likely to occur than with antibiotics; and iii) their specificity is easily tunable by protein engineering, thereby reducing possible side effects on the healthy microbiota (Vázquez et al., 2018). However, their rather short *in vivo* half-life (20–60 min) may hamper their therapeutic use (Loeffler Jutta M. et al., 2003). Thus, the development of tailored formulations has become a hotspot to improve the therapeutic properties of this new kind of antimicrobials (De Maesschalck et al., 2020), as proved by the recent efforts towards the immobilization or encapsulation of enzybiotics (Miao et al., 2011; Nithya et al., 2018; Gondil et al., 2020; Urbanek et al., 2021; Vázquez et al., 2021). *Streptococcus pneumoniae* remains the main cause of bacterial respiratory infections in children and the elderly worldwide (Sempere et al., 2020). Its biofilm lifestyle, together with the high percentage of antibiotic-resistant strains and insufficient coverage of serotypes in vaccination, are some of the reasons behind its inclusion in the priority list for the development of antimicrobials elaborated by the World Health Organization (World Health Organization, 2017). Nevertheless, enzybiotics have proven to be a powerful tool to overcome antibiotic resistance on this pathogen (Vázquez et al., 2018).

Within this context, the aim of this work was to develop a platform for affinity immobilization of enzybiotics on PHA-based materials that allows the antimicrobial activity of the enzyme to be maintained. Thus, we fused the antipneumococcal lysin Cpl-711, a very efficient enzybiotic against this pathogen (Díez-Martínez et al., 2015), to the minimal PHA affinity tag MinP (Mato et al., 2020) and developed a procedure to immobilize such fusion protein (M711) onto preformed PHA NPs. Finally, as a proof of concept, we assessed the antipneumococcal potential of such functionalized material.

2 Materials and methods

2.1 Materials

The poly-3-hydroxyoctanoate-*co*-3-hydroxyhexanoate (hereinafter PHA) copolymer, with a respective monomer molar ratio of 94% and 6%, was kindly supplied by Bioplastech Ltd (Dublin, Ireland).

2.2 Bacterial strains, media, and growth conditions

The bacteria and plasmids used in this study are listed in Table 1. *P. putida* and *Escherichia coli* strains were grown on lysogeny broth (LB) medium at 30 or 37°C respectively, with shaking (200 rpm). Kanamycin (Km) or ampicillin (Amp) were added when needed at a final concentration of 50 µg mL^{-1} (Km) or 100 µg mL^{-1} (Amp). The PHA accumulation conditions for *P. putida* cultures were as described in (Mato et al., 2020). Briefly, the biomass from a 20 mL LB overnight culture was pelleted and washed with 120 mM NaCl, and then used to inoculate fresh 0.1 N M63 medium (with 15 mM sodium octanoate as carbon source) to an OD$_{600}$ = 0.3 (Mato et al., 2020). *S. pneumoniae* R6 was grown at 37°C without shaking in Todd-Hewitt broth (Difco, NJ,

TABLE 1 Plasmids and bacterial strains used in this study.

Plasmid	Description	Plasmid
pTRD762	pUC derivative plasmid bearing the gene encoding Cpl-711 under the control of the T7 promoter. AmpR	Díez-Martínez et al. (2015)
pFB85	pBBR1 derivative plasmid bearing the gene encoding M711 under the control of the XylS/Pm system. KmR	This study
Strain	**Description**	**Reference**
E. coli BL21 (DE3) (pTRD762)	Strain for the production of Cpl-711	Díez-Martínez et al. (2015)
E. coli BL21 (DE3) (pFB85)	Strain for the production of M711	This study
P. putida PP00_01	*P. putida* KT2440 Δ*pha*, with PP_5003 (*phaC1*) integrated at the Tn7 site, which produces bare PHA granules, without the presence of GAPs	Mato et al. (2020)
P. putida PP00_01 (pFB85)	*P. putida* PP00_01 harboring the plasmid for M711 production, which produces M711 immobilized onto PHA granules	This study
S. pneumoniae R6	Laboratory standard strain. D39 derivative (serotype 2); Non-encapsulated	Hoskins et al. (2001)
S. pneumoniae P046	*S. pneumoniae* R6 derivative, *lytA::kan lytC::ermC*. Non autolytic strain of *S. pneumoniae*	Moscoso et al. (2006)

United States of America) with 2% yeast extract. *S. pneumoniae* P046 for biofilm assays was grown in C medium (Lacks and Hotchkiss, 1960) containing 33 mM potassium phosphate buffer pH 8.0 (CpH8) at 37°C without shaking. Blood agar plates (trypticase soy agar plus 0.05% defibrinated sheep blood) were used to culture *S. pneumoniae* in solid medium. Solid media for *E. coli* and *P. putida* cultures were LB-agar plates containing the corresponding antibiotic, and incubated at 37°C or 30°C, respectively.

2.3 DNA techniques

The synthetic gene *m711*, comprising the MinP PHA affinity tag directly fused to Cpl-711 (Supplementary Figure S1A) (thus M711 chimeric protein) was purchased from ATG:Biosynthetics (Merzhausen, Germany), and cloned at the NdeI-HindIII restriction sites in a pSEVA238 expression vector (Silva-Rocha et al., 2013). The resulting vector (pFB85) was then transformed either by heat shock into *E. coli* BL21 (DE3) competent cells or by electroporation into *P. putida* PP00_01 cells according to the methods described previously (Mato et al., 2020).

2.4 Protein techniques

2.4.1 Protein production
The production of Cpl-711 or M711 was carried out by culturing the corresponding *E. coli* or *P. putida* strain and inducing at an $OD_{600} = 0.6$ by the addition of 0.5 mM isopropyl-β-d-thiogalactopyranoside (IPTG) for Cpl-711, or 1 mM 3-methylbenzoate (3-MB) for M711. Incubation was then prolonged overnight at room temperature (RT). Cells were subsequently harvested by centrifugation (10,000 × *g*, 20 min, 4°C), resuspended in the binding buffer (20 mM sodium phosphate pH 6.0, 1.5 M NaCl) with two tablets of

protease inhibitor (Roche, Switzerland) per 10 mL of resuspended culture, and disrupted three times in a French Press (at ≈ 1,000 psi). Cell lysates were clarified by centrifugation (10,000 × *g*, 20 min, 4°C) to remove cell debris, and the remaining DNA present in the lysate was further eliminated by precipitation with 4% (w/v) of streptomycin sulfate under magnetic stirring (200 rpm, 20 min, 4°C) and further centrifugation (10,000 × *g*, 20 min, 4°C).

When the production of M711 was done in *P. putida* PP00_01 (pFB85) under PHA-accumulation conditions, the procedure was the same but the binding buffer additionally contained 1.6 mM sodium dodecyl sulfate (SDS) and the cell lysates were incubated for 2 h at 30°C with shaking (200 rpm) to promote M711 detachment from the PHA granules.

2.4.2 Protein purification
Proteins were purified based on Cpl-711 affinity towards the diethylaminoethyl (DEAE) group, a structural analogue to its natural ligand, choline (Sanz et al., 1988). The clarified cell extracts were loaded onto a DEAE-Sepharose column (HiTrap DEAE FF 5 mL, GE Healthcare, United States) equilibrated with binding buffer, then were washed with the same buffer and finally eluted with elution buffer (20 mM sodium phosphate pH 6.0, 1.5 M NaCl, 4% choline). The eluted protein fractions were analyzed by SDS-PAGE (12.5%) and dialyzed against 20 mM sodium phosphate buffer pH 6.0, 150 mM NaCl. This was also the buffer in which the antibacterial activity was tested (hereinafter "activity buffer").

Protein concentrations were calculated from A_{280} with the molar extinction coefficient as predicted with ProtParam (Gasteiger et al., 2005) (126,865 $M^{-1} cm^{-1}$ for Cpl-711, and 140,845 $M^{-1} cm^{-1}$ for M711).

2.4.3 N-terminal sequencing
To verify the identity of the purified proteins, N-terminal sequencing was performed. Samples from different

M711 production culture conditions were subjected to SDS-PAGE (12.5%) and then transferred onto methanol activated - polyvinylidene fluoride (PVDF) membranes in a semidry transfer device (Biorad, CA, United States) soaked in transfer buffer (25 mM Tris, 192 mM glycine, 20% methanol, pH 8.3) for 1 h 15 min at 15 mV. The resulting transferred membranes were stained with Ponceau S stain (ThermoFisher, MA, United States), and the visible protein bands were subjected to N-terminal sequencing by Edman degradation (Edman and Begg, 1967) in a Protein sequencer (Applied Biosystems, Procise 494, CA, United States), as performed by the Protein Chemistry service from the Margarita Salas Center for Biological Research.

2.5 Preparation of PHA granules

The PHA granules from *P. putida* PP00_01 (pFB85) were isolated as previously described (Dinjaski and Prieto, 2013). Bacteria from 20 mL cultures grown overnight under PHA-accumulation conditions were harvested (12,000 x g, 20 min, 4°C), resuspended in 8 mL of 15 mM Tris-HCl pH 8.0, and disrupted twice in a French press (≈1,000 psi). The resulting suspension was centrifuged (12,000 x g, 30 min, 4°C) and the supernatant was layered over 5 mL of 55% glycerol. The suspension was centrifuged (18,000 x g, 30 min, 4°C), and the granules were isolated with a Pasteur pipette from the glycerol-buffer interface. Granules were washed twice with 15 mM Tris-HCl buffer, pH 8.0.

2.6 PHA nanoparticle procedures

2.6.1 Nanoparticle formulation

PHA solid nanoparticles (PHA NPs) were produced by the nanoprecipitation method as previously reported (Beck-Broichsitter et al., 2010). 100 mg of PHA were dissolved in 50 mL of acetone, and the solution was added dropwise onto 10 mL of distilled water placed on ice water while magnetically stirred (250 rpm). The resulting suspension was vacuum evaporated at 65°C for 5 min to remove the acetone. The PHA NPs were then leveled to 10 mL of distilled water and stored as a 10 mg mL^{-1} PHA NPs stock solution at 4°C for up to 7 days.

2.6.2 Loading M711 onto PHA NPS

To functionalize PHA NPs with M711, 100 µL of the 10 mg mL^{-1} NPs stock solution were centrifuged (13,000 x g, 30 min), resuspended in 100 µL of a 250 nM M711 solution in activity buffer, and incubated in an orbital shaker (800 rpm, 30 min). The resulting M711-NPs and protein mixture was centrifuged (13,000 x g, 30 min), washed with activity buffer, and the pellet and supernatant fractions were evaluated for protein content by SDS-PAGE (12.5%).

2.6.3 Nanoparticle characterization

The Attenuated total reflectance Fourier transform infrared spectroscopy (ATR-FTIR) spectrum was evaluated before (PHA NPs) and after protein functionalization (M711-NPs) to confirm protein incorporation. Briefly, 100 µL of PHA NPs or M711-PHA NPs were centrifuged (13,000 x g, 30 min) and freeze-dried. The lyophilized NPs were analyzed in a Perkin–Elmer (Spectrum One) spectrometer equipped with an ATR accessory. Spectra were recorded in the range from 4,000 to 400 cm−1 by 4 scans and with a resolution of 4 cm^{-1}.

The PHA NPs formulations were evaluated for their size distribution by Dynamic light scattering (DLS) in terms of hydrodynamic diameter (D_H) and polydispersity index (PDI) in the activity buffer at 25°C. Measurements were taken in a Malvern Nanosizer NanoZS (Malvern, Worcestershire, United Kingdom) equipped with a 4 mW He-Ne laser (λ = 633 nm), with a scattering angle of 173°. Likewise, the zeta (ζ)-potential was measured by laser Doppler electrophoresis (LDE) using the Zetasizer NanoZS. Each measurement was performed in triplicate. Data are presented as the mean ± standard deviation.

To evaluate the stability of the NPs functionalized with either M711 or just Cpl-711 (*i.e.*, specific binding *versus* unspecific adsorption), equimolar amounts (250 nM) of each protein were incubated with 1 mg of PHA NPs. Then, the pellet fraction after centrifugation (13,000 x g, 30 min) containing the loaded NPs, was resuspended in the activity buffer containing Triton X-100 (0.01%, 0.1% or 1%) and incubated for 2 h at RT, which has been reported as an efficient strategy for MinP release from PHA granules (14). The resulting suspensions were centrifuged (13,000 x g, 30 min) and evaluated for protein release by SDS-PAGE (12.5%).
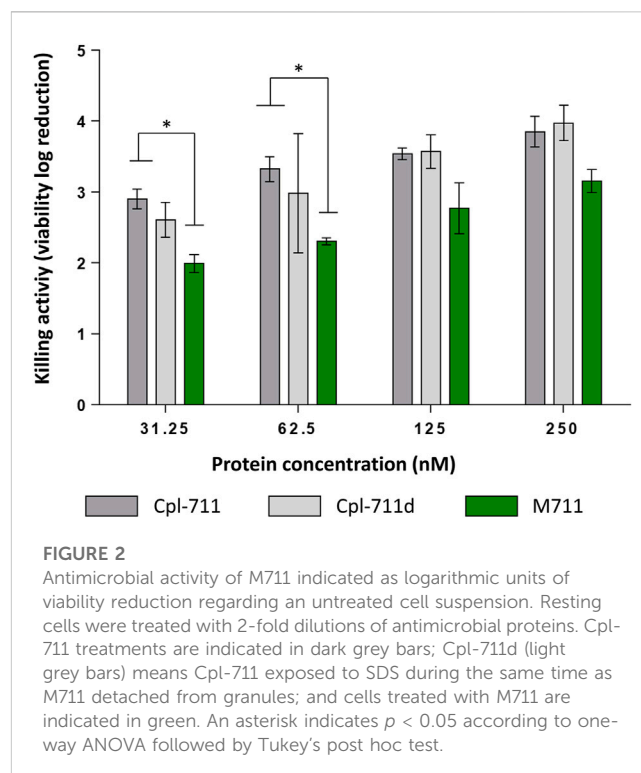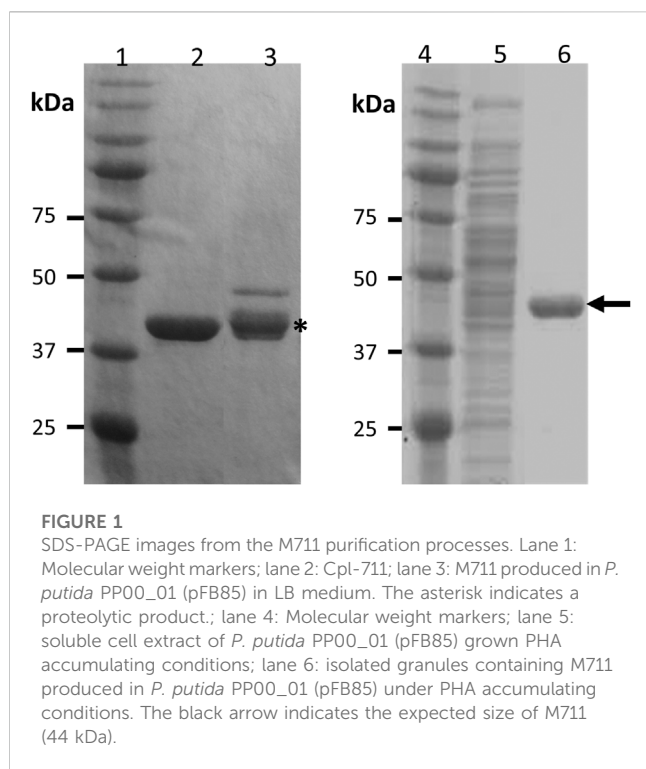
Likewise, the eventual release of M711 from the NPs was assessed by incubating M711-NPs for up to 4 h at 37°C in activity buffer, centrifuging them (13,000 x g, 30 min) and measuring protein release at the supernatant by spectrophotometry at 280 nm.

2.7 Antibacterial activity assays

2.7.1 On resting cell suspensions

Early-exponential phase cultures of *S. pneumoniae* R6 ($OD_{550} \approx$ 0.3) were centrifuged (2,100 x g, 20 min, 4°C), washed, and resuspended in half the initial volume of activity buffer. 180 µL of this resting cell suspension was added to each well in a microtiter plate and then mixed with 20 µL of a protein solution (M711 or Cpl-711) at the desired concentrations or just activity buffer. The plate was incubated at 37°C and OD_{550} was monitored for 1 h with a VersaMax microplate absorbance reader (Molecular Devices, CA, United States). After the incubation time, viable bacterial cell counts were performed by 10-fold serial diluting in activity buffer and plating onto blood agar plates.

Alternatively, the antibacterial activity of NPs formulations was assayed in test tubes by mixing 900 µL of the *S. pneumoniae* P046 resting cells prepared as described in the previous paragraph with 100 µL of i) activity buffer; ii) PHA NPs; iii) M711-loaded PHA NPs (M711-NPs); or iv) equimolar amount of free M711. The tubes were then incubated at 37°C for 4 h and samples were taken every hour to perform viable cell counts. All samples were also observed under the microscope after staining with BacLight LIVE/DEAD kit (Invitrogen, MA, United States) according to the manufacturer's instructions, in an epifluorescence microscope Leica DM4 B (Wetzlar, Germany) using a ×100 phase-contrast

FIGURE 1
SDS-PAGE images from the M711 purification processes. Lane 1: Molecular weight markers; lane 2: Cpl-711; lane 3: M711 produced in *P. putida* PP00_01 (pFB85) in LB medium. The asterisk indicates a proteolytic product.; lane 4: Molecular weight markers; lane 5: soluble cell extract of *P. putida* PP00_01 (pFB85) grown PHA accumulating conditions; lane 6: isolated granules containing M711 produced in *P. putida* PP00_01 (pFB85) under PHA accumulating conditions. The black arrow indicates the expected size of M711 (44 kDa).

FIGURE 2
Antimicrobial activity of M711 indicated as logarithmic units of viability reduction regarding an untreated cell suspension. Resting cells were treated with 2-fold dilutions of antimicrobial proteins. Cpl-711 treatments are indicated in dark grey bars; Cpl-711d (light grey bars) means Cpl-711 exposed to SDS during the same time as M711 detached from granules; and cells treated with M711 are indicated in green. An asterisk indicates $p < 0.05$ according to one-way ANOVA followed by Tukey's post hoc test.

objective, a Lumencor light source and an L5 filter system for green fluorescence observation. Images were analyzed using LAS X software from Leica.

2.7.2 On biofilm

To pre-form *S. pneumoniae* P046 biofilms, this strain was grown in CpH8 medium to $OD_{550} \approx 0.5–0.6$ ($\approx 10^8$ CFU mL^{-1}) and 100-fold diluted in CpH8 medium. 200 μL aliquots of this dilution were added into each well of 96-well polystyrene plates (Costar 3,595, Corning, NY, United States). These cultures were then statically incubated for 16 h at 37°C to allow the biofilms to form. After that time, the planktonic cells were aspirated and the OD_{550} corresponding to the total growth was measured using a microtiter plate reader (Molecular Devices, CA, United States). To evaluate the biofilm disaggregation activity of the loaded NPs, a crystal violet (CV) quantification assay was used (Domenech et al., 2015). The biofilms were thoroughly washed with activity buffer, and the remaining sessile cells were then incubated for 4 h at 37°C with different treatments in activity buffer: PHA NPs, M711-NPs, 250 nM M711, or just buffer as a control. Following the disaggregation treatment, the planktonic fraction was removed and the remaining biofilm was stained with 50 μL CV (1% w/V) for 15 min, rinsed twice with 200 μL of water, and finally solubilized with 200 μL 95% ethanol. The resulting CV suspension was measured at OD_{595} to evaluate the remaining biofilm. Viable cells were quantified from mechanically disaggregated biofilms in unstained wells.

Alternatively, antibiofilm activity was observed by Confocal Laser Scanning Microscopy (CLSM) (42). In this case, biofilms were grown on glass-bottomed dishes (WillCo-dish; WillCo Wells B.V., Netherlands) using the same conditions as specified

before. After incubation, the supernatant was removed, and the treatments were applied in a total volume of 1 mL. CLSM observations were done after LIVE/DEAD BacLight staining with a Leica spectral SP8 confocal microscope and analyzed with the LAS X software. Images represent the x–z projections from XZY stacks at 5-μm intervals planes.
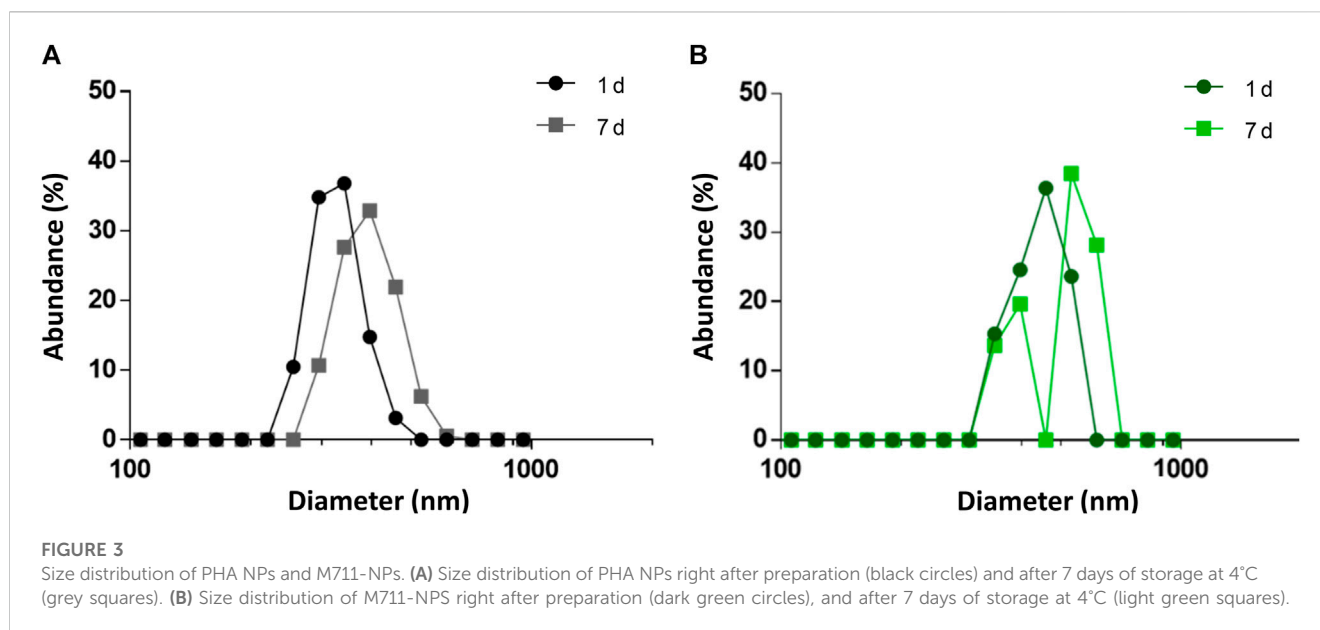
2.8 Statistical analysis

Data were obtained from, at least, three independent experiments. One-way ANOVA followed by Tukey's *post hoc* test was used for multiple comparisons as implemented in GraphPad InStat version 8.0. We indicate significant differences as $p < 0.05$ (*), $p < 0.01$ (**), and $p < 0.001$ (***).

3 Results and discussion

3.1 Soluble production and antimicrobial characterization of the tagged enzybiotic M711
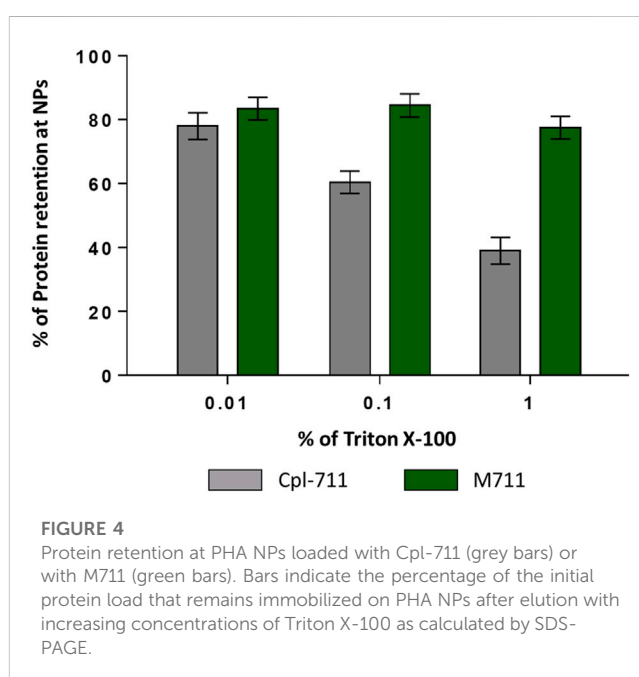
A transcriptional fusion between the PHA affinity tag MinP (Mato et al., 2020) and Cpl-711 (Díez-Martínez et al., 2015) was designed (termed M711) to produce an antipneumococcal protein able to bind to PHA-based materials while remaining functional (Supplementary Figure S1). The new fusion protein (M711) was expressed either in *E. coli* BL21 (DE3) or *P. putida* PP00_01 from pFB85 (Table 1). When expressed from any of the hosts in rich medium (LB), the subsequently purified fractions showed two

FIGURE 3
Size distribution of PHA NPs and M711-NPs. **(A)** Size distribution of PHA NPs right after preparation (black circles) and after 7 days of storage at 4°C (grey squares). **(B)** Size distribution of M711-NPS right after preparation (dark green circles), and after 7 days of storage at 4°C (light green squares).

bands on SDS-PAGE (Figure 1, lane 4). In neither *P. putida* nor *E. coli* did the lower band correspond to the expected size of M711 (43 kDa), but rather to an approximately 40 kDa truncated protein. To identify this product, this lower band was subjected to N-terminal sequencing. The resulting N-terminal amino acid sequence (LVKLE) did not correspond to the expected N-terminus of M711 (MAGKK) but to the C-terminus of the MinP moiety plus the first 3 amino acids of the linker sequence (Supplementary Figure S1B), indicating proteolytic degradation. To prevent this proteolysis, M711 was expressed in *P. putida* PP00_01 under PHA accumulation conditions to associate the MinP-tagged protein onto the granules concomitantly to its synthesis. In this way, the expressed protein would be expected to immediately bind the granules, so then it would remain protected from the potential protease activity. Using this approach, a single band was obtained, and its N-terminal sequence was as expected for M711 minus the processed first methionine (AGKKN, Figure 1, lane 2). This demonstrates direct protein immobilization onto PHA as a powerful tool for the expression of labile proteins.

The protein immobilized onto *P. putida* PHA granules was released by incubating cell extracts with SDS detergent (1.6 mM). In this way, a soluble, full version of M711 was obtained to later be bound to NPs formulated *in vitro*. The released protein was purified by affinity chromatography on a DEAE-Sepharose column (see *Materials and methods*).
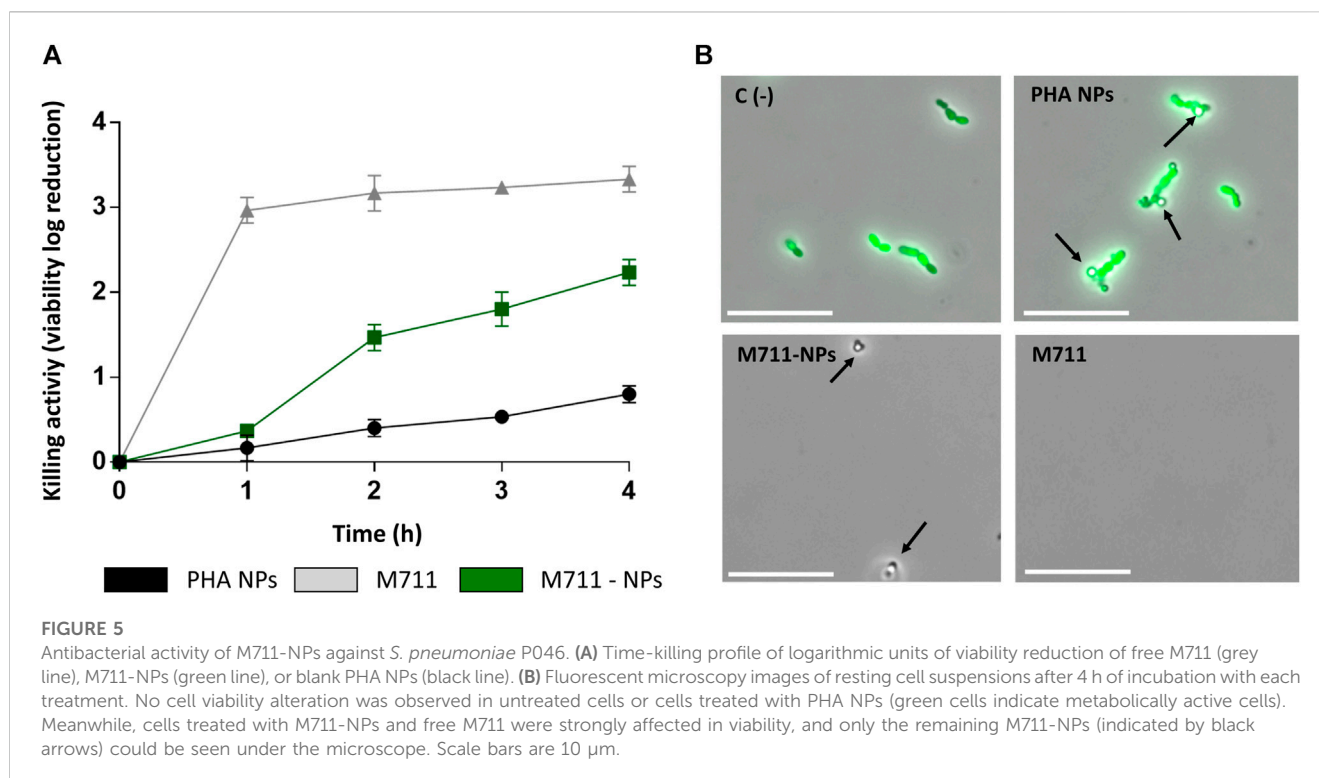
The antibacterial activity of purified M711 was assessed and compared with that of Cpl-711. An additional control of SDS-treated Cpl-711 (Cpl-711d) was also included to exclude the effect of SDS exposure, which could be potentially detrimental to the enzyme. Significant differences were only observed at the two lowest concentrations tested when comparing Cpl-711 with M711 in equimolar concentrations, showing a slight decrease in killing activity (of ~1 log killing) (Figure 2). No remarkable differences were observed by optical density decrease either (Supplementary Figure S2). This implies that the fused MinP tag does not

FIGURE 4
Protein retention at PHA NPs loaded with Cpl-711 (grey bars) or with M711 (green bars). Bars indicate the percentage of the initial protein load that remains immobilized on PHA NPs after elution with increasing concentrations of Triton X-100 as calculated by SDS-PAGE.

dramatically hinder the antimicrobial activity and confirms the methodology's efficiency in producing the tagged enzybiotic M711.

3.2 M711-NPs physicochemical characterization

The main infection niche of *S. pneumoniae* is the pneumocytes of the epithelial lung alveoli, below the LS layer (Julio et al., 2022). This means that an inhaled drug conjugate targeting pneumococcal cells, such as the one tested here, should be able to travel through the upper and lower airways to reach the alveoli. Then, the system should be translocated through the layer of LS without losing the

FIGURE 5
Antibacterial activity of M711-NPs against *S. pneumoniae* P046. **(A)** Time-killing profile of logarithmic units of viability reduction of free M711 (grey line), M711-NPs (green line), or blank PHA NPs (black line). **(B)** Fluorescent microscopy images of resting cell suspensions after 4 h of incubation with each treatment. No cell viability alteration was observed in untreated cells or cells treated with PHA NPs (green cells indicate metabolically active cells). Meanwhile, cells treated with M711-NPs and free M711 were strongly affected in viability, and only the remaining M711-NPs (indicated by black arrows) could be seen under the microscope. Scale bars are 10 μm.

loaded drug. The LS is a challenging body barrier consisting of a layer of phospholipids (92%) and hydrophobic proteins (8%) that avoid alveolar collapse during the respiratory mechanics reducing surface tension, as well as plays a role in immune innate defense (Hidalgo et al., 2017).

The ability to reach the lung alveoli is mainly determined by the NP's size. NPs with $D_H > 5$ μm are usually retained in the upper airways. Those ranging between 1–5 μm reach the lower respiratory tract by deposition, while those with $D_H \leq 1$ μm arrive at the lung alveoli by Brownian diffusion (Hidalgo et al., 2017).

The second condition, crossing the LS layer, depends on a combination of variables including size, shape, and the chemical nature and surface chemistry of the NPs (Hidalgo et al., 2015). Vehiculization through this surfactant layer needs the formation of an LS corona around the cargo so that it can translocate to the subphase. As LS is mainly composed of lipids, hydrophobic NPs have a better chance of interaction. Also, cationic or neutral NPs are preferred to anionic NPs that can sequester positively charged LS proteins, thus resulting in surfactant dysfunction (Arick et al., 2015). Accordingly, the ability of PHA NPs to translocate through the LS has been experimentally proven (Cañadas et al., 2021). Not only PHA NPs have been demonstrated to translocate through the LS, but also phasins, such as PhaF, from which the MinP tag is derived, have proven to interact with the LS (Mato et al., 2019).

Taking all the above mentioned into account, the PHA NPs formulation hereby tested was designed to meet those requirements. PHA NPs were obtained by nanoprecipitation (see Materials and methods 2.5) without the use of any stabilizer. The presence of surfactants may, on one hand, stabilize NPs systems, but, on the other hand, it interferes with phasin binding (Zhao et al., 2016).

Indeed, preliminary results of protein fractionation between supernatant and surfactant-stabilized PHA NPs showed that the detergents intensely interfered with protein binding (Supplementary Figure S3). M711 was then bound to bare PHA NPs by incubating the tagged enzybiotic with the NPs. The incorporation of M711 on the NPS (M711-NPs) was confirmed by ATR-FTIR (Supplementary Figure S4). PHA NPs presented a unimodal distribution with mean $D_H = 431 \pm 14$ nm (Figure 3A), which remained stable for a week (final $D_H = 458 \pm 15$ nm, also unimodally distributed). Likewise, the size distribution of NPs (M711-NPs) was unimodal but with a larger D_H (548 ± 12) (Figure 3B) as measured right after preparation, meeting the size targeted for an eventual alveolar delivery of the NPs. However, the M711-NPs showed a bimodal size distribution after 7 days of storage at 4°C in the activity buffer, with mean sizes at each peak of 392 and 531 nm.

This latter result shows that M711-NPs tend to interact with each other and aggregate over time but still maintaining the size requirements for an alveolar delivery MP system. Another interesting remark is the size increment of M711-NPs as compared to that of PHA NPs. Given the dimensions of the crystal structure of Cpl-1 (PDB 2IXU, 67.99 Å × 61.77 Å x 40.08 Å), which is 92% identical in sequence to Cpl-711, a difference in D_H of roughly 70 nm would indicate that several layers of protein were formed around the NPs. Although these broad layers of proteins are formed over PHA granules *in vivo* by the oligomerization of phasins through their leucine zipper motives (Tarazona et al., 2019b), these were removed in the design of MinP (Mato et al., 2020). It is however rather well established that the formation of a non-specifically associated protein corona at the NP's surface is a common phenomenon
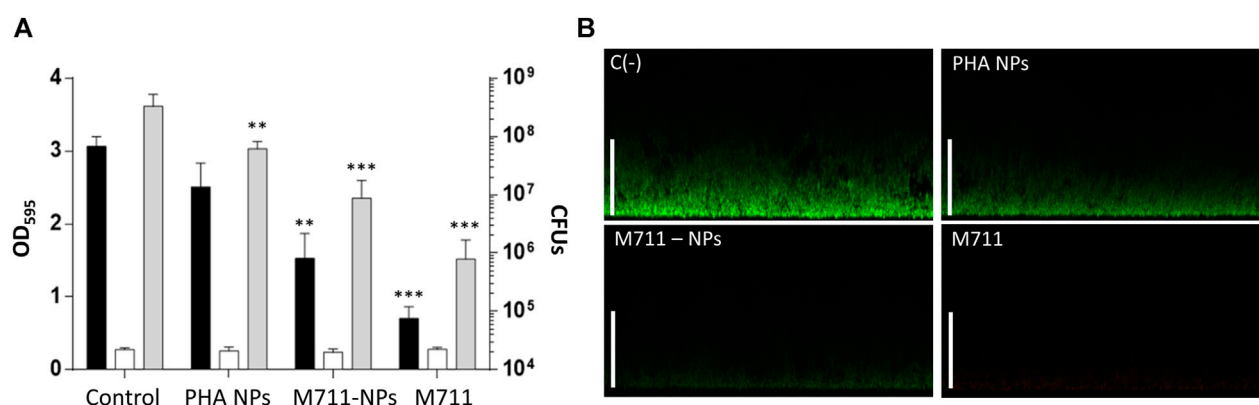
FIGURE 6
Antibiofilm activity of M711-NPS system. **(A)** Biofilm disaggregation and viable cells count from mature biofilms treated for 4 h with activity buffer, PHA NPs, M711-NPs, or free M711 in equimolar amounts (250 nM). Black bars indicate the remaining biofilm as assessed by CV staining, white bars indicate growth controls of the planktonic cell from the biofilm well, and grey bars indicate the number of viable cells in each biofilm per well. Asterisks indicate different levels of signification following a one-way ANOVA with a Tuckey post hoc test comparing each treatment with the control. (**) $p < 0.01$; (***) $p < 0.001$. **(B)** CLSM of untreated and treated biofilms with PHA NPs, M711-NPs, or free M711 for 4 h. Images are the views of the maximal projection on the x–z plane. Scale bars indicate 25 µm.

in protein-crowded solutions and biofluids (Lima et al., 2020). The existence of unspecific binding between the PHA NPs and the Cpl-711 moiety other than that driven by MinP was analyzed by assessing protein binding and release induced by exposure to Triton X-100 by SDS-PAGE. This detergent is known to effectively detach proteins from PHA granules, and it would also somehow mimic the surfactant environment at the LS (Olmeda et al., 2015; Mato et al., 2020). Indeed, the Cpl-711 attached to PHA NPs. However, a concentration-dependent elution was observed for Cpl-711 upon treatment with Triton X-100, while the amount of M711 retained in the NPs remained almost unchanged (at ≈ 80% of total protein) (Figure 4), in agreement with previous results (Mato et al., 2020). Taking this into account, a possible binding scheme could be the soft and hard corona model (García-Álvarez and Vallet-Regí, 2021), in which proteins bound to the PHA NPs via the MinP tag are tightly bound to the NPs while those bound via unspecific interactions of Cpl-711 are loosely attached. The fact that in the presence of surfactants such as Triton X-100 only small amounts of M711 are detached could correlate with smaller cargo losses during an eventual translocation at the LS. Furthermore, the aggregation effect observed when stored in an aqueous solution is likely to be prevented in the presence of LS, where the non-specifically bound protein would be released.

Also related to the colloidal stability of the system, PHA NPs showed a ζ-potential of −4.37 ± 0.34 mV, which was further reduced upon functionalization down to −7.46 ± 0.58 mV. Particulate systems are generally accepted to be stable with a ζ-potential of ±30 mV (Pochapski et al., 2021). In this case, a balance between the charge needed for stabilizing the system for long-term storage and the charge desired for facilitated transport through the LS (neutral or cationic) should be addressed. Our values are rather neutral, which was nevertheless expected given

the absence of charged moieties in PHA (Abid et al., 2016; Lee et al., 2022).

3.3 M711-NPs antimicrobial characterization

After proving the suitable physicochemical properties of M711-NPs, the antibacterial activity of the system was evaluated. Indeed, the immobilization of enzymes is very challenging, due to the need of maintaining the three-dimensional structure of the protein and its orientation to keep the biological activity. Because *S. pneumoniae* presents spontaneous autolysis when reaching the stationary growth phase, an autolysin-devoid pneumococcal strain P046 (Moscoso et al., 2006) was used to assess the antibacterial activity of the M711-NPs over time. Determination of the Minimal inhibitory concentration could not be performed due to the turbidity provided by the NPs. Thus, we directly assessed the M711-NPs with *S. pneumoniae* resting cells.

In a killing activity assay prolonged for 4 h (Figure 5) the free M711 outperformed both blank NPs and M711-NPs, with a killing curve that peaked already after 1 h. PHA NPs had a little killing effect on their own, while M711-NPs with a protein concentration equivalent to that of the free M711 treatment displayed a time-dependent sustained antibacterial activity. M711-NPs reached a killing activity of 2.2 units (Figure 5A), meaning that ≈99% of the *S. pneumoniae* cells were eliminated. Fluorescence microscopy results (Figure 5B) showed the aggregation of PHA-NPs around the cells without producing any apparent alteration in cell viability (green cells, Figure 5B). Conversely, after 4 h of incubation with M711-NPs, no cells could be observed, but only the remaining M711-NPs, which further confirmed bacterial cell lysis.

The MinP tag had been previously used to functionalize PHA granules *in vivo* leading to active immobilized enzymes (Mato et al., 2020). However, this is the first time this tag has been used to immobilize an enzyme *in vitro* while preserving its activity. While the conversion of small chemicals by enzymes immobilized on PHA granules can occur at the functionalized granule itself, the antibacterial drug delivery formulations usually imply the release of the active molecule. However, our results strongly suggest that the antimicrobial activity was due to the protein attached to the particle since no protein was detected by spectrophotometric measurements at 280 nm on the supernatant of M711-NPs incubated for up to 4 h at 37°C. The lack of release would also explain the observed lag in the activity kinetics (Figure 5A). Different causes could be argued for the kinetic retardation assuming the lack of cargo release, for example i) the steric hindrances partially blocking the access of immobilized enzymes to their substrate; ii) a lesser number of target bacteria reachable by clustered (immobilized) enzybiotics regarding an equimolar concentration of free enzymes, able to diffuse as individual molecules; iii) as multiple layers are probably formed as suggested by the increment in particle size, probably only the outermost layer displays an effective antimicrobial activity. Indeed, this behavior has been observed upon irreversible immobilization of enzybiotics. Recently, a study comparing covalent binding and simple adsorption of the antistaphylococcal enzybiotic Auresine*Plus* onto PLGA/chitosan fibers concluded lower and slower death rates for the permanently immobilized material than in the case of the enzybiotic-releasing material (Urbanek et al., 2021). However, a sustained activity due to immobilized, more stable enzybiotic could be preferred to a fast release in a clinical setting (Gao et al., 2011). Indeed, a major advantage of irreversible immobilization may be the protection of the enzyme against proteolytic activities (*e.g.* as observed in Figure 1). In contrast, in a self-releasing system, the released enzybiotic would still be susceptible to such degradation and would probably have a short residence time within the body.

Because the activity of the M711-NPs is thought to need the direct contact between the loaded NPs and bacteria, the antibacterial activity of the NPs was assessed on a solid substrate (biofilm). Due to this sessile lifestyle, the contact between the NPs and the *S. pneumoniae* cells will be more intimate than that on cell suspensions. Importantly, *S. pneumoniae* is able to form stable biofilms associated with up to 80% of chronic infections and persistent conditions (Wolcott and Ehrlich, 2008). The disaggregation of the biofilms was 13% for PHA NPs, 50% for the M711-NPs, and 77% for the free M711 treatment, with respect to an untreated control biofilm (Figure 6A), as assessed by CV staining. These results were further confirmed by CLSM, where observations indicated that the thickness of the biofilm was reduced from ≈25 μm to ≈15 μm, ≈5 μm or up to unmeasurable levels, when treated with PHA NPs, M711-NPs or free M711, respectively (Figure 6B). In terms of antibacterial activity, the viability reduction of the biofilms was significantly decreased by 0.5, 1.2, and 2.3 logarithmic units for PHA-NPs, M711-NPs, and free M711, respectively (Figure 6A). Altogether, these results indicate that M711-NPs display pneumococcus biofilm disaggregation activity despite the absence of enzybiotic release (Figure 5). Moreover, the reduced specific activity of the immobilized enzybiotic, is compensated by other functional advantages of immobilization, such as an increase of *in vivo* half-life regarding the administration of the free enzyme or by an enhanced ability to be vehiculized through the LS, as demonstrated for PHA NPs, in a possible M711-NPs inhaled formulation.

4 Conclusion

In this work, we proposed tag-mediated immobilization of enzybiotics as a method for the antimicrobial functionalization of PHA-based materials. We first achieved the *in vivo* immobilization of the fusion protein M711 onto PHA granules, which prevented the proteolytic degradation observed for the soluble production of the protein in two different heterologous hosts. This demonstrates *in vivo* PHA immobilization as a tool for the production of labile proteins. The protein purified from the granules through detergent washing was able to bind again onto preformed PHA NPs *in vitro*, and the functionalized NPs displayed antibacterial activity against both sessile and planktonic *S. pneumoniae* cells. Although the specific antimicrobial activity of M711-NPs was slightly reduced as compared with equimolar amounts of the free enzyme, this is expected to be compensated by other therapeutical properties of the NPs formulation, such as a prolonged half-life or the enhanced translocation through body barriers (*e.g.*, the LS, as described for PHA NPs). These advantages remain however to be explored in future studies.

Data availability statement

The original contributions presented in the study are included in the article/Supplementary Material, further inquiries can be directed to the corresponding author.

Author contributions

PG and MP conceived the study and provided funding acquisition. RV conceived the experimental approach and with AH-A. supervised the experimental procedures. FB performed the experimental procedures and wrote the initial draft. All authors contributed to the article and approved the submitted version.

Conflict of interest

The authors declare that the research was conducted in the absence of any commercial or financial relationships that could be construed as a potential conflict of interest.

Publisher's note

All claims expressed in this article are solely those of the authors and do not necessarily represent those of their affiliated organizations, or those of the publisher, the editors and the reviewers. Any product that may be evaluated in this article, or claim that may be made by its manufacturer, is not guaranteed or endorsed by the publisher.

Supplementary material

The Supplementary Material for this article can be found online at: https://www.frontiersin.org/articles/10.3389/fbioe.2023.1220336/full#supplementary-material

References

Abid, S., Raza, Z. A., and Rehman, A. (2016). Synthesis of poly(3-hydroxybutyrate) nanospheres and deposition thereof into porous thin film. *Mater. Res. Express* 3, 105042. doi:10.1088/2053-1591/3/10/105042

Amararathna, M., Hoskin, D. W., and Rupasinghe, H. P. V. (2022). Anthocyanin encapsulated nanoparticles as a pulmonary delivery system. *Oxidative Med. Cell. Longev.* 2022, 1–20. doi:10.1155/2022/1422929

Arick, D. Q., Choi, Y. H., Kim, H. C., and Won, Y.-Y. (2015). Effects of nanoparticles on the mechanical functioning of the lung. *Adv. Colloid Interface Sci.* 225, 218–228. doi:10.1016/j.cis.2015.10.002

Banik, B. L., Fattahi, P., and Brown, J. L. (2016). Polymeric nanoparticles: The future of nanomedicine. *WIREs Nanomedicine Nanobiotechnology* 8, 271–299. doi:10.1002/wnan.1364

Beck-Broichsitter, M., Rytting, E., Lebhardt, T., Wang, X., and Kissel, T. (2010). Preparation of nanoparticles by solvent displacement for drug delivery: A shift in the "ouzo region" upon drug loading. *Eur. J. Pharm. Sci.* 41, 244–253. doi:10.1016/j.ejps.2010.06.007

Bello-Gil, D., Maestro, B., Fonseca, J., Dinjaski, N., Prieto, M. A., and Sanz, J. M. (2018). Poly-3-Hydroxybutyrate functionalization with BioF-tagged recombinant proteins. *Appl. Environ. Microbiol.* 84, e02595-17. doi:10.1128/aem.02595-17

Blanco, F. G., Hernández, N., Rivero-Buceta, V., Maestro, B., Sanz, J. M., Mato, A., et al. (2021). From Residues to Added-Value Bacterial Biopolymers as Nanomaterials for Biomedical Applications, 11.*Nanomaterials*

Cabeza, L., Ortiz, R., Prados, J., Delgado, Á. V., Martín-Villena, M. J., Clares, B., et al. (2017). Improved antitumor activity and reduced toxicity of doxorubicin encapsulated in poly(ε-caprolactone) nanoparticles in lung and breast cancer treatment: An *in vitro* and *in vivo* study. *Eur. J. Pharm. Sci.* 102, 24–34. doi:10.1016/j.ejps.2017.02.026

Cañadas, O., García-García, A., Prieto, M. A., and Pérez-Gil, J. (2021). Polyhydroxyalkanoate nanoparticles for pulmonary drug delivery: Interaction with lung surfactant. *Nanomaterials* 11, 1482. doi:10.3390/nano11061482

De Maesschalck, V., Gutiérrez, D., Paeshuyse, J., Lavigne, R., and Briers, Y. (2020). Advanced engineering of third-generation lysins and formulation strategies for clinical applications. *Crit. Rev. Microbiol.* 46, 548–564. doi:10.1080/1040841x.2020.1809346

Díez-Martínez, R., De Paz, H. D., García-Fernández, E., Bustamante, N., Euler, C. W., Fischetti, V. A., et al. (2015). A novel chimeric phage lysin with high *in vitro* and *in vivo* bactericidal activity against *Streptococcus pneumoniae*. *J. Antimicrob. Chemother.* 70, 1763–1773. doi:10.1093/jac/dkv038

Dinjaski, N., and Prieto, M. A. (2015). Smart polyhydroxyalkanoate nanobeads by protein based functionalization. *Nanomedicine Nanotechnol. Biol. Med.* 11, 885–899. doi:10.1016/j.nano.2015.01.018

Dinjaski, N., and Prieto, M. A. (2013). Swapping of phasin modules to optimize the *in vivo* immobilization of proteins to medium-chain-length polyhydroxyalkanoate granules in *Pseudomonas putida*. *Biomacromolecules* 14, 3285–3293. doi:10.1021/bm4008937

Domenech, M., Damián, D., Ardanuy, C., Liñares, J., Fenoll, A., and García, E. (2015). Emerging, non-PCV13 serotypes 11A and 35B of *Streptococcus pneumoniae* show high potential for biofilm formation *in vitro*. *PLOS ONE* 10, e0125636. doi:10.1371/journal.pone.0125636

Edman, P., and Begg, G. (1967). A protein sequenator. *Eur. J. Biochem.* 1, 80–91. doi:10.1111/j.1432-1033.1967.tb00047.x

Gao, P., Nie, X., Zou, M., Shi, Y., and Cheng, G. (2011). Recent advances in materials for extended-release antibiotic delivery system. *J. Antibiotics* 64, 625–634. doi:10.1038/ja.2011.58

García-Álvarez, R., and Vallet-Regí, M. (2021). Hard and soft protein corona of nanomaterials: Analysis and relevance. *Nanomaterials* 11, 888. doi:10.3390/nano11040888

Gasteiger, E., Gattiker, A., Duvaud, S., Wilkins, M. R., Appel, R. D., and Bairoch, A. (2005). "Protein identification and analysis tools on the ExPASy server," in *The proteomics protocols handbook*. Editor John M. Walker (NJ: Humana Totwa), 571–607.

Gondil, V. S., Dube, T., Panda, J. J., Yennamalli, R. M., Harjai, K., and Chhibber, S. (2020). Comprehensive evaluation of chitosan nanoparticle based phage lysin delivery system; a novel approach to counter *S. pneumoniae* infections. *Int. J. Pharm.* 573, 118850. doi:10.1016/j.ijpharm.2019.118850

Gonzalez-Miro, M., Chen, S., Gonzaga, Z. J., Evert, B., Wibowo, D., and Rehm, B. H. A. (2019). Polyester as antigen carrier toward particulate vaccines. *Biomacromolecules* 20, 3213–3232. doi:10.1021/acs.biomac.9b00509

Guagliardo, R., Pérez-Gil, J., De Smedt, S., and Raemdonck, K. (2018). Pulmonary surfactant and drug delivery: Focusing on the role of surfactant proteins. *J. Control. Release* 291, 116–126. doi:10.1016/j.jconrel.2018.10.012

Hidalgo, A., Cruz, A., and Pérez-Gil, J. (2015). Barrier or carrier? Pulmonary surfactant and drug delivery. *Eur. J. Pharm. Biopharm.* 95, 117–127. doi:10.1016/j.ejpb.2015.02.014

Hidalgo, A., Cruz, A., and Pérez-Gil, J. (2017). Pulmonary surfactant and nanocarriers: Toxicity versus combined nanomedical applications. *Biochimica Biophysica Acta (BBA) - Biomembr.* 1859, 1740–1748. doi:10.1016/j.bbamem.2017.04.019

Hoskins, J., Alborn William, E., Arnold, J., Blaszczak, L. C., Burgett, S., DeHoff Bradley, S., et al. (2001). Genome of the Bacterium Streptococcus pneumoniae Strain R6. *J. Bacteriol.* 183, 5709–5717. doi:10.1128/JB.183.19.5709-5717.2001

Jia, J., Wang, Z., Yue, T., Su, G., Teng, C., and Yan, B. (2020). Crossing biological barriers by engineered nanoparticles. *Chem. Res. Toxicol.* 33, 1055–1060. doi:10.1021/acs.chemrestox.9b00483

Julio, S., Rossi Suélen, A., Chamorro-Herrero, I., González-Camacho, F., de Lucas María, P., et al. (2022). Minilungs from human embryonic stem cells to study the interaction of *Streptococcus pneumoniae* with the respiratory tract. *Microbiol. Spectr.* 10, e00453–22. doi:10.1128/spectrum.00453-22

Kniewel, R., Lopez, O. R., and Prieto, M. A. (2019). "Biogenesis of medium-chain-length polyhydroxyalkanoates," in *Biogenesis of fatty acids, lipids and membranes*. Editor O. Geiger (Cham: Springer International Publishing), 457–481.

Lacks, S., and Hotchkiss, R. D. (1960). A study of the genetic material determining an enzyme activity in Pneumococcus. *Biochimica Biophysica Acta* 39, 508–518. doi:10.1016/0006-3002(60)90205-5

Lee, S. J., Park, J. P., Park, T. J., Lee, S. Y., Lee, S., and Park, J. K. (2005). Selective immobilization of fusion proteins on poly(hydroxyalkanoate) microbeads. *Anal. Chem.* 77, 5755–5759. doi:10.1021/ac0505223

Lee, S. Y., Kim, S. Y., Ku, S. H., Park, E. J., Jang, D.-J., Kim, S. T., et al. (2022). Polyhydroxyalkanoate decelerates the release of paclitaxel from poly(lactic-co-glycolic acid) nanoparticles. *Pharmaceutics* 14, 1618. doi:10.3390/pharmaceutics14081618

Li, Z., and Loh, X. J. (2017). Recent advances of using polyhydroxyalkanoate-based nanovehicles as therapeutic delivery carriers. *WIREs Nanomedicine Nanobiotechnology* 9, e1429. doi:10.1002/wnan.1429

Lima, T., Bernfur, K., Vilanova, M., and Cedervall, T. (2020). Understanding the lipid and protein corona formation on different sized polymeric nanoparticles. *Sci. Rep.* 10, 1129. doi:10.1038/s41598-020-57943-6

Loeffler Jutta, M., Svetolik, D., and Fischetti Vincent, A. (2003). Phage lytic enzyme cpl-1 as a novel antimicrobial for pneumococcal bacteremia. *Infect. Immun.* 71, 6199–6204. doi:10.1128/iai.71.11.6199-6204.2003

Maestro, B., and Sanz, J. M. (2017). Polyhydroxyalkanoate-associated phasins as phylogenetically heterogeneous, multipurpose proteins. *Microb. Biotechnol.* 10, 1323–1337. doi:10.1111/1751-7915.12718

Mato, A., Blanco, F. G., Maestro, B., Sanz, J. M., Pérez-Gil, J., and Prieto, M. A. (2020). Dissecting the polyhydroxyalkanoate-binding domain of the PhaF phasin: Rational design of a minimized affinity tag. *Appl. Environ. Microbiol.* 86, e00570-20. doi:10.1128/aem.00570-20

Mato, A., Tarazona, N. A., Hidalgo, A., Cruz, A., Jiménez, M., Pérez-Gil, J., et al. (2019). Interfacial activity of phasin PhaF from *Pseudomonas putida* KT2440 at hydrophobic–hydrophilic biointerfaces. *Langmuir* 35, 678–686. doi:10.1021/acs.langmuir.8b03036

Mezzina, M. P., Manoli, M. T., Prieto, M. A., and Nikel, P. I. (2021). Engineering native and synthetic pathways in *Pseudomonas putida* for the production of tailored polyhydroxyalkanoates. *Biotechnol. J.* 16, 2000165. doi:10.1002/biot.202000165

Miao, J., Pangule, R. C., Paskaleva, E. E., Hwang, E. E., Kane, R. S., Linhardt, R. J., et al. (2011). Lysostaphin-functionalized cellulose fibers with antistaphylococcal activity for wound healing applications. *Biomaterials* 32, 9557–9567. doi:10.1016/j.biomaterials.2011.08.080

Moldes, C., Garcia, P., Garcia, J. L., and Prieto, M. A. (2004). *In vivo* immobilization of fusion proteins on bioplastics by the novel tag BioF. *Appl. Environ. Microbiol.* 70, 3205–3212. doi:10.1128/aem.70.6.3205-3212.2004

Moscoso, M., García, E., and López, R. (2006). Biofilm Formation by *Streptococcus pneumoniae:* Role of choline, extracellular DNA, and capsular polysaccharide in microbial accretion. *J. Bacteriol.* 188, 7785–7795. LP – 7795. doi:10.1128/jb.00673-06

Murray, C. J., Ikuta, K. S., Sharara, F., Swetschinski, L., Robles Aguilar, G., Gray, A., et al. (2022). Global burden of bacterial antimicrobial resistance in 2019: A systematic analysis. *Lancet* 399, 629–655. doi:10.1016/s0140-6736(21)02724-0

Murray, E., Draper, L. A., Ross, R. P., and Hill, C., 2021. The advantages and challenges of using endolysins in a clinical setting. Viruses 13.

Nithya, S., Nimal, T. R., Baranwal, G., Suresh, M. K., Anil Kumar, V., Gopi Mohan, C., et al. (2018). Preparation, characterization and efficacy of lysostaphin-chitosan gel against *Staphylococcus aureus*. *Int. J. Biol. Macromol.* 110, 157–166. doi:10.1016/j.ijbiomac.2018.01.083

Olmeda, B., García-Álvarez, B., Gómez, M. J., Martínez-Calle, M., Cruz, A., and Pérez-Gil, J. (2015). A model for the structure and mechanism of action of pulmonary surfactant protein B. *FASEB J.* 29, 4236–4247. doi:10.1096/fj.15-273458

Pochapski, D. J., Carvalho dos Santos, C., Leite, G. W., Pulcinelli, S. H., and Santilli, C. V. (2021). Zeta potential and colloidal stability predictions for inorganic nanoparticle dispersions: Effects of experimental conditions and electrokinetic models on the interpretation of results. *Langmuir* 37, 13379–13389. doi:10.1021/acs.langmuir.1c02056

Rojo, L., García-Fernández, L., Aguilar, M. R., and Vázquez-Lasa, B. (2022). Antimicrobial polymeric biomaterials based on synthetic, nanotechnology, and biotechnological approaches. *Curr. Opin. Biotechnol.* 76, 102752. doi:10.1016/j.copbio.2022.102752

Sanz, J. M., Lopez, R., and Garcia, J. L. (1988). Structural requirements of choline derivatives for 'conversion' of pneumococcal amidase A new single-step procedure for purification of this autolysin. *FEBS Lett.* 232, 308–312. doi:10.1016/0014-5793(88)80759-2

Sempere, J., Miguel, S., González-Camacho, F., Yuste, J., and Domenech, M. (2020). Clinical relevance and molecular pathogenesis of the emerging serotypes 22F and 33F of *Streptococcus pneumoniae* in Spain. *Front. Microbiol.* 11, 309. doi:10.3389/fmicb.2020.00309

Silva-Rocha, R., Martinez-Garcia, E., Calles, B., Chavarria, M., Arce-Rodriguez, A., Las Heras, A., et al. (2013). The standard European vector architecture (SEVA): A coherent platform for the analysis and deployment of complex prokaryotic phenotypes. *Nucleic Acids Res.* 41, D666–D675. doi:10.1093/nar/gks1119

Tarazona, N. A., Machatschek, R., Schulz, B., Prieto, M. A., and Lendlein, A. (2019a). Molecular insights into the physical adsorption of amphiphilic protein PhaF onto copolyester surfaces. *Biomacromolecules* 20, 3242–3252. doi:10.1021/acs.biomac.9b00069

Tarazona, N. A., Maestro, B., Revelles, O., Sanz, J. M., and Prieto, M. A. (2019b). Role of leucine zipper-like motifs in the oligomerization of Pseudomonas putida phasins. *Biochimica Biophysica Acta (BBA) - General Subj.* 1863, 362–370. doi:10.1016/j.bbagen.2018.11.002

Urbanek, O., Wysocka, A., Nakielski, P., Pierini, F., Jagielska, E., and Sabała, I. (2021). *Staphylococcus aureus* specific electrospun wound dressings: Influence of immobilization technique on antibacterial efficiency of novel enzybiotic. *Pharmaceutics* 13, 711. doi:10.3390/pharmaceutics13050711

Vázquez, R., Caro-León, F. J., Nakal, A., Ruiz, S., Doñoro, C., García-Fernández, L., et al. (2021). DEAE-chitosan nanoparticles as a pneumococcus-biomimetic material for the development of antipneumococcal therapeutics. *Carbohydr. Polym.* 273, 118605. doi:10.1016/j.carbpol.2021.118605

Vázquez, R., García, E., and García, P. (2018). Phage lysins for fighting bacterial respiratory infections: A new generation of antimicrobials. *Front. Immunol.* 9, 2252. doi:10.3389/fimmu.2018.02252

Wolcott, R. D., and Ehrlich, G. D. (2008). Biofilms and chronic infections. *JAMA* 299, 2682–2684. doi:10.1001/jama.299.22.2682

World Health Organization (2017). *Prioritization of pathogens to guide discovery, research and development of new antibiotics for drug-resistant bacterial infections, including tuberculosis (No. 9789240026438 (electronic version))*. Geneva: World Health Organization.

Xue, Q., Liu, X. B., Lao, Y. H., Wu, L. P., Wang, D., Zuo, Z. Q., et al. (2018). Anti-infective biomaterials with surface-decorated tachyplesin I. *Biomaterials* 178, 351–362. doi:10.1016/j.biomaterials.2018.05.008

Zhao, H., Wei, H., Liu, X., Yao, Z., Xu, M., Wei, D., et al. (2016). Structural insights on PHA binding protein PhaP from aeromonas hydrophila. *Aeromonas hydrophila Sci. Rep.* 6, 39424. doi:10.1038/srep39424

Check for updates

Continuous bioreactor production of polyhydroxyalkanoates in *Haloferax mediterranei*

Mariana Parroquin-Gonzalez and James Winterburn*

Department of Chemical Engineering University of Manchester, Manchester, United Kingdom

In this work, the viability of continuous poly(3-hydroxybutyrate-co-3-hydroxyvalerate) (PHBV) production with controlled composition in *Haloferax mediterranei* when fed volatile fatty acids is demonstrated. Continuous fermentations showed to greatly outperform batch fermentations with continuous feeding. Operating the bioreactor continuously allowed for PHBV productivity normalised by cell density to increase from 0.29 to 0.38 mg L^{-1} h^{-1}, in previous continuously fed-fed batch fermentations, to 0.87 and 1.43 mg L^{-1} h^{-1} in a continuous mode of operation for 0.1 and 0.25 M carbon concentrations in the media respectively. Continuous bioreactor experiments were carried out for 100 h, maintaining control over the copolymer composition at around 30 mol% 3-hydroxyvalerate 3HV. This work presents the first continuous production of PHBV in *Haloferax mediterranei* which continuously delivers polymer at a higher productivity, compared to fed-batch modes of operation. Operating bioreactors continuously whilst maintaining control over copolymer composition brings new processing opportunities for increasing biopolymer production capacity, a crucial step towards the wider industrialisation of polyhydroxyalkanoates (PHAs).

KEYWORDS

bioreactor, fermentation, continuous, *Haloferax mediterranei*, polyhydroxyalkanoates, Poly(3-hydroxybutryrate-co-3-hydroxyvalerate)

1 Introduction

With the high demand for plastics production worldwide and its associated processing and disposal problems there is an increasing interest in developing more environmentally friendly alternatives, including biodegradable plastics produced from a renewable source (Plastics-Europe, 2021; European Commision, 2022). Polyhydroxyalkanoates (PHAs) are a family of bioplastics that can be produced by a large range of microorganisms and possess similar mechanical properties to widely used plastics such as polypropylene and polyethylene (Doi et al., 1989; Renard et al., 2004; Platt, 2006; Khanna and Srivastava, 2008). The homopolymer poly-3-hydroxybutyrate (PHB) is one of the most commonly produced PHAs. However, when adding the 3-hydroxyvalerate (3HV) monomer into the chain to form the copolymer poly-3-hydroxybutyrate-co-3-hydroxyvalerate (PHBV) the high crystallinity of the PHB is disrupted and a more malleable and flexible polymer is created which presents suitability for a broader range of industrial applications (Anjum et al., 2016).

The main restrictions on PHA industrial scale-up lies on their relatively high production cost, with the estimated PHA market price ranging between 2.4 and 5.5 USD per kg while the petroleum-based alternatives cost around 1 USD per kg (Gholami et al., 2016; Crutchik et al., 2020). A large

Continuous process

FEED VFA

1.2 L

BROTH

PHBV

GRAPHICAL ABSTRACT
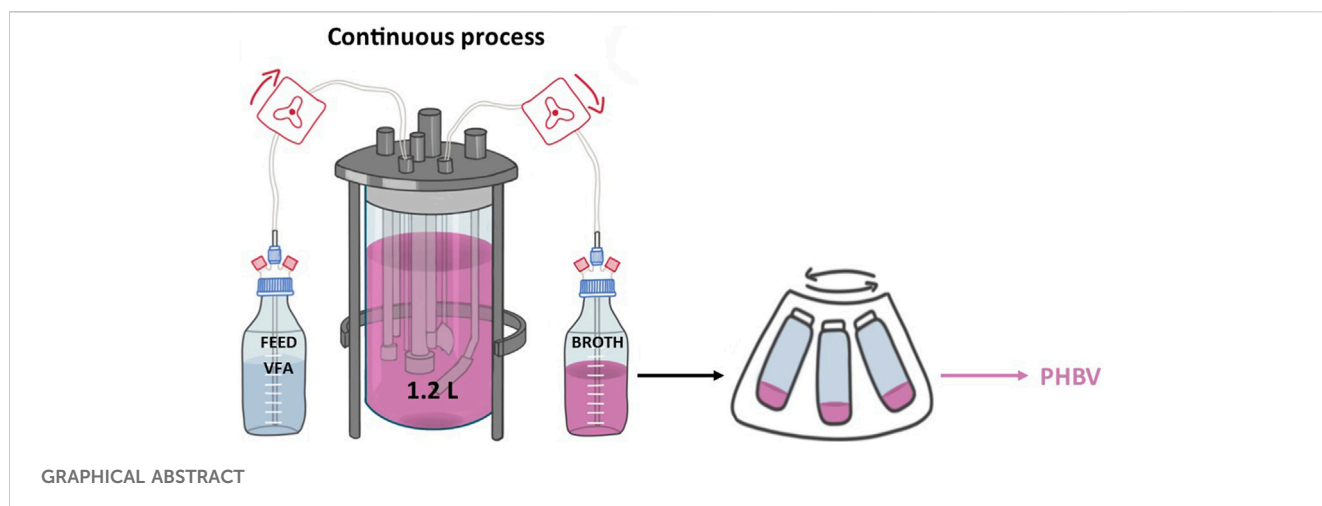
proportion of the costs are associated with creating sterile conditions, substrate carbon source refinement, use and disposal of solvents for polymer extraction and the low productivity, yields and other limitations such as short production campaigns and downtime for batch changeover of batch/fed-batch modes of operation (Arcos-Hernández et al., 2013; Kumar et al., 2016; Kourmentza et al., 2017; Chen and Jiang, 2018). Halophilic microorganisms have been suggested as suitable PHAs producers at a lower financial cost; the high salinity of the production medium needed (150–200 g/L of salts) for halophiles to grow minimises the risk of contamination, removing the need for sterile conditions and facilitates operation allowing for open vessels and low contamination risk continuous process (Chen and Jiang, 2018; Mahler et al., 2018; Kasirajan and Maupin-Furlow, 2021). Furthermore, the downstream process can be hugely simplified, extracting the polymer by simple osmotic shock when the cells are transferred into an isotonic media, removing the need for toxic and expensive solvents (Oren, 2010; Koller et al., 2017).

In most microorganisms, the 3HV percentage in PHBV is limited by the precursor toxicity with compositions above 50% being hard to obtain (McChalicher and Srienc, 2007; Han et al., 2015). However, *Haloferax mediterranei* can produce PHBV naturally without the need of precursors and can utilise a wide range of cheap carbon sources as substrate making it one of the preferred halophilic archaea for PHA production (Chen et al., 2006; Huang et al., 2006; Koller et al., 2007; Pais et al., 2016; Alsafadi and Al-Mashaqbeh, 2017; Montemurro et al., 2022). In addition, polymer composition could vary from batch to batch delivering a product with fluctuating mechanical properties. It has been shown that by feeding a mix of C4:0 and C5:0 volatile fatty acids (VFAs) the polymer composition can be controlled; in a fed-batch fermentation the 3HV content is directly proportional to the fraction of C5:0 fed (Ferre-Guell and Winterburn, 2018).

With sterilisation, extraction and carbon substrate simplified, the next productivity improvement can come from the operation mode selected. In addition to the fermentation time itself, batch operations include long periods of downtime, during which equipment is cleaned and sterilised, media is prepared, and a new inoculum is grown. This contributes to delayed product delivery or the need to set up several batches in series which complicates the process and requires more capital investment or result in less overall production from a given facility. Continuous

fermentations present an attractive alternative with an ease to control the fermentation allowing for a constant polymer harvest with a single longer production campaign.

A semi-continuous, fed batch, mode of operation has previously been tested, where the fermentation was continuously fed a mix of C4:0/C5:0 VFA in order to keep the concentration in the media constant, without an outlet stream (Parroquin Gonzalez and Winterburn, 2022). This strategy led to a productivity increase (12.8 mg L^{-1} h^{-1}) when compared to a pulse-feeding fed batch strategy (3.4 mg L^{-1} h^{-1}) (Ferre-Guell and Winterburn, 2018; Parroquin Gonzalez and Winterburn, 2022). However, the amount of polymer produced over time in the continuously fed fed-batch fermentation (CFFB) was limited by the reactor volume, increased cell density over time and accumulation of other metabolites and by-products, in addition the downstream process associated to a batch operation was still present. It has been shown that fully continuous operation can further increase the process productivity and simplify the operation generating a more industrially attractive process (Garcia Lillo and Rodriguez-Valera, 1990; Chen and Jiang, 2018; Amstutz et al., 2019). Therefore, a fully continuous fermentation is the crucial next step in improving polymer production. This has already been implemented for other PHA producing species showing promising results, including the genetically engineered *Halomonas TD01* (Yu et al., 2005) and *Ralstonia eutropha* (Fu et al., 2014). *Haloferax mediterranei* and the process described here present an opportunity for a non-engineered species that can operate under non-sterile conditions.

When performing a continuous fermentation, the genomic stability of the culture might be at risk. There are some halobacteria known to have high genomic stability. In 1990, Garcia Lillo & Rodriguez-Valera performed a continuous fermentation with *Haloferax mediterranei* for 3 months at a dilution rate of 0.12 h^{-1} which roughly corresponds to 370 generations. Afterwards they tested the PHB production of the strain and did not observe any significant difference from the original strain deeming *Haloferax mediterranei* as a stable culture for continuous operations (Garcia Lillo and Rodriguez-Valera, 1990).

The work presented in this paper details the first effort to continuously produce PHBV using *Haloferax mediterranei* in a continuous mode of bioreactor operation with VFAs as substrate, with the aim of further improving process productivity. Bioreactors were continuously fed a mix of C4:0/C5:0 VFAs maintaining steady state carbon concentration, cell density

and biopolymer concentration in the media, proving the viability of the process. Following this continuous bioreactor operation strategy improved both productivity normalised by optical density (OD) and yields, presenting a process that has the potential to be more industrially attractive. This work represents a crucial step for the wider industrialisation of biopolymer production.

2 Materials and methods

2.1 Microorganism and fermentation conditions

Haloferax mediterranei (DSM 1411, ATCC 33500) obtained from the Leibniz Institute DSMZ-German Collection of Microorganisms and Cell cultures, was used for all experiments. Cryovials of working stock were stored at −80°C. The seed culture was initiated by reviving the cryovial content in 20 mL minimal synthetic media (MSM) supplemented with 10 g/L of glucose and incubated during 24 h at 37°C and 200 rpm (INNOVA 42, New Brunswick Scientific). This was then transferred to a 1 L shake flask with 200 mL MSM supplemented with 10 g/L of glucose and incubated for further 36 h at 37°C and 200 rpm. Prior to starting the fermentations, cells were centrifuged to remove all media supplemented with glucose. For a final cultivation phase, the cells were resuspended in 200 mL MSM with 0.1 M carbon concentration of C4:0/C5:0 mix with a 50/50 ratio and inoculated for 48 h. This final cultivation phase was designed to adjust the cells to the fatty acids and reduce the lag phase at the beginning of the fermentation in the reactor. Finally, the cells were centrifuged at 7,000 rpm for 10 min and the supernatant was discarded. The pellet was then resuspended in fermentation media and added to the corresponding bio reactor.

The composition of the minimal synthetic media (MSM) was (g/L): 156.0 NaCl, 13.0 $MgCl_2 \cdot 6H_2O$, 20.0 $MgSO_4 \cdot 7H_2O$, 1.0 $CaCl_2 \cdot 6H_2O$, 4.0 KCl, 0.2 $NaHCO_3$ and 0.5 NaBr as marine salts; 0.5 KH_2PO_4, 0.005 (g/L) $FeCl_3$ and 1.0 (mL/L) trace elements solution SL6 (10×) as supplements; 2.0 NH_4Cl to supply the desired amount of nitrogen and 49.6 (mL/L) 1,4-piperazinediethane-sulfonic acid (PIPES) as pH buffer. The trace elements solution contained (g/L): 2.0 $ZnSO_4 \cdot 7H_2O$, 0.6 $MnCl_2 \cdot 4H_2O$, 6.0 H_3BO_3, 4.0 $CoCl_2 \cdot 6H_2O$, 0.2 $CuCl_2 \cdot 2H_2O$, 0.22 $NiCl_2$, 0.6 $Na_2MoO_4 \cdot 2H_2O$. In all cases, the pH of the media was adjusted to 6.8 with NaOH or HCl solutions and with no sterilisation prior to use.

Butyric (C4:0) and pentanoic (C5:0) acid with a ≥99% purity from Sigma-Aldrich were used in all fermentations.

2.2 PHA bioreactor fermentations

A 3-L cylindrical bioreactor (Applikon Biotechnology, 1 Rushton turbine, 3 baffles, 2.2 H/D ratio) with an initial working volume of 1.2 L was used for all fermentations. The temperature was maintained at 37°C, the pH kept at 6.8 using 3M HCl solution, air was delivered at 0.75 vvm and an agitation cascade with stirring speed between 200 and 800 rpm was set up to maintain the dissolved oxygen at 20% [26]. C4:0/C5:0 (56:44 mol%) VFAs were used as the carbon substrate, the media had the corresponding amounts added to constitute the 0.1 and 0.25 M working concentrations.

Fermentations were continuously fed MSM media supplemented with a mix of C4:0/C5:0 (56:44 mol%) of 0.5 and 0.4 M respectively for the 0.1 and 025 M working concentration respectively. Both inlet and outlet streams were pumped with a Watson Marlow (IP31) pump with flowrates adjusted accordingly to the fermentation specifications. Samples for analytical measurements were taken from the outlet stream. No significant salt deposits were observed inside the tubing for the duration of the fermentations. Outlet broth was stored in a cold-room prior to polymer extraction.

2.3 Downstream: PHBV extraction

PHA from *Haloferax mediterranei* can be isolated by osmotic shock. To extract the polymer for quantification and composition analysis, 2 mL of sample broth was centrifuged in an Eppendorf tube at 13,000 rpm for 5 min and the supernatant was discarded. The pellet was resuspended in 1 mL of 0.1% w/v Sodium Dodecyl Sulphate (SDS) (Sigma Aldrich) and vortexed for 1 min. This process was repeated 3 times to eliminate the light pink colour associated with *Haloferax mediterranei* fermentation broth. Finally, cells were washed one last time with distilled water and left to dry in a drying oven at 60°C. No evidence of PHBV degradation was observed, with no discernible difference in concentration detected using GC between polymer extracted immediately after sampling and that obtained from samples stored in a cold room for a period of time prior to extraction as shown in Figure 2.

2.4 Analytical techniques

2.4.1 Determination of optical density

Optical density was used to measure cell growth as specified in (Parroquin Gonzalez and Winterburn, 2022). 1 mL samples of fermentation broth were taken every 24 h. The sample was centrifuged for 5 min at 13,000 rpm, the supernatant retained for HPLC analysis, and the cells resuspended in a 10 w/v NaCl solution. The measurements were carried out by a US-visible spectrometer at 600 nm (UV mini-1240, UV-vis spectrometer, Shimadzu).

2.4.2 Dry cell weight (DCW) and biomass

Due to the high salinity of the media, dry cell weight could not be determined by standard solvent evaporation. 10 mL of sample were analysed following the procedure detailed by (Parroquin Gonzalez and Winterburn, 2022). Samples were centrifuged for 10 min at 7000 rpm and supernatant discarded. The pellet was then resuspended in 10% w/v NaCl solution. This process was repeated three times before transferring the samples to a ceramic crucible. Samples were then dried to constant weight, weighed and then all organic matter burnt at 400°C for 4 h in a P300 furnace (Nabertherm). This process degrades all organic matter leaving the salts in the crucible. The dry cell weight was calculated as the difference between the dry weight (salts plus organic matter) and the burnt sample (salts only). Biomass was calculated as the difference between DCW and PHA concentration.

2.4.3 PHA quantification and composition analysis with GC-FID

For sample preparation the method described by (Braunegg et al., 1978) was followed. 2 mL of sample were centrifuged, and the supernatant discarded. The pellet was then washed 3 times with

0.1% w/v sodium dodecyl sulphate (SDS) (Sigma Aldrich) solution before a final wash with distilled water. The pellet was then transferred to a pressure tube and left to dry. Once dried, the sample was treated at 95°C for 140 min with a chloroform: methanol:sulfuric acid solution (2:1.85:0.15 v/v) supplemented with 5 g/L of methyl benzoate as an internal standard. Following this procedure, 2 mL of water were added, and the mix was vortexed and left to settle. After settling the lower layer (organic phase) was extracted with the use of a syringe, filtered (0.45 µm PTFE filter) and transferred to a GC vial.

Gas chromatography with a flame ionization detector (GC-FID), a 30 m × 0.25 mm × 0.25 µm Zebron ZB-SemiVolatiles Capillary GC column capillary column (SGE Analytical Science) was used to analyse the PHA concentration. The method consisted of an initial temperature of 100°C for 3 min, followed by a ramp of 25°C/min to 200°C, followed by a second ramp of 30°C/min to 220°C, maintaining this temperature for 2 min. Helium was used as carrier gas. Standards were prepared from Methyl-(R)-3-hydroxybutyrate and Methyl-(R)-3-hydroxyvalerate (Sigma Aldrich) to create calibration curves.

2.4.4 Determination of PHBV microstructure by NMR

Nuclear Magnetic Resonance (NMR) (B500 MHz Avance II+, Bunker), was used to determine the microstructure of the PHA produced by analysing the presence of HV and HB monomers and their distribution in the copolymer which can be identified by the position of the ^1H and ^{13}C present. The results allow calculation of the D value (Eq. (1)) which gives an idea of the relative proximity of HB*HV and HV*HB groups. A large D value corresponds to a block polymer structure while values close to 1 indicate a random polymer structure (Kamiya et al., 1989). The D value is given by:

$$D = \frac{F_{HBHB} \times F_{HVHV}}{F_{HBHV} \times F_{HVHB}} \quad (1)$$

Where F_{HBHB} represents the fraction of 3HB adjacent to 3HB monomer units, F_{HBHV} represents the fraction of 3HB adjacent to 3HV monomer units, F_{HVHV} represents the fraction of 3HV adjacent to 3HV monomer units, F_{HVHB} represents the fraction of 3HB adjacent to 3HV monomer units.

2.4.5 Quantification of fatty acids with HPLC, yields

The supernatant from each OD sample was analysed to determine carbon substrate (VFA) content. Samples were passed through 0.45 µm Nylon filters before being transferred to HPLC vials. The C4:0 and C5: 0 concentrations were quantified by High Performance Liquid Chromatography (HPLC) (Ultimate 300 Dionex HPLC system, Thermo Scientific) using an Aminex HPX-87H (Biorad) column and UV detector. The mobile phase used was 0.5 mM H_2SO_4. The operating temperature was 50°C, 1.0 mL/min flow rate and 220 nm UV wavelength. Pure valeric and butyric acid were used to prepare standards.

Product yield ($Y_{PHA/S}$) and Biomass yield ($Y_{X/S}$) were calculated with the following equations $Y_{PHA/S} = [PHA_{average}]/\Delta S$ and $Y_{X/S} = X_{total}/\Delta S$. Where X represents the total biomass in g/L, = [$PHA_{average}$] shows the average PHA concentration in g/L and ΔS the substrate consumed in g/L.

2.4.6 Carbon consumption and feeding rate calculation

HPLC analysis results were used to obtain the fatty acid consumption rate which was calculated as the difference in VFA between two readings. The amount of VFA fed between samples was also taken into consideration. Substrate consumption was calculated as $\Delta S = [VFA]_{feed} - [VFA]_{outlet\ stream}$ for each 24 h period.

The feed flow rate (mL h^{-1}) was calculated as the product of reactor volume (mL) and dilution rate (h^{-1}). The dilution rate was selected based on previous experiments as the expected specific growth rate for each 24 h period. The feed concentration (g mL^{-1}) was determined based on the measured carbon consumption (g) and total volume fed over a 24 h period (mL).

3 Results and discussion

The results of two fully continuous bioreactor fermentations are presented, to prove the viability of a continuous mode of bioreactor operation for PHBV production in *Haloferax mediterranei* when fed a mix of C4:0/C5:0 volatile fatty acids (VFAs). Firstly, operating conditions, e.g., feeding rate, feed carbon concentration and steady state OD, are determined followed by discussion of continuous fermentation data and the analysis of the PHBV produced.

3.1 Design of continuous operating conditions

A continuous strategy, with feeding and broth removal, was designed to keep the cell density and carbon concentration constant inside the bioreactor. Two experiments were completed with a mix of C4:0/C5:0 VFAs at different media substrate concentrations; experiments A and B were performed at 0.1 M and 0.25 M carbon concentration respectively.

The natural PHBV production in *Haloferax mediterranei* is growth associated; maximum production occurs during the exponential growth phase (Koller et al., 2007). When looking to maximise productivity, elongating that exponential productive growth phase is of interest. When working in fed-batch and continuously fed fed-batch (CFFB) strategies, the maximum cell density observed was around OD 35 with exponential growth occulting in the range 8–35 OD (Ferre-Guell and Winterburn, 2019; Parroquin Gonzalez and Winterburn, 2022). Based on this a steady state OD between 10–12 was chosen for the continuous fermentations. These values fall at the beginning of the exponential phase which not only guarantees PHA production but also results in a relatively straight forward steady state at which to control and maintain the fermentation vs. a higher, late exponential stage, OD. Whilst operating at higher OD is possible it would require significantly greater dilution rates, achieved with high and difficult to control inlet and outlet flow rates.

To establish a steady state cell density and carbon concentration inside of the reactor for the duration of the continuous fermentation, the outlet stream had to be set to match cell growth rate and carbon consumption rate. The inlet stream was set to match the outlet stream to maintain

constant working volume in the reactor. The flowrates and feeding rate were initially calculated based on the growth rate in the CFFB fermentations averaging the same carbon concentration in the media. Both experiments were initially fed a C4:0/C5:0 (56:44 mol%) 0.3 M of carbon mix, same concentration as the CFFB experiments (Parroquin Gonzalez and Winterburn, 2022). However, with a continuous stream of cells leaving the reactor and hence limiting their natural exponential growth phase, cell growth and carbon consumption rates decreased when compared to CFFB fermentations and the outlet flow rate had to be adjusted; accordingly, experiments A and B had an outlet flow of 5.3 and 9.2 mL h^{-1} respectively. Once the outlet flow was stablished, the inlet flow had to be adjusted to keep the volume inside the reactor constant. The new consumption rate was calculated by analysing the carbon concentration change in the media over a 24 h period, samples were analysed by HPLC. A consumption rate of 54.1 and 30.9 mg h^{-1} were obtained for experiments A and B respectively. Research conducted in *Haloferax mediterranei* shows its preference for C4:0 over C5:0 during the growth phase (Ferre-Guell and Winterburn, 2019). Additionally, it has been documented that cells exhibit faster growth when the carbon concentration in the media is maintained at 0.25 M (Parroquin Gonzalez and Winterburn, 2022). As expected, B shows faster cell growth, as evidenced by the higher flow rate out (Table 1) which suggests that the cells are at a stage that further favors the consumption of C4:0 over C5:0. The carbon consumed is not only used by the cells for biomass growth but also for PHA production and formation of other fermentation products; experiment A shows slower growth with higher PHA production and a larger carbon consumption rate when compared to experiment B, a faster growing culture with less PHA production and lower carbon consumption. Figure 1
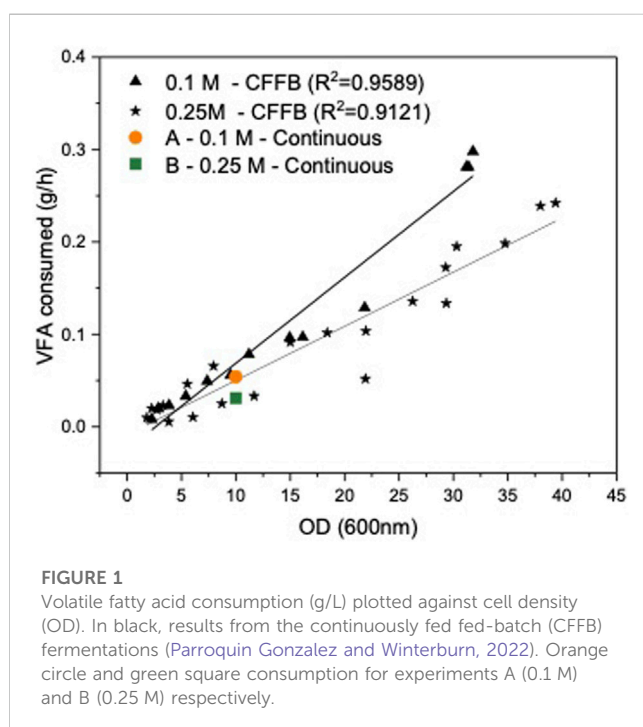
shows the consumption rate trends for the CFFB fermentation at increasing OD as well as the consumption rate values for experiments A and B. Knowing how much carbon had been consumed over that period as well as the required flowrate rate needed to keep the volume in the reactor at steady state, the final feeding concentrations for each experiment were calculated; experiments A and B where fed a media supplemented with 0.515 and 0.390 M of carbon respectively. The final design parameters used are presented in Table 1.

3.2 Continuous fermentation results

Results from two continuous fermentations are presented; experiments A and B were performed at steady state 0.1 M and 0.25 M carbon concentration in the media respectively. Both reactors were inoculated so that the initial cell density in the reactor would be within the desired 10–12 OD mark. Immediately following inoculation, the inlet and outlet streams were turned on and the continuous fermentation was initiated maintaining the working volume inside each bioreactor constant at 1.2 L. Both experiments were sampled every 24 h for 100 h; the data obtained for OD, VFA concentration in media, PHBV and 3HV concentration is presented in Figure 2. As desired, for both experiments A and B, each sample presented an OD value within the 10–12 mark. The carbon concentration in the media was successfully kept at 0.1 and 0.25 M of carbon concentration respectively through the 100 h analysed showing that the feeding concentrations and rates described in Table 1 were correctly calculated. In addition, both the concentration of the polymer and the 3HV fraction obtained remained constant over time. All these constant values demonstrate that steady state was successfully kept. Figure 2 shows steady state carbon concentration, cell density (OD) and polymer production remained constant for the duration of the continuous experiment. While the experiments presented in this work only lasted for 100 h, *Haloferax mediterranei* has been shown to be a stable culture for continuous processes with no genomic alterations observed after 3 months (Garcia Lillo and Rodriguez-Valera, 1990).

For the operations presented in this work, the continuous feed flow prevented salt deposits forming and salt accumulation was not observed in the tubing system, allowing for the feeding solution to include the required salts. This presents an additional advantage for the continuous operation granting greater control and assuring the fermentation is continuously provided the needed amount of micronutrients. While the high salinity might present an industrial scale up limitation due to potential for corrosion and salt build up, the experimental work presented in this paper shows that when there is a continuous flow of media salts do not accumulate, further careful material selection for bioreactor vessels and pipework can mitigate the corrosion risk when scaling up.

Overall, the results presented demonstrate that not only a continuous fermentation of *Haloferax mediterranei* is viable, but the PHBV produced is obtained continuously with constant concentration and 3HV fraction. This presents a huge industrial advantage as fermentations could be kept running for longer (at least 3 months), as opposed to being limited by the end of the exponential

FIGURE 1
Volatile fatty acid consumption (g/L) plotted against cell density (OD). In black, results from the continuously fed fed-batch (CFFB) fermentations (Parroquin Gonzalez and Winterburn, 2022). Orange circle and green square consumption for experiments A (0.1 M) and B (0.25 M) respectively.

TABLE 1 Fermentation design parameters.

Exp	Media concentration (M)	Working Volume (L)	Steady state OD	Dilution rate (h^{-1})	Flowrate out (mL h^{-1})	Feeding concentration (M of Carbon)	VFA consumption rate (mg h^{-1})	C4:0 consumption rate (mg h^{-1})	C5:0 consumption rate (mg h^{-1})
A	0.1	1.2	10–12	0.0044	5.3	0.515	54.1	27.2	26.9
B	0.25			0.0076	9.2	0.390	30.9	22.3	8.6
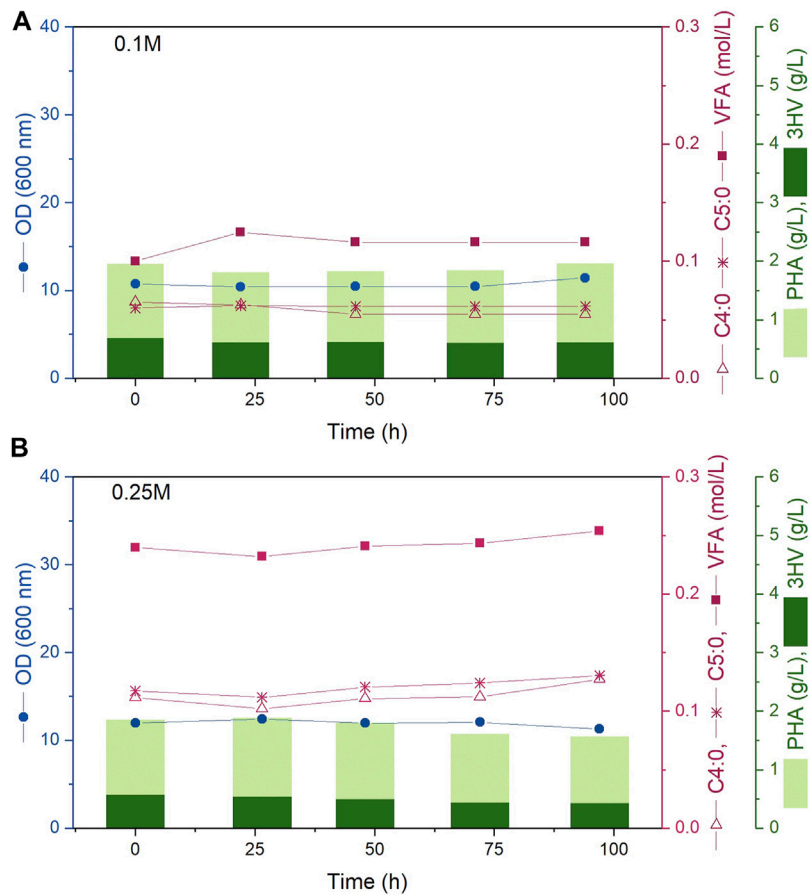
FIGURE 2
Bioreactor fermentation time course showing experiments **(A, B)** (top to bottom) corresponding to steady state carbon concentrations in the media of 0.1 and 0.25 M. The circles represent OD (600 nm), squares indicate VFA concentration (mol/L), empty triangles show C4:0 concentration (mol/L), asterisks represent C5:0 concentration (mol/L). The light bars represent the PHBV concentration while the dark bars represent the PHV concentration (g/L).

cell growth or by-products accumulation in batch fermentations, with product being harvested continuously whilst maintaining consistent material properties and quality. Continuous operation also minimises downtime, maximising the production possible from a given equipment asset.

3.3 PHA production and quantification in continuous fermentations

The main advantage of a continuous mode of operation is the ability of product to be harvested continuously. Figure 3 shows

the total amount of PHBV and volume of broth obtained throughout the 100 h sampled. An average of 130 mL of broth containing 250 mg of PHBV were obtained daily from experiment A. Experiment B delivered an average of 220 mL containing 376 mg of PHBV. By the end of the continuous production time more than 600 mL had been extracted from experiment A with a total of 1.2 g of PHBV produced while 1,100 mL and 2 g of PHBV were produced in experiment B (Figure 3).

Three different productivities were calculated for both experiments to characterise the fermentation and be able to compare them with the results previously obtained for CFFB

FIGURE 3
Total volume extracted, and polymer produced by continuous fermentations for experiments A (0.1 M) and B (0.25 M).

the fermentation life (fermentation reaching stationary phase) while the continuous total time only accounts for the 100 h tested while the fermentation could have continued for a much longer time at least tripling the CFFB time. In addition, the polymer produced in the continuous fermentations was made by a lower total cell count with the total cell density staying between 10–12; in the CFFB the amount of polymer produced increases proportionately with the cell density going up to 34 OD.

To be able to compare productivities, the overall productivity is normalised by the maximum OD obtained. When comparing these values, the productivity normalised by OD increased from 0.29 to 0.87 mg L^{-1} h^{-1} OD^{-1} (331%) and from 0.38 to 1.43 mg L^{-1} h^{-1} OD^{-1} (453%) for 0.1 and 0.25 M carbon concentration respectively for CFFB and continuous fermentation (Table 2). In this work, only one OD value was tested in continuous operation, higher cell densities could be tested in the future to further improve the overall productivity.

Steady state productivity and production rates were also calculated and are presented in Table 2. These values correspond to the 24 h period between samples and can be useful when comparing fermentations at different working volumes. Steady state productivities of 77.5 and 71.3 mg L^{-1} h^{-1} were obtained for experiments A and B respectively. One of the main features of continuous fermentations is the constant product delivery; steady state production rates of 9.9 and 15.8 mg h^{-1} were obtained for experiments A and B respectively.

Biomass yields of 0.07 and 0.32 (g g^{-1}) were obtained for experiments A and B respectively. As for the PHA yield, values of 0.18 and 0.51 (g g^{-1}) were obtained for experiments A and B respectively (Table 2). In the CFFB experiments conducted at the same carbon concentration the biomass yields obtained were of 0.29 (g g^{-1}) for both 0.1 and 0.25 M fermentations and PHA yields of 0.73 and 0.63 (g g^{-1}) were calculated for 0.1 and 0.25 M fermentations respectively (Parroquin Gonzalez and Winterburn, 2022). Experiment A did not show an improvement in terms of yield while experiment B presented an improved biomass yield and maintained a similar value for PHA yield. It is important to know than in CFFB cells were allowed to grow all the way to stationary phase producing polymer at higher cell density. Engineering the *Haloferax mediterranei* cells with an additional phaCAB operon and exploring higher cell density continuous fermentations can be ways to further increase the yields. However, even with the lower yields observed the greater productivity normalised by OD, continuous production and elimination down time associated with batch changeover means

operations (Table 2). Overall productivities of 9.6 and 17.2 mg L^{-1} h^{-1} for experiments A and B respectively were obtained. A productivity normalised by OD of 0.87 and 1.43 mg L^{-1} h^{-1} OD^{-1} was calculated for experiments A and B respectively. Finally, a steady state productivity of 77.5 and 71.3 mg L^{-1} h^{-1} for A and B respectively was obtained.

The overall productivity for CFFB fermentations was 10.0 and 12.8 mg L^{-1} h^{-1} when fed 0.1 and 0.25 M of carbon respectively (Parroquin Gonzalez and Winterburn, 2022). For the experiments at 0.1 M VFA the overall productivity calculated is numerically equal for CFFB and continuous fermentations (Table 2) while in the 0.25 M experiments there is a 34% increase in overall productivity from 12.8 mg L^{-1} h^{-1} in CFFB to 17.2 mg L^{-1} h^{-1} in the continuous process. However, while these values are mathematically calculated in the same manner accounting for the total polymer mass produced in the total working volume during the total fermentation time, the significance is of the value is different; the CFFB total fermentation time goes from the start to the actual end of

TABLE 2 Parameters for the PHBV produced in *Haloferax mediterranei* grown in different VFA constant concentrations and operation conditions.

	Operation mode	Carbon concentration (M)	Time (h)	PHBV (g L^{-1})	Total PHBV produced (g)	Overall Productivity (mg L^{-1} h^{-1})	Maximum OD	Productivity normalised by OD (mg L^{-1} h^{-1} OD^{-1})	Steady state productivity (mg L^{-1} h^{-1})	Steady state production rate (mg h^{-1})	$Y_{X/S}$ (g g^{-1})	Y_{PHA} (g g^{-1})
A	Continuous	0.1	104	1.86	1.2	9.6	11[b]	0.87	77.5	9.9	0.07	0.18
B	Continuous	0.25	97	1.71	2.0	17.2	12[b]	1.43	71.3	15.8	0.32	0.51
A[a]	Fed-batch	0.1	260	5.27	9.5	10.0	34	0.29	N/A	N/A	0.29	0.73
B[a]	Fed-batch	0.25	383	4.73	9.4	12.8	34	0.38	N/A	N/A	0.29	0.63

[a]Values for continuously fed fed-batch fermentations were taken from Parroquin Gonzalez and Winterburn (2022).
[b]Average OD values at steady state.

the continuous process is a more attractive mode of operation compared to fed-batch.

An in-depth techno-economical assessment for PHBV production *via* fermentation has been published (Policastro et al., 2021). In this study the productivity and 3HV fraction of different PHBV processes are compared. It is known that PHBV copolymers with 30–60 mol% 3HV composition are elastic and soft which makes them desirable over other polymeric compositions that are less elastic and brittle (Sudesh et al., 2000; Anjum et al., 2016). Furthermore, 3HV fractions higher than 30 mol% have a lower melting temperature, increasing the gap between melting and degradation temperatures facilitating their moulding into desired goods (Lauzier et al., 1992; Khanna and Srivastava, 2005). However, 3HV factions in *Haloferax mediterranei* are limited by precursor toxicity with higher than 15% are difficult to achieve; 3HV fractions higher than 40 mol% rarely being reported (Fernandez-Castillo et al., 1986; Chen et al., 2006). Overall productivities associated with these processes range between

9 and 360 mg L^{-1} h^{-1} with the highest values obtained when glucose or starch are used as carbon sources (Don et al., 2006; Hermann-Krauss et al., 2013). While said productivities are numerically larger than those presented here, when using a mix of C4:0 and C5:0 VFAs as carbon source it is possible to control the 3HV fraction and obtain compositions as high as 99.5 mol% without toxicity limitation (Ferre-Guell and Winterburn, 2018). 3HV plays an important role in the market price with higher fractions being more desirable. Furthermore, most processes use a batch operation mode hence process productivity is limited by fermentation cycles with time between batches having a large impact in overall production and product pricing. Having steady state PHBV production capacity makes the process more efficient despite the relatively low productivities. Whilst further process development is still required to further increase productivity in order for this system to become industrially viable, overall the productivities reported here confirm that a continuous fermentation in which high 3HV fractions are achievable has
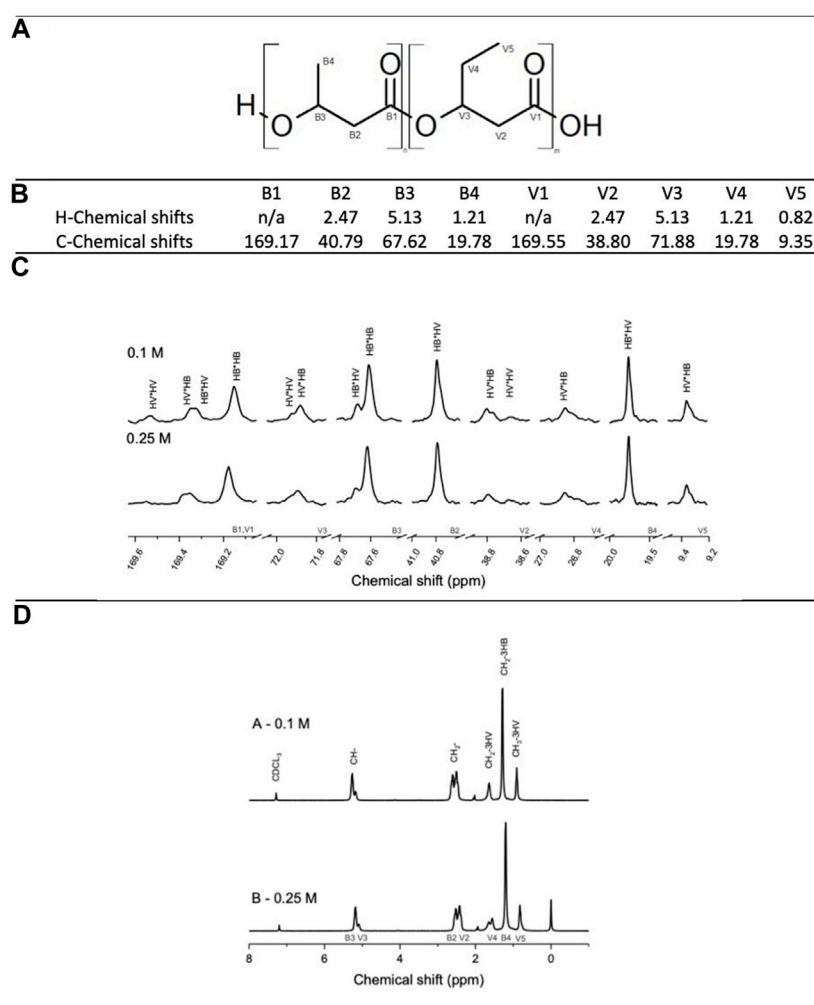
FIGURE 4
Top to bottom: **(A)** PHBV structure highlighting each carbon of the chain: B$_i$ and V$_i$ carbons correspond to PHB and PHV monomers respectively. **(B)** Characteristic chemical shifts for each carbon and proton in the PHBV molecule. **(C)** C-NMR and **(D)** H-NMR spectra of experiments A and B.

TABLE 3 D values for polymer structure characterisation.

Experiment	D Value	Polymer composition
A—0.1 M	1.12	Random
B—0.25 M	1.02	Random

a greater potential than the previously conducted batch fermentations.

With higher productivities, production rate and yields obtained for experiment B, it is shown that a higher carbon concentration in the media is recommended, whilst keeping in mind that concentrations close and above to 0.4 M will become toxic for *Haloferax mediterranei* (Parroquin Gonzalez and Winterburn, 2022).

3.4 Polymer structure

Nuclear magnetic resonance (NMR) was performed to determine the copolymer structure and to confirm the presence of PHB and PHV in the copolymer. Figure 4 shows the chemical shifts obtained in the ^{13}C-NMR and H-NMR spectrums. With the integrated value of the peaks corresponding to HB-HB, HB-HV, HV-HV and HV-HB neighbouring units, the *D* values were calculated, see Table 3. With a D values close to 1; 1.12 and 1.02 for experiments A and B respectively, a random polymeric structure is suggested for both experiments A and B (Žagar et al., 2006) (Table 3). Given that C4:0 and C5:0 were continuously co-fed the assimilation of the substrate and addition of PHB and PHV monomers into the PHBV polymeric chain would occur concurrently creating a chain with a random structure. A random allocation guarantees a well-mixed polymer with enhanced mechanical properties; with PHB being a more brittle and less elastic material it is not desirable to have long sections of it in the polymer chain (Anjum et al., 2016).

4 Conclusion

This work shows for the first time that continuous PHBV production in *Haloferax mediterranei* when fed volatile fatty acids is viable. Controlling and maintaining a steady state carbon concentration and cell density in the reactor resulted in a significant productivity normalised by OD improvement with respect to previous fed-batch strategies tested. When performing fermentations following this regime, productivity normalised by OD increased from 0.29 to 0.38 mg L^{-1} h^{-1} in continuously fed-fed batch fermentations to 0.87 and 1.43 mg L^{-1} h^{-1} when continuously operated for 0.1 and 0.25 M carbon concertation in the media respectively. Production rates of 9.9 and 15.8 mg h^{-1} for 0.1 and 0.25 M carbon concertation respectively were achieved, showing continuous product delivery is possible. Presenting the first continuous fermentation for PHBV production in *Haloferax mediterranei*, this paper offers a step towards the wider industrialisation of PHBV production by fermentation, offering a process that is relatively straight forward to operate and produces a relatively high product concentration.

Data availability statement

The raw data supporting the conclusions of this article will be made available by the authors, without undue reservation.

Author contributions

All authors contributed to the study conception and design. Material preparation, data collection and analysis were performed by MP-G. The first draft of the manuscript was written by MP-G and all authors commented on previous versions of the manuscript. All authors contributed to the article and approved the submitted version.

Conflict of interest

The authors declare that the research was conducted in the absence of any commercial or financial relationships that could be construed as a potential conflict of interest.

Publisher's note

All claims expressed in this article are solely those of the authors and do not necessarily represent those of their affiliated organizations, or those of the publisher, the editors and the reviewers. Any product that may be evaluated in this article, or claim that may be made by its manufacturer, is not guaranteed or endorsed by the publisher.

References

Alsafadi, D., and Al-Mashaqbeh, O. (2017). A one-stage cultivation process for the production of poly-3-(hydroxybutyrate-co-hydroxyvalerate) from olive mill wastewater by Haloferax mediterranei. *New Biotechnol.* 34, 47–53. doi:10.1016/j.nbt.2016.05.003

Amstutz, V., Hanik, N., Pott, J., Utsunomia, C., and Zinn, M. (2019). Tailored biosynthesis of polyhydroxyalkanoates in chemostat cultures. *Methods Enzym.* 627, 99–123. doi:10.1016/bs.mie.2019.08.018

Anjum, A., Zuber, M., Zia, K. M., Noreen, A., Anjum, M. N., and Tabasum, S. (2016). Microbial production of polyhydroxyalkanoates (PHAs) and its copolymers: A review of recent advancements. *Int. J. Biol. Macromol.* 89, 161–174. doi:10.1016/j.ijbiomac.2016.04.069

Arcos-Hernández, M. V., Laycock, B., Donose, B. C., Pratt, S., Halley, P., Al-Luaibi, S., et al. (2013). Physicochemical and mechanical properties of mixed culture polyhydroxyalkanoate (PHBV). *Eur. Polym. J.* 49 (4), 904–913. doi:10.1016/j.eurpolymj.2012.10.025

Brauneg, G., Sonnleitner, B., and Lafferty, R. M. (1978). A rapid gas chromatographic method for the determination of poly-β-hydroxybutyric acid in microbial biomass. *Eur. J. Appl. Microbiol. Biotechnol.* 6 (1), 29–37. doi:10.1007/BF00500854

Chen, C. W., Don, T. M., and Yen, H. F. (2006). Enzymatic extruded starch as a carbon source for the production of poly(3-hydroxybutyrate-co-3-hydroxyvalerate) by Haloferax mediterranei. *Process Biochem.* 41 (11), 2289–2296. doi:10.1016/j.procbio.2006.05.026

Chen, G. Q., and Jiang, X. R. (2018). Next generation industrial biotechnology based on extremophilic bacteria. *Curr. Opin. Biotechnol.* 50, 94–100. doi:10.1016/j.copbio.2017.11.016

Crutchik, D., Franchi, O., Caminos, L., Jeison, D., Belmonte, M., Pedrouso, A., et al. (2020). Polyhydroxyalkanoates (PHAs) production: A feasible economic option for the treatment of sewage sludge in municipal wastewater treatment plants? *Water* 12 (4), 1118. doi:10.3390/w12041118

Doi, Y., Kunioka, M., Kawaguch, Y., Segawa, A., Abe, C., and Kanesawa, Y. (1989). Production, properties, and biodegradation of microbial copolyesters of 3-hydroxybutyrate and 4-hydroxybutyrate. *Am. Chem. Soc. Polym. Prepr. Div. Polym. Chem.* 268, 1192.

Don, T. M., Chen, C. W., and Chan, T. H. (2006). Preparation and characterization of poly(hydroxyalkanoate) from the fermentation of Haloferax mediterranei. *J. Biomaterials Sci. Polym. Ed.* 17 (12), 1425–1438. doi:10.1163/156856206778937208

European Commison (2022). *European bioeconomy policy: Stocktaking and future developments: Report from the commission to the European parliament, the Council, the European economic and social committee and the committee of the regions.* Publications Office of the European Union.

Fernandez-Castillo, R., Rodriguez-Valera, F., Gonzalez-Ramos, J., and Ruiz-Berraquero, F. (1986). Accumulation of poly(β-hydroxybutyrate) by halobacteria. *Appl. Environ. Microbiol.* 51 (1), 214–216. doi:10.1128/aem.51.1.214-216.1986

Ferre-Guell, A., and Winterburn, J. (2018). Biosynthesis and characterization of polyhydroxyalkanoates with controlled composition and microstructure. *Biomacromolecules* 19 (3), 996–1005. doi:10.1021/acs.biomac.7b01788

Ferre-Guell, A., and Winterburn, J. (2019). Increased production of polyhydroxyalkanoates with controllable composition and consistent material properties by fed-batch fermentation. *Biochem. Eng. J.* 141, 35–42. doi:10.1016/j.bej.2018.10.004

Fu, X. Z., Tan, D., Aibaidula, G., Wu, Q., Chen, J. C., and Chen, G. Q. (2014). Development of Halomonas TD01 as a host for open production of chemicals. *Metab. Eng.* 23, 78–91. doi:10.1016/j.ymben.2014.02.006

Garcia Lillo, J., and Rodriguez-Valera, F. (1990). Effects of culture conditions on poly(β-hydroxybutyric acid) production by *Haloferax mediterranei*. *Appl. Environ. Microbiol.* 56 (8), 2517–2521. doi:10.1128/aem.56.8.2517-2521.1990

Gholami, A., Mohkam, M., Rasoul-Amini, S., and Ghasemi, Y. (2016). Industrial production of polyhydroxyalkanoates by bacteria: opportunities and challenges. *Minerva Biotechnol.* 28 (1), 59–74. doi:10.47277/JETT/8(4)1273

Han, J., Wu, L. P., Hou, J., Zhao, D., and Xiang, H. (2015). Biosynthesis, characterization, and hemostasis potential of tailor-made poly(3-hydroxybutyrate-co-3-hydroxyvalerate) produced by *Haloferax mediterranei*. *Biomacromolecules* 16 (2), 578–588. doi:10.1021/bm5016267

Hermann-Krauss, C., Koller, M., Muhr, A., Fasl, H., Stelzer, F., and Brauneg, G. (2013). Archaeal production of polyhydroxyalkanoate (PHA) Co- and terpolyesters from biodiesel industry-derived by-products *Archaea* 2013, 1–10. doi:10.1155/2013/129268

Huang, T. Y., Duan, K. J., Huang, S. Y., and Chen, C. W. (2006). Production of polyhydroxyalkanoates from inexpensive extruded rice bran and starch by Haloferax mediterranei. *J. Industrial Microbiol. Biotechnol.* 33 (8), 701–706. doi:10.1007/s10295-006-0098-z

Kamiya, N., Yamamoto, Y., Inoue, Y., Chujo, R., and Doi, Y. (1989). Microstructure of bacterially synthesized poly(3-hydroxybutyrate-co-3-hydroxyvalerate). *Macromolecules* 22 (4), 1676–1682. doi:10.1021/ma00194a030

Kasirajan, L., and Maupin-Furlow, J. A. (2021). Halophilic archaea and their potential to generate renewable fuels and chemicals. *Biotechnol. Bioeng.* 118 (3), 1066–1090. doi:10.1002/bit.27639

Khanna, S., and Srivastava, A. K. (2008). Continuous production of poly-β-hydroxybutyrate by high-cell-density cultivation of Wautersia eutropha. *J. Chem. Technol. Biotechnol.* 83 (6), 799–805. doi:10.1002/jctb.1868

Khanna, S., and Srivastava, A. K. (2005). Recent advances in microbial polyhydroxyalkanoates. *Process Biochem.* 40 (2), 607–619. doi:10.1016/j.procbio.2004.01.053

Koller, M., Hesse, P., Bona, R., Kutschera, C., Atlić, A., and Brauneg, G. (2007). Biosynthesis of high quality polyhydroxyalkanoate Co- and terpolyesters for potential medical application by the archaeon haloferax mediterranei. *Macromol. Symp.* 253, 33–39. doi:10.1002/masy.200750704

Koller, M., Maršálek, L., de Sousa Dias, M. M., and Brauneg, G. (2017). Producing microbial polyhydroxyalkanoate (PHA) biopolyesters in a sustainable manner. *New Biotechnol.* 37, 24–38. doi:10.1016/j.nbt.2016.05.001

Kourmentza, C., Plácido, J., Venetsaneas, N., Burniol-Figols, A., Varrone, C., Gavala, H. N., et al. (2017). Recent advances and challenges towards sustainable polyhydroxyalkanoate (PHA) production. *Bioengineering* 4 (2), 55. doi:10.3390/bioengineering4020055

Kumar, P., Mehariya, S., Ray, S., Mishra, A., and Kalia, V. C. (2016). Biotechnology in aid of biodiesel industry effluent (glycerol): biofuels and bioplastics. *Microb. Factories Biofuels, Waste Treat.* 1, 105–119. doi:10.1007/978-81-322-2598-0_7

Lauzier, C., Marchessault, R. H., Smith, P., and Chanzy, H. (1992). Structural study of isolated poly(β-hydroxybutyrate) granules. *Polymer* 33 (4), 823–827. doi:10.1016/0032-3861(92)90343-u

Mahler, N., Tschirren, S., Pflügl, S., and Herwig, C. (2018). Optimized bioreactor setup for scale-up studies of extreme halophilic cultures. *Biochem. Eng. J.* 130, 39–46. doi:10.1016/j.bej.2017.11.006

McChalicher, C. W. J., and Srienc, F. (2007). Investigating the structure-property relationship of bacterial PHA block copolymers. *J. Biotechnol.* 132 (3), 296–302. doi:10.1016/j.jbiotec.2007.04.014

Montemurro, M., Salvatori, G., Alfano, S., Martinelli, A., Verni, M., Pontonio, E., et al. (2022). Exploitation of wasted bread as substrate for polyhydroxyalkanoates production through the use of Haloferax mediterranei and seawater. *Front. Microbiol.* 13, 1000962. doi:10.3389/fmicb.2022.1000962

Oren, A. (2010). Industrial and environmental applications of halophilic microorganisms. *Environ. Technol.* 31 (8-9), 825–834. doi:10.1080/09593330903370026

Pais, J., Serafim, L. S., Freitas, F., and Reis, M. A. M. (2016). Conversion of cheese whey into poly(3-hydroxybutyrate-co-3-hydroxyvalerate) by Haloferax mediterranei. *New Biotechnol.* 33 (1), 224–230. doi:10.1016/j.nbt.2015.06.001

Parroquin Gonzalez, M., and Winterburn, J. (2022). Enhanced biosynthesis of polyhydroxyalkanoates by continuous feeding of volatile fatty acids in Haloferax mediterranei. *Biochem. Eng. J.* 179, 108307. doi:10.1016/j.bej.2021.108307

Plastics-Europe (2021). Plastics - the facts 2021. Avaliable At: https://plasticseurope.org/knowledge-hub/plastics-the-facts-2021/.

Platt, D. K. (2006). Biodegradable polymers, merket report. Report.

Policastro, G., Panico, A., and Fabbricino, M. (2021). Improving biological production of poly(3-hydroxybutyrate-co-3-hydroxyvalerate) (PHBV) co-polymer: A critical review. *Rev. Environ. Sci. Bio/Technology* 20 (2), 479–513. doi:10.1007/s11157-021-09575-z

Renard, E., Walls, M., Guérin, P., and Langlois, V. (2004). Hydrolytic degradation of blends of polyhydroxyalkanoates and functionalized polyhydroxyalkanoates. *Polym. Degrad. Stab.* 85 (2), 779–787. doi:10.1016/j.polymdegradstab.2003.11.019

Sudesh, K., Abe, H., and Doi, Y. (2000). Synthesis, structure and properties of polyhydroxyalkanoates: biological polyesters. *Prog. Polym. Sci. Oxf.* 25 (10), 1503–1555. doi:10.1016/S0079-6700(00)00035-6

Yu, S. T., Lin, C. C., and Too, J. R. (2005). PHBV production by Ralstonia eutropha in a continuous stirred tank reactor. *Process Biochem.* 40 (8), 2729–2734. doi:10.1016/j.procbio.2004.12.023

Žagar, E., Kržan, A., Adamus, G., and Kowalczuk, M. (2006). Sequence distribution in microbial poly(3-hydroxybutyrate-*co*-3-hydroxyvalerate) Co-polyesters determined by NMR and MS. *Biomacromolecules* 7 (7), 2210–2216. doi:10.1021/bm060201g

Check for updates

Heterologous constitutive production of short-chain-length polyhydroxyalkanoates in *Pseudomonas putida* KT2440: the involvement of IbpA inclusion body protein

Maria-Tsampika Manoli[1,2], Francisco G. Blanco[1,2], Virginia Rivero-Buceta[1,2], Ryan Kniewel[1,2], Sandra Herrera Alarcon[1,2], Sergio Salgado[1,2] and M. Auxiliadora Prieto[1,2]*

[1]Interdisciplinary Platform for Sustainable Plastics Towards a Circular Economy-Spanish National Research Council (SusPlast-CSIC), Madrid, Spain, [2]Polymer Biotechnology Group, Department of Microbial and Plant Biotechnology, Margarita Salas Center for Biological Research (CIB-CSIC), Madrid, Spain

Designing cell factories for the production of novel polyhydroxyalkanoates (PHAs) via smart metabolic engineering is key to obtain *à la carte* materials with tailored physicochemical properties. To this end, we used the model medium-chain-length-PHA producing bacterium, *P. putida* KT2440 as a chassis, which is characterized by its metabolic versatility and stress tolerance. Different PHA biosynthetic modules were assembled in expression plasmids using the Golden gate/MoClo modular assembly technique to implement an orthogonal short-chain-lengh-PHA (scl-PHA) switch in a "deaf" PHA mutant. This was specifically constructed to override endogenous multilevel regulation of PHA synthesis in the native strain. We generated a panel of engineered approaches carrying the genes from *Rhodospirillum rubrum, Cupriavidus necator* and *Pseudomonas pseudoalcaligenes,* demonstrating that diverse scl-PHAs can be constitutively produced in the chassis strain to varying yields from 23% to 84% PHA/CDW. Co-feeding assays of the most promising engineered strain harboring the PHA machinery from *C. necator* resulted to a panel of PHBV from 0.6% to 19% C5 monomeric incorporation. Chromosomally integrated PHA machineries with high PhaC[Cn] synthase dosage successfully resulted in 68% PHA/CDW production. Interestingly, an inverse relationship between PhaC synthase dosage and granule size distribution was demonstrated in the heterologous host. In this vein, it is proposed the key involvement of inclusion body protein IbpA to the heterologous production of tailored PHA in *P. putida* KT2440.

KEYWORDS

Pseudomonas putida, synthetic biology, polyhydroxyalkanoates, modular cloning assembly, IbpA inclusion body protein

1 Introduction

Polyhydroxyalkanoates (PHAs) are biotechnologically useful natural polyesters produced in many microorganisms. PHAs function as an intracellular carbon and energy storage reservoir with physical and mechanical properties that make them promising bioplastics with many possible applications (Zheng et al., 2019). Optimal PHA production generally occurs when a deficit exists in the nutritional conditions of the cell, with the deprivation of nitrogen being the most widely applied in bioproduction strategies (Kim and Lenz, 2001; Mahato et al., 2021; Ronďošová et al., 2022). Hydrophobic PHA accumulates in roughly spherical cellular inclusions called PHA granules that are segregated from the cytoplasm by a surface layer of amphipathic phasin proteins and other granule-associated proteins (Jendrossek, 2009). The Gram-negative *P. putida* KT2440 has been extensively studied as archetypal producer of medium-chain-length PHA (mcl-PHA) containing monomers of 6–14 carbon atoms in length (C6-C14) (Mezzina et al., 2021). The *P. putida pha* genomic locus contains the genetic machinery (Supplementary Figure S1, panel A) which along with its metabolic flexibility, allows for the production of mcl-PHA from a variety of substrates, including both PHA-like aliphatic fatty acids as well as PHA-unrelated carbon sources (Figure 1) (Cheng and Charles, 2016; Koller et al., 2017).

In contrast to *P. putida*, many bacterial species are capable of producing short-chain-length PHA (scl-PHA) with monomers of 3–5 carbon atoms in length (C3-C5) from PHA-unrelated carbon sources (Figure 1). For example, the production of polyhydroxybutyrate
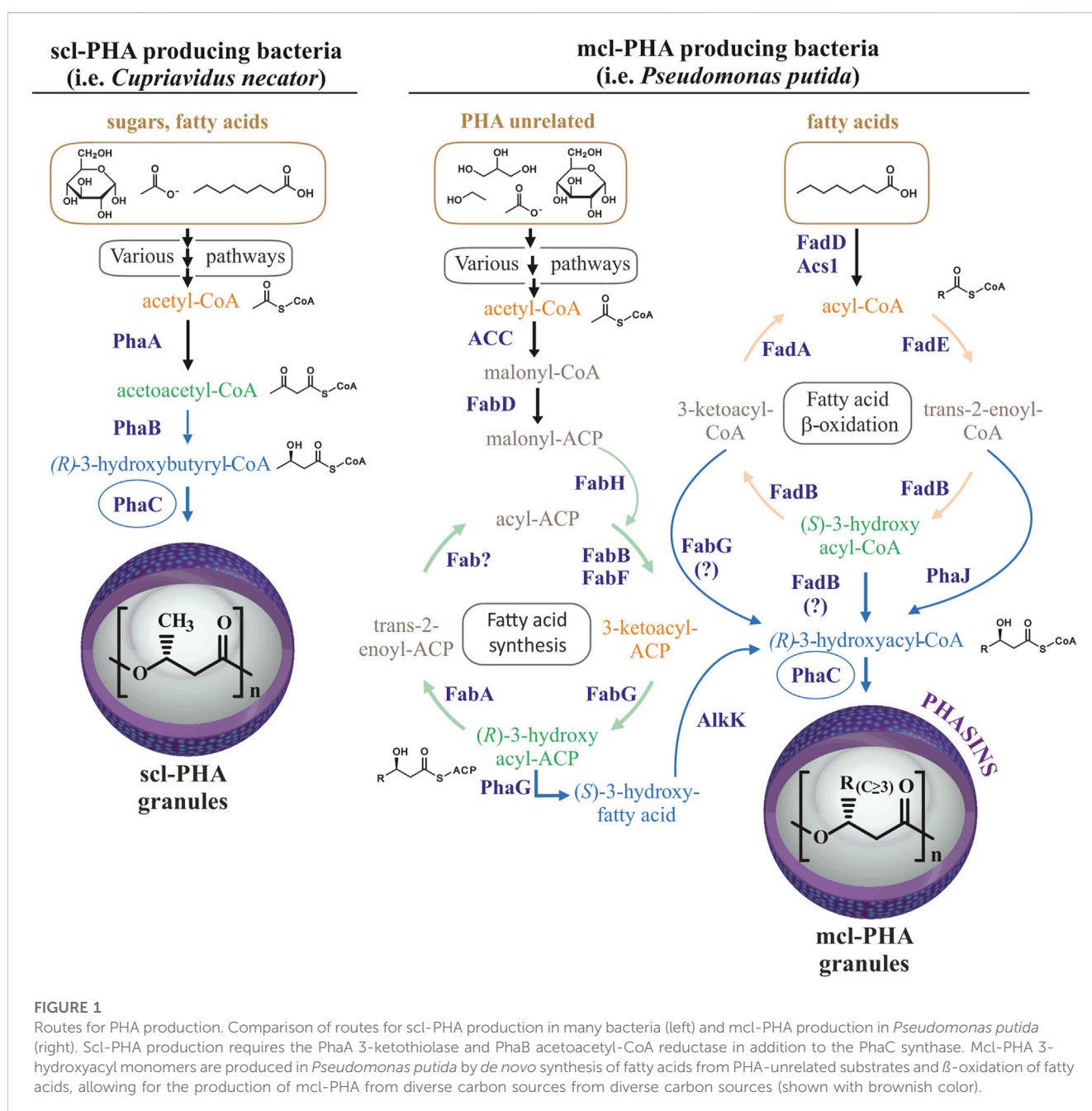

FIGURE 1
Routes for PHA production. Comparison of routes for scl-PHA production in many bacteria (left) and mcl-PHA production in *Pseudomonas putida* (right). Scl-PHA production requires the PhaA 3-ketothiolase and PhaB acetoacetyl-CoA reductase in addition to the PhaC synthase. Mcl-PHA 3-hydroxyacyl monomers are produced in *Pseudomonas putida* by *de novo* synthesis of fatty acids from PHA-unrelated substrates and ß-oxidation of fatty acids, allowing for the production of mcl-PHA from diverse carbon sources from diverse carbon sources (shown with brownish color).

(PHB) from sugars in *C. necator* requires the 3-ketothiolase PhaA to condense two glycolysis-derived acetyl-CoA molecules into acetoacetyl-CoA, and the acetoacetyl-CoA reductase PhaB to reduce acetoacetyl-CoA to four carbon 3-hydroxybutyryl-CoA, the substrate for PhaC synthase (Figure 1). Acetyl-CoA for PHB synthesis can also be provided by other carbon sources, such as the degradation of amino acids or ß-oxidation of fatty acids (Jendrossek and Pfeiffer, 2014). Some bacteria, such as *Rhodospirillum rubrum*, are capable of producing heteropolymers of both, scl-PHA with monomers of 4 and 5 carbon atoms, as well as mcl-PHA by incorporating 3-hydroxyhexanoate-CoA or 3-hydroxyheptanoate-CoA monomers when provided with medium-chain-length fatty acids (hexanoate) as the carbon source (Brandl et al., 1989; Jin and Nikolau, 2012; Godoy et al., 2023). Importantly, in addition to the supplied substrate and metabolic determinants, organism-specific PhaC synthase(s) determine the length monomers that can be incorporated into the polymer due to differences in substrate specificity (Kim et al., 2017). Thus, the class I PHA synthases, PhaC1 from *Cupriavidus necator* and PhaC2 from *R. rubrum* are generally able to incorporate monomers containing up to 5 or 7 carbons in length, respectively (Brandl et al., 1989). In contrast, the class II PHA synthases from *P. putida* can incorporate a wide variety of monomers of lengths between 6 and 14 carbons to produce mcl-PHAs. As mentioned above, wild type *P. putida* does not naturally produce scl-PHAs, which is likely due to the substrate specificity of its PHA synthases along with a metabolic propensity to produce longer chain 3-hydroxyacyl-CoA monomers (Huisman et al., 1989; Kim et al., 2017).

Pseudomonads gained special interest due to their metabolic versatility, adaptability to endogenous and exogenous stresses. Specifically, *P. putida* KT2440 has become a model organism for biotechnological, environmental and industrial applications due to the presence of different genome-scale metabolic models and high advances in synthetic biology and metabolic engineering fields (Mezzina et al., 2021). In fact, several studies have demonstrated the use of *P. putida* as a chassis for the heterologous expression of scl- or mcl-PHA machinery from other bacteria (Matsusaki et al., 1998; Clemente et al., 2000; Ouyang et al., 2007; Cha et al., 2020). For orthogonal scl-PHA production in this strain apart from the deletion of the native *pha* locus, the expression of *phb* genes is required (Figure 1) (Prieto et al., 2016). However, the majority of these studies were based on the heterologous inducible expression systems of *phb* gene clusters, which are not useful for scaling up processes. Digging into the optimization of the constitutive scl-PHA production in *P. putida,* in this work we have used as microbial chassis the PP05_01 strain with the entire native *pha* genomic locus deleted (Mato et al., 2020). To enhance the capacity for designing, building and testing of heterologous constitutive expression systems with different strengths, we adapted our Golden gate/MoClo modular assembly cloning method for obtaining plasmids suited for constitutive PHA production at different rates in *P. putida* (Blázquez et al., 2023). These approaches allowed us not only to control the monomer composition, but to identify the inclusion body protein IbpA as an important partner for heterologous production of scl-PHA in *P. putida* KT2440. We demonstrated an inverse relationship between PhaC synthase dosage and granule size/number distribution in the heterologous host driven by IbpA.

2 Materials and methods

2.1 Bacterial strains, media and culture conditions

Bacterial strains and plasmids used in this work are listed in Table 1 and Supplementary Table S1 respectively. Unless otherwise indicated, *E. coli* and *P. putida* strains pre-cultures were grown in lysogeny broth (LB) at 37°C and 30°C respectively, at 200 rpm. Streptomycin (75 µg/mL), ampicillin (100 µg/mL), kanamycin (50 µg/mL), gentamycin (10 µg/mL), chloramphenicol (34 µg/mL), IPTG (0.5–1 mM) and Xgal (40 µg/mL) were added as required. Solid media were made by the addition of 1.5% (w/v) agar.

For PHA production standard laboratory methods were performed as previously described (Manoli et al., 2022). Briefly, *P. putida* strains were grown overnight in LB, the cells were washed twice with 0.85% saline solution and adjusted to an optical density of 600 nm of 0.3. Then, *P. putida* cells were grown for 24 h at 30°C and 200 rpm in 0.1 N M63, a nitrogen-limited minimal medium (13.6 g/L KH_2PO_4, 0.2 g/L $(NH_4)_2SO_4$, 0.5 mg/L $FeSO_4 \cdot 7H_2O$, adjusted to pH 7.0 with KOH). This medium was supplemented with 1 mM $MgSO_4$, a solution of trace elements/Goodies (composition 1000X: 2.78 g $FeSO_4 \cdot 7H_2O$, 1.98 g $MnCl_2 \cdot 4H_2O$, 2.81 g $CoSO_4 \cdot 7H_2O$, 1.47 g $CaCl_2 \cdot 2H_2O$, 0.17 g $CuCl_2 \cdot 2H_2O$, 0.29 g $ZnSO_4 \cdot 7H_2O$ dissolved in 1 L water), 15 mM sodium octanoate or 20 mM glucose as the carbon source (C/N ratio was maintained at 40 mol/mol). Concerning the inducible P*trc* cultures 1 mM IPTG was used from the beginning of the assays. Culture growth was monitored in shaking Erlenmeyer flasks of 250 mL (maintaining a volume to air ratio of 1/5) by measuring optical density at 600 nm (OD600) using a portable spectrophotometer (ThermoFisher Scientific).

2.2 Transformation of *Pseudomonas putida* strains by electroporation

Pseudomonas putida strains were transformed following the protocol described by Choi et al. with some adaptations (Choi et al., 2006). Briefly, the strains of *P. putida* KT2440 and PP05_01 were grown overnight in 5 mL of LB at 30°C and 200 rpm and subcultured into 50 mL of LB to an OD600 between 0.5–1.0. These cultures were pelleted at 3,200 ×*g* for 8 min, washed five times with 300 mM sucrose and resuspended in 500 µL of 300 mM sucrose. 100 µL of cell suspension were mixed with 100 ng of desired plasmid and transferred to a 2 mm gap electroporation cuvette. After a pulse of 25 µF, 2.5 kV and 200 Ω; 900 µL of room temperature LB was added and transferred to a 100 × 16 mm round-bottom polypropylene tube and incubated for 1 h at 30°C, 200 rpm. 5 µL and 100 µL of the transformation cultures were plated on LB agar plates containing the corresponding antibiotic for the plasmid maintenance and grown at 30°C.

2.3 Molecular biology reagents

Plasmid DNA minipreps were made using the High Pure Plasmid Isolation Kit (Roche) following the manufacturer's protocol. Genomic extractions of *P. putida* KT2440, *R. rubrum* ATCC11170, *C. necator*

TABLE 1 Strains used in this study.

Strains	Relevant characteristics	References
Pseudomonas putida		
KT2440	Wild-type strain derived from *P. putida* mt-2 cured of the pWW0 plasmid	Bagdasarian et al. (1981)
PP05_01	KT2440 derivative strain with *pha* cluster deleted (PP_5003-PP_5008) _CECT 30020	Mato et al. (2020)
PP00_02	Km^r, PP05_01 derivative strain expressing P*trc:phaC^{Cn}-phaA^{Cn}-phaB^{Cn}* genes, integrated into the genome (via mini-Tn*5* transposon) using the pMAB26 plasmid	This work
PP00_03	Km^r, KT2440 strain expressing P*trc:phaC^{Cn}-phaA^{Cn}-phaB^{Cn}* genes integrated into the genome (via mini-Tn*5* transposon) using the pMAB26 plasmid	This work
PP01_02	Gm^r, PP05_01 derivative strain harboring 14f:BCD2-*phaC^{Cn}-rnpB*T1; 14a:BCD2-*phaA^{Cn}-rpoC*;14a:BCD2-*phaB^{Cn}-*λT1 at *att*Tn*7* site	This work
PP05_12	Gm^r, PP05_01 derivative strain harboring 14a:BCD2-*phaC^{Cn}-rnpB*T1; 14a:BCD2-*phaA^{Cn}-rpoC*;14a:BCD2-*phaB^{Cn}-*λT1, at *att*Tn*7* site	This work
PP05_15	Gm^r, PP01_02 derivative strain with *ibpA* locus deleted (PP_1982)	This work
PP05_16	Gm^r, PP05_01 derivative strain harboring 14a:BCD2-*phaC^{Cn}-rnpB*T1; 14a:BCD2-*phaA^{Cn}-rpoC*;14a:BCD2-*phaB^{Cn}-*λT1; 14a:BCD2-*phaP1^{Cn}-rnpB*T1, at *att*Tn*7* site	This work
KT2440 (pGG128)	Km^r, KT2440 strain harboring pGG128 empty plasmid	This work
PP05_01 (pGG128)	Km^r, PP05_01 strain harboring pGG128 empty plasmid	This work
PP05_01 (pSS126)	Km^r, PP05_01 strain harboring pSS126; 14a:BCD2-*phaC2^{Rr}-*λT0; 14a:BCD2-*phaA^{Rr}-*λT0; 14a:BCD2-*phaB^{Rr}-* λT0	This work
PP05_01 (pRK216)	Km^r, PP05_01 strain harboring pRK216; SynPro16-*phaC^{Cn}-rnpB*T1; SynPro16-*phaA^{Cn}-rpoC*; SynPro16-*phaB1^{Cn}-*T500	This work
PP05_01 (pMM85)	Km^r, PP05_01 strain harboring pMM85; 14a:BCD2-*phaC^{Cn}-rnpB*T1; 14a:BCD2-*phaA^{Cn}-rpoC*; 14a:BCD2-*phaB^{Cn}-*λT1; 14a:BCD2-*phaP1^{Cn}-rnpB*T1	This work
PP05_01 (pMM106)	Km^r, PP05_01 strain harboring pMM106; 14a:BCD2-*phaC5^{Pp}-rnpB*T1; 14a:BCD2-*phaA3^{Pp}-rpoC*; 14a:BCD2-*phaB^{Pp}-*λT1; 14a:BCD2-*phaP1^{Pp}-rnpB*T1	This work
PP05_12 (pMM194)	Km^r, Gm^r, PP05_12 strain harboring pMM194; 14a:BCD2-*ibpA^{Pp}-rnpB*T1	This work
PP05_15 (pMM194)	Km^r, Gm^r, PP05_15 strain harboring pMM194; 14a:BCD2-*ibpA^{Pp}-rnpB*T1	This work
PP01_02 (pBDN2-GFP)	Km^r, PP01_02 strain harboring pBDN2-GFP, empty plasmid	Blanco et al. (2023)
PP01_02 (pBDN2-PhaP)	Km^r, PP01_02 strain harboring pBDN2-PhaP, harboring the *PhaP1^{Cn}*	Blanco et al. (2023)
Escherichia coli		
DH5αλ*pir*	Tc^r, cloning host; DH5α lysogenized with λ*pir* phage. Host strain for *ori*R6K plasmids	Zobel et al. (2015)
DH10B	Sp^r, cloning host; F-, *mcrA* Δ(*mrr hsdRMS-mcrBC*) Φ80d*lac*ΔM15 Δ*lacX74 deoR recA1 araD139* Δ(*ara-leu*)7697	Invitrogen, Thermo Fisher Scientific, United States of America
HB101 (pRK600)	Cm^r, Conjugation helper strain; F$^-$ λ$^-$ *hsdS20*(r$_B^-$ m$_B^-$) *recA13 leuB6*(Am) *araC14* Δ(*gpt-proA*)62 *lacY1 galK2*(Oc) *xyl-5 mtl-1 rpsL20*(Sm^r) *glnX44* (AS)	Boyer and Roulland-Dussoix (1969)
R. rubrum ATCC 11170	*R. rubrum* type strain	Pfennig and Trüper (1971)
C. necator H16 DSM 428	*C. necator* H16	Makkar and Casida (1987)

H16 and *P. pseudoalcaligenes* CECT5344 were performed with the illustra bacteria genomicPrep Mini Spin Kit (GE Healthcare). DNA agarose gel bands, PCR products and digestion products were purified with illustraTM GFX PCR DNA and Gel Band Purification Kit (GE Healthcare). DNA concentration was measured using a NanoDrop 2000 Spectrophotometer (ThermoFisher Scientific). The Golden gate restriction enzymes, BbsI (BpiI) and BsaI (Eco31I) were from ThermoFisher Scientific. Phusion DNA polymerase, T4 DNA ligase and all other restriction enzymes were from New England

Biolabs. The MoClo toolkit was a gift from Sylvestre Marillonnet via Addgene (Kit #1000000044) (Weber et al., 2011; Werner et al., 2012).

2.4 Adapted golden gate/MoClo protocol

Golden gate/MoClo assembly is a hierarchical method requiring the establishment of a library of promoter + RBS, CDS and terminator parts (level 0) that are assembled into higher order promoter-CDS-
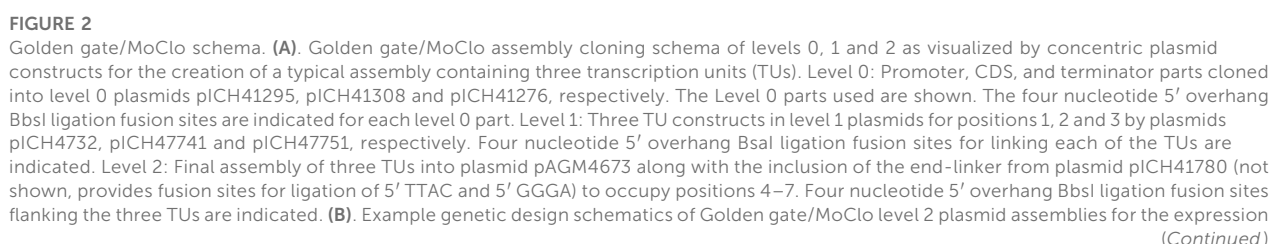
FIGURE 2

Golden gate/MoClo schema. **(A)**. Golden gate/MoClo assembly cloning schema of levels 0, 1 and 2 as visualized by concentric plasmid constructs for the creation of a typical assembly containing three transcription units (TUs). Level 0: Promoter, CDS, and terminator parts cloned into level 0 plasmids pICH41295, pICH41308 and pICH41276, respectively. The Level 0 parts used are shown. The four nucleotide 5′ overhang BbsI ligation fusion sites are indicated for each level 0 part. Level 1: Three TU constructs in level 1 plasmids for positions 1, 2 and 3 by plasmids pICH4732, pICH47741 and pICH47751, respectively. Four nucleotide 5′ overhang BsaI ligation fusion sites for linking each of the TUs are indicated. Level 2: Final assembly of three TUs into plasmid pAGM4673 along with the inclusion of the end-linker from plasmid pICH41780 (not shown, provides fusion sites for ligation of 5′ TTAC and 5′ GGGA) to occupy positions 4–7. Four nucleotide 5′ overhang BbsI ligation fusion sites flanking the three TUs are indicated. **(B)**. Example genetic design schematics of Golden gate/MoClo level 2 plasmid assemblies for the expression

(Continued)

FIGURE 2 (Continued)
of PHB machinery from *R. rubrum* (pSS126), *Pseudomonas pseudoalcaligenes* (pMM106) and *Cupriavidus necator* (pRK216, pMM85, pFB52). The TU assemblies contain the PHA synthase, thiolase, reductase, and optional phasin genes with their promoters and terminators indicated. Genetic design glyphs follow the Synthetic Biology Open Language (SBOL) visual standard for elements: promoter, RBS, CDS, terminator and assembly scar.

terminator transcription units (TU, level 1) and finally into assemblies containing 1 to 7 transcription units (level 2, Figure 2). The parts comprised the essential units needed to assemble the heterologous expression constructs for PHA production (i.e., *phaC* synthase, *phaA* 3-ketothiolase, *phaB* acetoacetyl-CoA, *phaP* phasin) from *C. necator*, *P. pseudoalcaligenes* and *R. rubrum*. Non-CDS parts included synthetic constitutive promoters of varying strengths. These promoters contained RBS sequences by the inclusion of the two Shine-Dalgarno sequences/ RBSs in the bicistronic translational coupler BCD2 for the low expression promoter BG28/14a from Zobel *et al.* (level 0 plasmid pSS15) or the AGGGGG RBS for the moderate expression promoter SynPro16 from Tiso *et al.* (level 0 plasmid pRK154) (Zobel et al., 2015; Tiso et al., 2016). Following the design of SynPro16 validated by Tiso et al., the presence of the upstream insulating terminator λT0 was maintained in this promoter part. These two promoters were chosen for the assemblies used in the proof-of-concept experiments described below as they were expected to confer low and moderate constitutive expression in *P. putida* due to the published descriptions of their activities (Zobel et al., 2015; Tiso et al., 2016). Finally, parts were made for five rho-independent terminators with efficiencies of ≥98%, including the natural terminators λT0, *rrnB*_T1, *rnpB*_T1, *rpoC* and the synthetic T500 (Stueber and Bujard, 1982; Lutz and Bujard, 1997; Yarnell and Roberts, 1999; Larson et al., 2008; Cambray et al., 2013).

Golden gate/MoClo plasmids were constructed following Weber et al. with some modifications and recently updated by Weber et al. (2011), Blázquez et al. (2023). For Level 0 plasmid construction, every part was PCR amplified with DNA oligos designed using Benchling (www.benchling.com) with the following characteristics: a tail containing the BbsI recognition site followed by the corresponding four nucleotide fusion site, 21 bp of minimal length for target complementarity, 50°C of minimal T_m for that region and a maximal T_m difference of ±1.5°C between both oligos. Promoter and CDS sequences were PCR amplified from *C. necator* H16, *R. rubrum* ATCC11170, *P. pseudoalcaligenes* CECT5344 and *P. putida* KT2440 genomic DNA or plasmid templates. Terminator sequences were PCR amplified from *E. coli* DH5α genomic DNA or plasmid templates. Oligo primers, templates and references for all Golden gate level 0 PCR amplifications are listed in Supplementary Table S2. Where needed DNA domestication (removal of naturally present internal BbsI or BsaI restriction sites was carried out using the strategy of Engler et al. (2008). This strategy generated PCR subparts with 5' cohesive end fusion sites overlapping the internal restriction sites to be eliminated. The primers used for PCR contained synonymous substitution point mutations in the fusion nucleotides of a BbsI site that eliminate the restriction site upon ligation in the golden gate level 0 reaction. PCR products were purified using a gel purification kit following manufacturer instructions. Golden gate digestion-ligation reactions were set up with 100 ng of level 0 acceptor plasmid (position *abc*, pICH41295; position *def*, pICH41308; or position *gh*, pICH41276; Supplementary Table S1) and the corresponding amount of gel

purified PCR product to achieve a 2:1 insert-vector molar ratio; 10 U BbsI, 400 U T4 DNA ligase and 1 mM ATP in Buffer G (10 mM Tris-HCl pH 7.5, 10 mM MgCl$_2$, 50 mM NaCl and 0.1 mg/mL bovine serum albumin; ThermoFisher Scientific) in a reaction volume of 20 μL. The reaction was incubated in a thermocycler with four cycles of 37°C for 10 min and 16°C for 10 min followed by 65°C for 20 min. A 100 μL aliquot of chemically competent *E. coli* DH5α was then transformed by heat shock with 5 μL of the Golden gate reaction. Transformed cells were plated on LB-agar supplementedwith 75 μg/mL streptomycin, 0.5 mM IPTG and 40 μL/mL X-gal and grown overnight at 37°C for selection of the disruption of *a*-complementation *ß*-galactosidase activity. Several white colonies per transformation were transferred to 4 mL LB medium with 75 μg/mL streptomycin and grown overnight at 37°C for plasmid purification. The extracted plasmids were digested with BsaI to check for the presence of the correct insert size and confirmed by sequencing with primers RK81 and RK82 (Supplementary Table S2).

For Level 1 construction of TUs, the reaction mix contained 100 ng of acceptor plasmid (depending on the TU position, Supplementary Table S1), the three level 0 plasmids containing a promoter plasmid part, a CDS plasmid part and a terminator plasmid part in a 2:1 donor plasmid:acceptor plasmid molar ratio; 10 U BsaI, 400 U T4 DNA ligase and 1 mM ATP in Buffer G in a reaction volume of 20 μL. The reaction was incubated in a thermocycler for four cycles of 40°C for 10 min and 16°C for 10 min, then at 50°C for 10 min and 80°C for 20 min. Reactions were transformed into *E. coli* DH5α and plasmids prepared as for level 0 golden gate reactions except that 100 μg/mL ampicillin, 0.5 mM IPTG and 40 μL/mL X-gal were present for selection. The extracted plasmids were digested with BbsI to check for the presence of the correct insert size and sequenced with primers RK155 and RK156 (Supplementary Table S2).

Level 2 assembly reactions were carried out with 100 ng of acceptor plasmid (pAGM4673, RK2 origin of replication providing some range in copy number in pseudomonads estimated to be maintained at 30 ± 10 copies per genome equivalent in *P. putida*, Supplementary Table S1), the corresponding end-linker plasmid depending on the number of TUs to be inserted, each level 1 plasmid in a 2:1 donor plasmid:acceptor plasmid molar ratio, 10 U BbsI, 400 U T4 DNA ligase and 1 mM ATP in Buffer G in a reaction volume of 20 μL. The reaction was incubated in a thermocycler with four cycles of 37°C for 10 min and 16°C for 10 min followed by 65°C for 20 min. Reactions were transformed into *E. coli* DH5α as for level 0 golden gate reactions except that 50 μg/mL kanamycin was added for selection. Red-white color selection was carried out (red color canthaxanthin produced by its operon in the cloning site of pAGM4673) and several white colonies were transferred to 4 mL of liquid LB medium with 50 μg/mL kanamycin for plasmid minipreps. The extracted plasmids were confirmed by digestion with DraIII or EcoRI and sequenced using primers RK157 and RK158 (Supplementary Table S2).
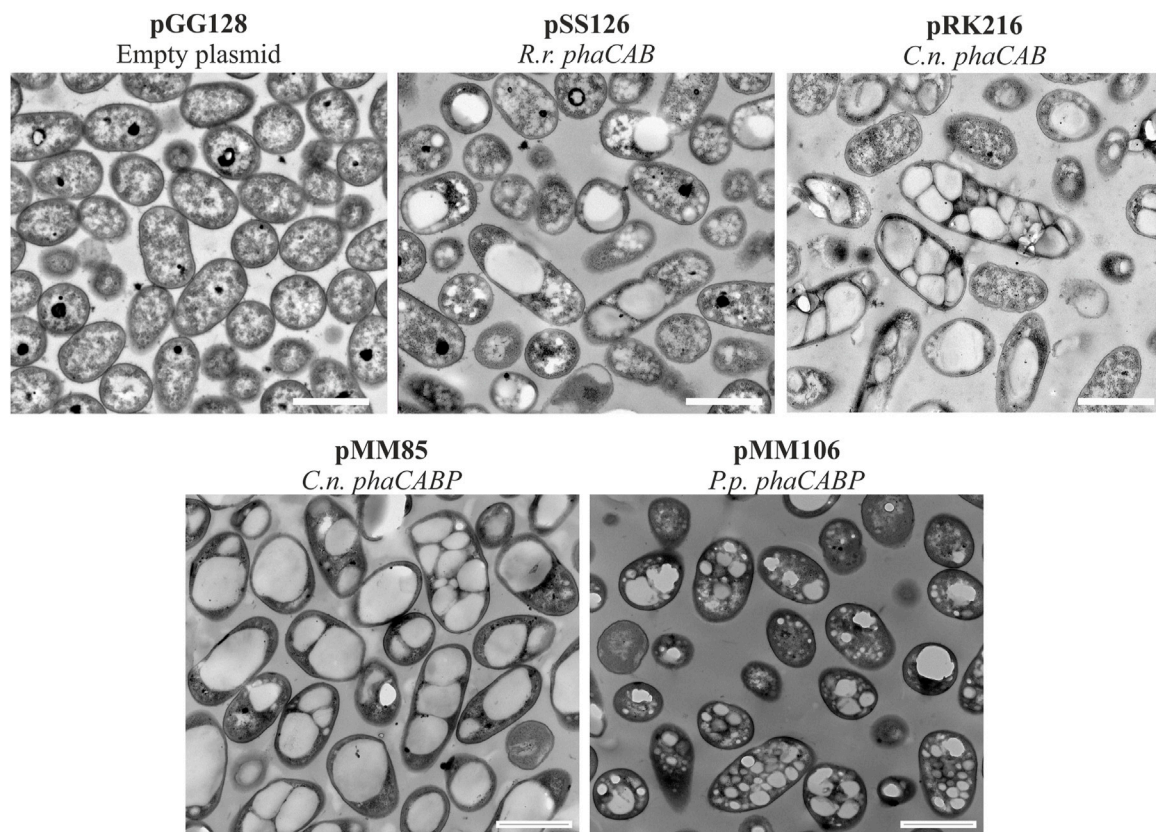
FIGURE 3
Transmission electron microscopy photos of heterologous PHA production. Pseudomonas putida PP05_01 strains expressing heterologous PHA machinery grown for 24 h in PHA production conditions with 15 mMoctanoate. Scale bars represent 1 μm. Abbreviations: R. r.: Rhodospirillum rubrum, C. n.: Cupriavidus necator, P. p.: Pseudomonas pseudoalcaligenes.

2.5 Strains construction for deletion, complementation assays, and chromosomic integration

For *ibpA* gene deletion, the pEMG knockout system was used, generating the PP05_15 strain. *ibpA* encodes a small heat shock protein, located in PP_1982 locus. Two pairs of primers (MM388-MM389, MM390-MM391, Supplementary Table S2) were designed to amplify the flanking fragments of the *ibpA* locus. An overlap PCR was carried out giving a product of 1.6 kb and was cloned into pEMG plasmid using EcoRI and BamHI restriction enzymes. For the first and second recombination steps, we followed the protocol described above. In this case for the confirmation of the second recombination event, external pair of primers (i.e., MM392-MM393) of to be deleted region were used.

For IbpA complementation assays, the PP05_15 strain was transformed with pMM194 plasmid (obtained using Golden gate/MoClo strategy) that contains the *ibpA* gene under the low strength 14a promoter and the BCD2 element. PHA accumulation assays were then performed as stated below.

For the co-localization experiments one multipurpose vector was constructed, with a phasin fusion position tags and under the control of the inducible *Pm* promoter. For the *in vivo* co-localization experiments the pBDN2 vector was used, since it contains the

cloning site for the phasin between two SapI restriction sites (Blanco et al., 2023). Then, PP01_02 strain was transformed with the pBDN2 derived plasmids (i.e., empty, including only the msf-GFP, as negative control and harboring the wild type *PhaP1^{Cn}*). The resulting strains were inoculated at OD600 nm of 0.3 under PHA accumulating conditions and were allowed to grow until the polymer accumulation was visible (i.e., OD600 = 0.7). At this point the cultures were induced with 1 mM 3 MB for the expression of the fusion protein phasin-GFP (Mato et al., 2020).

To facilitate the single-copy genes into bacterial chromosome (i.e., for the generation of PP05_12 and PP01_02 strains), an adapted for Golden gate broad host range mini-Tn*7* vector (pRK99) was used. The genome integration is based on a neutral and naturally evolved *att*Tn*7* site, located downstream of a highly conserved *glmS* gene (Zobel et al., 2015). A four parental mating process was carried out from overnight LB precultures of *E. coli* CC118λpir bearing pMM175 and pFB52 plasmids (donor strains), *E. coli* HB101 (pRK600) (helper strain), *E. coli* DH5αλpir (pTnS-1) (leading transposase strain), and *P. putida* PP05_01 (recipient strain). The transconjugants were selected on cetrimide agar containing 10 μg/mL gentamycin plates and incubated at 30°C for 18 h. The next day few colonies were picked on LB kanamycin, to verify the loss of the plasmid and LB gentamycin and incubated at 30°C for 18 h. Few gentamycin resistant and kanamycin sensitive clones were selected

to verify the correct insertion of the transposon into the *att*Tn*7* stie and checked via colony PCR and sequencing (Zobel et al., 2015).

2.6 PHA quantification and monomer composition

For PHA quantification, 20 mL of each *P. putida* strain grown in PHA production conditions (see 2.1 section) for 24 h were centrifuged for 30 min at 3,200 ×*g*. Cells were washed once with 0.85% NaCl and lyophilized for 24 h. Lyophilized pellets were weighed to obtain the cell dry weight (CDW) of total biomass. PHA monomer composition and PHA content were determined by Gas Chromatography-Mass Spectrometry (GC-MS) of the methanolysed polyester (Braunegg et al., 1978; Revelles et al., 2016; Manoli et al., 2022). In each condition, at least two independent biological replicates were performed. Where the statistical error was higher of 10%, four biological replicates were performed. During the methanolysis process, two technical replicates were included for each biological sample. 2–5 mg of lyophilized cells were resuspended in 2 mL of methanol acidified with 3% (v/v) H_2SO_4 for scl-PHA analysis, and resuspended in 2 mL of methanol containing 15% (v/v) H_2SO_4 for mcl-PHA analysis. 2 mL of chloroform containing 0.5 mg/mL 3-methylbenzoic acid was added to the samples as an internal standard. Samples were boiled in a screw-capped tube at 100°C for 4 or 5 h to assay scl-PHA or mcl-PHA, respectively. After cooling, the mixture was washed twice by adding 1 mL of distilled water, centrifuged for 10 min, and followed by the removal of the aqueous phase. The organic layer containing the resulting methyl ester of each monomer was analyzed by GC-MS using an Agilent 7890A GC equipped with a DB-5HT capillary column (30 m length, 0.25 mm internal diameter, 0.1 μm film thickness) and mass data were acquired and processed with an Agilent 5975C mass spectrometer. Samples (1 μL) of the organic phase were injected with helium as carrier gas at a ratio of 1:10 with 1 part sample to 10 parts helium, and the oven temperature was programmed to remain at 80°C for 2 min and then increased at a rate of 5°C/min up to 115°C for the efficient separation of peaks. The temperature of the injector was 250°C. Spectra were obtained as electron impacts with an ionizing energy for MS operation of 70 eV. Standard curves with known quantities of PHB (Sigma-Aldrich) or poly (3-hydroxyhexanoate-co-3-hydroxyoctanoate) (Bioplastech, Ltd.) dissolved in chloroform were used to calculate the monomer composition of the extracted polymers.

Monomer composition was also analysed by NMR. For these experiments, the used solvent was deuterated chloroform (chloroform-d 99.8%) that contains 0.03% (v/v) tetramethylsilane (TMS) ($CDCl_3$) (ref. 225,789 from Sigma-Aldrich). Proton NMR spectra (^{1}H-NMR) were recorded using a 90° pulse experiment under the following acquisition parameters: 128 scans with a fixed receiver gain value of 287, spectral width of 12.0164 ppm, 32,768 points in the time domain, and acquisition time of 2.27 s. COSY spectra were recorded using the standard Bruker sequence *cosygpqf*. Spectra were recorded under the following acquisition parameters: fixed receiver gain value of 1290, 128 scans and a spectral width of 13.0177 × 13.0177 ppm.

The 1D (1H), 2D Correlated Spectroscopy (COSY) NMR spectra of the extracted polymers were recorded on Bruker AV III 600 MHz spectrometer (Bruker, Rheinstetten, Germany) using a XI 600 MHz S3 5 mm probe with Z-gradient in $CDCl_3$. The resulting NMR spectra were processed by Mestrelab MNova software (Version 14.2.3–29241). Phasing and baseline correction were manually completed.

According to ^{1}H-NMR and COSY assays (Supplementary Figure S3), the signals assigned to the protons of the HB monomer are methyl at 1.27 ppm (4), methylene at 2.50 ppm (2) and methine at 5.25 ppm (3), and the protons assigned to the mcl-HA monomer are methyl at 0.90 ppm (9), methylene groups of the side chain at 1.28 and 1.59 ppm (8), methylene group at 2.50 ppm (6) and methine at 5.25 ppm (7).

2.7 Granule extraction and identification of key associated proteins

For granule extraction, cultures grown under PHA-producing conditions for 24 h as mentioned above were harvested by centrifugation for 20 min at 10,000 ×*g*. Cells were resuspended in 15 mM Tris-HCl pH 8.0 buffer and then disrupted twice using French Press (at ≈ 1 000 psi). PHB granules from pellets (resuspended in 15 mM Tris-HCl pH 8.0) were purified by two subsequent glycerol density gradient centrifugations at 18,000 ×*g* for 40 min. The first gradient consisted of 6 mL of sample layered over 3 mL of 85% glycerol and 6 mL of 50% glycerol. Granules were isolated after centrifugation with a Pasteur pipette at the glycerol 50%–85% interface. The second gradient consisted of 3 mL of granule fraction from the first gradient over 4 layers of 3 mL of glycerol at 85%, 80%, 60%, and 40% glycerol. Granules were isolated after centrifugation from the glycerol 40%–60% interface.

For granule-associated protein detection, independent granule isolations were normalized to the same PHB content by PHA quantification as explained above. Aliquots containing 22.5 μg of PHB from each extraction were run onto 12.5% SDS-PAGE gels and stained using BlueSafe (Nzytech).

For N-terminal sequencing of granule-associated proteins, these SDS-PAGE (12.5%) gels were transferred onto methanol activated-polyvinylidene fluoride (PVDF) membranes in a semidry transfer device (Biorad) soaked in transfer buffer (25 mM Tris, 192 mM glycine, 20% methanol, pH 8.3) for 1 h 15 min at 15 mV. The resulting transferred membranes were stained with Ponceau S stain (ThermoFisher), and the visible protein bands of selected proteins were subjected to N-terminal sequencing by Edman degradation in a protein sequencer (Applied Biosystems, Procise 494).

2.8 Microscopy assays

Cultures were routinely visualized with a 100× phase-contrast objective using an epifluorescence microscope Leica DM4B (Wetzlar, Germany) and images were taken with an attached camera (Leica DFC345 FX). Where needed a filter system L5 was used for GFP observation. In order to fix cells and achieve a correct superposition of images from the different channels, microscope slides were covered by a thin layer of 0.1% poly-L-lysine. Then, 5 μL of the cell suspension was deposited on the covered slide and immediately observed under microscopy.

For Transmission electron microscopy (TEM) experiments, *P. putida* cells previously grown during 24 h under M63 0.1 N

minimal medium supplemented with 15 mM octanoate, were harvested and washed twice with 1 X PBS. Then, the cells were fixed for 1 h in 3% glutaraldehyde in PBS and washed twice with PBS. Samples were post-fixed in 1% osmium tetroxide and 0.8% potassium ferricyanide for 1 h at 4°C. Samples were washed with PBS prior to dehydration with an increasing gradient of ethanol (30%, 50%, 70%, 80%, 90% and 100%) of 10 min per step. Samples were embedded in LX112 resin and were polymerized for 48 h at 60°C. 60–80 nm sections were placed in copper grids of 75 mesh and stained with 5% uranyl acetate for 15 min and lead citrate for 3 min. Samples were viewed in a JEOL 1230 TEM and images were taken with a CMOS TVIPS 16 mp camera.

To determine the size of PHA granules from TEM micrographs, 50 cells of each engineered strain were selected, in which PHA granule diameters were measured using ImageJ software. In each case, 100 granules with sharp boundaries were selected and analyzed. Thus, to avoid measuring cells in different section plans, only granules from cells with a size of 0.9-1 x 2–2.2 μm (width x length) were considered (Galán et al., 2011).

3 Results

3.1 Generating a *Pseudomonas putida* chassis for customized constitutive scl-PHA production

The chassis applied in this work was the PHA-deficient strain (*P. putida* KT2440 Δ*pha*, named as PP05_01). This lacks the native *pha* gene cluster, including *phaC1ZC2DFI* that encodes the two PHA synthases, the depolymerase, the transcriptional activator PhaD and the two phasins (including promoters and regulatory regions that drive the expression of *pha* genes) (Supplementary Figure S1 and Supplementary Table S3).

Phenotypic evaluation of the PP05_01 (Δ*pha*) strain confirmed that it does not produce PHA as determined microscopically by the complete lack of PHA granules when cultured in LB or 0.1 N M63 supplemented with 15 mM octanoate (Supplementary Figure S1) and by the lack of detectable PHA by GC-MS (Table 2). Growth of the PP05_01 strain was highly similar to wild type. Comparison of the two strains revealed lower relative CFUs in the wild type (Supplementary Figure S1). This was expected due to the allocation of metabolic resources towards PHA production in the wild type that were instead dedicated to biomass accumulation in the Δ*pha* strain (De Eugenio et al., 2010a; Manoli et al., 2022).

Since PP05_01 strain will be the foundation for implanting an orthogonal, synthetic *phb* gene cluster designed for constitutive scl-PHA production, we firstly validated the scl-PHA production capacity when carrying an inducible monocopy system that allows the production of the PHA machinery in the presence of an inducer. Thus, we chromosomally inserted via mini Tn5 transposon the P*trc*: *phaC*Cn-*phaA*Cn-*phaB*Cn cluster from *C. necator* driven by the P*trc* promoter inducible by IPTG. Two strains were obtained on wild type background and *pha* null, PP00_03 and PP00_02, respectively. By initial screening of PP00_03 using octanoate as carbon and energy source, we obtained 60% PHA/CDW, composed of 43% C4, 4% C6 and

53% C8 (data not shown). For the purpose of this study, the influence of different carbon sources under nitrogen limited conditions on PHA accumulation was evaluated in the resulting *pha* null background strain PP00_02 (Table 2). The best PHA accumulation was observed when a fatty acid precursor such as octanoic acid was used compared to glucose or acetate. In fact, PP00_02, lacking the *pha* cluster, reached high amounts of PHA accumulation with octanoate (e.g., nearly 70% PHA/ CDW) and 50% of PHA/CDW under glucose conditions. Taking into account the toxicity effect of acetate and the low growth performance under these conditions (e.g., reaching up to 0.3 g/L total biomass), PP00_02 produced slight amounts of 3% PHA/CDW. Taken together, these experiments validated the PP05_01 chassis as modifiable to enable orthogonal constitutive PHA production.

3.2 Custom golden gate/MoClo assembly for constitutive *pha* expression constructs

For the installation of efficient constitutive PHA production machinery, we aimed to develop a modular, extensible system for the creation of PHA gene expression constructs that would be easy to deploy with the chassis strain. To this end, we adapted the Golden gate/MoClo assembly cloning technique to rapidly generate gene expression constructs organized in synthetic operons containing multiple transcription units with the minimum *phb* genes needed (Weber et al., 2011; Blázquez et al., 2023). The resulting synthetic *phb* clusters followed the modular structure shown in the synthetic *phb* orthogonalization pathway (Figure 2), which enabled interchangeability of genetic parts across modules as needed.

Since dosage of the different synthetic *phb* modules is crucial for proper functioning of the PHA machinery (Hiroe et al., 2012; Li et al., 2016; Li et al., 2017), we varied the strength of synthetic promoters driving the expression of these genes using low (14a) and medium (SynPro16 or SP16) strength constitutive promoters, previously validated in *P. putida* (Zobel et al., 2015; Tiso et al., 2016; Blázquez et al., 2023). During the strains' construction, we considered the specificity of the *phb* module as a potential tool for diversification of the monomeric content and possibly different catalytic capacities of these enzymes in a heterologous chassis. For this, the wild type genes were obtained from bacteria able to produce different types of scl-PHA (i.e., *R. rubrum*, *P. pseudoalcaligenes* and *C. necator*). Numerous plasmid-based synthetic *phb* modules were generated and tested (Figure 2, Supplementary Table S1), each module contained the three minimal *phb* transcriptional units necessary for PHB production (i.e., PHA synthase, *phaC*; 3-ketoacyl-CoA thiolase, *phaA*; 3-ketoacyl-CoA reductase, *phaB*).

We assessed the production of scl-PHA (i.e., consisting of C4 or C5 monomers) and mcl-PHA (i.e., consisting of predominantly C6 and C8 monomers) following 24 h of growth in 0.1 N M63 minimal medium supplemented with 15 mM octanoate as the sole carbon source. The strain PP05_01 (pSS126), expressing the PHA machinery from *R. rubrum* under the low strength 14a constitutive promoter, yielded ~25% CDW of PHB (Table 3). TEM images of PP05_01 (pSS126) strain revealed that most cells contained a single PHB granule occupying a large proportion of the cytoplasm (Figure 3). To improve the

TABLE 2 PHA yield following 24 h of growth under the corresponding conditions using 0.1 N M63 minimal medium. The data correspond to the mean values and standard deviations of four biological replicates (with two technical replicates for the methanolysis analysis). Residual biomass indicates the biomass free of PHA. N.D.: not detected *data obtained from (Manoli et al., 2022).

Conditions	Strains	Total biomass (g/L)	PHB (%CDW)	PHA (g/L)	Residual biomass (g/L)
15 mM octanoate	PP05_01	0.56 ± 0.07*	N.D.*	N.D.*	0.60 ± 0.10*
	PP00_02	1.40 ± 0.09	69.39 ± 7.12	0.97 ± 0.09	0.48 ± 0.08
20 mM glucose	PP00_02	0.68 ± 0.05	48.96 ± 4.15	0.33 ± 0.04	0.35 ± 0.03
30 mM acetate	PP00_02	0.34	3.46 ± 0.46	0.01 ± 0.00	0.32 ± 0.00

TABLE 3 Properties of heterologous PHA production in *Pseudomonas putida* chassis strain. GC-MS analysis of PHA content in 0.1 N M63 minimal medium supplemented with 15 mM octanoate for 24 h. The data correspond to the mean values and standard deviations of at least two independent biological replicates. TR.: Traces; N.D.: not detected.

Strain	Total CDW (g/L)	PHA (%CDW)	PHA (g/L)	Residual biomass (g/L)	%C4	%C6	%C8
KT2440 (pGG128; empty plasmid)	1.42 ± 0.01	61.73 ± 1.25	0.88 ± 0.01	0.54 ± 0.02	N.D.	7.11 ± 0.14	92.89 ± 0.14
PP05_01 (pGG128; empty plasmid)	0.43 ± 0.05	N.D.	N.D.	0.43 ± 0.05	N.D.	N.D.	N.D.
PP05_01 (pSS126; *R.r. phaCAB*)	0.67 ± 0.01	23.11 ± 1.04	0.15 ± 0.00	0.51 ± 0.02	99.57 ± 0.07	<0.5	<0.5
PP05_01 (pRK182; *R.r. phaCABP*)	0.60 ± 0.03	25.37 ± 1.59	0.15 ± 0.02	0.45 ± 0.01	100.00	TR.	TR.
PP05_01 (pRK216; *C.n. phaCAB*)	0.87 ± 0.04	47.13 ± 2.83	0.41 ± 0.05	0.46 ± 0.00	99.87 ± 0.02	<0.5	<0.5
PP05_01 (pMM85; *C.n. phaCABP*)	1.32 ± 0.10	84.31 ± 0.12	1.11 ± 0.08	0.21 ± 0.02	98.45 ± 0.54	0.98 ± 0.32	0.56 ± 0.21
PP05_01 (pMM106; *P.p. phaCABP*)	0.68 ± 0.02	44.90 ± 0.08	0.30 ± 0.01	0.37 ± 0.01	100.00	TR.	TR.

granule stability, in the same construct the three phasins from *R. rubrum* (i.e., A3283[Rr], A2817[Rr], A2111[Rr]) were additionally expressed under the SynPro16 promoter generating the PP05_01 (pRK182) strain. However, no major effect on the overall PHA production properties were observed by yielding 25% PHB/CDW (Table 3).

Similarly, the PHA machinery of *P. pseudoalcaligenes* (pMM106) and *C. necator* (pMM85) were expressed under the 14a constitutive promoter reaching 45%–84% PHA/CDW, respectively (Table 3; Figure 3). These were encouraging results, since we were able to obtain similar PHA content from *C. necator* genes expressed in a constitutive multicopy system compared to the inducible monocopy strain PP00_02 (Table 2). From TEM images, we could confirm that cells producing PHB generally contained multiple PHB granules that occupied the majority of the intracellular space (Figure 3). We also tested the influence of expressing the PHA machinery of *C. necator* under the moderate SynPro16 promoter (PP05_01 (pRK216)). However, assessing PP05_01 (pRK216) under the same growth scenario, there was no apparent improvement in the PHA production capabilities compared to the pMM85 plasmid (47% PHB/CDW, Table 3). In general, the PHA machinery constructs with SynPro16 promoter showed a more variable phenotype compared to 14a constitutive promoter. This can be also observed by the TEM images, where several cells harboring pRK216 did not produce PHA, leading to an overall decrease of the %PHA/CDW quantified by GC-MS analyses (Figure 3). Considering the unstableness issues raised by the

SynPro16 promoter, in this study, we did not pursue the combination of the different genetic parts with this expression system.

As a product of a synthetic pathway involving four enzymes, PHA content relies heavily on the activity and relative ratios of these enzymes and the applied growth conditions. Thus, the best candidate strain harboring *C. necator* PHA machinery was tested for the feasibility to produce tailored PHA towards diverse personalized applications. For this purpose, several nutritional scenarios were planned for the production of copolymers (i.e., PHBV) in PP05_01 harboring pMM85 with the wild type *phb*[Cn] cassette. As listed in Table 4, a panel of PHBV copolymers was successfully obtained with varying C4: C5 compositions. In fact, co-feeding with 5 mM propionic acid yielded 35% of PHA/CDW with 3% C5 monomeric composition while 1 mM undecenoic acid co-feeding yielded 44% PHA/CDW with 19% of C5. Overall, we demonstrated the successful deployment of custom assembled plasmids to produce à la carte PHB/PHBV polymers in the engineered *P. putida* strains.

3.3 Phenotypic evaluation of chromosomally integrated PHB constructs

For scale up processing the ideal strain would not rely on antibiotic resistance for plasmid maintenance nor the use of an inducer for expression of the heterologous cassette. Additionally, the chromosomic PHA machinery integration would result to a more
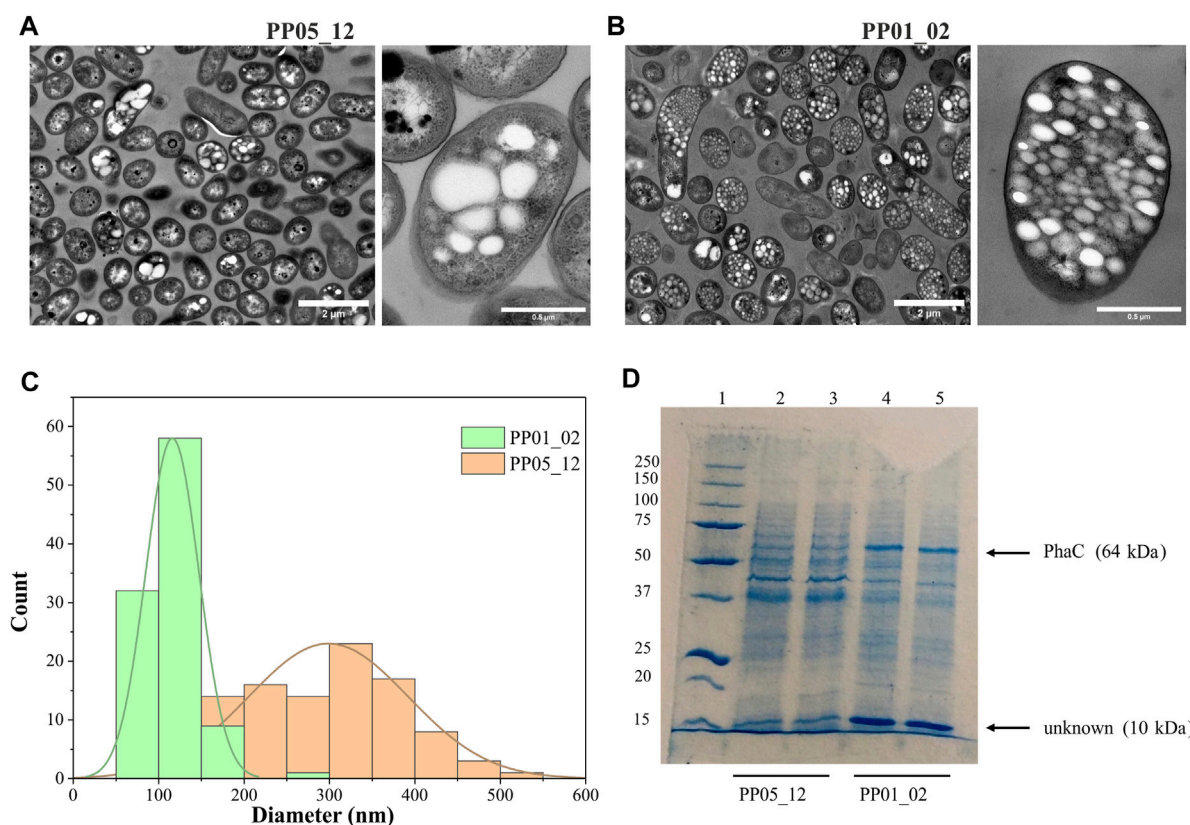
FIGURE 4
Impact of synthase dosage on granule number and size. **(A, B)**. TEM images of PP01_02 and PP05_12, respectively under standard PHA accumulation conditions supplemented with 15 mM octanoate. **(C)**. Granule size distribution obtained from 100 granules measured from TEM images using ImageJ software, PP01_02 (green) and PP05_12 (orange). **(D)**. SDS - PAGE gels of granule extractions. Lane 1 MW marker; lanes 2−3: PP05_ 12 independently extracted PHB granules; lanes 4−5: PP01_02 independently extracted PHB granules. MW of the corresponding GAPs are indicated. Precision Plus Protein Standards (Biorad) was used as a molecular weight marker using Tris-Glycine 4%−20% conditions.

TABLE 4 PHA yield of PP05_01 harboring pMM85 (*C.n. phaCABP*) following 24 h growth with 0.1 N M63 supplemented with 20 mM glucose and co-fed with the indicated odd length fatty acids. The data correspond to the mean values and standard deviations of two independent biological replicates.

Conditions	Total biomass (g/L)	PHA (%CDW)	PHA (g/L)	Residual biomass (g/L)	%C4	%C5
not-cofed	0.97 ± 0.04	39.04 ± 3.09	0.38 ± 0.04	0.59 ± 0.03	100	N.D.
1 mM propionic	0.95 ± 0.03	33.00 ± 1.05	0.31 ± 0.00	0.64 ± 0.03	99.41 ± 0.01	0.59 ± 0.01
5 mM propionic	0.98 ± 0.08	34.61 ± 2.72	0.34 ± 0.05	0.64 ± 0.02	96.91 ± 0.61	3.09 ± 0.61
1 mM undecenoic	1.08 ± 0.12	44.26 ± 2.83	0.48 ± 0.08	0.60 ± 0.04	81.36 ± 4.52	18.64 ± 4.52

stable and homogeneous phenotype compared to plasmid. For this reason, a strain was generated to efficiently produce PHB in a monocopy constitutive expression system inserted in the *P. putida* chromosome. As a starting point, the *phb* cassette from *C. necator* was specifically inserted into the *att*Tn*7* loci of *P. putida* PP05_01, generating the PP05_16 and PP05_12 strains (Table 1). PP05_16 strain contained the four genes necessary to drive PHB synthesis under the low strength constitutive promoter 14a and PP05_12 did not contain the PhaP^{Cn} phasin (please refer to Table 1 and (Supplementary Table S1) for strains, plasmids and genomic information).

As expected, under the same growth conditions supplemented with 15 mM octanoate, the monocopy expression of the *phb*^{Cn} cassette led to a decrease in percent PHA/CDW accumulation (Table 5) that was also reflected in a decrease in total biomass (12%–15% by PP05_12 and PP05_16 *versus* 84% with pMM85 plasmid). To improve on PHB productivity observed in PP05_12 and PP05_16, the PP01_02 strain was generated. PP01_02 harbored the same *phb* cassette as PP05_12 in the *att*Tn*7* chromosomic locus but with the *phaC*^{Cn} synthase under control of a stronger 14f promoter (Table 5; Zobel et al., 2015). PP01_ 02 resulted in 69% PHA/CDW accumulation, which by NMR quantification we confirmed that 92% of the produced polymer was

TABLE 5 PHA yield in PP05_01 modified strain following 24 h growth with 0.1 N M63 supplemented with 15 mM octanoate as the sole carbon source. N.D.: not detected. Mean values and standard deviations of at least two independent biological replicates are shown. *Data derived from NMR quantification.

Plasmid	Total biomass (g/L)	PHA (%CDW)	PHA (g/L)	Residual biomass (g/L)	%C4	%C6	%C8
PP05_01 (pMM85)	1.32 ± 0.10	84.31 ± 0.12	1.11 ± 0.08	0.21 ± 0.02	98.45 ± 0.54	0.98 ± 0.32	0.56 ± 0.21
PP05_16	0.69 ± 0.02	14.56 ± 1.16	0.10 ± 0.01	0.59 ± 0.01	100.00	N.D.	N.D.
PP05_12	0.63 ± 0.02	11.78 ± 0.97	0.07 ± 0.01	0.56 ± 0.01	100.00	N.D.	N.D.
PP05_12 (pMM194)	0.62 ± 0.01	15.10 ± 1.81	0.09 ± 0.01	0.53 ± 0.01	100.00	N.D.	N.D.
PP01_02	1.02 ± 0.04	68.51 ± 5.78	0.70 ± 0.06	0.32 ± 0.06	92*	8*	N.D.
PP05_15	1.07 ± 0.05	63.47 ± 4.86	0.68 ± 0.04	0.39 ± 0.07	95.88 ± 1.25	2.80 ± 0.79	1.31 ± 0.49
PP05_15 (pMM194)	1.00 ± 0.05	65.29 ± 1.68	0.65 ± 0.05	0.35 ± 0.00	97.82 ± 0.06	1.51 ± 0.01	0.67 ± 0.07

C4 and 8% C6 monomer (Supplementary Figure S3). Altogether, we successfully obtained a battery of chromosomic integrated PHB constructs that resulted in tuned PHA productivities (e.g., from 12%–69% PHA/CDW). These observations strongly suggested the impact of *pha* synthase dosage on PHA yield and monomeric composition.

3.4 Impact of PHA synthase dosage on number and size distribution of granules and the identification of a granule-associated heat shock protein

It is well known that PHA synthesis is tightly controlled by a number of regulatory networks that govern PHA content, granule size and distribution in cells (recently reviewed by (Mitra et al., 2022)). However, the heterologously produced phasins in engineered strains did not show an obvious influence over PHA production properties or granule size (Table 3; Figure 3).

To elucidate other factors that might impact granule number and size (i.e., synthase dosage), TEM microscopic photos were taken after 24 h of growth using 15 mM octanoate as the sole carbon and energy source. For this, PP05_12 and PP01_02 strains were used, expressing the *pha* synthase under the control of 14a (low strength) and 14f (high strength) promoters, respectively. Figure 4 shows that low synthase dosage in the PP05_12 strain, generated a heterogeneous cell population, with several cells without PHB inclusions and others with few, but large PHB granules. However, high synthase doses in the PP01_02 strain resulted in a more homogeneous population of cells that contained numerous smaller granules. Granule size analysis of the PP05_12 strain showed a broader size distribution with an average size of 300 nm, while PP01_02 strain had a narrower size distribution with a smaller average size of 180 nm (Figure 4C).

To further confirm the relative increase in PhaC synthase expression, granule preparations were extracted and run on SDS-PAGE to estimate GAPs present on the granule surface (Figure 4D). To ascertain that the same granule quantity was run on the gels, methanolysis of granule preparations were performed to quantify the actual amount of PHB in each preparation. The control experiments with the empty plasmid may be found in the Supplementary Figure S2. As expected, PP05_01 (pGG128) strain did not produce any detectable PHA and, thus, no granule formation was visible in the SDS-PAGE gels (Supplementary Figure S2). Comparing with the control band pattern, the presence of acetoacetyl-CoA-reductase

PhaB (26 kDa) and acetyl-CoA-transferase PhaA (40 kDa) in both strains' granule preparation resulted challenging. This could be explained to some extent by their low abundance in the granule surface since they were expressed under the low 14a promoter's strength. However, as expected, the PP01_02 strain with a higher strength promoter for PhaC synthase (64 kDa) showed higher levels of PhaC protein than PP05_12 (Figure 4D). N-terminal sequencing of the 64 kDa band confirmed that this corresponded to PhaC.

In this granule preparations, we could observe a repeated pattern of a co-increased protein dosage of approximately 10 kDa protein together with the increase in PhaC^{Cn}. Interestingly, this low molecular weight protein was also observed in the granules' extraction harboring the PHA machinery from *R. rubrum* (Supplementary Figure S2). To elucidate the identity of this unknown protein, we performed N-terminal sequencing. A protein BLAST of "TTAFSLAPLF" against the *P. putida* KT2440 proteome revealed the presence of the small heat shock protein, IbpA (PP_1982).

3.5 Involvement of inclusion body protein IbpA in PHA production

Small heat-shock proteins (sHSP), are characterized by a molecular mass of 12–43 kDa, and function as ubiquitous and diverse molecular chaperones that prevent protein aggregation under heat shock conditions. Two sHSP from *E. coli*, IbpA/B have been previously reported to bind to the inclusion bodies of recombinant proteins (Han et al., 2006). IbpA is also considered a stress-related chaperone with an intrinsic holdase activity. This ATP-independent holding function allows them to bind to denatured and partly unfolded proteins under stress conditions. The proteins bound to sHSPs are maintained in a refolding-competent state and are thereby protected from irreversible aggregation (Han et al., 2006; Roy et al., 2014).

To assess the involvement of IbpA on bacterial PHA machinery, an *ibpA* deletion mutant was constructed in the PP01_02 background, generating strain PP05_15. Phenotypic evaluation of PP05_15 showed no major impact on the growth capacity at 30°C compared to the parental PP01_02 strain (e.g., similar residual biomass, Table 5). These results are in agreement with previous observations to *ibpA* deletion mutant in KT2440, where the growth was only significantly affected at 40°C (Krajewski et al., 2013). Looking at the PHA profile properties, PP05_15 revealed no
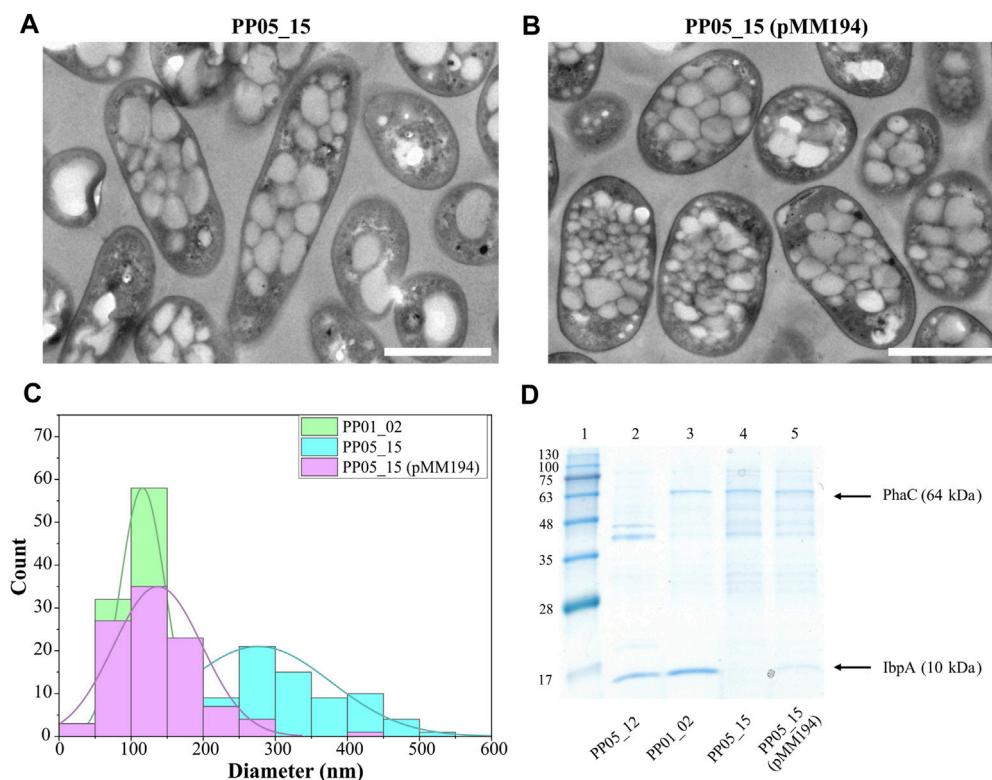
FIGURE 5
Impact of IbpA deletion on granule number and size. **(A, B)**. TEM images of PP05_15 and PP05_15 (pMM194), respectively under standard PHA accumulation conditions supplemented with 15 mM octanoate. **(C)**. Granule size distribution obtained from 100 granules measured from TEM images using ImageJ software, in green PP01_02, blue PP05_15 and purple PP05_15 (pMM194). Scale bars represent 1 µm. **(D)**. SDS - PAGE gels of granule extractions. Lane 1 MW marker; lanes 2: PP05_12; lane 3: PP01_02; lane 4: PP05_15; lane 5: PP05_15 (pMM194). The MW of the corresponding GAPs are indicated. BlueStar Prestained protein marker (Nippon Genetics) was used as a molecular weight marker using Tris-Glycine 4%−20% conditions.

major differences concerning the PHA accumulation profile compared with the parental strain, PP01_02; 63.5% PHA/CDW *versus* 68.5% PHA/CDW, respectively (Table 5). These observations are in accordance with the recombinant *E. coli* IbpA/B null strain behavior, which also slightly affected PHA production, when carried the *C. necator* PHA machinery (Han et al., 2006). To look closer on the involvement of the IbpA deletion on granule size distribution, TEM analyses were performed (Figure 5A). In fact, PP05_15 strain showed a broader granule size distribution with an average size of about 300 nm compared with 180 nm of PP01_02 (Figure 5C). Finally, the influence of IbpA over other granule-associated proteins was analyzed by granule extraction assay (Figure 5D). As expected for granules extracted from the *ibpA* null (PP05_15) strain, the 10 kDa band corresponding to IbpA disappeared, while showing little change in the other bands corresponding to GAPs involved in PHA production (i.e., PhaC). It is worth mentioning that during the extraction procedure granules from the PP05_15 strain appeared to be more aggregated and adherent compared to granules from PP01_02. This aspect could be explained, at least to some extent, from the deletion of IbpA, which could lead to higher protein aggregation.

Complementation assays with pMM194 plasmid were performed by introducing the *ibpA* gene expressed by the constitutive 14a promoter:BCD2 element. Similar PHA production properties were obtained by the complemented strains PP05_12 (pMM194) and PP05_15 (pMM194), reaching 15% and 65% PHA/CDW, similar to the parental strains (Table 5). This could be explained to some extent by the low dosage of complemented IbpA. We cannot discard that higher IbpA dosage could lead to higher PHA content to the engineered strains. Even though no major effect was observed by PHA production, TEM images revealed that PP05_15 (pMM194) successfully reverted the granule formation pattern, with a clear tendency towards smaller granule size compared to PP01_02 strain (Figures 5B, C). Additionally, granule extraction assays confirmed that the presence of IbpA by pMM194 resulted in less granule aggregation (data not shown) and a re-appearance of the IbpA band to the SDS-PAGE (Figure 5D).

IbpA/B seem to exhibit several different functions depending on physiological conditions, among them it has been ascribed that these phasin-like proteins might function as a phase stabilizer at the interface of hydrophilic cytoplasm and hydrophobic PHB granules when this polymer is heterologously produced in *E. coli* (Han et al., 2006). To elucidate if the presence of IbpA in the granule could inhibit the binding of other GAPs, we tested the binding of the PhaP phasin from *C. necator* to scl-PHA granules. For this, PhaP1^{Cn} was fused to the green fluorescent protein (msf-GFP) and heterologously expressed in the PP01_02 strain (Figure 6A). For the co-localization experiments, as expected, the control PP01_02 strain harboring (pBDN2-GFP), empty
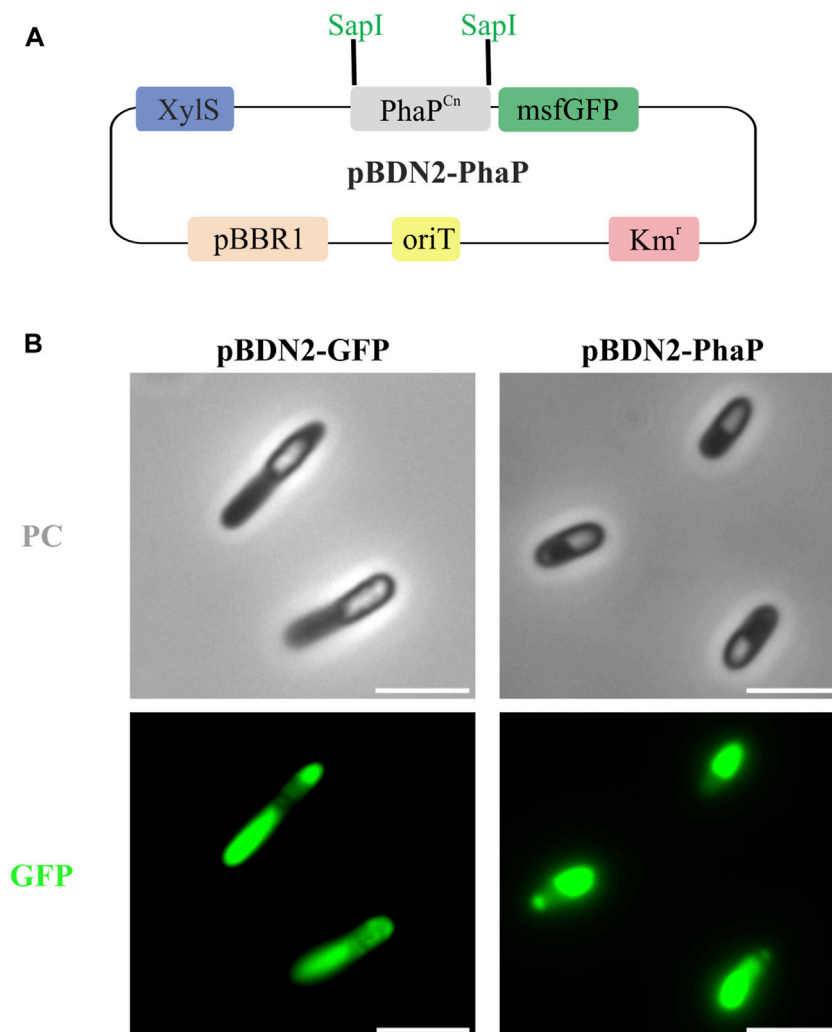
FIGURE 6
Co-localization experiments in the scl-PHA chassis (PP01_02). **(A)**. Schematic representation of pBDN2-PhaP vector. **(B)**. Fluorescence images with phase contrast (PC) amd GFP, left panel PP01_02 (pBDN2-GFP) negative control of binding, the strain that expresses the msf-GFP gene and right panel PP01_02 (pBDN2-PhaP) that expresses the PhaP1 from *Cupriavidus necator*. The scale bar corresponds to 3 μm.

plasmid including only the msf-GFP, showed a diffuse cytoplasmic fluorescence surrounding the scl-PHA granules (Figure 6B). This observation confirmed the non-binding affinity of msf-GFP towards scl-PHA. As anticipated, the scl-family phasin (e.g., PhaP1^{Cn} in pBDN2-PhaP plasmid) showed a co-localized fluorescence to the polymer, thus, maintaining its ability to bind to scl-PHA even in the presence of IbpA (Figure 6B).

4 Discussion

4.1 *P. putida* as a PHA production chassis

Pseudomonas putida is a model bacterium for mcl-PHA production with a complex regulatory system driving the expression of genes encoding the PHA machinery. When grown on fatty acids, transcription of *pha* locus genes is augmented when compared to growth on simple carbon sources (De Eugenio et al.,

2010b; Wang and Nomura, 2010; Manoli et al., 2020). Additionally, the Crc catabolite repression regulator influences transcription of *phaC1* such that its transcription is inhibited in balanced carbon/ nitrogen conditions (La Rosa et al., 2014). While other global transcriptional factors, including RpoS, PsrA and GacS/GacA also influence transcription of genes in the *pha* locus, though their precise roles remain to be fully elucidated (De Eugenio et al., 2010b; Mezzina et al., 2021). In fact, from previous works from our group, we showed a complex interactome among key components of PHA production (i.e., PhaF-PhaD) (Tarazona et al., 2020). However, a deletion of the entire *pha* locus disengages these regulatory functions from the native production of mcl-PHA, making orthogonal PHA production independent of cellular regulators of gene expression. Nevertheless, we cannot discard the involvement of other cellular components during the heterologously expressed scl-PHA machinery. A full *pha* locus deletion chassis strain can then serve to host heterologous *pha* expression constructs. This allows for *à la carte* production of

bespoke PHAs in *P. putida* using custom expression constructs coupled with growth of the resulting strain on any number of carbon sources.

There have been numerous examples of the production of orthogonal PHA in *pha* null *Pseudomonas* through the heterologous expression of *pha* genes. These include the expression of *phaC* synthase genes from scl-/mcl-PHA producing *C. necator, Rhodobacter sphaeroides, Nocardia corrallina, Thiocystis violacea*, or various pseudomonads in Δ*pha* mutants of *P. putida* to generate scl- and mcl-PHAs with unique compositions (Huisman et al., 1991; Preusting et al., 1993; Timm et al., 1994; Lee et al., 1995; Dennis et al., 1998; Matsusaki et al., 1998; Clemente et al., 2000; Ouyang et al., 2007). Another study created a *P. putida* KT2440 *phaC1⁻*, Δ*phaZ, phaC2⁻ Ω* interposon mutant and used this Δ*pha* strain as a host for the functional screening of soil metagenomic cosmid clones to identify novel PHA synthases (Cheng and Charles, 2016). Our work expands upon these previous investigations by generating a sequence-confirmed *P. putida* KT2440 Δ*pha* locus chassis, PP05_01 strain coupled with the advantage of using a highly flexible assembly cloning system for the generation of custom, stable and constitutively produced scl- and mcl-PHAs.

Pseudomonads can utilize direct PHA precursor pathways to convert fatty acids and PHA unrelated carbon sources (i.e., acetate, ethanol, glycerol, sugars, etc.) via ß-oxidation and *de novo* synthesis of fatty acids, respectively, into various (*R*)-3-hydroxyacyl-CoAs (Figure 1). In contrast, *R. rubrum, P. pseudoalcaligenes,* and *C. necator* are limited in their ability to channel fatty acid metabolites into PHA and instead PHA production relies upon the availability of acetyl-CoA derived from the catabolism of carbon sources (Senior and Dawes, 1971; Budde et al., 2010). The creation of the PP05_01 chassis strain lacking the entire *pha* locus allows for the decoupling of the natural cycle of mcl-PHA production and consumption that is an integral part of energy apportionment and central carbon flux in *P. putida* (Escapa et al., 2012). As mentioned above, mcl-PHA production in *P. putida* is connected to central and peripheral metabolic pathways. The PP05_01 chassis is not subject to catabolite repression of PHA machinery expression and thus, avoids the dependence on certain carbon sources for PHA production. Generally, a nutritional imbalance (i.e., excess carbon and/or the limitation of nutrients such as nitrogen) favors PHA production in *P. putida* (Madison and Huisman, 1999). This imbalance is most significant for PHA production when substrates other than fatty acids are used as carbon sources (Sun et al., 2007; Wang and Nomura, 2010; Follonier et al., 2011). In the presence of fatty acids, nitrogen limitation is not necessary for PHA production, yet greatly improves PHA yields (Poblete-Castro et al., 2012). Notwithstanding, for our studies in the majority of cases, PHA production was carried out in nitrogen limited conditions with octanoate as the sole carbon source.

4.2 Expanding the range of PHA production in *P. putida*

The modular and hierarchical nature of biological designs reveals new possibilities for the development of rational and standardized mechanisms in order to improve the engineering process of specific biological solutions. DNA assembly is a widely used method to build synthetic genetic circuits. Traditionally, these cloning strategies were performed by digestion and ligation of DNA fragments using BioBricks or Gibson assembly. However, these approaches require specific designs for each step that can hamper complete standardization and parts reuse. Modular Cloning (MoClo) methodology has emerged as a powerful tool for standardizing the assembly of genetic parts. MoClo is based on Golden gate cloning, which allows simultaneous and directional assembly of multiple DNA parts.

PHA polyesters can be derived from over 150 different (*R*)-3-hydroxyalkanoic acid monomers, giving rise to a huge variety of physical and mechanical properties in the resulting polymers (Steinbüchel and Valentin, 1995; Hazer and Steinbüchel, 2007). Production of orthogonal PHAs in *P. putida* greatly expands the envelope of polymer diversity. Due to its metabolic flexibility and ability to use a variety of substrates, such as fatty acids or aromatic compounds, it is expected that our *P. putida* toolkit can be exploited to generate new and useful PHAs (Linger et al., 2014; Blázquez et al., 2023).

By using Golden gate/MoClo technology, we demonstrated the successful production of PHB and PHBV copolymers in *P. putida* PP05_01 through the expression of heterologous PHB machinery from *R. rubrum, P. pseudoalcaligenes* or *C. necator*. Indeed, since the synthetic *phb* clusters used in this study followed the same brick structure, this could enable the interchangeability of the genetic parts across the modules, if needed. Thus, we could discover the best synthetic parts' (i.e., promoter, RBS, CDS) combination for most optimal PHA production. Additionally, the involvement of phasins in PHA accumulation and granule stability was studied, suggesting that the presence of these proteins in a heterologous host is not crucial. The absence or presence of phasins did not demonstrate significant differences in PHA accumulation and granule formation. However, we observed that the dosage of PhaC in the chromosome integrated constructs significantly impacted PHA production in several ways. In this sense, we identified interesting patterns: i) higher scl-PHA production, ii) production of a panel of PHAs with increased mcl-PHA (predominantly C6) composition (i.e. 90% C4 and approximately 10% mcl-PHA, iii) more numerous and smaller size granules, and iv) that the presence of the small heat shock protein IbpA augments heterologous PHA production.

4.3 IbpA is an additional player in PHB granule stability

IbpA/B belong to the alpha-crystalline type small heat-shock proteins (sHSP) with a molecular mass of 12–43 kDa, and are known to act as holding chaperones (Krajewski et al., 2013; Roy et al., 2014). Most chaperones possess intrinsic holdase activity, where the ATP-independent holding function is used to bind unstable proteins and prevent the formation of dysfunctional aggregates. Then, misfolded proteins can be transferred from holdase chaperones to downstream ATP-dependent chaperones. These use energy from ATP hydrolysis to power conformational changes in the chaperone, which promotes unfolding, refolding, or translocation of bound substrate proteins as part of their processing. Therefore, the combined action of molecular chaperones may increase the cellular pool of native proteins while minimizing inactive proteins and potentially harmful protein aggregates (Jewett and Shea, 2006).

Indeed, two sHSP from *E. coli*, IbpA/B have been previously reported to bind to the inclusion bodies of recombinant proteins. Han and collaborators demonstrated that a recombinant *E. coli* IbpA/B deletion mutant led to significant changes in PHB granule morphology, whereby they were shown to become distorted and wrinkled (Han et al., 2006). Therefore, it was suggested that in the absence of IbpA/B, PHB granules were expected to bind more cytosolic proteins in a non-specific manner compared to the parental strain. For this, IbpA/B in *E. coli* were proposed to act as phasin-like proteins that function as a phase stabilizer at the interface of the hydrophobic PHB granules and the hydrophilic cytoplasm (Han et al., 2006).

In this work, we constructed a viable IbpA null, PP05_15 strain. Even though the phenotypic evaluation revealed no major changes in PHA production, differences were observed in granule size distribution. Indeed, in the absence of IbpA, the tendency was towards overall larger granules compared to parental PP01_02 strain. Interestingly, this granule size distribution of PP05_15 is quite similar to PP05_12 (containing low PhaC synthase expression), suggesting that the deletion of IbpA may decrease the effective level or function of PhaC. We did not observe an obvious lower PhaC synthase level in the granule extracts of PP05_15 compared to PP01_02, indicating that the IbpA either modulates the function of PhaC by allowing its proper folding or operates on granule size in a PhaC-independent manner. Whether or not the PhaC/other granule-associated proteins could be partially aggregated in the PP05_15 strain was not determined, yet our findings confirmed the importance of IbpA protein in granule size determination and GAPs localization.

Altogether, in this study we demonstrated that *P. putida* optimized cell factories can be used for the production of tailored scl-PHA. Our results also suggest that native mcl-PHA regulatory network might be different to that of orthogonal scl-PHA system and we cannot discard the involvement of non-envisaged players such as IbpA.

Data availability statement

The raw data supporting the conclusion of this article will be made available by the authors, without undue reservation.

Author contributions

M-TM: Conceptualization, Supervision, Writing–review and editing, Investigation, Methodology, Writing–original draft, Validation, Data curation. FB: Writing–review and editing, Investigation, Methodology. VR-B: Methodology, Writing–review and editing. RK: Conceptualization, Supervision, Writing–review and editing, Investigation, Methodology, Writing–original draft, Project administration. SA: Writing–review and editing, Methodology. S: Writing–review and editing, Investigation, Methodology. MP: Conceptualization, Funding acquisition, Resources, Supervision,

Writing–review and editing, Investigation, Project administration, Writing–original draft.

Conflict of interest

The authors declare that the research was conducted in the absence of any commercial or financial relationships that could be construed as a potential conflict of interest.

Publisher's note

All claims expressed in this article are solely those of the authors and do not necessarily represent those of their affiliated organizations, or those of the publisher, the editors and the reviewers. Any product that may be evaluated in this article, or claim that may be made by its manufacturer, is not guaranteed or endorsed by the publisher.

Supplementary material

The Supplementary Material for this article can be found online at: https://www.frontiersin.org/articles/10.3389/fbioe.2023.1275036/full#supplementary-material

References

Bagdasarian, M., Lurz, R., Rückert, B., Franklin, F. C., Bagdasarian, M. M., Frey, J., et al. (1981). Specific-purpose plasmid cloning vectors. II. Broad host range, high copy number, RSF1010-derived vectors, and a host-vector system for gene cloning in *Pseudomonas*. *Gene* 16, 237–247. doi:10.1016/0378-1119(81)90080-9

Jewett, A. I., and Shea, J.-E. (2006). Folding on the chaperone: yield enhancement through loose binding. *J. Mol. Biol.* 363 (5), 945–957. doi:10.1016/j.jmb.2006.08.040

Blanco, F. G., Machatschek, R., Keller, M., Hernández-Arriaga, A. M., Godoy, M. S., Tarazona, N. A., et al. (2023). Nature-inspired material binding peptides with versatile

polyester affinities and binding strengths. *Int. J. Biol. Macromol.* 253, 126760. doi:10.1016/j.ijbiomac.2023.126760

Blázquez, B., León, D. S., Torres-Bacete, J., Gómez-Luengo, Á., Kniewel, R., Martínez, I., et al. (2023). Golden Standard: a complete standard, portable, and interoperative MoClo tool for model and non-model proteobacteria. *Nucleic Acids Res.* 23, gkad758. doi:10.1093/nar/gkad758

Boyer, H. W., and Roulland-Dussoix, D. (1969). A complementation analysis of the restriction and modification of DNA in *Escherichia coli*. *J. Mol. Biol.* 41, 459–472. doi:10.1016/0022-2836(69)90288-5

Brandl, H., Knee, E. J., Fuller, R. C., Gross, R. A., and Lenz, R. W. (1989). Ability of the phototrophic bacterium *Rhodospirillum rubrum* to produce various poly (β-hydroxyalkanoates): potential sources for biodegradable polyesters. *Int. J. Biol. Macromol.* 11, 49–55. doi:10.1016/0141-8130(89)90040-8

Braunegg, G., Sonnleitner, B., and Lafferty, R. M. (1978). A rapid gas chromatographic method for the determination of poly-β-hydroxybutyric acid in microbial biomass. *Eur. J. Appl. Microbiol. Biotechnol.* 6, 29–37. doi:10.1007/BF00500854

Budde, C. F., Mahan, A. E., Lu, J., Rha, C., and Sinskey, A. J. (2010). Roles of multiple acetoacetyl coenzyme A reductases in polyhydroxybutyrate biosynthesis in *Ralstonia eutropha* H16. *J. Bacteriol.* 192, 5319–5328. doi:10.1128/JB.00207-10

Cambray, G., Guimaraes, J. C., Mutalik, V. K., Lam, C., Mai, Q.-A., Thimmaiah, T., et al. (2013). Measurement and modeling of intrinsic transcription terminators. *Nucleic Acids Res.* 41, 5139–5148. doi:10.1093/nar/gkt163

Cha, D., Ha, H. S., and Lee, S. K. (2020). Metabolic engineering of *Pseudomonas putida* for the production of various types of short-chain-length polyhydroxyalkanoates from levulinic acid. *Bioresour. Technol.* 309, 123332. doi:10.1016/j.biortech.2020.123332

Cheng, J., and Charles, T. C. (2016). Novel polyhydroxyalkanoate copolymers produced in *Pseudomonas putida* by metagenomic polyhydroxyalkanoate synthases. *Appl. Microbiol. Biotechnol.* 100, 7611–7627. doi:10.1007/s00253-016-7666-6

Choi, K.-H., Kumar, A., and Schweizer, H. P. (2006). A 10-min method for preparation of highly electrocompetent *Pseudomonas aeruginosa* cells: application for DNA fragment transfer between chromosomes and plasmid transformation. *J. Microbiol. Methods* 64, 391–397. doi:10.1016/j.mimet.2005.06.001

Clemente, T., Shah, D., Tran, M., Stark, D., Padgette, S., Dennis, D., et al. (2000). Sequence of PHA synthase gene from two strains of *Rhodospirillum rubrum* and *in vivo* substrate specificity of four PHA synthases across two heterologous expression systems. *Appl. Microbiol. Biotechnol.* 53, 420–429. doi:10.1007/s002530051636

De Eugenio, L. I., Escapa, I. F., Morales, V., Dinjaski, N., Galán, B., García, J. L., et al. (2010a). The turnover of medium-chain-length polyhydroxyalkanoates in *Pseudomonas putida* KT2442 and the fundamental role of PhaZ depolymerase for the metabolic balance. *Environ. Microbiol.* 12, 207–221. doi:10.1111/j.1462-2920.2009.02061.x

De Eugenio, L. I., Galán, B., Escapa, I. F., Maestro, B., Sanz, J. M., García, J. L., et al. (2010b). The PhaD regulator controls the simultaneous expression of the pha genes involved in polyhydroxyalkanoate metabolism and turnover in *Pseudomonas putida* KT2442. *Environ. Microbiol.* 12, 1591–1603. doi:10.1111/j.1462-2920.2010.02199.x

Dennis, D., McCoy, M., Stangl, A., Valentin, H. E., and Wu, Z. (1998). Formation of poly(3-hydroxybutyrate-co-3-hydroxyhexanoate) by PHA synthase from *Ralstonia eutropha*. *J. Biotechnol.* 64, 177–186. doi:10.1016/S0168-1656(98)00110-2

Engler, C., Kandzia, R., and Marillonnet, S. (2008). A one pot, one step, precision cloning method with high throughput capability. *PLOS ONE* 3, e3647. doi:10.1371/journal.pone.0003647

Escapa, I. F., García, J. L., Bühler, B., Blank, L. M., and Prieto, M. A. (2012). The polyhydroxyalkanoate metabolism controls carbon and energy spillage in *Pseudomonas putida*. *Environ. Microbiol.* 14, 1049–1063. doi:10.1111/j.1462-2920.2011.02684.x

Follonier, S., Panke, S., and Zinn, M. (2011). A reduction in growth rate of *Pseudomonas putida* KT2442 counteracts productivity advances in medium-chain-length polyhydroxyalkanoate production from gluconate. *Microb. Cell Factories* 10, 25. doi:10.1186/1475-2859-10-25

Galán, B., Dinjaski, N., Maestro, B., De Eugenio, L. I., Escapa, I. F., Sanz, J. M., et al. (2011). Nucleoid-associated PhaF phasin drives intracellular location and segregation of polyhydroxyalkanoate granules in *Pseudomonas putida* KT2442. *Mol. Microbiol.* 79, 402–418. doi:10.1111/j.1365-2958.2010.07450.x

Godoy, M. S., de Miguel, S. R., and Prieto, M. A. (2023). Aerobic-anaerobic transition boosts poly(3-hydroxybutyrate-co-3-hydroxyvalerate) synthesis in *Rhodospirillum rubrum*: the key role of carbon dioxide. *Microb. Cell Factories* 22, 47. doi:10.1186/s12934-023-02045-x

Han, M.-J., Park, S.-J., Lee, J.-W., Min, B.-H., Lee, S.-Y., Kim, S.-J., et al. (2006). Analysis of poly (3-hydroxybutyrate) granule-associated proteome in recombinant *Escherichia coli*. *J. Microbiol. Biotechnol.* 16, 901–910.

Hazer, B., and Steinbüchel, A. (2007). Increased diversification of polyhydroxyalkanoates by modification reactions for industrial and medical applications. *Appl. Microbiol. Biotechnol.* 74, 1–12. doi:10.1007/s00253-006-0732-8

Hiroe, A., Tsuge, K., Nomura, C. T., Itaya, M., and Tsuge, T. (2012). Rearrangement of gene order in the *phaCAB* operon leads to effective production of ultrahigh-molecular-weight poly[(R)-3-Hydroxybutyrate] in genetically engineered *Escherichia coli*. *Appl. Environ. Microbiol.* 78, 3177–3184. doi:10.1128/AEM.07715-11

Huisman, G. W., de Leeuw, O., Eggink, G., and Witholt, B. (1989). Synthesis of poly-3-hydroxyalkanoates is a common feature of fluorescent pseudomonads. *Appl. Environ. Microbiol.* 55, 1949–1954. doi:10.1128/aem.55.8.1949-1954.1989

Huisman, G. W., Wonink, E., Meima, R., Kazemier, B., Terpstra, P., and Witholt, B. (1991). Metabolism of poly(3-hydroxyalkanoates) (PHAs) by *Pseudomonas oleovorans*. Identification and sequences of genes and function of the encoded proteins in the synthesis and degradation of PHA. *J. Biol. Chem.* 266, 2191–2198. doi:10.1016/s0021-9258(18)52227-4

Jendrossek, D. (2009). Polyhydroxyalkanoate granules are complex subcellular organelles (carbonosomes). *J. Bacteriol.* 191, 3195–3202. doi:10.1128/JB.01723-08

Jendrossek, D., and Pfeiffer, D. (2014). New insights in the formation of polyhydroxyalkanoate granules (carbonosomes) and novel functions of poly(3-hydroxybutyrate). *Environ. Microbiol.* 16, 2357–2373. doi:10.1111/1462-2920.12356

Jin, H., and Nikolau, B. J. (2012). Role of genetic redundancy in polyhydroxyalkanoate (PHA) polymerases in PHA biosynthesis in *Rhodospirillum rubrum*. *J. Bacteriol.* 194, 5522–5529. doi:10.1128/JB.01111-12

Kim, J., Kim, Y.-J., Choi, S. Y., Lee, S. Y., and Kim, K.-J. (2017). Crystal structure of *Ralstonia eutropha* polyhydroxyalkanoate synthase C-terminal domain and reaction mechanisms. *Biotechnol. J.* 12, 1600648. doi:10.1002/biot.201600648

Kim, Y. B., and Lenz, R. W. (2001). Polyesters from microorganisms. *Adv. Biochem. Eng. Biotechnol.* 71, 51–79. doi:10.1007/3-540-40021-4_2

Koller, M., Maršálek, L., de Sousa Dias, M. M., and Braunegg, G. (2017). Producing microbial polyhydroxyalkanoate (PHA) biopolyesters in a sustainable manner. *N. Biotechnol.* 37, 24–38. doi:10.1016/j.nbt.2016.05.001

Krajewski, S. S., Nagel, M., and Narberhaus, F. (2013). Short ROSE-like RNA thermometers control IbpA synthesis in *Pseudomonas* species. *PLoS ONE* 8, e65168. doi:10.1371/journal.pone.0065168

La Rosa, R., de la Peña, F., Prieto, M. A., and Rojo, F. (2014). The Crc protein inhibits the production of polyhydroxyalkanoates in *Pseudomonas putida* under balanced carbon/nitrogen growth conditions. *Environ. Microbiol.* 16, 278–290. doi:10.1111/1462-2920.12303

Larson, M. H., Greenleaf, W. J., Landick, R., and Block, S. M. (2008). Applied force reveals mechanistic and energetic details of transcription termination. *Cell* 132, 971–982. doi:10.1016/j.cell.2008.01.027

Lee, E. Y., Jendrossek, D., Schirmer, A., Choi, C. Y., and Steinbüchel, A. (1995). Biosynthesis of copolyesters consisting of 3-hydroxybutyric acid and medium-chain-length 3-hydroxyalkanoic acids from 1,3-butanediol or from 3-hydroxybutyrate by *Pseudomonas*. *Appl. Microbiol. Biotechnol.* 42, 901–909. doi:10.1007/BF00191189

Li, D., Lv, L., Chen, J.-C., and Chen, G.-Q. (2017). Controlling microbial PHB synthesis via CRISPRi. *Appl. Microbiol. Biotechnol.* 101, 5861–5867. doi:10.1007/s00253-017-8374-6

Li, T., Ye, J., Shen, R., Zong, Y., Zhao, X., Lou, C., et al. (2016). Semirational approach for ultrahigh poly(3-hydroxybutyrate) accumulation in *Escherichia coli* by combining one-step library construction and high-throughput screening. *ACS Synth. Biol.* 5, 1308–1317. doi:10.1021/acssynbio.6b00083

Linger, J. G., Vardon, D. R., Guarnieri, M. T., Karp, E. M., Hunsinger, G. B., Franden, M. A., et al. (2014). Lignin valorization through integrated biological funneling and chemical catalysis. *Proc. Natl. Acad. Sci. U. S. A.* 111, 12013–12018. doi:10.1073/pnas.1410657111

Lutz, R., and Bujard, H. (1997). Independent and tight regulation of transcriptional units in *Escherichia coli* via the LacR/O, the TetR/O and AraC/I1-I2 regulatory elements. *Nucleic Acids Res.* 25, 1203–1210. doi:10.1093/nar/25.6.1203

Madison, L. L., and Huisman, G. W. (1999). Metabolic engineering of poly(3-hydroxyalkanoates): from DNA to plastic. *Microbiol. Mol. Biol. Rev.* 63, 21–53. doi:10.1128/mmbr.63.1.21-53.1999

Mahato, R. P., Kumar, S., and Singh, P. (2021). Optimization of growth conditions to produce sustainable polyhydroxyalkanoate bioplastic by *Pseudomonas aeruginosa* EO1. *Front. Microbiol.* 12, 711588. doi:10.3389/fmicb.2021.711588

Makkar, N. S., and Casida, L. E. (1987). Technique for estimating low numbers of a bacterial strain(s) in soil. *Appl. Environ. Microbiol.* 53, 887–888. doi:10.1128/aem.53.4.887-888.1987

Manoli, M.-T., Nogales, J., and Prieto, A. (2022). Synthetic control of metabolic states in *Pseudomonas putida* by tuning polyhydroxyalkanoate cycle. *mBio* 13, 01794–e1821. doi:10.1128/mbio.01794-21

Manoli, M. T., Tarazona, N., Mato, A., Maestro, B., Sanz, J. M., Nogales, J., et al. (2020). "Molecular basis of medium-chain length-PHA metabolism of *Pseudomonas putida*," in *The handbook of polyhydroxyalkanoates* (United States: CRC Press), 89–114.

Mato, A., Blanco, F. G., Maestro, B., Sanz, J. M., Pérez-Gil, J., and Prieto, M. A. (2020). Dissecting the polyhydroxyalkanoate-binding domain of the PhaF phasin: rational design of a minimized affinity tag. *Appl. Environ. Microbiol.* 86, 00570–e620. doi:10.1128/AEM.00570-20

Matsusaki, H., Manji, S., Taguchi, K., Kato, M., Fukui, T., and Doi, Y. (1998). Cloning and molecular analysis of the Poly(3-hydroxybutyrate) and Poly(3-hydroxybutyrate-co-

3-hydroxyalkanoate) biosynthesis genes in *Pseudomonas* sp. strain 61-3. *J. Bacteriol.* 180, 6459–6467. doi:10.1128/jb.180.24.6459-6467.1998

Mezzina, M. P., Manoli, M. T., Prieto, M. A., and Nikel, P. I. (2021). Engineering native and synthetic pathways in *Pseudomonas putida* for the production of tailored polyhydroxyalkanoates. *Biotechnol. J.* 16, 2000165. doi:10.1002/biot.202000165

Mitra, R., Xu, T., Chen, G., Xiang, H., and Han, J. (2022). An updated overview on the regulatory circuits of polyhydroxyalkanoates synthesis. *Microb. Biotechnol.* 15, 1446–1470. doi:10.1111/1751-7915.13915

Ouyang, S.-P., Liu, Q., Fang, L., and Chen, G.-Q. (2007). Construction of *pha*-operon-defined knockout mutants of *Pseudomonas putida* KT2442 and their applications in poly(hydroxyalkanoate) production. *Macromol. Biosci.* 7, 227–233. doi:10.1002/mabi.200600187

Pfennig, N., and Trüper, H. G. (1971). Type and neotype strains of the species of phototrophic bacteria maintained in pure culture. *Int. J. Syst. Evol. Microbiol.* 21, 19–24. doi:10.1099/00207713-21-1-19

Poblete-Castro, I., Escapa, I. F., Jäger, C., Puchalka, J., Lam, C. M. C., Schomburg, D., et al. (2012). The metabolic response of *P. putida* KT2442 producing high levels of polyhydroxyalkanoate under single- and multiple-nutrient-limited growth: highlights from a multi-level omics approach. *Microb. Cell Factories* 11, 34. doi:10.1186/1475-2859-11-34

Preusting, H., Kingma, J., Huisman, G., Steinbüchel, A., and Witholt, B. (1993). Formation of polyester blends by a recombinant strain of *Pseudomonas oleovorans*: different poly(3-hydroxyalkanoates) are stored in separate granules. *J. Environ. Polym. Degrad.* 1, 11–21. doi:10.1007/BF01457649

Prieto, A., Escapa, I. F., Martínez, V., Dinjaski, N., Herencias, C., de la Peña, F., et al. (2016). A holistic view of polyhydroxyalkanoate metabolism in *Pseudomonas putida*. *Environ. Microbiol.* 18, 341–357. doi:10.1111/1462-2920.12760

Revelles, O., Tarazona, N., García, J. L., and Prieto, M. A. (2016). Carbon roadmap from syngas to polyhydroxyalkanoates in *Rhodospirillum rubrum*. *Environ. Microbiol.* 18, 708–720. doi:10.1111/1462-2920.13087

Ronďošová, S., Legerská, B., Chmelová, D., Ondrejovič, M., and Miertuš, S. (2022). Optimization of growth conditions to enhance PHA production by *Cupriavidus necator*. *Fermentation* 8, 451. doi:10.3390/fermentation8090451

Roy, S., Patra, M., Nandy, S., Banik, M., Dasgupta, R., and Basu, T. (2014). *In vitro* holdase activity of *E. coli* small heat-shock proteins IbpA, IbpB and IbpAB: a biophysical study with some unconventional techniques. *Protein Pept. Lett.* 21, 564–571. doi:10.2174/0929866521666131224094408

Senior, P. J., and Dawes, E. A. (1971). The role and regulation of poly-beta-hydroxybutyrate synthesis in *Azotobacter beijerinckii*. *Biochem. J.* 123, 29P. doi:10.1042/bj1230029pa

Steinbüchel, A., and Valentin, H. E. (1995). Diversity of bacterial polyhydroxyalkanoic acids. *FEMS Microbiol. Lett.* 128, 219–228. doi:10.1111/j.1574-6968.1995.tb07528.x

Stueber, D., and Bujard, H. (1982). Transcription from efficient promoters can interfere with plasmid replication and diminish expression of plasmid specified genes. *EMBO J.* 1, 1399–1404. doi:10.1002/j.1460-2075.1982.tb01329.x

Sun, Z., Ramsay, J. A., Guay, M., and Ramsay, B. A. (2007). Carbon-limited fed-batch production of medium-chain-length polyhydroxyalkanoates from nonanoic acid by *Pseudomonas putida* KT2440. *Appl. Microbiol. Biotechnol.* 74, 69–77. doi:10.1007/s00253-006-0655-4

Tarazona, N. A., Hernández-Arriaga, A. M., Kniewel, R., and Prieto, M. A. (2020). Phasin interactome reveals the interplay of PhaF with the polyhydroxyalkanoate transcriptional regulatory protein PhaD in *Pseudomonas putida*. *Environ. Microbiol.* 22, 3922–3936. doi:10.1111/1462-2920.15175

Timm, A., Wiese, S., and Steinbüchel, A. (1994). A general method for identification of polyhydroxyalkanoic acid synthase genes from pseudomonads belonging to the rRNA homology group I. *Appl. Microbiol. Biotechnol.* 40, 669–675. doi:10.1007/BF00173327

Tiso, T., Sabelhaus, P., Behrens, B., Wittgens, A., Rosenau, F., Hayen, H., et al. (2016). Creating metabolic demand as an engineering strategy in *Pseudomonas putida* – rhamnolipid synthesis as an example. *Metab. Eng. Commun.* 3, 234–244. doi:10.1016/j.meteno.2016.08.002

Wang, Q., and Nomura, C. T. (2010). Monitoring differences in gene expression levels and polyhydroxyalkanoate (PHA) production in *Pseudomonas putida* KT2440 grown on different carbon sources. *J. Biosci. Bioeng.* 110, 653–659. doi:10.1016/j.jbiosc.2010.08.001

Weber, E., Engler, C., Gruetzner, R., Werner, S., and Marillonnet, S. (2011). A modular cloning system for standardized assembly of multigene constructs. *PLOS ONE* 6, e16765. doi:10.1371/journal.pone.0016765

Werner, S., Engler, C., Weber, E., Gruetzner, R., and Marillonnet, S. (2012). Fast track assembly of multigene constructs using Golden Gate cloning and the MoClo system. *Bioengineered* 3, 38–43. doi:10.4161/bbug.3.1.18223

Yarnell, W. S., and Roberts, J. W. (1999). Mechanism of intrinsic transcription termination and antitermination. *Science* 284, 611–615. doi:10.1126/science.284.5414.611

Zheng, Y., Chen, J.-C., Ma, Y.-M., and Chen, G.-Q. (2019). Engineering biosynthesis of polyhydroxyalkanoates (PHA) for diversity and cost reduction. *Metab. Eng.* 58, 82–93. doi:10.1016/j.ymben.2019.07.004

Zobel, S., Benedetti, I., Eisenbach, L., De Lorenzo, V., Wierckx, N., and Blank, L. M. (2015). Tn7-Based device for calibrated heterologous gene expression in *Pseudomonas putida*. *ACS Synth. Biol.* 4, 1341–1351. doi:10.1021/acssynbio.5b00058

Degradation kinetics of medium chain length Polyhydroxyalkanoate degrading enzyme: a quartz crystal microbalance study

Fabien Millan and Nils Hanik*

Institute of Life Technologies, School of Engineering, University of Applied Science and Arts Western Switzerland, Sion, Switzerland

This study investigates the enzymatic degradation processes of different classes of polyhydroxyalkanoates (PHAs), a group of biopolymers naturally synthesized by various microorganisms. Medium chain length PHAs (mcl-PHAs) are distinguished biopolymers due to their biodegradability and diverse material properties. Using quartz crystal microbalance measurements as a valuable tool for accurate real-time monitoring of the enzymatic degradation process, the research provides detailed kinetic data, describing the interaction between enzymes and substrates during the enzymatic degradation process. Thin films of poly-3-hydroxybutyrate (PHB) and polyhydroxyoctanoate copolymer (PHO), containing molar fractions of about 84% 3-hydroxyoctanoate and 16% 3-hydroxyhexanoate, were exposed to scl-depolymerases from *Pseudomonas lemoignei* LMG 2207 and recombinant mcl-depolymerase produced in *Escherichia coli* DH5α harboring the plasmid pMAD8, respectively. Analyses based on a heterogeneous kinetic model for the polymer degradation indicated a six-fold stronger adsorption equilibrium constant of mcl-depolymerase to PHO. Conversely, the degradation rate constant was approximately twice as high for scl-depolymerases acting on PHB. Finally, the study highlights the differences in enzyme-substrate interactions and degradation mechanisms between the investigated scl- and mcl-PHAs.

KEYWORDS

polyhydroxyalkanoates, depolymerase enzymes, quartz crystal microbalance, degradation kinetics, biodegradable polymers, enzymatic degradation

Introduction

Polyhydroxyalkanoates (PHAs) are aliphatic polyesters naturally produced by several microorganisms, including *Bacillus*, *Pseudomonas*, *Azotobacter*, *Hydrogenomonas*, and *Chromatium*. These microorganisms synthesize PHAs intracellularly for carbon and energy storage, typically through the fermentation of carbon-rich substrates. The accumulation process often occurs under unbalanced growth conditions such as carbon excess and limitation of essential elements like phosphorus, nitrogen, or oxygen (Raza et al., 2018). Based on the number of carbon atoms in their monomers, PHAs can be grouped into subclasses. Short-chain length PHA (scl-PHA) consists of monomers with three to five carbon atoms, while medium-chain length PHA (mcl-PHA) contains monomers with 6–14 carbon atoms.

A distinctive characteristic of PHAs lies in the vast range of physicochemical, mechanical, and thermal properties they can exhibit, owing to the broad substrate specificity of PHA polymerases and the myriad of potential monomers (Matsumoto et al., 2009; Amstutz et al., 2019). This versatility has placed PHAs as the largest group among natural polyesters (Kim et al., 2007). The advent of genetically engineered strains and innovations in carbon sources and feeding strategies further enhances our ability to produce tailored PHAs with a more recent focus on the production of mcl-PHAs and their industrial applications (Tortajada et al., 2013; Oliveira et al., 2020; Muthuraj et al., 2021; Reddy et al., 2022). Consequently, these polymers find applications in diverse fields, from bioplastics and biomaterials to medical implants and biofuels (Hazer and Steinbüchel, 2007; Brigham and Sinskey, 2012; Panchal et al., 2013; Li et al., 2016).

The proliferation of petroleum-based plastics in the environment has raised pressing concerns due to their prolonged persistence (Singh and Sharma, 2016). Both terrestrial and marine ecosystems face the mounting challenge of plastic debris accumulation, with marine regions being especially burdened by sizable aggregations known as "plastic gyres" (Derraik, 2002; Law, 2017; Drzyzga and Prieto, 2019). The widespread occurrence of microplastics, tiny fragments resulting from larger plastic breakdown or direct release, intensifies the issue, affecting a great number of species across diverse habitats (de Souza Machado et al., 2018; Hanik et al., 2019; Soo et al., 2021). Current recycling and waste management efforts address only a portion of the total plastic waste, leading to increased calls for sustainable alternatives. In this context, biobased polymers like PHAs are gaining attention. PHAs are naturally produced by microorganisms and, crucially, are biodegradable. Their ability to serve as a direct replacement for many petroleum-based plastic applications while offering a reduced environmental footprint makes them a promising candidate in the quest for sustainable materials. Although PHAs available on the market are more expensive than those derived from petroleum, they have the advantage of not necessarily being derived from nonrenewable energy and fossil raw materials. Their production is not only possible from edible substrates such as sugars or vegetable oils but also substrates obtained from agricultural and food industry waste (Khardenavis et al., 2007). From a financial and environmental point of view, a considerable potential for optimization exists for the manufacturing processes, mainly with the use of bioenergy, biocatalyst, and carbon source from waste (Chen, 2009; Chen et al., 2020). The integration of PHAs into industrial and consumer applications could not only reduce the inflow of non-degradable plastics but also provide a model for how bioengineering can offer tangible solutions to pressing global environmental issues.

However, there are still many economic and technological challenges to overcome in the field of PHAs (Wang et al., 2014). One of them is to develop unique and tailored material properties for specific applications. For example, the degradability of biopolymers is an essential property which needs to be well adapted for biomedical or packaging applications (Gumel et al., 2013; Keskin et al., 2017; Kalia et al., 2021). Biopolymers can undergo degradation through different mechanisms, which depend on the polymer structure and exposure conditions. Physical and chemical degradation are the two main types of degradation. Physical

degradation results from physical changes, such as thermal embrittlement and environmental stress cracking. Chemical degradation occurs through chemical reactions, with common examples including photo-induced, thermal, thermal-oxidative, solvolytic, hydrolytic, and biological degradation. Understanding the mechanisms of biodegradation is essential for designing more sustainable and environmentally friendly materials (Meereboer et al., 2020; Silva et al., 2023). In this regard, the monitoring of the biopolymers degradation has become a key area of research.

Secretion of PHA depolymerases by microorganisms represents one of the possibilities for the biodegradation of extracellular PHA in the environment. While many extracellular scl-PHA depolymerases have been purified and well characterized (Handrick et al., 2001; Braaz et al., 2003; García-Hidalgo et al., 2012), only few mcl-PHA depolymerases have been described so far (Schirmer and Jendrossek, 1994; Gangoiti et al., 2012; Martínez et al., 2015). These enzymes play a crucial role in the biodegradation process, as they catalyze the breakdown of the larger polymer molecules into smaller units that can be metabolized by microorganisms. Several techniques have been developed for monitoring the enzymatic degradation of plastics, such as turbidimetric powder and film assay (Timmins et al., 1997a; Timmins et al., 1997b), Taylor dispersion analysis (Chamieh et al., 2015), and Blue-ray-based micromechanical characterization (Ceccacci et al., 2017). However, these techniques often suffer from time-consuming sample preparation and complex experimental set up. Some require the polymer to be formulated into stable suspensions or free-standing films which limits their application to specific mechanical polymer properties for monitoring the enzymatic degradation. One tool that has been proven to be useful for this purpose is the quartz crystal microbalance (QCM). Based on the inverse piezoelectric effect the QCM can be used to measure very small changes in the mass of a material in real time (Sabot and Krause, 2002; Marx, 2003). QCM sensors are commonly 5 or 10 MHz AT-cut quartz crystals with gold electrodes on both sides that vibrate in the thickness-shear mode during measurements, where the two surfaces move in an antiparallel fashion. The use of these sensors as microbalances is based on the linear relationship between the resonance frequency variation and the mass variation of the quartz crystal, which can be described by the Sauerbrey equation (Eq. 1), where Δf and f_0 represent the normalized frequency variation and the resonant frequency of the fundamental mode, respectively. The active area, the density, and the shear modulus describe the crystal used for the measurement and are represented by A, ρ_q, and μ_q, respectively. The corresponding mass variation is represented by Δm (Sauerbrey, 1959; Johannsmann, 2015).

$$\Delta f = -\frac{2 f_0^2}{A \sqrt{\rho_q \mu_q}} \Delta m \qquad (1)$$

Applying this equation to a quartz crystal with a fundamental resonance frequency (RF) of about 5 MHz, assigns a change in the RF of 1 Hz to a mass variation of about 17 ng on the sensor surface. This information is useful for designing experiments that use QCM to monitor the degradation of biodegradable plastics, such as PHA. QCMs have been used to study the enzymatic degradation of polyester films in several scientific publications. Yamashita et al.,

used the combination of QCM with atomic force microscopy (AFM) to study interactions between an enzyme and a biopolymer film at the molecular level Yamashita et al. (2005). In our experimental set up, a continuously circulating enzyme solution is introduced into a fluidic cell and brought in contact with a PHA coated sensors. The changes in the RF due to the degradation of PHA are monitored over time.

Various models have been developed to characterize the depolymerization kinetics of enzymes, taking into account different mechanisms, kinetics, and environmental factors. The heterogeneity of the reaction (i.e., the interaction between a soluble enzyme and an insoluble substrate in the case of PHA films) requires more complex models. The observed degradation behavior was found to be inconsistent with classical Michaelis-Menten homogenous enzymatic kinetic where both enzyme and substrate are considered as soluble. At high enzyme concentrations, the reaction rate becomes inversely proportional to the enzyme concentration. The heterogenous kinetic model proposed by Mukai et al., assumes that the depolymerase first binds to the substrate surface and then hydrolyzes polymer chains. However, if the adsorption process is faster than the rate-limiting hydrolysis, surface crowding limits the unhindered access of the enzymes catalytic domain to the substrate. This eventually leads to a decrease in the degradation rate of the poly-3-hydroxybutyrate (PHB) film when increasing the enzyme concentration (Mukai et al., 1993). This kinetic model successfully described the experimental data reported for the enzymatic degradation of PHB films by several PHB depolymerases. However, to the best of our knowledge, this approach was never applied to other classes of PHA polymers and their corresponding depolymerases.

In this study, we apply the QCM technique to model the degradation kinetics of PHA films from different PHA classes. The model we use was adapted from Mukai et al. and can be written in the form of the rate equation (Eq. 2), where v_0 represents the highest degradation rate observed for the corresponding enzyme concentration $[E]_0$. The adsorption equilibrium constant and the degradation rate constant are represented by K et k', respectively.

$$v_0 = \frac{k'K[E]_0}{\left(1 + K[E]_0\right)^2} \qquad (2)$$

We characterize mcl-PHA degradation and compare it with scl-PHA degradation by their respective depolymerases. As far as we know, this is the first detailed study of the enzymatic degradation of mcl-PHA in direct comparison of scl-PHA degradation. In this approach the QCM technique is especially useful as the mcl-PHAs are commonly highly amorphous polymers which are not readily available as free-standing films or stable polymer suspensions (Jendrossek and Handrick, 2002). Based on our experiments, we find a distinguished difference between the scl- and mcl-PHA depolymerases investigated. The results highlight the importance of understanding not only the molecular structure of the enzyme and its substrates but also their degradation mechanism. The applied analytical method allows to distinguish the parameters for adsorption equilibrium and degradation rate, providing a deeper understanding of the key features of the PHA degradation by their specific depolymerases.

Materials and methods

PHB powder was purchased from Biomer (Germany) and polyhydroxyoctanoate copolymer (PHO), containing molar fractions of about 84% 3-hydroxyoctanoate and 16% 3-hydroxyhexanoate as determined by gas chromatography, was kindly provided by Prof. Dr. Manfred Zinn (University of Applied Science and Arts Western Switzerland). All other chemicals and reagents were purchased from Sigma-Aldrich (Switzerland) and used without any further purification.

Strains, plasmid, media, and cultivation conditions

Pseudomonas lemoignei LMG 2207 was kindly provided by Prof. Dr. Dieter Jendrossek (Stuttgart University, Germany) and received on filter paper blots. The filter paper blots were stored at 4°C. The strain was used for all cultivations in the following sterilized minimal medium (adapted from Stinson and Merrick, 1974): Disodium succinate (15 mM), KH_2PO_4 (33 mM), $Na_2HPO_4 \times 2\ H_2O$ (33 mM), NH_4Cl (18 mM), $MgSO_4 \times 7\ H_2O$ (2 mM), $FeCl_3 \times 6\ H_2O$ (0.037 mM) and $CaCl_2 \times 2\ H_2O$ (0.045 mM).

Escherichia coli DH5α [*supE*44, Δ*lac*U169 (Ø80lacZΔM15), *hsdR*17, *recA*1, *endA*1, *gyrA*96, *thi*-1, *relA*1] was used as host for the expression of modified mcl-depolymerase from *Pseudomonas fluorescens* GK13 with the previously described plasmid pMAD8 (Ihssen et al., 2009). The preculture and agar slant was performed in LB-Amp medium: 5 g L^{-1} yeast extract, 10 g L^{-1} tryptone and 5 g L^{-1} NaCl, 100 mg L^{-1} ampicillin. The bioreactor cultivation was conducted in Terrific Broth (TB): 24 g L^{-1} yeast extract, 12 g L^{-1} tryptone, 4 mL L^{-1} glycerol, 0.25 mL L^{-1} PPG 2000, 0.017 M KH_2PO_4 and 0.072 M K_2HPO_4, 100 mg L^{-1} ampicillin.

Colony selection for producers of scl-depolymerases

In order to identify colonies of *P. lemoignei* producing extracellular scl-depolymerases, colonies were incubated on the solid media supplemented with 1.5% w/v of PHB powder at 30°C for 72 h. The selected colonies, distinguished by a circular halo around them, were used to inoculate precultures.

Preculture preparation

Pseudomonas lemoignei LMG 2207 was cultivated in shake flasks for precultures. For the preparation of the minimal medium, $CaCl_2 \times 2\ H_2O$, $FeCl_3 \times 6\ H_2O$, NH_4Cl, and $MgSO_4 \times 7\ H_2O$ were autoclaved separately and mixed at room temperature to avoid the formation of precipitates. The resulting solution was supplemented with 5 g L^{-1} of disodium succinate. A gas-liquid ratio of 5 was respected for all cultivations to keep sufficient microbial culture aeration. Colonies from solid media plates were selected for medium inoculation. These cultures were incubated at 30°C and 160 RPM in an orbital shaker incubator. The biomass growth was monitored by measuring the optical density at 600 nm

TABLE 1 Degradation rates extracted from raw data processing according to the protein concentration for all degradation experiments.

	Protein concentration [µg mL^{-1}]	Degradation rate υ_0 [ng cm^{-2} s^{-1}]
Degradation of PHB by scl-depolymerases	828.4	11.5
	414.2	17.2
	207.1	18.2
	145.0	14.4
	82.8	13.0
	41.4	7.8
	16.6	6.5
	4.1	2.9
	0.8	1.0
	0.2	0.2
Degradation of PHO by mcl-depolymerase	122.2	7.0
	24.4	8.7
	12.2	7.1
	2.4	2.3
	0.5	0.8
	0.1	0.2

(OD_{600}) of 1 mL samples. The incubation was stopped once the desired OD_{600} was reached.

In a similar way, *E. coli* DH5α strain harboring the plasmid pMAD8 was streaked on LB-Amp Agar at 37°C and incubated overnight, providing single colonies to inoculate LB-Amp medium. The precultures were cultivated overnight at 37°C with 200 RPM agitation.

Batch cultivation with pH shift

For the optimization of scl-depolymerases production from *P. lemoignei* in a 3 L benchtop bioreactor (KLF, Bioengineering), the cultivation was carried out as reported by Terpe et al. (1999). A preculture of 200 mL with an OD600 of 1.0 was used to inoculate the main culture medium to obtain an OD600 of approximately 0.1. The fermentation was separated into biomass accumulation and depolymerase production phases, differentiated only by the pH setting of 6.3 and 7.6, respectively. The pH adjustment was realized by adding smaller volumes of NaOH 5 M or H_3PO_4 5 M. Furthermore, the process parameters were set to a temperature of 30°C, a stirring speed of 400 RPM, and an aeration of 2 vvm with air. The pO_2 was prevented to fall below 30% by addition of O_2 to the inlet gas. Samples of 5 mL were taken regularly during the whole cultivation. The OD_{600} of samples was measured to follow the biomass growth and to apply the pH shift during the late exponential phase. Moreover, the enzyme activity was measured on crude culture medium samples with a spectrophotometric enzyme assay.

For the expression of mcl-depolymerase by *E. coli* harboring the plasmid pMAD8, a stock solution of 0.17 M KH_2PO_4 and 0.72 M

K_2HPO_4 was separately autoclaved and added to the main solution together with the ampicillin. Cultivation conditions in the 3 L benchtop bioreactor were set to 37°C, a pH of 7.0 (adjusted with NaOH 5 M and H_3PO_4 2 M), an aeration of 1 vvm, and agitation starting at 700 RPM and gradually increasing to 1,200 RPM to prevent the pO_2 to drop below 30%. The bioreactor was inoculated with 100 mL of the LB-Amp preculture. The OD_{600} was monitored and once it reached 6, the temperature was reduced to 25°C and 0.5 mM IPTG was added for induction. After 16 h of induction, cells were harvested and isolated by centrifugation.

Spectrophotometric enzyme activity assay

To follow the production of extracellular depolymerases, the enzyme activity was monitored using the model substrate *para*-nitrophenyl butyrate (pNPB) according to the spectrophotometric assay described by Rios et al. (2019).

Isolation and concentration of depolymerases

For scl-depolymerases from *P. lemoignei*, the isolation of extracellular enzymes was performed by centrifugation of the crude culture medium at 2500 × g for 45 min at 4°C. The enzymes present in the supernatant fraction were concentrated by two consecutive ultrafiltration (UF) cycles using centrifugal concentrator tubes of 15 mL with a 50 kDa molecular weight cut-off regenerated cellulose membrane (Vivaspin Turbo 15 RC 50kDa,
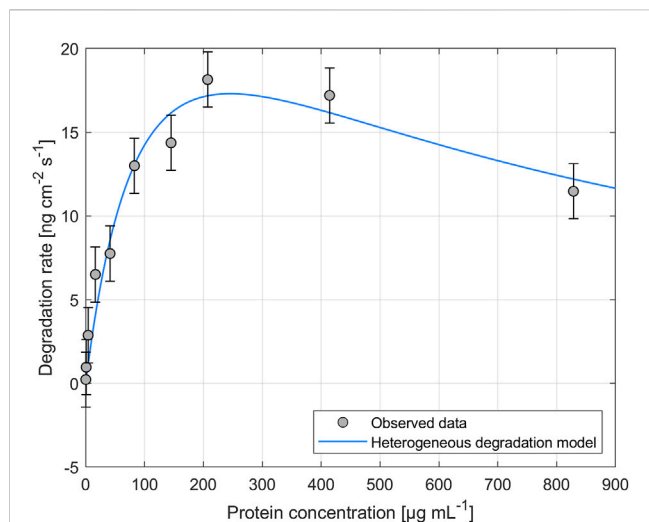
FIGURE 1
Degradation of PHB thin films exposed to depolymerases from *Pseudomonas lemoignei* LMG 2207 at various protein concentrations. The heterogeneous degradation model was fitted to the observed data through non-linear regression using the Levenberg-Marquardt algorithm. The degradation rate measurement for an enzyme concentration of C_{prot} = 82.8 μg mL^{-1} was carried out in triplicate and the standard deviation was used to calculate the error bars assuming a constant error.
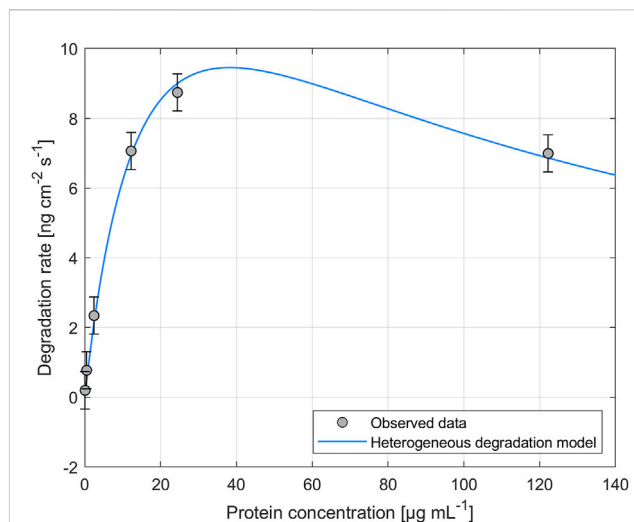
FIGURE 2
Degradation of PHO thin films exposed to recombinant mcl-depolymerases from *Escherichia coli* DH5α harboring the plasmid pMAD8, at various protein concentrations. The heterogeneous degradation model was fitted to the observed data through non-linear regression using the Levenberg-Marquardt algorithm. The degradation rate measurement for an enzyme concentration of C_{prot} = 2.4 μg mL^{-1} was carried out in triplicate and the standard deviation was used to calculate the error bars assuming a constant error.

Sartorius). The concentrator tubes were filled with 10 mL of supernatant and centrifuged 5000 × g for 15 min at 4°C for the first concentration step and 7 min at 4°C for the second step.

For mcl-depolymerases from recombinant *E. coli*, the crude culture medium was centrifuged at 7000 × g for 30 min at 4°C. The pellet was resuspended in a lysis buffer consisting of 30 mM Tris-HCl (pH 8.0) and 1 mM EDTA. The cells were disrupted using a French press at 1,000 bar for two cycles, keeping the mixture on ice throughout the process. The mixture was then centrifuged at 9384 × g for 15 min at 4°C to obtain the supernatant containing the depolymerase. The solution was concentrated using a 30 kDa centrifugal concentrator tubes (Amicon, Millipore). The final step of purification was performed by preparative chromatography (Äkta start, Cytiva) using a high-flow amylose resin (n°E8022S from neb, Bioconcept Ltd.).

Protein quantification

For protein quantification, a sample volume of 1 μL was directly deposited onto the measurement pedestal of a Nanodrop spectrophotometer (DS-11 FX +, DeNovix) and measured at 280 nm. As the exact composition of the mixture of depolymerases was not known, the concentrations were calculated based on the percent extinction coefficient of bovine serum albumin provided by the device manufacturer (0.667 L g^{-1} cm^{-1}).

PHA thin film preparation

PHA solutions were prepared for the coating step of thin films on quartz crystal sensors. Surface electron microscopy (SEM) was

employed to support the development of a suitable coating procedure (Supplementary Figure S1). The solution was made from PHB powder or PHO film solubilized in trichloromethane (1% w/v) and heated at 50°C for 1 h to fully solubilize the polymer. A fraction of 10% v/v of toluene was added to the solutions to optimize the evaporation speed and film thickness during the spin coating process. For dynamic spin coating of quartz crystal sensors, the speed of the spin coater (Ossila Ltd.) was set at 4,000 RPM and 140 μL of polymer solution was cast on the rotating sensor center. The spinning was continued for 40 s, followed by drying the coated sensor in a vacuum oven at 37.5°C and 50 mbar for 20 min. Finally, the film was examined visually for any imperfections such as irregularities, pinholes, or scratches.

QCM measurements procedure

Experiments were carried out with a QCM (Q-1, openQCM) allowing the measurement of the RF, dissipation, and sensor temperature. The sensor type was a 5 MHz quartz crystal with a blank diameter of 13.95 mm, a frontal gold electrode diameter of 11.20 mm, an AT-fundamental cut, a quartz density of 2649.7 kg m^{-3}, and one gold electrode on both sides. For data acquisition and real-time monitoring, the openQCM Q-1 Python Software (GUI Python version 2.0) was used.

Film stability assessment

Before any degradation experiment, the film stability was assessed by monitoring the RF variations of coated quartz

TABLE 2 Kinetic constants calculated by non-linear regression of experimentally observed data to the heterogeneous degradation model for the PHB and PHO degradation.

	Adsorption equilibrium constant (K) [mL μg^{-1}]	Degradation rate constant (k') [ng cm^{-2} s^{-1}]
Degradation of PHB by scl-depolymerases	0.004	69
Degradation of PHO by mcl-depolymerase	0.026	38

sensors dispensed in circulating buffer solution. Chemical-resistant tubes (Tygon 2375-C, Saint Gobain) of 1.6 mm inner diameter, connected the measuring module to a magnetically stirred reservoir. Phosphate buffer at pH 7 was introduced into the reservoir and a constant flow was installed by a peristaltic pump, set to a flow rate of 0.5 mL min^{-1}. Once the measuring chamber was filled, measurements were started for 1 h. For acceptable frequency variations in phosphate buffer (typically below 30 Hz), the degradation experiment was started. Otherwise, another sensor was calibrated, coated, and assessed.

Enzymatic degradation

The measuring chamber, the stirred container, and circulation tubes were kept filled with the phosphate buffer solution to avoid air bubbles. Enzyme solution was introduced into the stirred container and mixed for 1 min at 700 RPM. Afterwards, the peristaltic pump was switched on and set at a flow rate of 0.5 mL min^{-1}. As soon as the enzyme solution circulated, measurements were started. Finally, once the enzymatic degradation was finished, measurements were kept for approximately one more hour.

Results

The degradation of thin films made of PHB and PHO was investigated using scl-depolymerases from *P. lemoignei* LMG 2207 and recombinant mcl-depolymerases from *E. coli* DH5α harboring the plasmid pMAD8, respectively. To assess the degradation process, QCM measurements were carried out. The results revealed a sigmoidal degradation rate profile, consisting of an initial acceleration phase, an inflection point representing the highest degradation rate (v_0) and a subsequent deceleration phase (Supplementary Figure S2). The raw data were analyzed to obtain the degradation rate for each experiment and are compiled in Table 1.

The impact of different enzyme concentrations on degradation rate was investigated. The protein concentrations tested for PHB and PHO films differed, with a wider range of 0.2–828.4 μg mL^{-1} for PHB and a narrower range of 0.1–122.2 μg mL^{-1} for PHO. Consistent with findings in the literature for scl-PHA, QCM measurements revealed that the degradation rate initially increased with increasing enzyme concentration, reaching a maximum value, and followed by a decreasing degradation rate with further increasing enzyme concentrations. The enzyme concentration corresponding to the maximum degradation rate was higher when using scl-depolymerases to degrade PHB thin films than when using mcl-depolymerases to degrade PHO thin films. According to these observations, results were analyzed using

the heterogeneous degradation model, which was fitted to the observed degradation rate data through non-linear regression with the Levenberg-Marquardt algorithm. Figures 1, 2 display the observed data and the corresponding fitted models for the degradation of PHB and PHO, respectively. We like to point out, that in the case of the used experimental set-up, the observed mass loss cannot directly be correlated with the hydrolysis rate of the enzymes. Although both enzyme classes are known to primarily produce water soluble monomers, dimers, and trimers as degradation products (Abe and Doi, 1999; Handrick et al., 2004; Martínez et al., 2015), the fragmentation of the PHA polymer into non soluble degradation products would lead to their deposition on the surface and would not be observed as a frequency change in the QCM measurement. However, due to the stability testing prior to each experiment in the absence of polymer degrading enzyme, mass loss as observed by a resonance frequency increase can be attributed to the degradation of the polymer by the enzyme into soluble products. We therefore refer to the constant k' of the heterogeneous degradation model as degradation rate constant, rather than hydrolysis rate constant as originally proposed by Mukai et al. By applying the kinetic model, it was determined that the maximum degradation rate for PHB films was 17.3 ng cm^{-2} s^{-1} and occurred at a scl-depolymerases concentration of 245.6 μg mL^{-1}. For PHO films, the maximum degradation rate was 9.5 ng cm^{-2} s^{-1} and occurred at a mcl-depolymerases concentration of 38.2 μg mL^{-1}.

The kinetic constants were obtained through non-linear regression analysis of QCM measurements and are compiled in Table 2. The adsorption equilibrium constant (K) represents the affinity of the enzyme to the substrate and reflects the initial adsorption step of the depolymerization process. The higher K value for mcl-depolymerases on PHO films compared to scl-depolymerases on PHB films indicates a stronger affinity of the mcl-depolymerases for the PHO substrate. Concerning the degradation rate constant (k'), it reflects the enzymatic degradation activity of the enzyme and represents the rate of mass reduction after adsorption. The lower k' value for mcl-depolymerases compared to scl-depolymerases suggests that mcl-depolymerases have a lower enzymatic efficiency in degrading PHO films. These results indicate that the enzyme-substrate interactions and degradation activity play key functions in the degradation of PHB and PHO films by scl- and mcl-depolymerases.

Discussion

The interaction strength between an enzyme and its substrate is represented by the constant K in the heterogeneous degradation model. The QCM measurements showed that the K value was six times higher for mcl-depolymerases and PHO when compared to

scl-depolymerases and PHB. It indicates a stronger adsorption of mcl-depolymerase to PHO than the adsorption of scl-depolymerases to PHB. We attribute the differences in K values between these two systems to the higher hydrophobicity of the PHO polymer. Although structurally different, with a C-terminal substrate binding domain for scl-depolymerases (Behrends et al., 1996) and an N-terminal substrate binding domain for mcl-depolymerases (Gangoiti et al., 2012), both enzymes have a hydrophobic site that promotes absorption to the substrate. However, the presence of longer aliphatic side chains of the PHO polymer reduces the competitive effect of solvent absorption at the polymer surface when compared to the more polar PHB surface where water molecules will absorb to a higher extend, leading to a lower number of absorbed enzyme molecules in the equilibrium state.

The degradation rate of a biopolyester under the catalytic effect of an enzyme is expressed by the constant k' in the heterogeneous degradation model. The QCM measurements showed that the k' value was approximately twice as high for scl-depolymerases and PHB than for mcl-depolymerases and PHO. Possible explanations, apart from the different specific environments of the Serine-Histidine-Aspartate motif (i.e., catalytic triad), can be found in the different nature of the PHA-backbones. PHA hydrolysis takes place at the ester forming carbonyl groups of the polymers. For mcl-PHAs these are sterically more challenging due to their longer aliphatic side chains. This sidechain length also reduces the quality of the leaving group and the nucleophilicity of the carbonyl group.

Considering the mechanism of the degradation of PHA as proposed by Mukai et al., this leads not only to a reduced maximum degradation rate for the mcl-depolymerase when compared to the scl-depolymerases of this study but also to a lower optimal enzyme concentration since the fast adsorption accompanied by a relatively slow and rate-limiting hydrolysis process leads to faster surface crowding by the absorbed enzyme molecules on the substrate surface (Figures 1, 2).

In conclusion, we believe that these findings will support the process of developing applications for mcl-PHAs and the critical consideration of end-of-life scenarios. A low abundance of natural mcl-PHA producers in the environment, concomitant scarcity of mcl-PHA depolymerases and the observed lower degradation rate constant when compared to scl-PHA depolymerases, invite to consider new routes for monomer reutilization and upcycling. In this respect, enzymatic engineering might offer a viable solution to improve the enzymatic degradation of PHA depolymerases by addressing their substrate binding and hydrolysis profiles.

Data availability statement

The raw data supporting the conclusion of this article will be made available by the authors, without undue reservation.

Author contributions

FM: Formal Analysis, Investigation, Methodology, Software, Writing–original draft. NH: Conceptualization, Methodology, Resources, Supervision, Writing–review and editing.

Funding

Conflict of interest

The authors declare that the research was conducted in the absence of any commercial or financial relationships that could be construed as a potential conflict of interest.

Publisher's note

All claims expressed in this article are solely those of the authors and do not necessarily represent those of their affiliated organizations, or those of the publisher, the editors and the reviewers. Any product that may be evaluated in this article, or claim that may be made by its manufacturer, is not guaranteed or endorsed by the publisher.

Supplementary material

The Supplementary Material for this article can be found online at: https://www.frontiersin.org/articles/10.3389/fbioe.2023.1303267/full#supplementary-material

References

Abe, H., and Doi, Y. (1999). Structural effects on enzymatic degradabilities for poly [(R)-3-hydroxybutyric acid] and its copolymers. *Int. J. Biol. Macromol.* 25 (1-3), 185–192. doi:10.1016/s0141-8130(99)00033-1

Amstutz, V., Hanik, N., Pott, J., Utsunomia, C., and Zinn, M. (2019). Tailored biosynthesis of polyhydroxyalkanoates in chemostat cultures. *Methods Enzym.* 627, 99–123. doi:10.1016/bs.mie.2019.08.018

Behrends, A., Klingbeil, B., and Jendrossek, D. (1996). Poly(3-hydroxybutyrate) depolymerases bind to their substrate by a C-terminal located substrate binding site. *FEMS Microbiol. Lett.* 143 (2-3), 191–194. doi:10.1111/j.1574-6968.1996.tb08479.x

Braaz, R., Handrick, R., and Jendrossek, D. (2003). Identification and characterisation of the catalytic triad of the alkaliphilic thermotolerant PHA depolymerase PhaZ7 of Paucimonas lemoignei. *FEMS Microbiol. Lett.* 224 (1), 107–112. doi:10.1016/s0378-1097(03)00425-7

Brigham, C. J., and Sinskey, A. J. (2012). Applications of polyhydroxyalkanoates in the medical industry. *Int. J. Biotechnol. Wellness Industries* 1, 52–60. doi:10.6000/1927-3037.2012.01.01.03

Ceccacci, A. C., Chen, C.-H., Hwu, E.-T., Morelli, L., Bose, S., Bosco, F. G., et al. (2017). Blu-Ray-based micromechanical characterization platform for biopolymer degradation assessment. *Sensors Actuators B-chemical* 241, 1303–1309. doi:10.1016/j.snb.2016.09.190

Chamieh, J., Biron, J. P., Cipelletti, L., and Cottet, H. (2015). Monitoring biopolymer degradation by taylor dispersion analysis. *Biomacromolecules* 16 (12), 3945–3951. doi:10.1021/acs.biomac.5b01260

Chen, G. (2009). A microbial polyhydroxyalkanoates (PHA) based bio- and materials industry. *Chem. Soc. Rev.* 38 8, 2434–2446. doi:10.1039/b812677c

Chen, G.-Q., Chen, X.-Y., Wu, F.-Q., and Chen, J.-C. (2020). Polyhydroxyalkanoates (PHA) toward cost competitiveness and functionality. *Adv. Industrial Eng. Polym. Res.* 3 (1), 1–7. doi:10.1016/j.aiepr.2019.11.001

Derraik, J. G. B. (2002). The pollution of the marine environment by plastic debris: a review. *Mar. Pollut. Bull.* 44 9, 842–852. doi:10.1016/s0025-326x(02)00220-5

de Souza Machado, A. A., Kloas, W., Zarfl, C., Hempel, S., and Rillig, M. C. (2018). Microplastics as an emerging threat to terrestrial ecosystems. *Glob. Chang. Biol.* 24 (4), 1405–1416. doi:10.1111/gcb.14020

Drzyzga, O., and Prieto, A. (2019). Plastic waste management, a matter for the 'community. *Microb. Biotechnol.* 12 (1), 66–68. doi:10.1111/1751-7915.13328

Gangoiti, J., Santos, M., Prieto, M. A., de la Mata, I., Serra, J. L., and Llama, M. J. (2012). Characterization of a novel subgroup of extracellular medium-chain-length polyhydroxyalkanoate depolymerases from actinobacteria. *Appl. Environ. Microbiol.* 78 (20), 7229–7237. doi:10.1128/aem.01707-12

García-Hidalgo, J., Hormigo, D., Prieto, M. A., Arroyo, M., and de la Mata, I. (2012). Extracellular production of Streptomyces exfoliatus poly(3-hydroxybutyrate) depolymerase in Rhodococcus sp. T104: determination of optimal biocatalyst conditions. *Appl. Microbiol. Biotechnol.* 93 (5), 1975–1988. doi:10.1007/s00253-011-3527-5

Gumel, A. M., Annuar, M. S. M., and Heidelberg, T. (2013). Current application of controlled degradation processes in polymer modification and functionalization. *J. Appl. Polym. Sci.* 129, 3079–3088. doi:10.1002/app.39006

Handrick, R., Reinhardt, S., Focarete, M. L., Scandola, M., Adamus, G., Kowalczuk, M., et al. (2001). A new type of thermoalkalophilic hydrolase of Paucimonas lemoignei with high specificity for amorphous polyesters of short chain-length hydroxyalkanoic acids. *J. Biol. Chem.* 276 (39), 36215–36224. doi:10.1074/jbc.M101106200

Handrick, R., Reinhardt, S., Kimmig, P., and Jendrossek, D. (2004). The "intracellular" poly(3-hydroxybutyrate) (PHB) depolymerase of Rhodospirillum rubrum is a periplasm-located protein with specificity for native PHB and with structural similarity to extracellular PHB depolymerases. *J. Bacteriol.* 186 (21), 7243–7253. doi:10.1128/jb.186.21.7243-7253.2004

Hanik, N., Amstutz, V., and Zinn, M. (2019). Microplastics - from anthropogenic to natural. *Chim. (Aarau)* 73 (10), 841–843. doi:10.2533/chimia.2019.841

Hazer, B., and Steinbüchel, A. (2007). Increased diversification of polyhydroxyalkanoates by modification reactions for industrial and medical applications. *Appl. Microbiol. Biotechnol.* 74, 1–12. doi:10.1007/s00253-006-0732-8

Ihssen, J., Magnani, D., Thony-Meyer, L., and Ren, Q. (2009). Use of extracellular medium chain length polyhydroxyalkanoate depolymerase for targeted binding of proteins to artificial poly[(3-hydroxyoctanoate)-co-(3-hydroxyhexanoate)] granules. *Biomacromolecules* 10 (7), 1854–1864. doi:10.1021/bm9002859

Jendrossek, D., and Handrick, R. (2002). Microbial degradation of polyhydroxyalkanoates. *Annu. Rev. Microbiol.* 56, 403–432. doi:10.1146/annurev.micro.56.012302.160838

Johannsmann, D. (2015). *The quartz crystal microbalance in soft matter research.* Cham: Springer.

Kalia, V. C., Singh Patel, S. K., Shanmugam, R., and Lee, J.-K. (2021). Polyhydroxyalkanoates: trends and advances toward biotechnological applications. *Bioresour. Technol.* 326, 124737. doi:10.1016/j.biortech.2021.124737

Keskin, G., Kizil, G. V., Bechelany, M., Pochat-Bohatier, C., and Öner, M. (2017). Potential of polyhydroxyalkanoate (PHA) polymers family as substitutes of petroleum based polymers for packaging applications and solutions brought by their composites to form barrier materials. *Pure Appl. Chem.* 89, 1841–1848. doi:10.1515/pac-2017-0401

Khardenavis, A. A., Kumar, M. S., Mudliar, S. N., and Chakrabarti, T. (2007). Biotechnological conversion of agro-industrial wastewaters into biodegradable plastic, poly(β-hydroxybutyrate). *Bioresour. Technol.* 98 (18), 3579–3584. doi:10.1016/j.biortech.2006.11.024

Kim, H. W., Chung, M. G., and Rhee, Y. H. (2007). Biosynthesis, modification, and biodegradation of bacterial medium-chain-length polyhydroxyalkanoates. *J. Microbiol.* 45 (2), 87–97.

Law, K. L. (2017). Plastics in the marine environment. *Annu. Rev. Mar. Sci.* 9, 205–229. doi:10.1146/annurev-marine-010816-060409

Li, Z., Yang, J., and Loh, X. J. (2016). Polyhydroxyalkanoates: opening doors for a sustainable future. *NPG Asia Mater.* 8 (4), e265. doi:10.1038/am.2016.48

Martínez, V., De Santos, P. G., García-Hidalgo, J., Hormigo, D., Prieto, M. A., Arroyo, M., et al. (2015). Novel extracellular medium-chain-length polyhydroxyalkanoate depolymerase from Streptomyces exfoliatus K10 DSMZ 41693: a promising biocatalyst for the efficient degradation of natural and functionalized mcl-PHAs. *Appl. Microbiol. Biotechnol.* 99, 9605–9615. doi:10.1007/s00253-015-6780-1

Marx, K. A. (2003). Quartz crystal microbalance: a useful tool for studying thin polymer films and complex biomolecular systems at the solution-surface interface. *Biomacromolecules* 4 (5), 1099–1120. doi:10.1021/bm020116i

Matsumoto, K. i., Shozui, F., Satoh, Y., Tajima, K., Munekata, M., and Taguchi, S. (2009). Kinetic analysis of engineered polyhydroxyalkanoate synthases with broad substrate specificity. *Polym. J.* 41, 237–240. doi:10.1295/polymj.pj2008253

Meereboer, K. W., Misra, M., and Mohanty, A. K. (2020). Review of recent advances in the biodegradability of polyhydroxyalkanoate (PHA) bioplastics and their composites. *Green Chem.* 22, 5519–5558. doi:10.1039/d0gc01647k

Mukai, K., Yamada, K., and Doi, Y. (1993). Kinetics and mechanism of heterogeneous hydrolysis of poly[(R)-3-hydroxybutyrate] film by PHA depolymerases. *Int. J. Biol. Macromol.* 15 (6), 361–366. doi:10.1016/0141-8130(93)90054-p

Muthuraj, R., Valerio, O., and Mekonnen, T. H. (2021). Recent developments in short- and medium-chain- length Polyhydroxyalkanoates: production, properties, and applications. International *Journal of Biological Macromolecules. Int. J. Biol. Macromol.* 187, 422–440. doi:10.1016/j.ijbiomac.2021.07.143

Oliveira, G. H. D., Zaiat, M., Rodrigues, J. A. D., Ramsay, J. A., and Ramsay, B. A. (2020). Towards the production of mcl-PHA with enriched dominant monomer content: process development for the sugarcane biorefinery context. *J. Polym. Environ.* 28, 844–853. doi:10.1007/s10924-019-01637-2

Panchal, B., Bagdadi, A., and Roy, I. (2013). "Polyhydroxyalkanoates: the natural polymers produced by bacterial fermentation," in *Advances in natural polymers: composites and nanocomposites*. Editors S. Thomas, P. M. Visakh, and A. P. Mathew (Berlin, Heidelberg: Springer Berlin Heidelberg), 397–421.

Raza, Z. A., Abid, S., and Banat, I. M. (2018). Polyhydroxyalkanoates: characteristics, production, recent developments and applications. *Int. Biodeterior. Biodegrad.* 126, 45–56. doi:10.1016/j.ibiod.2017.10.001

Reddy, V. U. N., Ramanaiah, S. V., Reddy, M. V., and Chang, Y.-C. (2022). Review of the developments of bacterial medium-chain-length polyhydroxyalkanoates (mcl-PHAs). *Bioengineering* 9 (5), 225. doi:10.3390/bioengineering9050225

Rios, N. S., Mendez-Sanchez, C., Arana-Peña, S., Rueda, N., Ortiz, C., Gonçalves, L. R. B., et al. (2019). Immobilization of lipase from Pseudomonas fluorescens on glyoxyl-octyl-agarose beads: improved stability and reusability. *Biochim. Biophys. Acta BBA - Proteins Proteomics* 1867, 741–747. doi:10.1016/j.bbapap.2019.06.005

Sabot, A., and Krause, S. (2002). Simultaneous quartz crystal microbalance impedance and electrochemical impedance measurements. Investigation into the degradation of thin polymer films. *Anal. Chem.* 74 14, 3304–3311. doi:10.1021/ac0200724

Sauerbrey, G. (1959). Verwendung von schwingquarzen zur wagung dunner schichten und zur mikrowagung. *Z. Fur Phys.* 155 (2), 206–222. doi:10.1007/Bf01337937

Schirmer, A., and Jendrossek, D. (1994). Molecular characterization of the extracellular poly(3-hydroxyoctanoic acid) [P(3HO)] depolymerase gene of Pseudomonas fluorescens GK13 and of its gene product. *J. Bacteriol.* 176 (22), 7065–7073. doi:10.1128/jb.176.22.7065-7073.1994

Silva, R. R. A., Marques, C. S., Arruda, T. R., Teixeira, S. C., and de Oliveira, T. V. (2023). Biodegradation of polymers: stages, measurement, standards and prospects. *Macromol* 3 (2), 371–399. doi:10.3390/macromol3020023

Singh, P., and Sharma, V. P. (2016). Integrated plastic waste management: environmental and improved health approaches. *Procedia Environ. Sci.* 35, 692–700. doi:10.1016/j.proenv.2016.07.068

Soo, C. L., Sabana, S., Chen, C. A., and Hii, Y. S. (2021). Understanding microplastics in aquatic ecosystems – a mini review. *Borneo J. Mar. Sci. Aquac. (BJoMSA)* 5 (2), 63–69. doi:10.51200/bjomsa.v5i2.3386

Stinson, M. W., and Merrick, J. M. (1974). Extracellular enzyme secretion by Pseudomonas lemoignei. *J. Bacteriol.* 119 (1), 152–161. doi:10.1128/jb.119.1.152-161.1974

Terpe, K., Kerkhoff, K., Pluta, E., and Jendrossek, D. (1999). Relationship between succinate transport and production of extracellular poly(3-hydroxybutyrate) depolymerase in Pseudomonas lemoignei. *Appl. Environ. Microbiol.* 65 (4), 1703–1709. doi:10.1128/AEM.65.4.1703-1709.1999

Timmins, M. R., Gilmore, D. F., Lotti, N., Scandola, M., Fuller, R. C., and Lenz, R. W. (1997a). A spectrophotometric method for detection of enzymatic degradation of thin polymer films. *J. Environ. Polym. Degrad.* 5 (1), 1–15. doi:10.1007/BF02763564

Timmins, M. R., Lenz, R. W., and Clinton Fuller, R. (1997b). Heterogeneous kinetics of the enzymatic degradation of poly(β-hydroxyalkanoates). *Polymer* 38 (3), 551–562. doi:10.1016/S0032-3861(96)00530-7

Tortajada, M., da Silva, L. F., and Prieto, M. A. (2013). Second-generation functionalized medium-chain-length polyhydroxyalkanoates: the gateway to high-value bioplastic applications. *Int. Microbiol.* 16, 1–15. doi:10.2436/20.1501.01.175

Wang, Y., Yin, J., and Chen, G. Q. (2014). Polyhydroxyalkanoates, challenges and opportunities. *Curr. Opin. Biotechnol.* 30, 59–65. doi:10.1016/j.copbio.2014.06.001

Yamashita, K., Kikkawa, Y., Kurokawa, K., and Doi, Y. (2005). Enzymatic degradation of poly(l-lactide) film by proteinase K: quartz crystal microbalance and atomic force microscopy study. *Biomacromolecules* 6 (2), 850–857. doi:10.1021/bm049395v

frontiers | Frontiers in Bioengineering and Biotechnology

Marine biodegradation of poly [(R)-3-hydroxybutyrate-co-4-hydroxybutyrate] elastic fibers in seawater: dependence of decomposition rate on highly ordered structure

Taku Omura[1], Sakura Tsujimoto[1,2], Satoshi Kimura[1],
Akira Maehara[3], Taizo Kabe[1] and Tadahisa Iwata[1]*

[1]Graduate School of Agricultural and Life Sciences, The University of Tokyo, Bunkyo, Tokyo, Japan,
[2]Graduate School of Industrial Technology, Nihon University, Narashino, Japan, [3]Niigata Research
Laboratory, Mitsubishi Gas Chemical Co., Inc., Niigata, Japan

Here, we report the marine degradability of polymers with highly ordered structures in natural environmental water using microbial degradation and biochemical oxygen demand (BOD) tests. Three types of elastic fibers (non-porous as-spun, non-porous drawn, and porous drawn) with different highly ordered structures were prepared using poly[(R)-3-hydroxybutyrate-co-16 mol%-4-hydroxybutyrate] [P(3HB-co-16 mol%-4HB)], a well-known polyhydroxyalkanoate. Scanning electron microscopy (SEM) images indicated that microorganisms attached to the fiber surface within several days of testing and degraded the fiber without causing physical disintegration. The results of BOD tests revealed that more than 80% of P(3HB-co-16 mol%-4HB) was degraded by microorganisms in the ocean. The plastisphere was composed of a wide variety of microorganisms, and the microorganisms accumulated on the fiber surfaces differed from those in the biofilms. The microbial degradation rate increased as the degree of molecular orientation and porosity of the fiber increased: as-spun fiber < non-porous drawn fiber < porous drawn fiber. The drawing process induced significant changes in the highly ordered structure of the fiber, such as molecular orientation and porosity, without affecting the crystallinity. The results of SEM observations and X-ray measurements indicated that drawing the fibers oriented the amorphous chains, which promoted enzymatic degradation by microorganisms.

1 Introduction

Currently, 400 million tons of plastics, which are considered essential to our daily lives, are produced annually worldwide, representing a historic growth in production (Plastics Europe, 2016). At least 8 to 11 million tons of this plastic is released into the ocean each year, and if no action is taken, this amount is estimated to increase four-fold by 2050

(World Economic Forum, 2017; The Pew Charitable Trusts and SYSTEMIQ, 2020). In recent years, the negative effects of marine pollution, especially non-biodegradable plastics leaked into the ocean, on marine life have become a global problem. Depending on the location, plastic debris from fishing gear accounts for 10%–90% of marine debris (Lebreton et al., 2018). For example, around Korea, fishing gear generates approximately 75% of marine debris annually (Jang et al., 2014), while in the open ocean, fishing gear accounts for 50%–90% of marine debris (Hammer et al., 2012), most of which is fiber. Fishing nets, fishing lines, ropes, and other fibers used in fishing gear break during use and are lost or abandoned. Subsequently, they unintentionally become entangled with marine creatures and continue to function as fishing gear, known as the ghost fishing cycle (ghost gear). Therefore, to address this problem, there has been active development of plastic fibers that can be completely degraded by microorganisms in the environment into water and carbon dioxide, known as marine biodegradation.

To date, the biodegradability of plastics has been investigated using compost, soil, and river water under aerobic and anaerobic conditions in accordance with methods developed by standardization organizations, such as the International Organization for Standardization (ISO) and the American Society for Testing and Materials International (ASTM International). Compared with these media, the marine environment has fewer microorganisms, resulting in slower or no decomposition (Wang et al., 2021). Therefore, it is impossible to simply extrapolate the results of standard testing to evaluate biodegradability in the marine environment. The marine biodegradation of plastics has been evaluated using seawater and biochemical oxygen demand (BOD)-based tests (Kasuya et al., 1998; Nakayama et al., 2019) as well as field tests at shore (Briassoulis et al., 2019; Lott et al., 2020). These tests also investigate the effects of specific particle size, surface area, and shape on biodegradation (César et al., 2009; Chinaglia et al., 2018; Hino et al., 2023). In addition, polymer crystals (Nishida and Tokiwa, 1992; Nishida and Tokiwa, 1993), lamellar thickness (Koyama and Doi, 1997; Abe et al., 1998), and molecular orientation (Cai et al., 1996; Yoo and Im, 1999; Cho et al., 2003; Fischer et al., 2004; Komiyama et al., 2021) are some parameters that affect the degradation rate of biodegradable plastics. Therefore, the rate of biodegradation could be controlled by adjusting these parameters. To use biodegradable polymers in fiber applications, the polymers must possess enough strength which in turn can be tuned by changing the drawing ratio and the orientation of the molecular chains. However, multiple reports suggest that highly oriented molecular chains of poly[(R)-3-hydroxybutyrate] (PHB), poly(ε-caprolactone) (PCL), and poly(L-lactic acid) (PLLA) decreases the hydrolysis rate (Mochizuki et al., 1995; Cai et al., 1996; Yoo and Im, 1999; Cho et al., 2003; Fischer et al., 2004; Tsuji et al., 2007). These papers cannot be directly compared because as the orientation degree of the molecular chains increases, the degree of crystallinity also increases significantly, making it unclear which of these parameters affects the degradation rate. In fact, some studies have shown that the microbial degradation rate of biodegradable plastics decrease if the crystallinity is increased without orienting the molecular chains (Nishida and Tokiwa, 1992; Nishida and Tokiwa, 1993).

Polyhydroxyalkanoates (PHAs) are one of the few biodegradable plastics that can be degraded in the ocean, which is a critical issue today, and is attracting particular attention because of its potential to produce high-strength fibers (Iwata et al., 2004). A PHA copolymer that includes a 4HB unit as the second constituent, poly[(R)-3-hydroxybutyrate-co-4-hydroxybutyrate] [P(3HB-co-4HB)], is a promising alternative to non-biodegradable elastic materials owing to its ability to produce fibers with both strength and elasticity, excellent environmental degradability, and biocompatibility/absorbability (Omura et al., 2021; Murayama et al., 2023). The crystals of P(3HB-co-4HB) are representative of the Flory exclusion model because the 4HB units are excluded from the crystals formed from 3HB units, and thus the crystallinity saturates at a certain value (Kunioka et al., 1989; Doi et al., 1995). Therefore, even when uniaxial stretching is performed, there is no significant change in crystallinity, indicating that the degree of orientation can be strictly controlled.

PHA crystals have two crystalline phases: an α-form and a β-form (Yokouchi et al., 1973; Orts et al., 1990). In general, when PHA crystallizes, it forms lamellae crystals of the α-form, which is a thermodynamically stable crystalline phase. This form is easily obtained by hot-pressing or casting films. In contrast, the β-form is a stress-induced crystalline phase in uniaxially stretched PHA films (Iwata et al., 2004). In previous research on PHA, researchers have controlled not only the highly ordered structure, such as the melt-cooled α-form and the stress-induced β-form, but also the degree of crystallinity and porosity of the material (Iwata et al., 2003; Tanaka et al., 2007; Kabe et al., 2015; Phongtamrug and Tashiro, 2019; Komiyama et al., 2022). Moreover, studies on enzymatic and environmental degradation (Kumagai et al., 1992; Iwata et al., 1997; Kasuya et al., 1998) have been conducted. However, research on the correlation between these highly ordered structures and environmental degradability remains insufficient. To investigate this relationship, it is necessary to investigate the biodegradation of fibers with controlled highly ordered structures in terms of not only degradation rate but also BOD-curves changes.

The purpose of this study was to investigate the individual effect of uniaxial orientation and porous structure on the microbial degradation rate and BOD-based biodegradation of P(3HB-co-16 mol%-4HB), which has a highly ordered structure and is expected to be used in many environmental applications owing to its elasticity. Three types of P(3HB-co-16 mol%-4HB) fibers, non-porous as-spun, non-porous drawn, and porous drawn, with different highly ordered structures were prepared by melt spinning, and microbial degradation was performed using seawater from Tokyo Bay. The degradation of each fiber was evaluated using weight measurements, scanning electron microscopy (SEM), wide-angle X-ray diffraction (WAXD), small-angle X-ray scattering (SAXS), gel permeation chromatography (GPC), and BOD testing.

2 Experimental study

2.1 Materials

P(3HB-co-16 mol%-4HB) with a weight-average molecular weight (M_w) of 6.6×10^5 g/mol and polydispersity index (PDI) of 2.9 was provided by Mitsubishi Gas Chemical Co., Japan.

P(3HB-*co*-16 mol%-4HB) was obtained in the pure form and used without further purification. The powder (5 g) was dissolved in chloroform (500 mL) and cast into a film.

2.2 Processing of non-porous P(3HB-*co*-16 mol%-4HB) fiber

P(3HB-*co*-16 mol%-4HB) fibers were fabricated according to the method described previously (Omura et al., 2021). The cast film of P(3HB-*co*-16 mol%-4HB) (1.5 g) was placed in the furnace of a melt-spinner (IMC-19F8; Imoto Manufacturing Co., Japan) set to 150°C (i.e., lower than the melting temperature of the lamellar crystals), melted for 1 min, and then spun with an extruder rod at a rate of 1 mm/s. A nozzle with a length to diameter (L/D) ratio of 3 and diameter of 1 mm was used, and the fibers were taken up at a rate of 1.8 m/min. The fibers were then stretched by hand until they necked and drawn by five-fold at room temperature. The fibers obtained in this experiment were not heat treated.

2.3 Processing of porous P(3HB-*co*-16 mol%-4HB) fiber

P(3HB-*co*-16 mol%-4HB) powder was melt-spun using the same procedure as in 2.2. The melt-spun fibers were taken up at a speed of 1.8 m/min in an ice water bath at 4°C. After isothermal crystallization at 4°C for 72 h, porous fibers were obtained by necking and drawing by 12-fold at room temperature using a manual stretching machine. The fibers obtained in this experiment were not heat treated.

2.4 Microbial degradation tests

Seawater used as the source of microbial inoculum was collected from Tokyo Bay: Odaiba Seaside Park (35°37′41.1″N 139°46′16.5″E) in Minato-ku, Tokyo, Japan. Table 1 shows the detailed conditions under which the samples were collected.

Sediment (soil and sand) was also collected at the same location the natural environmental water (seawater) was collected. Sediment (2 kg) was added to 10 L of the natural water and stirred well. An ethanol-sterilized polyethylene mesh with a 122 μm gap was used to remove impurities, such as leaves, stones, and wood, with stirring. The resulting water was used as the test water.

Degradation tests were performed by adding approximately 20 mg of three P(3HB-*co*-16 mol%-4HB) fibers with different highly ordered structures and 100 mL of test water to each open container. The test was conducted at 25°C with agitation at a rate of 30 rpm for a total of 28 days. Samples were collected every 7 days, ultrasonically cleaned to remove the biofilm from the fiber surface, vacuum dried overnight at room temperature, and weighed for weight loss measurements. For each fiber, three different samples ($n = 3$) were collected every 7 days for weight loss measurements, and the average and deviation were calculated.

2.5 Media and culture conditions of bacteria

The total number of viable bacteria in the environmental water was determined using the plate count method (Nishida et al., 1998). Standard agar medium Daigo (23.5 g) and sodium chloride (29.2 g) were added to 1 L of distilled water, and the pH of the solution was adjusted to 7.0 using NaOH (1 mol/L) or HCl (1 mol/L) solution. The solution was autoclaved at 121°C for 15 min and poured into sterile polystyrene petri dishes to prepare the Luria–Bertani (LB) medium. A 10-fold diluted sample solution was prepared by adding 100 μL of collected seawater to 900 μL of sterile artificial seawater (NaCl: 29.2 g/L). This was repeated to prepare 100-, 1,000-, and 10,000-fold diluted sample solutions. Each sample solution (50 μL) was plated on the standard agar medium and incubated at 25°C for 24 h. Colonies formed on the plate were counted, and the number was expressed as colony forming units per mL (CFU/mL).

2.6 BOD-based test (BOD-biodegradability)

Biodegradation in the environmental water was evaluated using a BOD measuring device (OxiTop IDS, WTW, and Germany). The BOD test was performed by modifying the method of Suzuki et al. (Suzuki et al., 2017) In a cultivation bottle (internal volume 250 mL), 100 mL of seawater was mixed with 100 μL of buffer solution (Na$_2$HPO$_4$· 2H$_2$O 33.3 g/L, K$_2$HPO$_4$ 21.8 g/L, KH$_2$PO$_4$ 8.5 g/L, NH$_4$Cl 1.7 g/L), 0.5 g/L NH$_4$Cl, 0.1 g/L Na$_2$HPO$_4$, and 5 mg/L allylthiourea. The sample weight was 6-7 mg. BOD tests were conducted in an incubator (25°C) for approximately 1 month, and BOD data were acquired daily. BOD-biodegradability was calculated using Eqs 1, 2:

$$\text{BOD biodegradability } (\%) = \frac{\text{BOD}_s - \text{BOD}_b}{\text{ThOD}} \times 100 \qquad (1)$$

where BOD_s (mg) is the BOD value measured when the sample was added, BOD_b (mg) is the BOD value measured in blank tests, and ThOD is the theoretical oxygen demand (see Eq. 2).

$$\text{ThOD (mg)} = \frac{w \text{ (mg)}}{M \text{ (g/mol)}} \times \frac{4x + y - 2z}{4} \times 32 \text{ (g/mol)} \qquad (2)$$

where w is the initial sample weight (mg), and M is the molecular weight of the monomer unit (C$_x$H$_y$O$_z$) (g/mol).

The weight loss was calculated using Eq. 3:

$$\text{Weight loss } (\%) = \frac{W_i - W_f}{W_i} \times 100 \qquad (3)$$

where W_i is the initial sample weight (mg) and W_f is the sample weight after microbial degradation (mg).

2.7 Characterization

2.7.1 Scanning electron microscopy

The surface morphology of the fibers was observed using a scanning electron microscope (JCM-7000, JEOL, and Japan) operated at an accelerating voltage of 5 kV. Two different methods were used to treat the fibers after microbial degradation to obtain fibers with and without adhered bacteria. First, the

Type	Place	Date	Time	Weather	Temp /℃	Water temp /℃	pH	Viable microorganism counts ×10^5/CFU mL^{-1}
Seawater	Tokyo-bay	Mar 2nd	14:00	Cloudy/Rainy	18	15	7.6	2.1

collected fibers were soaked overnight in a 3% sodium chloride formaldehyde solution, and samples with microorganisms attached to the fiber surface were freeze-dried after solvent displacement with ethanol/t-butanol and then analyzed with SEM. Second, the collected samples were ultrasonically cleaned to remove the biofilm adhering to the fiber surface and vacuum dried overnight at room temperature. These samples were gold-coated using an ionic stepper (MSP-1S, Vacuum Device Co., Japan) before observation.

2.7.2 Gel permeation chromatography

The molecular weights (M_w and number-average, M_n) and PDI of the samples were measured using gel permeation chromatography (GPC; RID-20A differential refractive index detector, Shimadzu). Samples in chloroform were passed through columns (K-806M, K-802) with a flow rate of 0.8 mL/min at 40℃. A calibration curve was prepared using polystyrene (PS) standards (Shodex).

2.7.3 X-ray diffraction

Two-dimensional (2D) WAXD measurements were performed using a Micromax-007HF system (Rigaku, Japan) equipped with a CuKα irradiation source (λ = 0.15418 nm, operated at 40 kV and 30 mA), imaging plate reader (RAXIA-Di, Rigaku, Japan), and imaging plates (BAS-SR 127, 2,540 × 2,540 pixels, 50 × 50 μm2/pixel, Fujifilm Corporation, Japan). The distance between the sample and camera was 83 mm, and the sample and detector were placed in a vacuum chamber at room temperature. Single fibers were measured with an irradiation time of 5 min. The obtained 2D-WAXD diffractograms were converted to 1D-WAXD patterns using the 2DP software (Rigaku) to determine the crystallinity X_c and crystal orientation $f_{(020)}$.

2D SAXS measurements were performed on the BL03XU beamline at the SPring-8 synchrotron radiation facility (Harima, Japan) using an X-ray wavelength of 0.1 nm, and 2D diffractograms were recorded on an array detector (PILATUS3 S 1M, Rigaku). The distance between the sample and camera was 2,278 mm, and silver behenate (BeAg) was used as the calibration sample. The sample and detector were placed at room temperature and atmospheric pressure. Single fiber measurements were performed with an irradiation time of 1 s. The obtained 2D-SAXS images were analyzed using the MDIP software. The long period, L_p was obtained by analyzing the meridional region of the SAXS pattern.

3 Results and discussions

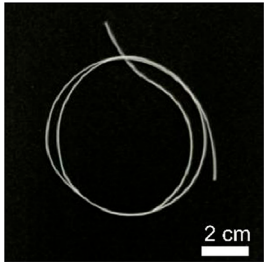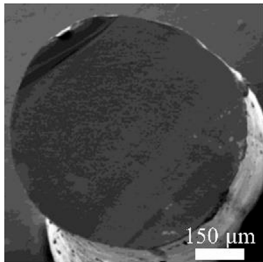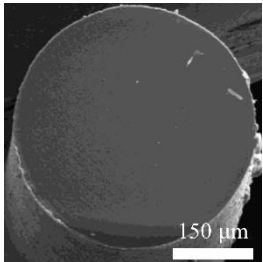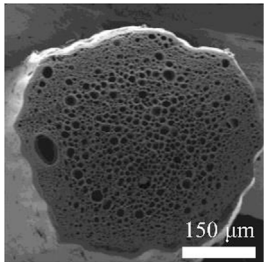### 3.1 Details of P(3HB-co-16 mol%-4HB) fibers
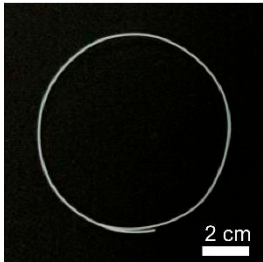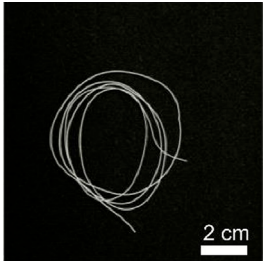
Details of the three types of P(3HB-co-16 mol%-4HB) fibers prepared are shown in Table 2. The weight of the fibers used in the degradation tests with seawater was approximately 20 mg, and the

corresponding fiber length and diameter are shown in Table 2. As-spun and 5-fold drawn fibers were densely packed with polymer chains inside the fiber. In contrast, fibers drawn by 12-fold after 72 h of isothermal crystallization at 4℃ had numerous discontinuous pores of approximately 5 μm inside the fiber, which was equivalent to a porosity of 45%. The crystals of P(3HB-co-4HB) are representative of the Flory exclusion model, in which 4HB units are excluded from crystals formed from 3HB units, and thus the crystallinity saturates at a certain value (Kunioka et al., 1989; Doi et al., 1995). This suggests that crystallization of 3HB unit is inhibited by the 4HB unit randomly incorporated during copolymerization, and thus crystallization can be controlled by drawing and heat treatment. Moreover, it is possible to control the degree of orientation without affecting the degree of crystallinity by drawing and heat treatment, thus obtaining samples with different degrees of orientation only. This enables a comparison of the samples without considering the effect of crystallinity. The 2D-WAXD image (Supplementary Figure S1A) of the as-spun fiber showed a ring pattern, indicating that the crystals were randomly distributed and unoriented, with a crystallinity of 41%. In contrast, the 2D-WAXD images (Supplementary Figures S1F, K) of both drawn fibers (non-porous and porous) indicated that the fibers were oriented in the α-form, with an orientation of 0.9 and crystallinity of 36% and 38%, respectively. In the previously reported uniaxial drawing of PCL, the crystallinity increases from 40% to 64% with drawing, and therefore it was impossible to simply attribute the enzymatic degradation rate to either the molecular orientation or the crystallinity (Mochizuki et al., 1995). However, in this study, the crystallinity of the P(3HB-co-16 mol%-4HB) elastic fibers did not change significantly before and after drawing, and thus the effect of orientation only on the degradation rate could be evaluated. In addition, the effect of the internal pores on the degradation rate could be evaluated.

3.2 Effect of highly ordered structure on marine biodegradability of P(3HB-co-16 mol%-4HB) fibers

To investigate the effect of morphology on the degradation rate, the weight losses of three types of P(3HB-co-16 mol%-4HB) fibers (non-porous as-spun, non-porous drawn, and porous drawn) immersed in seawater from Tokyo Bay were evaluated. After 28 days of microbial degradation in seawater from Tokyo Bay, the weight losses of the two types of drawn fibers (non-porous and porous) were approximately 100%, indicating good marine degradability (Figure 2). In the case of the porous drawn fiber, the internal porous surfaces were exposed as the smooth external surfaces were degraded by the microorganisms, further increasing the exposed surface area, which likely contributed to the fast marine

TABLE 2 Detail of various P(3HB-co-16 mol%-4HB) elastic fibers with different higher-ordered structure.
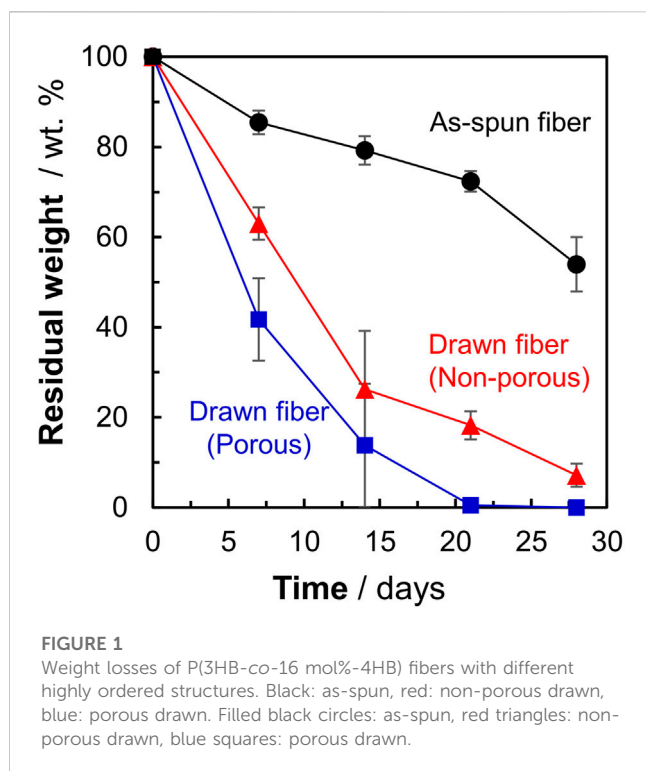
	As spun	Non-porous	Porous
Overall pictures			
Cross section, SEM Image			
Draw ratio, λ	1	5	12
Crystallinity, X_c/%	41	36	38
(020) orientation, f	-	0.9	0.9
Weight/mg	15–19	18–20	15–19
Diameter/μm	850	312	364
Length/cm	2.2	14.1	16.1

degradation rate (Figure 4, discussed later). In contrast, the as-spun fibers were not completely degraded in 28 days, and the weight loss after 28 days was only 46%. In this study, the weight of the fibers used was standardized to approximately 20 mg in order to make comparisons by weight loss. Fiber length and fiber surface area differ due to the thicker fiber diameter of the as-spun fiber (850 μm) compared to the fiber diameter of the two drawn fibers (about 300 μm). Since microbial degradation generally proceeds from the surface, the rate of biodegradation is strongly influenced by the surface area of the sample. Therefore, microbial degradation of samples with different surface areas must be evaluated by degradation rates considering the surface area. The degradation rate was 3.3 mg/cm²/week for the as-spun fiber, 5.1 mg/cm²/week for the drawn fiber (non-porous) and 5.5 mg/cm²/week for the drawn fiber (porous), indicating that the degradation rate for the drawn fibers (non-porous and porous) was about 1.5 times faster than that for the as-spun fiber.

3.3 Effect of P(3HB-co-16 mol%-4HB) morphology on BOD biodegradation

Figure 1 shows that the P(3HB-co-16 mol%-4HB) fibers lost weight in seawater. This indicated that the P(3HB-co-16 mol%-4HB) fibers were hydrolyzed by microorganism-secreted enzymes into substances with low molecular weights and high water solubility. However, weight loss is not equivalent to complete biodegradation into water and carbon dioxide. Therefore, the BOD test was conducted to confirm that the fibers were broken down into water and carbon dioxide by the microorganisms. The shape of the sample is reported to have a significant effect on the BOD test (Komiyama et al., 2021; Hino et al., 2023). It can be assumed that the faster the rate of enzymatic degradation by microorganisms to low molecular weight compounds (the faster the weight loss), the steeper the BOD-biodegradability curve. Here, in addition to the reference, P(3HB-co-16 mol%-4HB) powder, three types of P(3HB-co-16 mol%-4HB) fibers (as-spun non-porous fiber, drawn non-porous fiber, and drawn porous fiber), with evaluated microbial degradability by weight loss (Figure 1), were used to investigate the effect of shape on the BOD test (Figure 2). For P(3HB-co-16 mol%-4HB) powder and the two types of drawn fibers, which showed 100% weight loss in 28 days, BOD-biodegradability was approximately 70%–90% or more in 28 days. This indicated complete biodegradation because the rest of about 10%–30% is considered to be used for biomass formation in microorganism cells (Ohura et al., 1999). The rise of the BOD curve during the period in which low-molecular-weight compounds are completely degraded by microorganisms into carbon dioxide depends on the shape of the sample. The rise was steepest for the powder and flattened in the order of porous drawn fiber (with the fastest weight loss rate) > non-porous drawn fiber > non-porous as-spun fiber. As shown, the shape and highly ordered structure of the

FIGURE 1
Weight losses of P(3HB-*co*-16 mol%-4HB) fibers with different highly ordered structures. Black: as-spun, red: non-porous drawn, blue: porous drawn. Filled black circles: as-spun, red triangles: non-porous drawn, blue squares: porous drawn.

FIGURE 2
Effect of sample morphology on BOD-biodegradability of P(3HB-co-16 mol%-4HB) fibers in seawater from Tokyo Bay. Open circles : P(3HB-*co*-16 mol%-4HB) powder, open diamonds: reference cellulose, filled black circles: as-spun, red triangles: non-porous drawn, blue squares: porous drawn.

fibers had a remarkable effect on BOD biodegradation. In addition, the BOD curves obtained for the three fiber types did not rise in the early stage of the BOD test (5–10 days) because the surface area of the fiber was smaller than that of the powder, and it took time for the microorganisms on the fiber surface to form a biofilm and oligomerize through enzyme secretion and enzymatic hydrolysis.

3.4 Microorganisms on fibers after biodegradation

To confirm whether the P(3HB-*co*-16 mol%-4HB) fibers were degraded by microorganisms, the fibers were soaked in seawater and then treated with formaldehyde without washing for SEM observation. After 7 days, the P(3HB-*co*-16 mol%-4HB) fiber surface was covered with a biofilm (Figure 3A). This indicated that the P(3HB-*co*-16 mol%-4HB) fibers were not degraded physically but by microorganisms. Interestingly, different forms of microorganisms were accumulated inside the biofilm (Figure 3B) and on the fiber surface where the biofilm had not formed (Figure 3C). Round-shaped bacteria (cocci) were observed inside the biofilm, while rod-shaped bacteria (elongated bacilli) were found on the fiber surface where no biofilm had formed (Figure 3D). In general, depolymerase-secreting microorganisms that enzymatically degrade polymers may not always metabolize water-soluble low-molecular-weight substances. In contrast, microorganisms that do not participate in enzymatic degradation may metabolize low-molecular-weight compounds. The diverse microorganisms observed in the fibers after degradation suggested that the P(3HB-*co*-16 mol%-4HB) plastisphere was composed of diverse polyester degraders and microorganisms
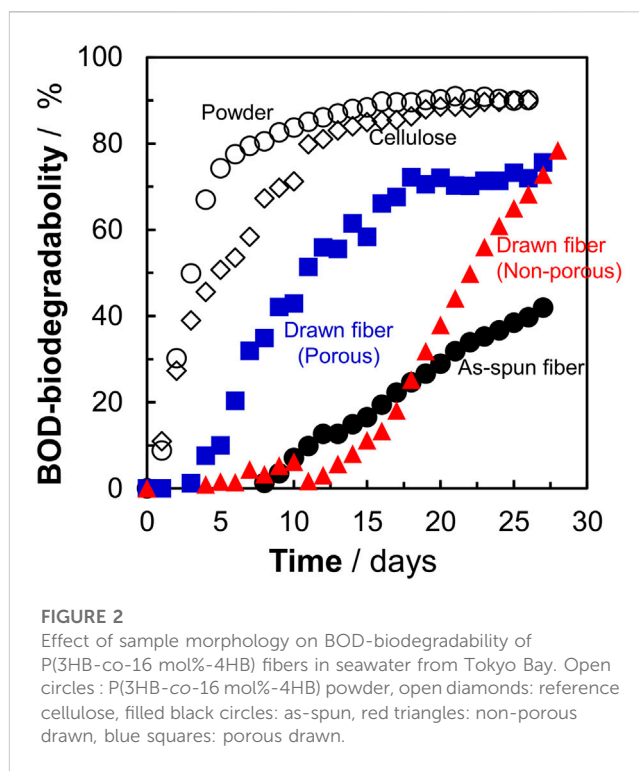
that metabolized the byproducts of enzymatic degradation, stabilized the biofilm, and preyed on other microorganisms, meaning that they coexisted.

3.5 Morphological changes of P(3HB-*co*-16 mol%-4HB) fibers during marine biodegradation

SEM images of the fiber surfaces showed that all ultrasonically washed fibers were degraded by microorganisms (Figures 4A–F). After microbial degradation, the surface of the as-spun fiber was rough and irregular, indicating that microbial biodegradation proceeded randomly (Figure 4G). In contrast, the two types of drawn fibers had a stacked lamellar structure perpendicular to the stretch direction (Figures 4H, I). Illustration of assumed biodegradation patterns of fibers with different higher-order structure are shown in Figure 5. This suggested that the lamellar crystals were oriented by drawing and biodegradation proceeded from the amorphous region of the fiber (Omura et al., 2021). This is because the amorphous region of polymers is less dense and thus more susceptible to attack than the crystalline region. As Abe et al. has reported that the erosion rate of amorphous phase is much larger than that of crystalline phase (Abe et al., 1998). By drawing and orienting the fibers, the amorphous chains are also oriented, and enzymatic degradation by microorganisms can easily proceed from the amorphous chains. Therefore, the biodegradation rate of the drawn fibers may be faster than that of the as-spun fiber. Furthermore, in the porous drawn fiber, the numerous pores inside the fiber are exposed, which increases the surface area. For these reasons, among the fibers investigated, the porous drawn fiber exhibited the fastest degradation rate (Figure 1). The results
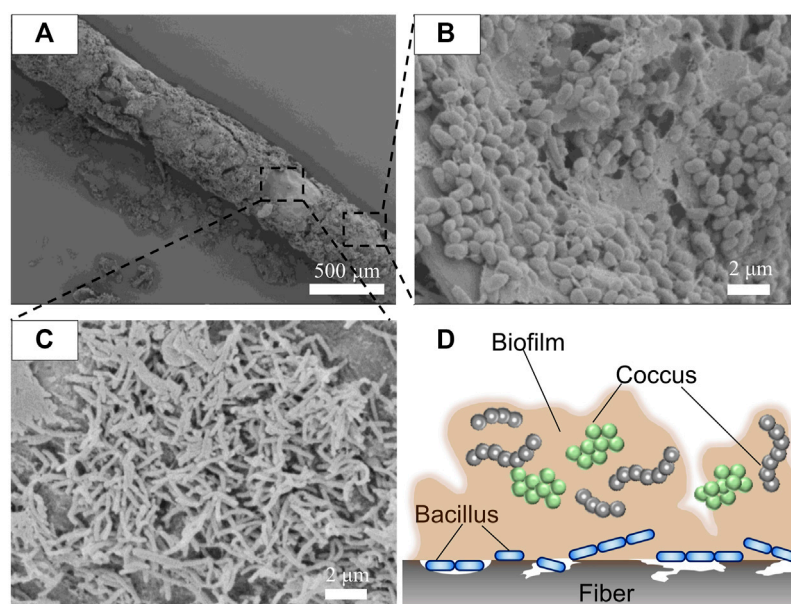
FIGURE 3
SEM images of **(A)** P(3HB-*co*-16 mol%-4HB) drawn elastic fiber (porous) with the biofilm attached after biodegradation in seawater for 7 days, **(B)** microorganisms present in the biofilm, and **(C)** microorganisms on the fiber surface. **(D)** Schematic model of microorganisms in the plastisphere.
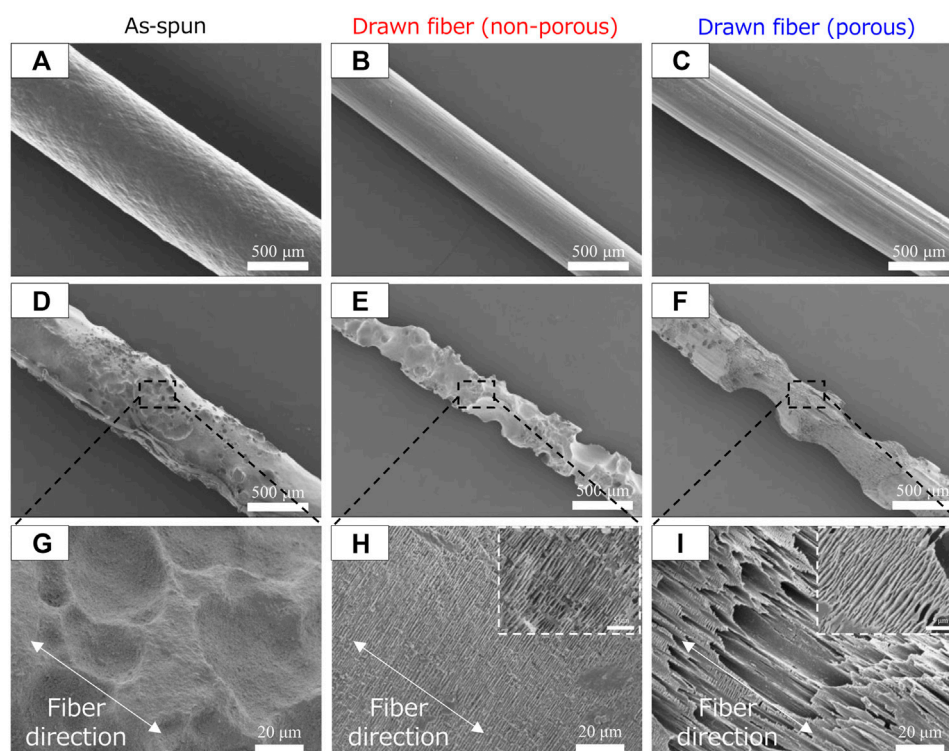

FIGURE 4
SEM images of P(3HB-*co*-16 mol%-4HB) fibers before **(A–C)** biodegradation and **(D–I)** after 1 week in seawater from Tokyo Bay: **(A, D, G)** asspun, **(B, E, H)** non-porous drawn, and **(C, F, I)** porous drawn.
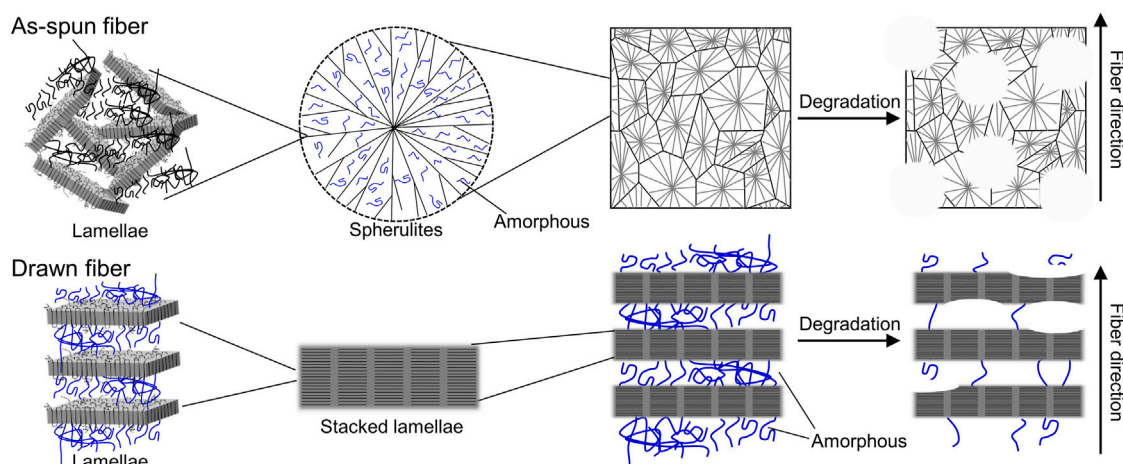
FIGURE 5
Illustration of assumed biodegradation patterns of fibers with different higher-order structures.
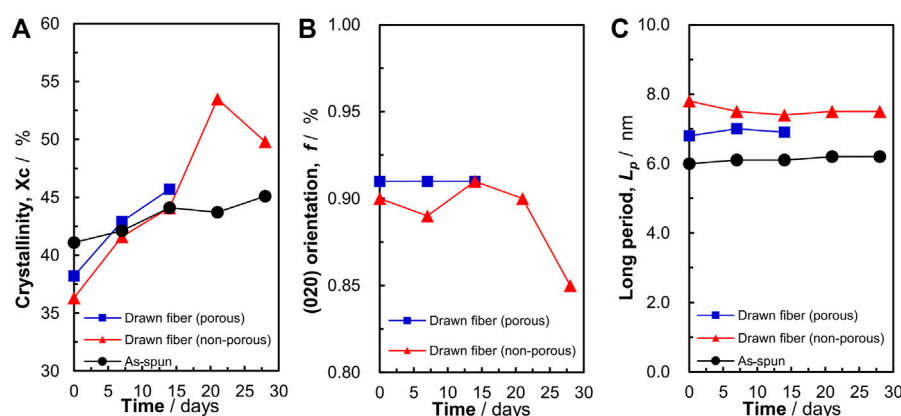
FIGURE 6
Changes in the **(A)** crystallinity, **(B)** (020) orientation, and **(C)** long period of P(3HB-*co*-16 mol%-4HB) fibers resulting from biodegradation. Black: as-spun, red: non-porous drawn, blue: porous drawn.

indicated that it was possible to increase the rate of marine degradation by changing the highly ordered structure of the fibers, such as fiber orientation and porous structure.

3.6 Changes in crystallinity with biodegradation

As shown in Figure 4, P(3HB-*co*-16 mol%-4HB) fibers were decomposed from the amorphous part. Therefore, we evaluated the P(3HB-*co*-16 mol%-4HB) fibers after degradation using WAXD and SAXS measurements (Supplementary Figures S1, S2). In the 2D-WAXD image of the as-spun fiber before biodegradation, ring diffraction of randomly distributed crystals was observed (Supplementary Figure S1A). In contrast, in the images of the two types of drawn fibers (non-porous and porous fibers) before decomposition, diffraction of

lamellar crystals derived from the α-form oriented with the fiber axis was observed (Supplementary Figures S1F, K). Notably, for all fibers, only diffraction of lamellar crystals composed of the α-form was observed, and diffraction of the β-form in a planar zigzag structure was not observed. Iwata et al. reported that for P(3HB) fibers with two types of molecular chains, α-form and β-form, which are controlled and oriented, enzymatic degradation of the β-form occurs at a faster rate than that of the α-form (Iwata et al., 2006). However, because the β-form was not observed in the fibers used for the biodegradation tests in this study, we discuss the degradation of the crystalline (α-form) and amorphous region. For all fibers, the crystallinity tended to increase with degradation time (Figure 6A). This indicated that the relative degree of crystallinity increased because biodegradation proceeded from the amorphous region, and thus the crystalline region remained intact. After biodegradation, the crystallinity of the as-spun fiber did not change as much as

FIGURE 7
Change in the molecular weight, M_w, of non-porous drawn P(3HB-*co*-16 mol%-4HB) fiber resulting from biodegradation. Black: original fiber, red: 7 days, blue: 14 days, and green: 21 days.
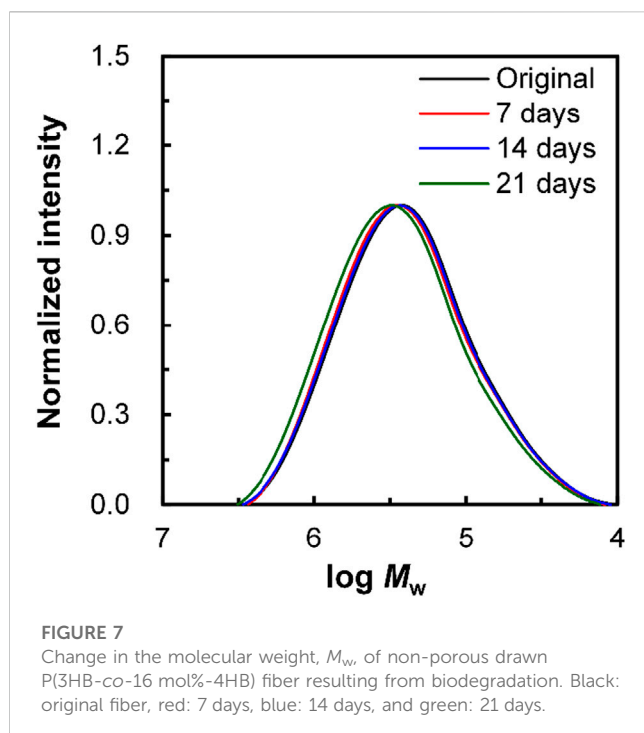
that of the two types of drawn fibers (non-porous and porous). This is because the amorphous and crystalline regions of the as-spun fiber are randomly decomposed, whereas the amorphous regions of the drawn fibers are preferentially decomposed, as shown in Figures 4H, I. After 20 days of biodegradation, the crystallinity of the non-porous drawn fiber decreased, which was attributed to the decomposition of the lamellar crystals as well as the progressive decomposition of the amorphous region. The crystal orientation remained almost constant during decomposition, and the orientation decreased just before the end of decomposition (Figure 6B). This suggested that the amorphous molecules that held the lamellae or stacked lamellae in place were decomposed, which destabilized and rotated the lamellae or stacked lamellae. Similarly, the long period remained constant as decomposition proceeded (Figure 6C). Yoo et al. reported a similar trend for the hydrolysis of PCL (Yoo and Im, 1999), suggesting that the crystals remain oriented to some extent, irrespective of microbial degradation.

3.7 Changes in molecular weight with biodegradation

To confirm whether enzymatic hydrolysis proceeded via surface or bulk degradation, the molecular weight of porous drawn P(3HB-*co*-16 mol%-4HB) fibers was determined (Figure 7). The molecular weight did not change before and after the degradation test, suggesting that microbial degradation progressed from the surface. Surface decomposition proceeding intensively on the surface of the material produces a continuous succession of water-soluble low-molecular-weight compounds. In addition, degradation by hydrolysis requires enzymes secreted by microorganisms, which cannot reach the inside of

the material owing to their size, and thus degradation proceeds only on the surface of the material (Tsuji and Ishida, 2002). Von Burkersroda et al. reported that the degradation mechanism of biodegradable plastics changes from bulk degradation to surface degradation when the thickness exceeds a critical value ($L_{critical}$) (Von Burkersroda et al., 2002). Considering that the fibers used in this study exceeded the critical value (fiber diameter >100 μm), the enzymatic degradation of P(3HB-*co*-16 mol%-4HB) fibers in seawater from Tokyo Bay likely proceeded by surface degradation. In addition, we found that the highly ordered structure of the fiber surface had a significant effect on the degradation rate.

4 Implication

These results provide information not only for controlling the degradation rate of biodegradable plastics, but also for future internationally standardized biodegradability tests. The P(3HB-*co*-16 mol%-4HB) elastic fiber prepared in this study shows not only excellent marine biodegradability but also bio-absorbability, and is expected to be applied to surgical sutures. Even in the case of use as surgical sutures, which are temporary fixative materials, the results obtained in this study may be used to fabricate various fibers with controlled duration (rate) of decomposition *in vivo*.

5 Conclusion

In this study, the effect of different highly ordered structures on the marine degradability of P(3HB-*co*-16 mol%-4HB) elastic fibers was investigated. The environmental degradation of P(3HB-*co*-16 mol%-4HB) fibers in seawater from Tokyo Bay was evaluated. The biodegradation rates of the three types of P(3HB-*co*-16 mol%-4HB) fibers (non-porous as-spun, non-porous drawn, and porous drawn) were different and decreased in the order of porous drawn > non-porous drawn > non-porous as-spun. BOD tests revealed that the P(3HB-*co*-16 mol%-4HB) elastic fibers were completely biodegraded by microorganisms in the ocean, which was significantly influenced by the morphology of the fibers. Microorganisms adhered to the fiber surface during degradation, suggesting that microorganisms coexisted and decomposed the fiber, indicative of microbial degradation. The SEM images showed that fibers oriented by drawing had a stacked lamellar structure perpendicular to the direction of drawing after the degradation test. In addition, X-ray analysis revealed that the crystallinity of the fibers increased after degradation, suggesting that enzymatic degradation of biodegradable plastics proceeded from the amorphous region, which was easily promoted by increasing the orientation of the molecular chains.

Data availability statement

The original contributions presented in the study are included in the article/Supplementary Material, further inquiries can be directed to the corresponding author.

Author contributions

Funding

Acknowledgments

Conflict of interest

Publisher's note

Supplementary material

The Supplementary Material for this article can be found online at: https://www.frontiersin.org/articles/10.3389/fbioe.2023.1303830/full#supplementary-material

References

Abe, H., Doi, Y., Aoki, H., and Akehata, T. (1998). Solid-state structures and enzymatic degradabilities for melt-crystallized films of copolymers of (R)-3-Hydroxybutyric acid with different hydroxyalkanoic acids. *Macromolecules* 31, 1791–1797. doi:10.1021/ma971559v

Briassoulis, D., Pikasi, A., Briassoulis, C., and Mistriotis, A. (2019). Disintegration behaviour of bio-based plastics in coastal zone marine environments: a field experiment under natural conditions. *Sci. Total Environ.* 688, 208–223. doi:10.1016/j.scitotenv.2019.06.129

Cai, H., Dave, V., Gross, R. A., and McCarthy, S. P. (1996). Effects of physical aging, crystallinity, and orientation on the enzymatic degradation of poly(lactic acid). *J. Polym. Sci. B Polym. Phys.* 34, 2701–2708. doi:10.1002/(SICI)1099-0488(19961130)34:16<2701::AID-POLB2>3.0.CO;2-S

César, M. E. F., Mariani, P. D. S. C., Innocentini-Mei, L. H., and Cardoso, E. J. B. N. (2009). Particle size and concentration of poly(ε-caprolactone) and adipate modified starch blend on mineralization in soils with differing textures. *Polym. Test.* 28, 680–687. doi:10.1016/j.polymertesting.2009.05.002

Chinaglia, S., Tosin, M., and Degli-Innocenti, F. (2018). Biodegradation rate of biodegradable plastics at molecular level. *Polym. Degrad. Stab.* 147, 237–244. doi:10.1016/j.polymdegradstab.2017.12.011

Cho, D. K., Park, J. W., Kim, S. H., Kim, Y. H., and Im, S. S. (2003). Effect of molecular orientation on biodegradability of poly(glycolide-co-ε-caprolactone). *Polym. Degrad. Stab.* 80, 223–232. doi:10.1016/S0141-3910(02)00402-0

Doi, Y., Kitamura, S., and Abe, H. (1995). Microbial synthesis and characterization of poly(3-hydroxybutyrate-co-3-hydroxyhexanoate). *Macromolecules* 28, 4822–4828. doi:10.1021/ma00118a007

Fischer, J. J., Aoyagi, Y., Enoki, M., Doi, Y., and Iwata, T. (2004). Mechanical properties and enzymatic degradation of poly([R]-3-hydroxybutyrate-co-[R]-3-hydroxyhexanoate) uniaxially cold-drawn films. *Polym. Degrad. Stab.* 83, 453–460. doi:10.1016/j.polymdegradstab.2003.08.006

Hammer, J., Kraak, M. H. S., and Parsons, J. R. (2012). Plastics in the marine environment: the dark side of a modern gift. *Rev. Environ. Contam. Toxicol.* 220, 1–44. doi:10.1007/978-1-4614-3414-6_1

Hino, S., Kawasaki, N., Yamano, N., Nakamura, T., and Nakayama, A. (2023). Effects of particle size on marine biodegradation of poly(L-lactic acid) and poly(ε-caprolactone). *Mater Chem. Phys.* 303, 127813. doi:10.1016/j.matchemphys.2023.127813

Iwata, T., Aoyagi, Y., Fujita, M., Yamane, H., Doi, Y., Suzuki, Y., et al. (2004). Processing of a strong biodegradable poly[(R)-3-hydroxybutyrate] fiber and a new fiber structure revealed by micro-beam x-ray diffraction with synchrotron radiation. *Macromol. Rapid Commun.* 25, 1100–1104. doi:10.1002/marc.200400110

Iwata, T., Aoyagi, Y., Tanaka, T., Fujita, M., Takeuchi, A., Suzuki, Y., et al. (2006). Microbeam X-ray diffraction and enzymatic degradation of poly[(R)-3-hydroxybutyrate] fibers with two kinds of molecular conformations. *Macromolecules* 39, 5789–5795. doi:10.1021/ma060908v

Iwata, T., Doi, Y., Kasuya, K.-I., and Inoue, Y. (1997). Visualization of enzymatic degradation of poly[(R)-3-hydroxybutyrate] single crystals by an extracellular PHB depolymerase. *Macromolecules* 30, 833–839. doi:10.1021/ma961352m

Iwata, T., Tsunoda, K., Aoyagi, Y., Kusaka, S., Yonezawa, N., and Doi, Y. (2003). Mechanical properties of uniaxially cold-drawn films of poly([R]-3-hydroxybutyrate). *Polym. Degrad. Stab.* 79, 217–224. doi:10.1016/s0141-3910(02)00274-4

Jang, Y. C., Lee, J., Hong, S., Lee, J. S., Shim, W. J., and Song, Y. K. (2014). Sources of plastic marine debris on beaches of Korea: more from the ocean than the land. *Ocean Sci. J.* 49, 151–162. doi:10.1007/s12601-014-0015-8

Kabe, T., Hongo, C., Tanaka, T., Hikima, T., Takata, M., and Iwata, T. (2015). High tensile strength fiber of poly[(R)-3-hydroxybutyrate-co-(R)-3-hydroxyhexanoate] processed by two-step drawing with intermediate annealing. *J. Appl. Polym. Sci.* 132, 1–8. doi:10.1002/app.41258

Kasuya, K., Takagi, K. I., Ishiwatari, S. I., Yoshida, Y., and Doi, Y. (1998). Biodegradabilities of various aliphatic polyesters in natural waters. *Polym. Degrad. Stab.* 59, 327–332. doi:10.1016/s0141-3910(97)00155-9

Komiyama, K., Omura, T., and Iwata, T. (2021). Effect of morphology and molecular orientation on environmental water biodegradability of poly[(R)-3-hydroxybutyrate-co-(R)-3-hydroxyvalerate]. *Polym. Degrad. Stab.* 193, 109719. doi:10.1016/j.polymdegradstab.2021.109719

Komiyama, K., Omura, T., Kabe, T., and Iwata, T. (2022). Mechanical properties and highly-ordered structural analysis of elastic poly[(R)-3-hydroxybutyrate-co-(R)-3-hydroxyvalerate] fibers fabricated by partially melting crystals. *Polym. Guildf.* 247, 124772. doi:10.1016/j.polymer.2022.124772

Koyama, N., and Doi, Y. (1997). Effects of solid-state structures on the enzymatic degradability of bacterial poly(hydroxyalkanoic acids). *Macromolecules* 30, 826–832. doi:10.1021/ma961195r

Kumagai, Y., Kanesawa, Y., and Doi, Y. (1992). Enzymatic degradation of microbial poly(3-hydroxybutyrate) films. *Makromol. Chem.* 193, 53–57. doi:10.1002/macp.1992.021930105

Kunioka, M., Tamaki, A., and Doi, Y. (1989). Crystalline and thermal properties of bacterial copolyesters: poly(3-hydroxybutyrate-co-3-hydroxyvalerate) and poly(3-hydroxybutyrate-co-4-hydroxybutyrate). *Macromolecules* 22, 694–697. doi:10.1021/ma00192a031

Lebreton, L., Slat, B., Ferrari, F., Sainte-Rose, B., Aitken, J., Marthouse, R., et al. (2018). Evidence that the great pacific garbage patch is rapidly accumulating plastic. *Sci. Rep.* 8, 4666–4715. doi:10.1038/s41598-018-22939-w

Lott, C., Eich, A., Unger, B., Makarow, D., Battagliarin, G., Schlegel, K., et al. (2020). Field and mesocosm methods to test biodegradable plastic film under marine conditions. *PLoS One* 15, e0236579. doi:10.1371/journal.pone.0236579

Mochizuki, M., Hirano, M., Kanmuri, Y., Kudo, K., and Tokiwa, Y. (1995). Hydrolysis of polycaprolactone fibers by lipase: effects of draw ratio on enzymatic degradation. *J. Appl. Polym. Sci.* 55, 289–296. doi:10.1002/app.1995.070550212

Murayama, A., Yoneda, H., Maehara, A., Shiomi, N., and Hirata, H. (2023). A highly elastic absorbable monofilament suture fabricated from poly(3-hydroxybutyrate-co-4-hydroxybutyrate). *Sci. Rep.* 13, 3275. doi:10.1038/s41598-023-30292-w

Nakayama, A., Yamano, N., and Kawasaki, N. (2019). Biodegradation in seawater of aliphatic polyesters. *Polym. Degrad. Stab.* 166, 290–299. doi:10.1016/j.polymdegradstab.2019.06.006

Nishida, H., Suzuki, S., and Yutaka, T. (1998). Distribution of poly(β-propiolactone) aerobic degrading microorganisms in different environments. *J. Environ. Polym. Degrad.* 6, 43–58. doi:10.1023/a:1022878512743

Nishida, H., and Tokiwa, Y. (1992). Effects of higher-order structure of poly(3-hydroxybutyrate) on its biodegradation. I. Effects of heat treatment on microbial degradation. *J. Appl. Polym. Sci.* 46, 1467–1476. doi:10.1002/app.1992.070460818

Nishida, H., and Tokiwa, Y. (1993). Effects of higher-order structure of poly(3-hydroxybutyrate) on its biodegradation. II. Effects of crystal structure on microbial degradation. *J. Environ. Polym. Degrad.* 1, 65–80. doi:10.1007/bf01457654

Ohura, T., Aoyagi, Y., Takagi, K., Yoshida, Y., Kasuya, K., and Doi, Y. (1999). Biodegradation of poly(3-hydroxyalkanoic acids) fibers and isolation of poly(3-hydroxybutyric acid)-degrading microorganisms under aquatic environments. *Polym. Degrad. Stab.* 63, 23–29. doi:10.1016/s0141-3910(98)00057-3

Omura, T., Komiyama, K., Maehara, A., Kabe, T., and Iwata, T. (2021). Elastic marine biodegradable fibers produced from poly[(R)-3-hydroxybutyrate-co-4-hydroxybutylate] and evaluation of their biodegradability. *ACS Appl. Polym. Mater* 3, 6479–6487. doi:10.1021/acsapm.1c01212

Orts, W. J., Marchessault, R. H., Bluhm, T. L., and Hamer, G. K. (1990). Observation of strain-induced β form in poly(β-hydroxyalkanoates). *Macromolecules* 23, 5368–5370. doi:10.1021/ma00228a014

Phongtamrug, S., and Tashiro, K. (2019). X-Ray crystal structure analysis of poly(3-hydroxybutyrate) β-form and the proposition of a mechanism of the stress-induced α-to-β phase transition. *Macromolecules* 52, 2995–3009. doi:10.1021/acs.macromol.9b00225

Plastics Europe (2016). *Plastics-the Facts 2016 an analysis of European plastics production, demand and waste data*. Italy: Plastics Europe.

Suzuki, M., Tachibana, Y., Kazahaya, J., Takizawa, R., Muroi, F., and Kasuya, K. (2017). Difference in environmental degradability between poly(ethylene succinate) and poly(3-hydroxybutyrate). *J. Polym. Res.* 24, 217. doi:10.1007/s10965-017-1383-4

Tanaka, T., Yabe, T., Teramachi, S., and Iwata, T. (2007). Mechanical properties and enzymatic degradation of poly[(R)-3-hydroxybutyrate] fibers stretched after isothermal crystallization near Tg. *Polym. Degrad. Stab.* 92, 1016–1024. doi:10.1016/j.polymdegradstab.2007.02.017

The Pew Charitable Trusts and SYSTEMIQ (2020). Breaking the plastic wave: a comprehensive assessment of pathways towards stopping ocean plastic pollution. Available at: https://www.pewtrusts.org/en.

Tsuji, H., and Ishida, T. (2002). Poly(L-lactide). X. Enhanced surface hydrophilicity and chain-scission mechanisms of poly(l-lactide) film in enzymatic, alkaline, and phosphate-buffered solutions. *J. Appl. Polym. Sci.* 87, 1628–1633. doi:10.1002/app.11605

Tsuji, H., Kidokoro, Y., and Mochizuki, M. (2007). Enzymatic degradation of poly(L-lactic acid) fibers: effects of small drawing. *J. Appl. Polym. Sci.* 103, 2064–2071. doi:10.1002/app.25366

Von Burkersroda, F., Schedl, L., and Opferich, A. G. (2002). Why degradable polymers undergo surface erosion or bulk erosion. *Biomaterials* 23, 4221–4231. doi:10.1016/s0142-9612(02)00170-9

Wang, G. X., Huang, D., Ji, J. H., Völker, C., and Wurm, F. R. (2021). Seawater-Degradable polymers—fighting the marine plastic pollution. *Adv. Sci.* 8, 2001121. doi:10.1002/advs.202001121

World Economic Forum (2017). *The New plastics economy- rethinking the future of plastics*. Geneva, Switzerland: World Economic Forum.

Yokouchi, M., Chatani, Y., Tadokoro, H., Teranishi, K., and Tani, H. (1973). Structural studies of polyesters: 5. Molecular and crystal structures of optically active and racemic poly(β-hydroxybutyrate). *Polym. Guildf.* 14, 267–272. doi:10.1016/0032-3861(73)90087-6

Yoo, E. S., and Im, S. S. (1999). Effect of molecular orientation on the biodegradability of aliphatic polyester. *Macromol. Symp.* 142, 13–21. doi:10.1002/masy.19991420104

Check for updates

Novel methods to monitor the biodegradation of polylactic acid (PLA) by *Amycolatopsis orientalis* and *Amycolatopsis thailandensis*

Najwa Mat Yasin[1,2], Farlash Pancho[1], Md Yasin[1],
Jan F. M. Van Impe[1]* and Simen Akkermans[1]

[1]BioTeC+ - Chemical and Biochemical Process Technology and Control, KU Leuven, Ghent, Belgium,
[2]Faculty of Ocean Engineering and Informatics, Universiti Malaysia Terengganu (UMT), Kuala Nerus,
Terengganu, Malaysia

Plastics are essential in modern life, but their conventional production is problematic due to environmental pollution and waste management issues. Polylactic acid (PLA) is a widely used bioplastic that is bio-based and biodegradable, making it a key player in the bioeconomy. PLA has been proven to be degradable in various settings, including aqueous, soil, and compost environments. However, monitoring and optimizing PLA biodegradation remains challenging. This study proposes methods to improve the quantification of PLA biodegradation by *Amycolatopsis* spp. Ultrasound treatments (10 s) significantly improved the enumeration of viable *Amycolatopsis* cells by breaking the pellets into quantifiable individual cells. A separation technique combining ultrasound (120 s) and 40 µm cell strainers effectively isolated PLA particles from biomass to quantify PLA weight loss. This enabled the monitoring of PLA biofragmentation. Finally, CO_2 production was measured according to ISO 14852 to quantify mineralization. Integrating these methods provides an improved quantification for PLA biodegradation along its different stages. In a case study, this led to the construction of a carbon balance where 85.1% of initial carbon content was successfully tracked. The developed techniques for monitoring of PLA biodegradation are essential to design future waste management strategies for biodegradable plastics.

1 Introduction

Plastics are essential in modern life, as they offer quality products for many uses. These sophisticated attributes of synthetic polymers have led to an annual plastic production of approximately 140 million tons (Teixeira et al., 2021). However, most conventional plastics are fossil-based, causing environmental pollution and waste management problems. The durability of plastics hampers their degradation in the biosphere, resulting in the long-term retention of plastic waste in the environment (Shimao, 2001; Mayekar et al., 2023). Chemical recycling is at its forefront as an economically viable technology for plastic waste management (JRC Technical Report, 2023). However, these processes are often energy intensive, for example, gasification requires a temperature up to 700°C (Shah et al., 2023). In response to these challenges, stakeholders have taken a paradigm shift to leverage

bioplastics that are environmentally friendly. However, not all bioplastics are biodegradable, even if they are bio-based. Polylactic acid (PLA) is a widely used bioplastic in the market and accounts for 20.7% of global bioplastic production (European Bioplastic, 2022). Owing to its bio-based and biodegradable characteristics, it is one of the key players in the bioeconomy (Butbunchu and Pathom-Aree, 2019). PLA has been proven to be degradable in various controlled settings at the laboratory stage, including aqueous, soil, and compost environments (Apinya et al., 2015; Castro-Aguirre et al., 2017; Benn and Zitomer, 2018; Hobbs et al., 2019; Choe et al., 2022; García-Depraect et al., 2023; Mayekar et al., 2023). The *Amycolatopsis* genus, specifically *Amycolatopsis orientalis* and *Amycolatopsis thailandensis* are the most dominant PLA degraders in mesophilic conditions, which they accomplish by secreting extracellular enzymes such as lipases, esterases and cutinases to depolymerize ester bonds within the polymer (Li et al., 2008; Chomchoei et al., 2011; Butbunchu and Pathom-Aree, 2019).

However, most studies on bioplastics have utilized microbial consortia isolated from local waste compost, activated sludge from wastewater, dumping sites, and soil environments (Adhikari et al., 2016; Hottle et al., 2016; Hobbs et al., 2019; Mayekar et al., 2023). Due to their methodology based on the isolation of local bacteria, these studies are difficult to reproduce. Further optimization under controlled conditions, e.g., using pure microbial cultures and at specific temperatures, could pave the way for reproducible biological recycling. To optimize such a controlled biodegradation process, accurate monitoring of this process is essential. Therefore, to improve PLA biodegradation, it is required to be able to accurately monitor the growth of degrading microbes, the weight loss of the PLA and the production of biogas. Even though these measurements seem evident, their implementation for aerobic PLA degradation by *Amycolatopsis* species is still lacking from literature.

Both the quantification of viable cells and of PLA weight reduction are hampered by the specific growth morphology of bacteria from the *Amycolatopsis* genus. These bacteria form branched filamentous structures that resemble a fungal aerial mycelium. When grown on agar medium, these actinobacteria form branch fragmenting into squarish and rod-shaped elements (Tan and Goodfellow, 2015) and they exhibit pellet morphology in liquid medium. When using the traditional viable plate count method to quantify *Amycolatopsis* on agar media, the numerous aggregated cells of pellets are perceived as an individual colony forming unit. On the other hand, these pellets are difficult to separate from bioplastics as is required for the quantification of bioplastic weight loss.

This research proposes sonication treatment as the solution for both quantification problems. In microbiology, sonication is primarily used as an effective method for cell lysis and elimination of biofilms from surfaces (Ganesan et al., 2015; Dudek et al., 2020; Ferdous et al., 2021). The ultrasound mechanism works by the propagation of sound waves from the sonicator along the medium, which induces a distinctive pressure difference. This causes the formation of high-energy gas bubbles, also known as cavitations, with a localized temperature reaching 5000 K, which then quickly dissipates (Pitt and Ross, 2003). The collapse of these gas bubbles radiates a shockwave that can release the cells from the aggregated pellets into the planktonic form

(Ganesan et al., 2015; Branck et al., 2017). The intensity of the ultrasound treatment is tuned by changing the amplitude, temperature, and treatment time. As such, sonication treatment was optimized in this study to balance the release of aggregated cells to make them quantifiable against the inactivation of cells (Dudek et al., 2020). With respect to the determination of PLA weight loss, the commonly used powder form in the range of 125–250 μm complicates the separation from the bacteria in the pellet morphology. This range of powder is commonly used as it is recommended by ISO 14 852 for plastic biodegradation studies. However, this PLA powder cannot be separated from bacterial pellets by centrifugation or filtration. Using the sonication method can form a solution by breaking the pellets into individual cells, making a separation based on particle size possible. Therefore, this research studies the combined use of sonication and filtration by cell strainers to determine the weight loss of PLA powder.

A complete biodegradation process of plastic involves either the determination of oxygen demand or carbon dioxide production (CO_2) (and methane, CH_4). The biodegradation step in which these processes occur, known as mineralization, determines the amount of polymeric carbon that is microbially converted into CO_2 (or CH_4) and biomass. Hence, monitoring of respirometry during biodegradation is crucial to monitor the biogas produced as end products (Choe et al. (2022). There is currently a wide array of techniques to measure CO_2 evolution including direct measurement respirometry, gravimetric measurement respirometry and cumulative measurement respirometry (Ruggero et al., 2019). Owing to the slow CO_2 evolution process for biodegradation of plastics, an established standard based on biogas cumulative measurement, ISO 14 852, was selected in this study. This method allows reliable, yet simple quantification of CO_2 based on titrimetric measurements using barium hydroxide as a carbon capture solution.

In this study, we focus on developing a set of methodologies to monitor the degradation of PLA by *A. orientalis* and *A. thailandensis* in aqueous conditions using PLA powder ranging from 125 to 250 μm. Three methods have been proposed to improve the monitoring of the biodegradation process: 1) viable cell enumeration, 2) gravimetric weight loss of PLA plastics, and 3) cumulative biogas quantification. In the first methodology, low-frequency ultrasound (20 kHz, 50 W) was used to enumerate the viable cell growth of the microorganisms in their rich medium via process optimization using a series of short exposure times of 5, 10, and 15 s. To validate the sonication methods for cell enumeration, extracellular leakage was observed using the optical density at 260 nm. Parameter estimation analysis was performed to further characterize the differences in observing cell growth with and without sonication, also in the presence of PLA. Next, gravimetric PLA weight loss was conducted to measure the PLA weight loss caused by bacterial degradation. Because the biodegradation process involves a mixture of PLA powder and aggregated cells, mechanical separation using a cell strainer was adopted. To enable the separation of these particles, a sonication method was implemented to degrade aggregated cell pellets to smaller sizes that passed as filtrate through these cell strainers, separating them from the PLA in the retentate. Finally, the ISO
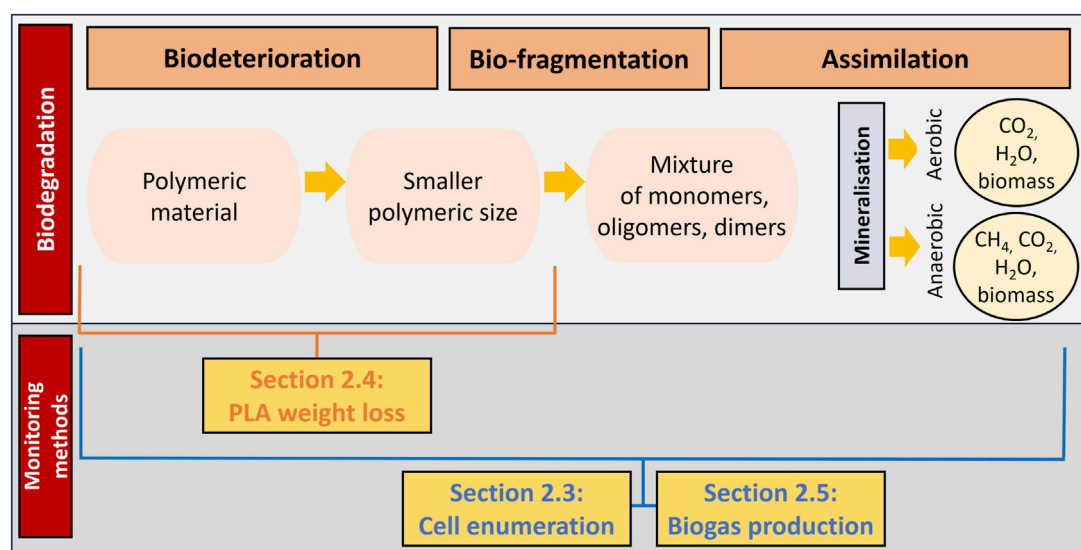
FIGURE 1
Representation of the link between the monitoring methods and the various phases of the biodegradation process (adapted from Yasin et al. (2022)).

14 852 method was implemented to monitor CO_2 production from PLA degradation to quantify the mineralization process. A simple carbon balance was calculated based on CO_2 evolution. To the best of our knowledge, this is the first effort to enumerate the kinetic growth of *A. orientalis* and *A. thailandensis*, which will serve as stepping stones for controlled biodegradation of PLA in the future.

2 Materials and methods

The new methods that have been developed within this research are described in the sections below. Specifically, the developed method for the quantification of the viable cell population is explained in Section 2.3 and the new method for studying PLA weight loss is provided in Section 2.4. Moreover, the implementation of the ISO method for quantifying cumulative biogas production in the form of CO_2 is provided in Section 2.5. The link between these three experimental methods and the biodegradation process is illustrated in Figure 1.

2.1 Strain and cultivation condition

Amycolatopsis orientalis and *Amycolatopsis thailandensis* were acquired from the NITE Biological Research Center (NBRC), Chiba, Japan. Storage and culturing of the strains were performed using yeast extract medium (YEM) containing 4 g yeast extract (Millipore, Merck, Darmstadt, Germany), 10 g malt extract (Carl Roth, Karlsruhe, Germany), 4 g glucose (Thermo Scientific, Kandel, Germany), and 20 g bacteriological agar (VWR International, Leuven, Belgium) per liter. Stock cultures of the strains were kept frozen at −80°C in YEM supplemented with 20% (v/v) glycerol (Acros Organics, Geel, Belgium), and thawed at room temperature

prior to utilization. Purity plates for each microorganism were prepared by spreading the stock on YEM agar plates, containing 20 g/L agar (NBRC), and incubating at 30°C for 5 days. Precultures were prepared by transferring one colony from the purity plate into 75 mL of freshly prepared YEM broth, which was incubated at 30°C for 5 days. The preculture was cultivated in 100 mL baffled shake flasks while shaken at 180 rpm until the cells reached the stationary phase.

In the biodegradation experiments, where PLA was used as the sole carbon source, following cultivation in rich medium, the cells were pelleted by centrifugation (4629 g for 20 min) and resuspended in minimal medium (MM). Minimal medium composition per liter was 200 mg magnesium sulphate heptahydrate ($MgSO_4.7H_2O$), 1600 mg potassium phosphate dibasic (K_2HPO_4), 200 mg monopotassium phosphate (KH_2PO_4), 1000 mg ammonium sulphate (($NH_4)_2SO_4$), 100 mg sodium chloride (NaCl), 20 mg calcium chloride dihydrate ($CaCl_2.2H_2O$), 0.5 mg sodium molybdate dihydrate ($Na_2MoO_4.2H_2O$), 0.5 mg sodium tungstate dihydrate ($Na_2WO_4.2H_2O$), 0.5 mg manganese sulphate ($MnSO_4$) and 25 mg ferrous chloride ($FeCl_2.4H_2O$). All chemicals were prepared as stock solutions under sterile conditions and were of analytical grade. MM was freshly prepared prior to each experiment by adding a proportionate amount of stock solution into sterile distilled water under continuous stirring. The pH of the minimal medium was 7.5.

2.2 Bioplastics

The PLA plastics used in this paper were IngeoTM 2003D (NatureWorks © LLC, Minnetonka, MN, United States) and Futerro PLA was provided by Futerro S.A. (Escanaffles, Belgium). These bioplastics were originally in granulated form. Prior to all experimental work, the PLA bioplastics were processed to transform

the granules into powder (Choe et al., 2022; García-Depraect et al., 2022). PLA granules (100 g) were ground together with alternate layers of dry ice (200 g, IJsfabriek, Belgium) using a commercial blender (Krups Blender, Prep Expert S7000; 1,000-W). A total of 15 grinding cycles (5 min grind; 3 min rest) was used to avoid overheating of the appliance and reduce sublimation.

The grounded PLA powder was dried overnight at room temperature. Finally, manual sieving using stainless steel sieves of 100, 125, 150, and 250 μm (Test Sieve ISO 3310/1, Fisherbrand) was conducted to classify the powders based on particle size. The particle size used was from 125 to 250 μm as recommended by ISO 14 852 for aerobic aqueous conditions. These particles were sterilized with 70% ethyl alcohol prior to working under aseptic conditions.

2.3 Viable cell enumeration

2.3.1 Sonicator treatment for quantifying viable cells

Sonication was implemented to decompose the flocs formed by *A. orientalis* and *A. thailandensis* into planktonic cells for enumeration. Experiments were conducted in 75 mL YEM in baffled shake flasks at 180 rpm and 30°C for 5 days. Samples of 900 μL were taken regularly and sonicated at 100% amplitude for 5, 10 and 15 s in a 1 mL Eppendorf tube using a Fisherbrand Model 50 Sonic Dismembrator with 1/8" probe. Samples were then serially diluted and plated on YEM agar (100 μL sample per plate for each dilution). Each sample was taken in quadruplicate and a comparison was made with samples without sonication. Agar plates were incubated at 30°C for 5 days. Similar experiments were conducted to monitor growth of both strains in a setting for biodegradation, where PLA served as the sole carbon source. Considering longer degradation for PLA would take place, this experiment lasted for 14 days.

2.3.2 Growth characteristics

The growth characteristics were quantified by performing a parameter estimation with the model of Baranyi and Roberts (1994) on the experimental data. This parameter estimation led to the identification of the initial population density (N_0), the lag phase duration (λ), the maximum specific growth rate (μ_{max}) and the maximum population density (N_{max}). The model equations are formulated as follows:

$$\frac{dN(t)}{dt} = \frac{Q(t)}{1 + Q(t)} \cdot \mu_{max} \cdot \left(1 - \frac{N(t)}{N_{max}}\right) \cdot N(t) \text{ with } N(t = 0) = N_0$$

$$\frac{dQ(t)}{dt} = \mu_{max} \cdot Q(t) \quad \text{with} \quad Q(t = 0) = Q_0$$

$$\lambda = \frac{\ln(1 + 1/Q_0)}{\mu_{max}}$$

where Q is the physiological state of the cell and its initial condition is Q_0. This physiological state is used to describe the lag phase of the bacteria. The model parameters were estimated using the function *lsqnonlin* of MATLAB (MathWorks) while the viable cell counts were transformed as follows: $n(t) = \ln(N(t))$, to stabilize the variance (Smet et al., 2017).

2.3.3 Effect of sonication on viability

To examine the applicability of sonicator treatments for cell enumeration, the integrity of sonicated *A. orientalis* and *A. thailandensis* cells was evaluated by measuring the leakage of intracellular constituents to the supernatant (Huang et al., 2019; Umair et al., 2022). Precultures (40 mL) were prepared in YEM, inoculated and stored shaken at 180 rpm for 5 days at 30°C. On the last day, the preculture was resuspended in 8 g/L sodium chloride solution after centrifugation at 13,600 g for 15 min. For each strain and treatment time, 1 mL of preculture was transferred into a sterile 1.5 mL Eppendorf tube three times. The tubes were subjected to sonication for 5, 10, 15, 60 and 120 s. The samples were centrifuged at 10,000 g for 10 min (4°C), and the supernatant of three identical tubes was transferred into a 3 mL quartz cuvette to examine the release of extracellular constituents at 260 nm (VWR UV-6300PC, Haasrode, Belgium). Samples were prepared in triplicate, with untreated samples as controls.

2.4 Gravimetric weight loss of PLA bioplastics

2.4.1 Optimization of PLA and cell separation following inoculation

Determining the weight loss of PLA powder is complicated by the bacterial flocs that are difficult to separate from this powder. In this study, a new method was developed to separate PLA powder from the bacteria by sonicating samples followed by filtration with 40 μm cell strainers (nylon mesh, Fisherbrand). Optimization studies were conducted to compare the percentage of PLA recovery at sonication times of 30, 60, 120, 180, and 240 s. All cell strainers were pre-weighed and covered with aluminum foil to keep them clean. First, 4 g/L of PLA powder was re-suspended in a 10 mL preculture combined with 20 mL MM in a 50 mL Falcon tube (Cellstart®, Greiner Bio-Lab, Vilvoorde, Belgium). The Falcon tube was placed in an ice bath during sonication. Sonicated samples were filtered by pouring them through the cell strainer and the cell strainer was rinsed 5 times with 1 mL of ultrapure water using a micropipette. Used cell strainers were dried at 55°C for 24 h and weighed again to determine the amount of PLA powder in the retentate. All samples were prepared in five replicates.

2.4.2 PLA biodegradation using *Amycolatopsis orientalis* and *Amycolatopsis thailandensis*

To validate the developed method for quantifying PLA weight loss, a PLA degradation study was implemented to compare biodegradation of two PLA types (Futerro and NatureWorks) by both microorganisms. The preculture was directly inoculated in the system. Centrifuge tubes containing 40 mL of preculture were sonicated at an amplitude of 100 for 10 s to homogenize them. Then, 1 mL was transferred to a disposable cuvette (Polystyrene, Fisherbrand™) to determine the absorption at 595 nm. The measured optical density OD_i was used to determine the inoculation volume V_i required to achieve the same cell density after inoculation according to the following equation:
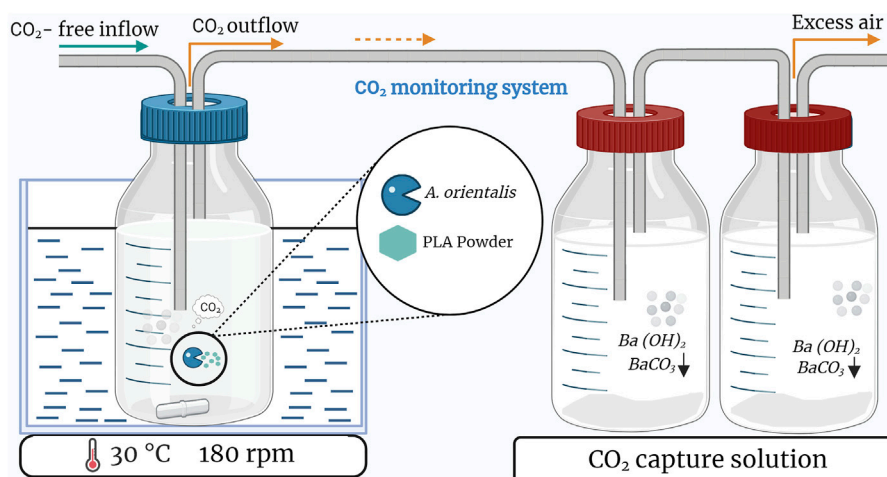
$$V_i = \frac{V_r \cdot OD_r}{OD_i}$$

FIGURE 2
Schematic of the setup used to monitor biodegradation based on carbon dioxide production in a single bioreactor. Triplicate samples are based on three of these setups in parallel.

In this equation the reference volume V_r and reference optical density OD_r were fixed to 10 mL and 0.173. Petri dishes (∅ 90 Gosselin, Fisher Scientific) were filled with 120 mg of PLA, V_i mL of inoculum and 30-V_i mL of minimal medium and incubated at 30°C.

On the fourth week of inoculation, Petri dishes were removed from the incubator. The content from each Petri dish was transferred to a 50 mL centrifuge tube and any residue was removed from the Petri dish by adding 5 mL ultrapure water and using a cell scraper, after which it was added to the centrifuge tube. The PLA degradation was then quantified using the method in Section 2.4.1 using a treatment time of 120 s. Gravimetric weight loss for the residual PLA was determined by weighing the PLA samples (KERN Precision balance, EWJ 300–3). In this way, the residual PLA in the samples, which determines the extent of degradation, could be measured. The weight loss of PLA was determined by using the equation below. Blank samples were prepared for both types of bioplastics using only minimal medium and PLA powder without bacteria. All samples were prepared in four replicates.

$$\text{PLA loss (\%)} = \frac{(W_i - W_f)}{W_i} \times 100$$

where W_i is the initial weight of the PLA powder g) and W_f is the final weight (i.e., after degradation) g).

2.5 Cumulative biogas quantification via CO_2 evolution

The PLA biodegradability was assessed following the ISO 14852 standard. The biogas production from the aerobic biodegradation was monitored by determining cumulative CO_2 production. Therefore, an experimental system was used consisting of: 1) a controlled flow of CO_2-free air, 2) a bioreactor and 3) a CO_2 scrubbing system (Baldera-Moreno et al., 2022; Choe et al., 2022), as illustrated in Figure 2. This biodegradation setup was

implemented to monitor the CO_2 evolution by *A. orientalis* using two different carbon substrates: glucose (4 g/L) and PLA powder (1 g/L, 120–250 μm), for 7 and 30 days, respectively. All samples consisted of 200 mL MM and were inoculated with similar inoculum concentrations, as described in Section 2.4.2 with V_r and OD_r fixed to 10 mL and 0.173 (in triplicate). The duplicate blanks contained only the MM and cells. CO_2-free air with less than 0.1 ppm-mol (ALPHAGAZ™ 2, Air Liquide) was supplied through a 0.2 μm filter at a flowrate of 0.05 lpm for each bioreactor using a flow meter. The biodegradability test was performed in 250 mL bottles equipped with a multi-inlet cap, stirred at 180 rpm and heated to 30 °C in a water bath (IKA IBR RO 15, Fisher Scientific). The CO_2 biogas was transferred directly into a gas washing bottle filled with 300 mL of barium hydroxide solution (12.5 mM) according to this reaction. This led to the following reaction that decreases the pH of the barium hydroxide solution:

$$Ba(OH)_2 + CO_2 \rightarrow BaCO_3 \downarrow + H_2O$$
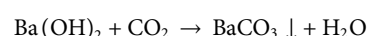
Two CO_2 scrubbing bottles were placed in series on the outflow of every bioreactor bottle. At the time of sampling, the first bottle was replaced by the second one and a fresh bottle was added. A 40 mL sample was taken from the first barium hydroxide bottle and filtered through 0.45 μm membrane filter (Filtropur S PES, Sarstedt) to remove precipitate. The solution was titrated to pH 7 with 50 mM HCl using a pH meter (Mettler Toledo, ECOLAB):

$$Ba(OH)_2 + 2HCl \rightarrow BaCl_2 + 2H_2O$$
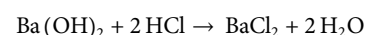
The amount of HCl needed to achieve the equivalence point was measured to determine the quantity of CO_2 that was captured:

$$n_{CO_2} = n_{Ba(OH)_2} - \frac{n_{HCl}}{2}$$

where n_{CO_2} is the quantity of CO_2 captured, $n_{Ba(OH)_2}$ is the original quantity of $Ba(OH)_2$ in the scrubbing bottle and n_{HCl} is the quantity of HCl that would be required to neutralize this entire bottle to pH 7. The mineralization (%) is calculated based on the amount (in mg or
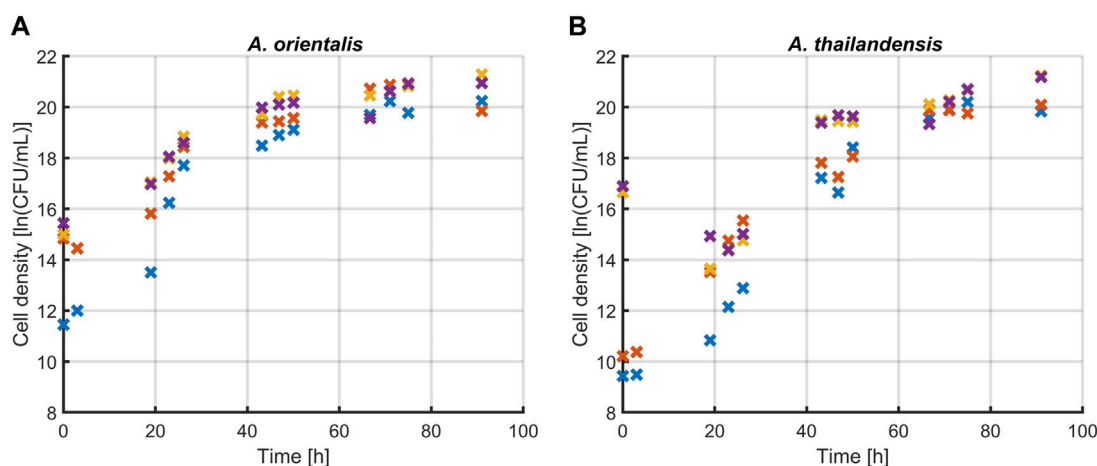
FIGURE 3
Effect of sonication on the quantification of viable **(A)** *Amycolatopsis orientalis* and **(B)** *Amycolatopsis thailandensis* cells through plate counts. The effects of 5 (**x**), 10 (**x**) and 15 (**x**) s of sonication were compared to a control without sonication (**x**). Data points are the averages of four technical replicates.

mole) of CO_2 captured in the sample ($CO_{2,S}$) and in the blank ($CO_{2,B}$) compared to the theoretical amount of CO_2 produced when fully oxidizing the carbon substrate ($CO_{2,T}$):

$$\text{Mineralization (\%)} = \frac{CO_{2,S} - CO_{2,B}}{CO_{2,T}} \cdot 100$$

At the end of the experiment, the PLA weight loss was determined according to the method of Section 2.4 with a sonication time of 120 s by distributing the bioreactor content over 3 centrifuge tubes of 50 mL. Biomass was measured based on dry cell weight determination after centrifugation. A carbon balance was determined to track the fate of carbon content conversion along the biodegradation process chain using carbon fraction that 1) converted to CO_2, 2) converted to biomass (calculated based on the average biomass molecular formula of CH1.7O0.4N0.2 according to Popovic (2019)), 3) undegraded PLA and 4) unaccounted residual PLA.

3 Results and discussion

In this paper, three methodologies were developed to enhance the monitoring of polylactic acid (PLA) degradation in aqueous media by utilizing *A. orientalis* and *A. thailandensis*. These methodologies are linked to the various stages of biodegradation as illustrated in Figure 1 and include monitoring 1) viable cell enumeration, 2) gravimetric weight loss of PLA plastics, and 3) cumulative biogas quantification. Following these monitoring methods, the carbon balance was computed.

3.1 Viable cell enumeration

To evaluate the performance of *A. orientalis* and *A. thailandensis* in the degradation of PLA under controlled conditions, it is crucial to employ appropriate enumeration techniques to monitor cell growth. To this end, a sonication method is developed in this section. The developed technique was validated by measuring the cell membrane integrity at 260 nm. This sonication method was limited to improving the cell quantification and was applied directly after taking sample. As such, it was not used in biodegradation process itself and therefore did not affect the degradation process or the final carbon balance.

3.1.1 Optimizing sonication for quantifying viable cells growth

The first step was to determine the effect of sonication treatments on the quantification of *Amycolatopsis* spp. during population growth. Figure 3 presents the comparison between three different treatment times (5, 10 and 15 s) and untreated controls for both *A. orientalis* and *A. thailandensis*. The results were analyzed with a two-way ANOVA ($p < 0.05$) that considers treatment time and culturing time. For *A. orientalis*, this analysis demonstrated that treating samples at any sonication time led to significantly higher counts compared to untreated samples. On the other hand, there was no statistical difference between the three different treatment times for this strain. In the case of *A. thailandensis*, there was no significant effect of treating the samples for 5 s compared to untreated samples. Only when treating samples for 10 or 15 s, a significant increase in the cell count was found. Also, for *A. thailandensis*, there was no significant difference between these two treatments. When combining these sonication results, it is concluded that a minimum sonication time of 10 s is required to obtain a statistically significant improvement in the quantification of *A. spp*. Figure 3 also indicates that the increase in cell recovery due to sonication differs during different phases of cell growth. The effect of sonication treatment on the characterization of the various phases of growth is discussed in Section 3.1.2. On average, the quantity of viable cells that was detected (before logarithmic transformation) increased 7-fold for *A. orientalis* and 6-fold for *A. thailandensis* compared to untreated samples.

The sonication treatment successfully improved the quantification of the total viable population by releasing
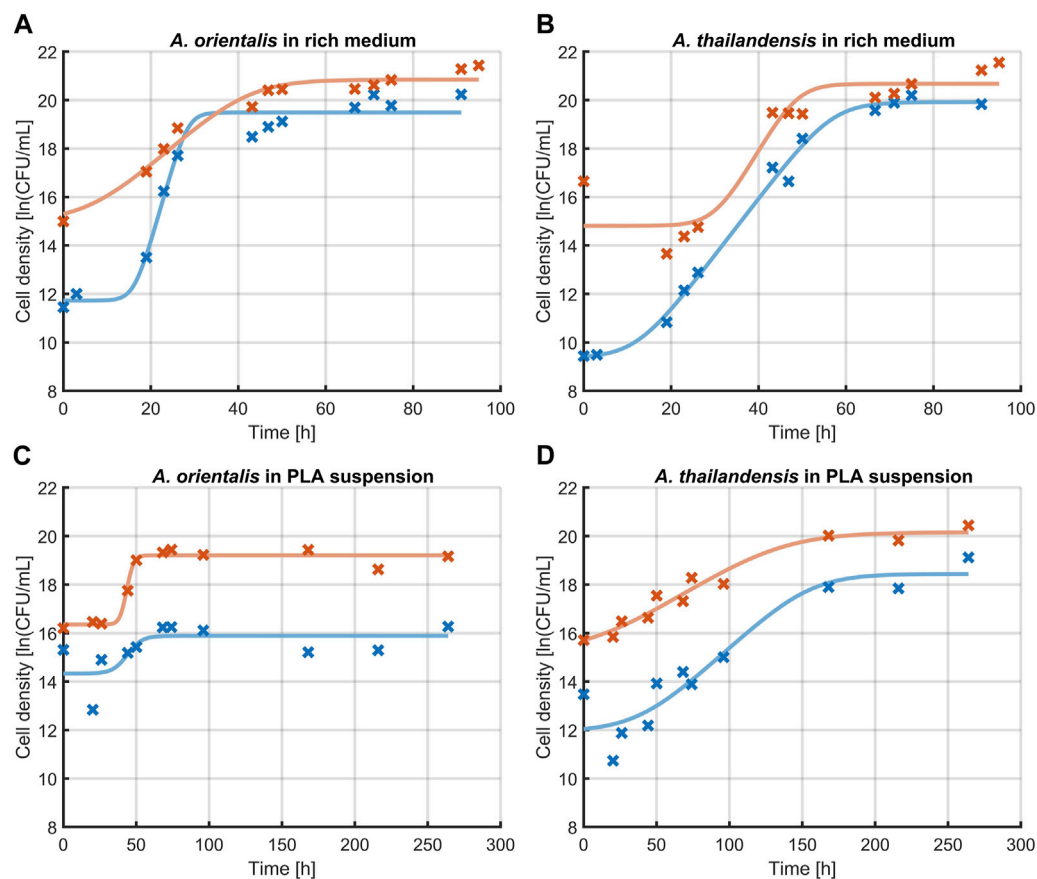
FIGURE 4
Effect of sonication on the measurement of growth kinetics of *Amycolatopsis orientalis* **(A,C)** and *Amycolatopsis thailandensis* **(B,D)** in rich medium **(A,B)** and PLA suspension **(C,D)**. A comparison is made between cell quantification without sonication (**x, —**) and after 10 s of sonication (**x, —**). Data points (x) have been fitted with the growth model of Baranyi and Roberts (1994) (–).

individual cells from agglomerates. When culturing *A.* spp., cells agglomerate in the form of dense pinpoint flocs (Tan and Goodfellow, 2015). These flocs appear as single colony forming units when applying plate count methods. The ultrasound waves of the sonication treatment apply strong shear forces on these flocs that led to the release of agglomerated cells into the planktonic form. This was visibly verified during the experiments as flocs were no longer observed after the applied sonication treatments. Ultrasound has been shown to effectively detach cells, which in this case resulted in an increase in the number of enumerated cells (Huang et al., 2017). Previous research has demonstrated that the use of sonication has a combined deagglomerating and inactivating effect. The research of Joyce et al. (2011) found these effects to be frequency dependent. In their research, low frequencies such as 20 and 40 kHz were causing a decrease in cell viability, rather than an increase in cultivability as seen in this study. This difference could be due to the fact that Gram-negative bacteria were studied in Joyce et al. (2011) whereas *A. orientalis* and *thailandensis* are Gram-positive.

3.1.2 Effect of sonication on evaluating growth kinetics

The effect of sonication on the characterization of growth kinetics was studied. Figure 4 illustrates the change in microbial growth kinetics as determined with or without sonicating the samples before quantification through viable plate counts. Specifically, the effect of 10 s of sonication was evaluated on the determination of the initial population density, the lag phase duration, the maximum specific growth rate in the exponential phase and the maximum population density that is reached in the stationary phase. These characteristics of microbial growth were determined by fitting the model of Baranyi and Roberts (1994) on the experimental data that was obtained and significant differences were analyzed between the model parameters that quantify each of these growth characteristics. The model parameters are compared in Table 1. The comparison was made for *A.* spp. growing in a rich medium and in PLA that was suspended in minimal medium (without any other carbon source aside from PLA). In all cases, the growth curve that was found through sonicating samples had higher population densities compared to growth curves from the untreated control. This increase in the measured cell densities is demonstrated by the initial cell densities and maximum cell densities that are consistently significantly higher when using ultrasound treated samples.

In the case of cell growth in PLA suspensions, there were no significant differences in the lag phase duration or the exponential growth rate. As such, the use of the sonication treatments leads to an upwards shift of the growth curve. This represents the increased detection of individual cells by applying sonication before further sample processing during viable plate counts.

TABLE 1 Evaluation of the growth characteristics of *Amycolatopsis orientalis* and *Amycolatopsis thailandensis* as evaluated without sample treatment (control) compared to using 10 s of sonication before diluting and plating. Different superscript indices between parameters of the control and sonicated samples indicate statistical differences ($p < 0.05$).

	A. orientalis			
	Rich medium		PLA	
	Control	10 s sonication	Control	10 s sonication
n_0 [ln (CFU/mL)]	11.7 ± 0.4^a	15.3 ± 0.4^b	14.3 ± 0.5^a	16.3 ± 0.2^b
λ [h]	16.3 ± 1.7^a	8.0 ± 5.6^b	40.2 ± 21.2^a	38.8 ± 3.9^a
μ_{max} [1/h]	0.64 ± 0.15^a	0.16 ± 0.04^b	0.21 ± 0.61^a	0.30 ± 0.16^a
n_{max} [ln (CFU/mL)]	19.5 ± 0.2^a	20.8 ± 0.2^b	15.9 ± 0.3^a	19.2 ± 0.1^b
	A. thailandensis			
	Rich medium		PLA	
	Control	10 s sonication	Control	10 s sonication
n_0 [ln (CFU/mL)]	9.4 ± 0.3^a	14.8 ± 0.7^b	12.0 ± 0.7^a	15.7 ± 0.4^b
λ [h]	12.3 ± 2.3^a	30.3 ± 12.2^b	40.6 ± 31.9^a	20.8 ± 25.6^a
μ_{max} [1/h]	0.24 ± 0.02^a	0.32 ± 0.24^a	0.06 ± 0.03^a	0.04 ± 0.01^a
n_{max} [ln (CFU/mL)]	19.9 ± 0.2^a	20.7 ± 0.4^b	18.4 ± 0.7^a	20.2 ± 0.3^b

Symbols: n_0, initial population density; λ, lag phase duration; μ_{max}, maximum specific growth rate in the exponential phase; n_{max}, maximum population density that is reached in the stationary phase.

When looking at the growth parameters of the *A.* spp. in rich medium, also the lag phase duration and exponential growth rate are defined differently when using sonication. These differences are caused by the fact that the increase in cell recovery is not equal in all phases of growth. The same phenomenon is seen to a lesser extent for cells growing in a PLA suspension. Given that the sonicated samples lead to an improved quantification of the individual cells, the respective characterization of the growth phases is considered more representative compared to untreated samples.

3.1.3 Effect of sonication on cell membrane integrity

The last part of the evaluation of the sonication method was to determine the effect of these treatments on the cell membrane integrity. The cavitations that lead to the disaggregation of flocculated *A.* spp. are known to cause damage to the bacterial cell membrane. Li et al. (2016) found that ultrasound causes damage on the cytoplasmic membrane of Gram-positive bacteria. This membrane damage leads to leakage of essential intracellular components such as DNA. Depending on the amount of damage, cells will transition into a non-viable or non-culturable state, causing them to be undetectable with the viable plate count method (Böllmann et al., 2016). Therefore, the membrane damage caused by sonication was studied for both *A. orientalis* and *A. thailandensis*. Membrane damage was quantified by measuring the amount of leakage of cytoplasmic components based on the absorbance of the supernatant at 260 nm (Chen and Cooper, 2002). The results of these absorbance measurements after treatments of 0, 5, 10, 15, 60 and 120 s are illustrated in Figure 5. The longest treatment times of 60 and 120 s were included as cases with a high degree of

membrane damage for comparison. In the case of treatments of 120 s, no viable cells could be detected. As such, this can be considered as a reference for membrane damage when all cells are inactivated to a non-viable or non-culturable state. For both strains, it is seen that there is a significant increase in the cell leakage when long treatments of 60 or 120 s are applied. In the case of short treatments of 5–15 s, there appears to be an increase in cell leakage for both strains, but this was not found to be statistically significant. As such, it is concluded that the use of sonication at the current conditions leads to membrane damage, which causes part of the population to become non-viable or non-culturable. However, in case of short treatments, there is a much higher increase in the quantity of colony forming units due to disaggregation of flocs than there is a decrease in viability or culturability. As such, short sonication times are beneficial to improve the accuracy of viable plate counts and the selected treatment time of 10 s leads to a desirable trade off between a significant amount of disaggregation and an insignificant amount of membrane damage.

3.2 Gravimetric weight loss of PLA

The quantification of degraded PLA samples is an important parameter in biodegradation. Separation between the PLA samples and cells is crucial prior to measuring the polymer weight loss of degraded samples. In this study, a PLA powder of 125–250 μm was used in an aqueous medium. Based on these powders, a separation method was first developed and then validated based on a case study in which the biodegradation of PLA by *A. orientalis* and *A. thailandensis* was compared for PLA from two different manufacturers.
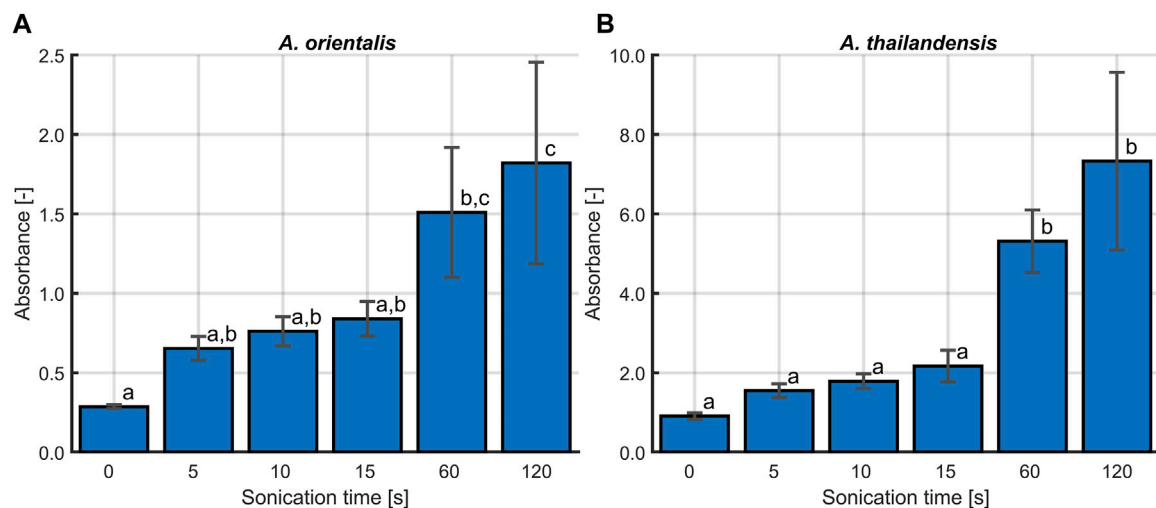
FIGURE 5
The effect of sonication time on the cell membrane integrity for **(A)** *Amycolatopsis orientalis* and **(B)** *Amycolatopsis thailandensis*. The membrane integrity is quantified by determining the amount of cell leakage, which is proportional to the absorbance of the supernatant at 260 nm. Bars bearing different letter indices have a statistically different mean ($p < 0.05$).
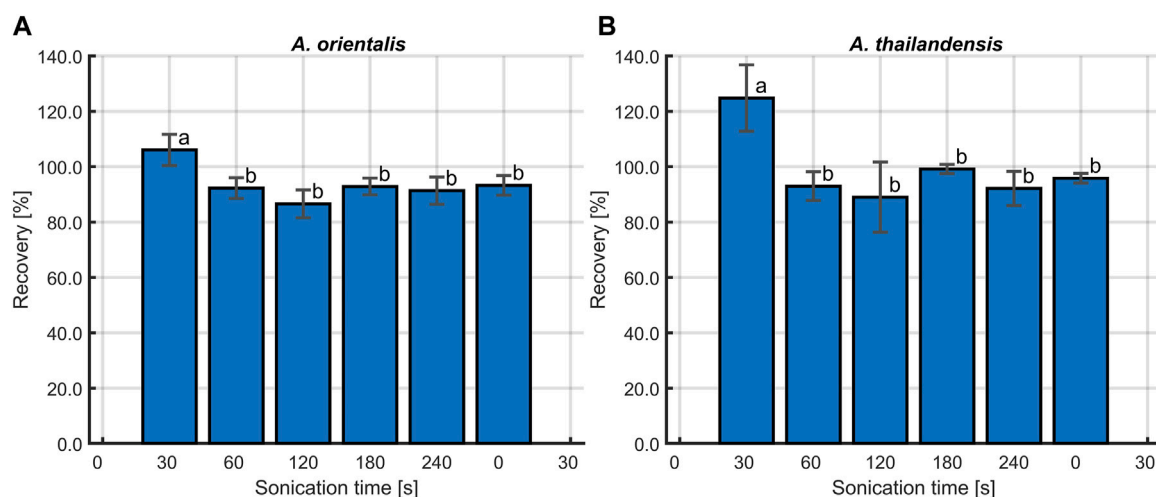

FIGURE 6
Percentage of PLA recovery at different sonication times, following inoculation with **(A)** *Amycolatopsis orientalis* and **(B)** *Amycolatopsis thailandensis*. Bars bearing different letter indices have a statistically different mean ($p < 0.05$).

3.2.1 Optimization of PLA and cells separation

A separation method was implemented that relied on sonication to disrupt cell agglomerates and to remove cells that are attached to the polymer surface. The individual planktonic cells are then separated from the larger PLA particles by using a cell strainer of 40 μm. This method was optimized on samples containing *A. orientalis* and *A. thailandensis* with the PLA powder. The percentage of PLA recovery in untreated samples was compared with samples treated by sonication for 30, 60, 120, 180, and 240 s. As shown in Figure 6, untreated samples had a recovery rate of about 125%. This overestimation of the recovery rate above 100% indicates the inclusion of cell pellets in the measured weight. The retention of agglomerated cells was visually confirmed when analyzing the dried strainers. Statistical analysis using one-way

ANOVA ($p < 0.05$) revealed that all sonication treatments had a significant effect on recovery compared to the untreated samples. As such, the ultrasound waves were efficient in deagglomerating cells to a size that was sufficiently small to pass through the cell strainer. On the other hand, there was no significant difference between the percentage of PLA recovery for any of the sonication treatment times for both *A. orientalis* and *A. thailandensis*. As such, it appears to be unlikely that an increased sonication time would lead to mechanical degradation of the PLA powder and would cause an overestimation of the biodegradation. As such, a sonication time of 120 s was selected to decrease the risk of overestimations of the PLA weight under conditions that would lead to stronger attachment or aggregation of cells.

The weight loss measurement requires an effective separation technique to retrieve polymer residue from samples containing biomass prior to weighing (Shah et al., 2008). The traditional separation methods such as centrifugation and filtration that were commonly employed to measure degraded plastics in the form of films or sheets in aqueous environments (Ayar-Kayali and Tarhan, 2007; Grause et al., 2022; Samat et al., 2023) were not effective when suspension of cells and PLA powders were used. The combination of a cell strainer and sonication proposed in this method has proven to be effective to separate cells and PLA powders at any treatment time tested compared to untreated sample.

When the PLA powder is reduced in size to particles smaller than the cell strainer pore size, i.e., 40 μm, the PLA will pass through, indicating that the first stage of degradation (biodeterioration) has occurred. When assuming a spherical size of the PLA powder, particles of 125–250 μm in diameter would have to be degraded respectively over 96% and 99% in volume to be able to pass through the 40 μm cell strainers. As such, this method enables the quantification of the biofragmentation step by monitoring PLA weight loss. This new method for the quantification of plastic biodegradation is a new application for cell strainers, which have already found applications in various fields (Qiu et al., 2018; Takino et al., 2018; Wang et al., 2019). To the authors' knowledge, this is the first study reporting on the combined use of cell strainers and sonication to analyze the biodegradation of plastics. A previous study has determined the residual quantity of PLA using a dialysis bag with at molecular weight cut off of 10 kDa (Youngpreda et al., 2017). However, given the small pore size, such a dialysis bag would not be suitable in the current application to separate biomass from PLA.

3.2.2 PLA biodegradation by *Amycolatopsis orientalis* and *Amycolatopsis thailandensis*

The combined application of 120 s of sonication and cell strainers for separating degraded PLA samples was validated in a biodegradation case study. In this study, two PLA types from different manufacturers (NatureWorks and Futerro), were incubated in the presence of *A. orientalis* and *A. thailandensis* for biodegradation. Figure 7 depicts the comparison of gravimetric weight loss after an incubation period of 4 weeks for both the biodegraded samples and control samples. Although for *A. thailandensis* there appears to be some increase in the weight loss compared to the control samples, there is no statistical difference between the untreated samples from either manufacturer and the respective *A. thailandensis*-biodegraded samples. When using *A. orientalis* on the other hand, there is a statistically significant increase in weight loss to 43% and 64% for NatureWorks and Futerro PLA, respectively. However, there was no statistical difference between any of the results from the two manufacturers under the same treatment conditions. The small quantity of weight loss in control samples (2% and 9%) is in line with results from the optimization study of the sonication time. As such, this is likely due to some losses of particles during sample processing.

Whereas plastic biodegradation has been broadly studied, until now there have been limited efforts in studying microbial degradation of powdered samples. Instead, most research efforts focus on the use of granulated particles or extruded films that represent waste fractions and are easier to retrieve from samples (Jarerat and Tokiwa, 2001; Jarerat and Tokiwa, 2003). The milling of
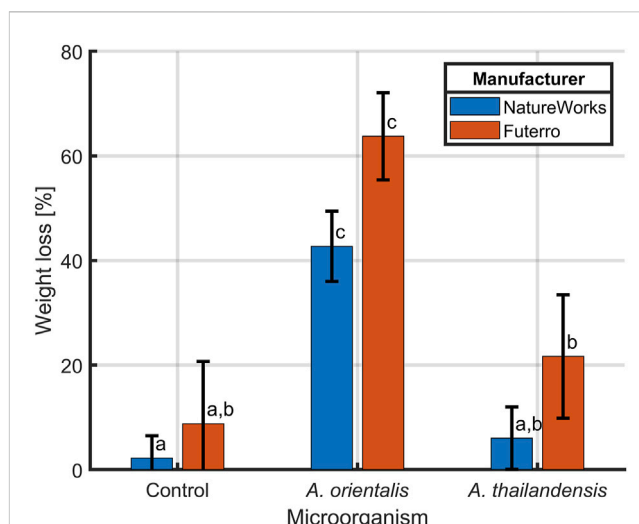

FIGURE 7
Biodegradation of PLA from two manufacturers NatureWorks and Futerro by *Amycolatopsis orientalis* or *Amycolatopsis thailandensis* compared to non-biodegraded control samples. The PLA weight loss was evaluated after sonication and separation from biomass using a 40 μm cell strainer. Bars bearing different letter indices have a statistically different mean ($p < 0.05$).
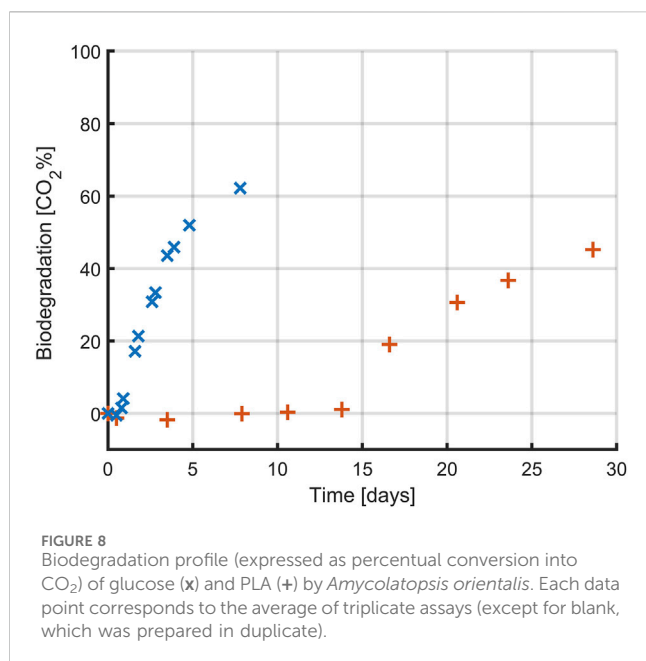
plastics to powders is however considered as pretreatment step that can significantly enhance biodegradation by increasing the accessible surface area (Yasin et al., 2022). In cases where powdered PLA has been used, the biodegradation process was monitored through different degradation parameters, such as carbon dioxide production and biological oxygen demand, which indicate the amount of carbon that was transformed into carbon dioxide and the amount of mineralized oxygen, respectively (Benn and Zitomer, 2018; Choe et al., 2022; García-Depraect et al., 2022; López-Ibáñez and Beiras, 2022). While these measurements provide information on the final stage of the biodegradation process, i.e., biomineralization, the weight loss method is suitable for monitoring the first steps of biodegradation, i.e., until biofragmentation (Yasin et al., 2022). Therefore, the developed method plays a crucial role in enabling researchers to obtain a better view of the individual stages of the biodegradation process when working with powdered plastics.

3.3 Monitoring the biodegradation process

Measuring biogas production serves for monitoring the final stage of the biodegradation process to the end products, i.e., biomineralization. In this study, biogas production was monitored according to the standard method ISO 14 852 for aerobic plastic biodegradation by determining the carbon dioxide production. In combination with the separation method that was proposed, a carbon balance was calculated by considering the carbon conversion throughout the biodegradation process.

3.3.1 CO₂ evolution

The production of biogas by *A. orientalis* on was studied when using either glucose or PLA as a sole carbon source for respectively

FIGURE 8
Biodegradation profile (expressed as percentual conversion into CO_2) of glucose (**x**) and PLA (**+**) by *Amycolatopsis orientalis*. Each data point corresponds to the average of triplicate assays (except for blank, which was prepared in duplicate).

FIGURE 9
Carbon mass balance % represented by the amount of initial carbon content converted into, biomass (C-Biomass), carbon dioxide (C-evolved CO_2), residual (C- PLA residual) and undefined carbon when using *Amycolatopsis orientalis* for PLA biodegradation.

7 and 30 days. Glucose was used as an easily accessible carbon source to validate the implementation of the CO_2 monitoring method. PLA on the other hand was used to confirm the application of this method for monitoring the various biodegradation phases of bioplastics and to construct a carbon balance. *A. orientalis* was selected for the experiments in this section following the promising results when studying the weight loss of PLA during biodegradation. The profiles for the cumulative production of CO_2 by *A. orientalis* based on the two carbon sources are presented in Figure 8. These profiles are the result of comparing the averages of 3 samples for each carbon source with 2 blanks, where no carbon source was present.

In both conditions, the highest conversion rate of carbon to CO_2 was approximately 60%, but this conversion happened faster when glucose was used as carbon source. In the case of glucose, CO_2 production was quantifiable within the first day of experimentation whereas for the PLA samples it took over 15 days before the first CO_2 production could be measured. For both carbon sources, CO_2 production occurred in a close to linear process after this lag period, although at a slower rate for the PLA samples. In the case of glucose, the CO_2 production rate decreased towards the end of the experiment, indicating that all carbon had been consumed. However, in the case of PLA the final samples still followed a linear trend, indicating that there is more PLA present that could be biodegraded. As such, a full biodegradation process would have taken even longer than 30 days. However, since the goal of the PLA-based experiments was to construct a carbon balance, full conversion of all PLA was not desirable.

Whereas glucose is readily accessible for uptake by the *A. orientalis* metabolism, as seen from the from the short delay until CO_2 production, this is not the case for PLA. Several steps are required before biopolymers can be used by microorganisms, as the polymer size and semi-crystalline structure hinder microbial attacks (Yasin et al., 2022). As the PLA in these experiments had a powder form with a large specific surface area, it can be assumed that untreated PLA material with a much smaller specific surface area
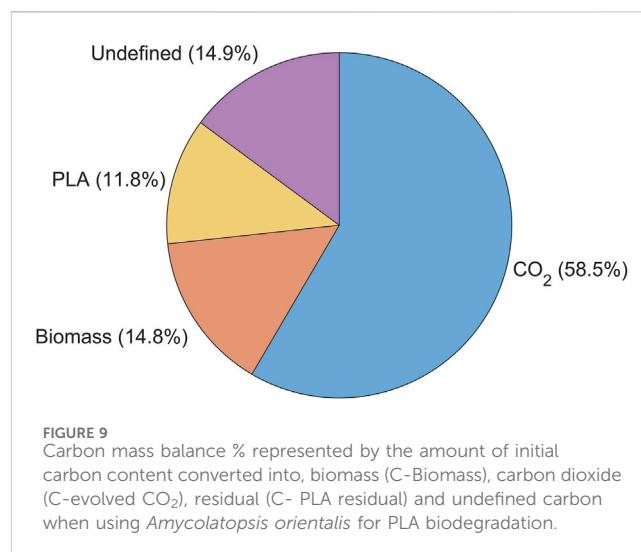
would lead to an even longer time before CO_2 production and that it would occur at a slower rate. The slow biodegradation rate of PLA in aqueous media has been commonly reported. In separate studies, only 2.0%–8.7% of PLA was degraded after incubation of 28–365 h in the presence of microbial community extracted from wastewater plants (Massardier-Nageotte et al., 2006; Choe et al., 2022) and in artificial aquatic system (Bagheri et al., 2017). The type of microbial inoculum plays a key role in the degradation of polymers. In this study, *A. orientalis* was used as it is a well-studied PLA-degrading bacterium that secretes serine-like protease to degrade PLA. Given that this process is marked by a slow CO_2 production rate, it is particularly suitable for monitoring with a cumulative measurement method as described by ISO 14 852.

3.3.2 Carbon balance

To assess the progress of the various phases of PLA biodegradation, a carbon balance was computed based on the experiments conducted with *A. orientalis* in the previous section. Figure 9 illustrates percentage of carbon from the initial quantity of PLA that 1) has been converted to CO_2, 2) has been converted to biomass, 3) remains as undegraded PLA and 4) is unaccounted for. From this analysis, 85.1% of the carbon from the initial PLA was successfully tracked and measured. More than half (58.5%) of the initial carbon content from PLA was mineralized into biogas, which in this case was CO_2. Meanwhile, 14.8% of the PLA led to the growth of additional biomass. Finally, 11.8% of the PLA was retrieved from the bioreactor on the final day of sampling. This sample represents the undegraded mass of PLA, which was separated and measured using the method described in Section 2.4.

By using a minimal medium containing only inorganic salts, the only carbon source in the samples was PLA. As expected, a higher biofragmentation rate of PLA was observed compared to the amount converted into CO_2. On the one hand, the former process reflects the stage of biodegradation in which PLA powder is fragmented into smaller particles by microbial attack. Any particle size larger than the cell strainer was retained, whereas particles smaller than 40 μm passed through and were not accounted for in the residual PLA fraction. Considering that PLA powder of 125–250 μm was used, any particle that passed the strainer had already undergone substantial size

reduction. Thus, particle sizes smaller than 40 μm, oligomers and monomers appear in the fraction of unaccounted carbon.

On the other hand, the cumulative CO_2 production only represents carbon that has been fully biodegraded until the final stage of mineralization (García-Depraect et al., 2022). Any PLA fractions that are larger than 1,000 Da cannot be taken up into the cell and are therefore not yet accessible for mineralization (Sander et al., 2023). As such, the fraction of PLA smaller than 40 μm and larger than 1,000 Da are considered to be the product from the biofragmentation that are broken down further in the bioassimilation step. This PLA fraction forms the unaccounted fraction of PLA, together with dissolved inorganic and organic carbon. Given that the degradation of larger PLA particles to oligomers, dimers, and monomers is slower than the enzymatic degradation of monomers to CO_2, it can be considered that the PLA fraction undergoing assimilation makes up the majority of the carbon that was unaccounted for.

4 Conclusion

This work proposes novel approaches for monitoring the viable cell density and polymer gravimetric weight loss during PLA biodegradation by *A. orientalis* and *A. thailandensis*. First, it was demonstrated that the total population of viable cells can be quantified more accurately by performing a 10 s sonication treatment before diluting and plating the sample. Secondly, powdered PLA was separated from biomass by performing a 120 s sonication treatment that breaks all cell agglomerates and removes attached cells from the PLA surface followed by a filtration step that retains the PLA on a 40 μm cell strainer while letting biomass pass through. Finally, the ISO 14 852 method was implemented to measure the cumulative production of CO_2 as a function of time. When combining these methods, an overview is obtained of the carbon balance consisting mostly of 1) CO_2, ii) biomass, 3) PLA that is undergoing the biofragmentation stage to form particles of a size less than 40 μm and 4) PLA that is undergoing the bioassimilation stage towards fractions of about 1,000 Da that can be taken up within the cell membrane.

As such, integrating these newly proposed and existing methods leads to an improved quantifying and understanding of the various stages and aspects of PLA biodegradation by *Amycolatopsis* species.

Data availability statement

The original contributions presented in the study are included in the article/supplementary material, further inquiries can be directed to the corresponding author.

References

Adhikari, D., Mukai, M., Kubota, K., Kai, T., Kaneko, N., Araki, K. S., et al. (2016). Degradation of bioplastics in soil and their degradation effects on environmental microorganisms. *J. Agric. Chem. Environ.* 5 (01), 23–34. doi:10.4236/jacen.2016.51003

Apinya, T., Sombatsompop, N., and Prapagdee, B. (2015). Selection of a *Pseudonocardia* sp. RM423 that accelerates the biodegradation of poly (lactic) acid in submerged cultures and in soil microcosms. *Int. Biodeterior. Biodegrad.* 99, 23–30. doi:10.1016/j.ibiod.2015.01.001

Author contributions

NY: Conceptualization, Data curation, Funding acquisition, Investigation, Methodology, Writing–original draft, Writing–review and editing. FP: Investigation, Writing–original draft. MY: Investigation, Writing–original draft. JV: Conceptualization, Funding acquisition, Writing–review and editing. SA: Conceptualization, Data curation, Formal Analysis, Funding acquisition, Methodology, Supervision, Writing–original draft, Writing–review and editing.

Funding

Acknowledgments

Conflict of interest

The authors declare that the research was conducted in the absence of any commercial or financial relationships that could be construed as a potential conflict of interest.

The author(s) declared that they were an editorial board member of Frontiers, at the time of submission. This had no impact on the peer review process and the final decision.

Publisher's note

Ayar-Kayali, H., and Tarhan, L. (2007). Balance between aerobic and anaerobic metabolites production of *Amycolatopsis orientalis* depending on initial glucose concentration. *Prep. Biochem. Biotechnol.* 37 (3), 247–263. doi:10.1080/10826060701386737

Bagheri, A. R., Laforsch, C., Greiner, A., and Agarwal, S. (2017). Fate of so-called biodegradable polymers in seawater and freshwater. *Glob. Challenges* 1 (4), 1700048. doi:10.1002/gch2.201700048

Baldera-Moreno, Y., Pino, V., Farres, A., Banerjee, A., Gordillo, F., and Andler, R. (2022). Biotechnological aspects and mathematical modeling of the biodegradation of plastics under controlled conditions. *Polymers* 14 (3), 375. doi:10.3390/polym14030375

Baranyi, J., and Roberts, T. A. (1994). A dynamic approach to predicting bacterial growth in food. *Int. J. food Microbiol.* 23 (3-4), 277–294. doi:10.1016/0168-1605(94)90157-0

Benn, N., and Zitomer, D. (2018). Pretreatment and anaerobic co-digestion of selected PHB and PLA bioplastics. *Front. Environ. Sci.* 5, 93. doi:10.3389/fenvs.2017.00093

Böllmann, J., Rathsack, K., and Martienssen, M. (2016). The precision of bacterial quantification techniques on different kinds of environmental samples and the effect of ultrasonic treatment. *J. Microbiol. Methods* 126, 42–47. doi:10.1016/j.mimet.2016.05.006

Branck, T. A., Hurley, M. J., Prata, G. N., Crivello, C. A., and Marek, P. J. (2017). Efficacy of a sonicating swab for removal and capture of *Listeria monocytogenes* in biofilms on stainless steel. *Appl. Environ. Microbiol.* 83 (10), e00109–e00117. doi:10.1128/aem.00109-17

Butbunchu, N., and Pathom-Aree, W. (2019). Actinobacteria as promising candidate for polylactic acid type bioplastic degradation. *Front. Microbiol.* 10, 2834. doi:10.3389/fmicb.2019.02834

Castro-Aguirre, E., Auras, R., Selke, S., Rubino, M., and Marsh, T. (2017). Insights on the aerobic biodegradation of polymers by analysis of evolved carbon dioxide in simulated composting conditions. *Polym. Degrad. Stab.* 137, 251–271. doi:10.1016/j.polymdegradstab.2017.01.017

Chen, C. Z., and Cooper, S. L. (2002). Interactions between dendrimer biocides and bacterial membranes. *Biomaterials* 23 (16), 3359–3368. doi:10.1016/s0142-9612(02)00036-4

Choe, S., Kim, Y., Park, G., Lee, D. H., Park, J., Mossisa, A. T., et al. (2022). Biodegradation of 3D-printed biodegradable/non-biodegradable plastic blends. *ACS Appl. Polym. Mater.* 4 (7), 5077–5090. doi:10.1021/acsapm.2c00600

Chomchoei, A., Pathom-aree, W., Yokota, A., Kanongnuch, C., and Lumyong, S. (2011). *Amycolatopsis thailandensis* sp. nov., a poly(L-lactic acid)-degrading actinomycete, isolated from soil. *Int. J. Syst. Evol. Microbiol.* 61, 839–843. doi:10.1099/ijs.0.023564-0

Dudek, P., Grajek, A., Kowalczewski, J., Madycki, G., and Marczak, D. (2020). Ultrasound frequency of sonication applied in microbiological diagnostics has a major impact on viability of bacteria causing PJI. *Int. J. Infect. Dis.* 100, 158–163. doi:10.1016/j.ijid.2020.08.038

European Bioplastic (2022). European bioplastic. Available at: https://docs.european-bioplastics.org/publications/EUBP_Facts_and_figures.pdf.

Ferdous, S., Dopp, J. L., and Reuel, N. F. (2021). Optimization of E. coli tip-sonication for high-yield cell-free extract using finite element modeling. *AIChE J.* 67 (10), e17389. doi:10.1002/aic.17389

Ganesan, B., Martini, S., Solorio, J., and Walsh, M. K. (2015). Determining the effects of high intensity ultrasound on the reduction of microbes in milk and orange juice using response surface methodology. *Int. J. Food Sci.* 2015, 1–7. doi:10.1155/2015/350719

García-Depraect, O., Lebrero, R., Martínez-Mendoza, L. J., Rodriguez-Vega, S., Börner, R. A., Börner, T., et al. (2023). Enhancement of biogas production rate from bioplastics by alkaline pretreatment. *Waste Manag.* 164, 154–161. doi:10.1016/j.wasman.2023.04.009

García-Depraect, O., Lebrero, R., Rodriguez-Vega, S., Bordel, S., Santos-Beneit, F., Martínez-Mendoza, L. J., et al. (2022). Biodegradation of bioplastics under aerobic and anaerobic aqueous conditions: kinetics, carbon fate and particle size effect. *Bioresour. Technol.* 344, 126265. doi:10.1016/j.biortech.2021.126265

Grause, G., Kuniyasu, Y., Chien, M. F., and Inoue, C. (2022). Separation of microplastic from soil by centrifugation and its application to agricultural soil. *Chemosphere* 288, 132654. doi:10.1016/j.chemosphere.2021.132654

Hobbs, S. R., Parameswaran, P., Astmann, B., Devkota, J. P., and Landis, A. E. (2019). Anaerobic codigestion of food waste and polylactic acid: effect of pretreatment on methane yield and solid reduction. *Adv. Mater. Sci. Eng.* 2019, 1–6. doi:10.1155/2019/4715904

Hottle, T. A., Agüero, M. L., Bilec, M. M., and Landis, A. E. (2016). Alkaline amendment for the enhancement of compost degradation for polylactic acid biopolymer products. *Compost Sci. Util.* 24 (3), 159–173. doi:10.1080/1065657x.2015.1102664

Huang, F., Kong, J., Ju, J., Zhang, Y., Guo, Y., Cheng, Y., et al. (2019). Membrane damage mechanism contributes to inhibition of trans-cinnamaldehyde on *Penicillium italicum* using Surface-Enhanced Raman Spectroscopy (SERS). *Sci. Rep.* 9 (1), 490. doi:10.1038/s41598-018-36989-7

Huang, G., Chen, S., Dai, C., Sun, L., Sun, W., Tang, Y., et al. (2017). Effects of ultrasound on microbial growth and enzyme activity. *Ultrason. sonochemistry* 37, 144–149. doi:10.1016/j.ultsonch.2016.12.018

Jarerat, A., and Tokiwa, Y. (2001). Degradation of poly (L-lactide) by a fungus. *Macromol. Biosci.* 1 (4), 136–140. doi:10.1002/1616-5195(20010601)1:4<136::aid-mabi136>3.3.co;2-v

Jarerat, A., and Tokiwa, Y. (2003). Poly (L-lactide) degradation by *Saccharothrix waywayandensis*. *Biotechnol. Lett.* 25, 401–404. doi:10.1023/a:1022450431193

Joyce, E., Al-Hashimi, A., and Mason, T. J. (2011). Assessing the effect of different ultrasonic frequencies on bacterial viability using flow cytometry. *J. Appl. Microbiol.* 110 (4), 862–870. doi:10.1111/j.1365-2672.2011.04923.x

Li, F., Wang, S., Liu, W., and Chen, G. (2008). Purification and characterization of poly (L-lactic acid)-degrading enzymes from *Amycolatopsis orientalis* ssp. orientalis. *FEMS Microbiol. Lett.* 282 (1), 52–58. doi:10.1111/j.1574-6968.2008.01109.x

Li, J., Ahn, J., Liu, D., Chen, S., Ye, X., and Ding, T. (2016). Evaluation of ultrasound-induced damage to *Escherichia coli* and *Staphylococcus aureus* by flow cytometry and transmission electron microscopy. *Appl. Environ. Microbiol.* 82 (6), 1828–1837. doi:10.1128/aem.03080-15

López-Ibáñez, S., and Beiras, R. (2022). Is a compostable plastic biodegradable in the sea? A rapid standard protocol to test mineralization in marine conditions. *Sci. Total Environ.* 831, 154860. doi:10.1016/j.scitotenv.2022.154860

Massardier-Nageotte, V., Pestre, C., Cruard-Pradet, T., and Bayard, R. (2006). Aerobic and anaerobic biodegradability of polymer films and physico-chemical characterization. *Polym. Degrad. Stab.* 91 (3), 620–627. doi:10.1016/j.polymdegradstab.2005.02.029

Mayekar, P. C., Limsukon, W., Bher, A., and Auras, R. (2023). Breaking it down: how thermoplastic starch enhances poly (lactic acid) biodegradation in Compost— A comparative analysis of reactive blends. *ACS Sustain. Chem. Eng.* 11 (26), 9729–9737. doi:10.1021/acssuschemeng.3c01676

Pitt, W. G., and Ross, S. A. (2003). Ultrasound increases the rate of bacterial cell growth. *Biotechnol. Prog.* 19 (3), 1038–1044. doi:10.1021/bp0340685

Popovic, M. (2019). Thermodynamic properties of microorganisms: determination and analysis of enthalpy, entropy, and Gibbs free energy of biomass, cells and colonies of 32 microorganism species. *Heliyon* 5 (6), e01950. doi:10.1016/j.heliyon.2019.e01950

Qiu, X., Lombardo, J. A., Westerhof, T. M., Pennell, M., Ng, A., Alshetaiwi, H., et al. (2018). Microfluidic filter device with nylon mesh membranes efficiently dissociates cell aggregates and digested tissue into single cells. *Lab a Chip* 18 (18), 2776–2786. doi:10.1039/c8lc00507a

Ruggero, F., Gori, R., and Lubello, C. (2019). Methodologies to assess biodegradation of bioplastics during aerobic composting and anaerobic digestion: a review. *Waste Manag. Res.* 37 (10), 959–975. doi:10.1177/0734242x19854127

Samat, A. F., Carter, D., and Abbas, A. (2023). Biodeterioration of pre-treated polypropylene by *Aspergillus terreus* and *Engyodontium album*. *npj Mater. Degrad.* 7 (1), 28. doi:10.1038/s41529-023-00342-9

Sander, M., Weber, M., Lott, C., Zumstein, M., Künkel, A., and Battagliarin, G. (2023). "Polymer biodegradability 2.0: a holistic view on polymer biodegradation in natural and engineered environments," in *Synthetic biodegradable and biobased polymers. Advances in polymer science*. Editors A. Künkel, G. Battagliarin, M. Winnacker, B. Rieger, and G. Coates (Cham.: Springer).

Shah, A. A., Hasan, F., Hameed, A., and Ahmed, S. (2008). Biological degradation of plastics: a comprehensive review. *Biotechnol. Adv.* 26 (3), 246–265. doi:10.1016/j.biotechadv.2007.12.005

Shah, H. H., Amin, M., and Pepe, F. (2023). Maximizing resource efficiency: opportunities for energy recovery from municipal solid waste in Europe. *J. Material Cycles Waste Manag.* 25 (5), 2766–2782. doi:10.1007/s10163-023-01733-5

Shimao, M. (2001). Biodegradation of plastics. *Curr. Opin. Biotechnol.* 12 (3), 242–247. doi:10.1016/s0958-1669(00)00206-8

Smet, C., Akkermans, S., Baka, M., Valdramidis, V., and Van Impe, J. (2017). "Multiscale modelling in predictive microbiology: macroscopic approach," in *Quantitative tools for sustainable food and energy in the food chain*. Editors V. Valdramidis, E. Cummins, and J. Van Impe (Ostend, Belgium: Eurosis), 15–49.

Takino, T., Sato, H., and Seiki, M. (2018). Simple and cost-effective assay for isolating invasive living cells. *BioTechniques* 65 (3), 137–142. doi:10.2144/btn-2018-0036

Tan, G. Y. A., and Goodfellow, M. (2015). *Amycolatopsis. Bergey's manual of systematics of archaea and bacteria*, 1–40.

Teixeira, S., Eblagon, K. M., Miranda, F., R. Pereira, M. F., and Figueiredo, J. L. (2021). Towards controlled degradation of poly (lactic) acid in technical applications. *C* 7 (2), 42. doi:10.3390/c7020042

Umair, M., Sultana, T., Xiaoyu, Z., Senan, A. M., Jabbar, S., Khan, L., et al. (2022). LC-ESI-QTOF/MS characterization of antimicrobial compounds with their action mode extracted from vine tea (*Ampelopsis grossedentata*) leaves. *Food Sci. Nutr.* 10 (2), 422–435. doi:10.1002/fsn3.2679

Wang, H., Sheng, J., He, H., Chen, X., Li, J., Tan, R., et al. (2019). A simple and highly purified method for isolation of glomeruli from the mouse kidney. *Am. J. Physiology-Renal Physiology* 317, F1217–F1223. doi:10.1152/ajprenal.00293.2019

Yasin, N. M., Akkermans, S., and Van Impe, J. F. (2022). Enhancing the biodegradation of (bio) plastic through pretreatments: a critical review. *Waste Manag.* 150, 1–12. doi:10.1016/j.wasman.2022.06.004

Youngpreda, A., Panyachanakul, T., Kitpreechavanich, V., Sirisansaneeyakul, S., Suksamrarn, S., Tokuyama, S., et al. (2017). Optimization of poly (DL-lactic acid) degradation and evaluation of biological re-polymerization. *J. Polym. Environ.* 25, 1131–1139. doi:10.1007/s10924-016-0885-1

frontiers | Frontiers in Bioengineering and Biotechnology

Check for updates

Key challenges in the advancement and industrialization of biobased and biodegradable plastics: a value chain overarching perspective

Tim Börner[1,2]* and Manfred Zinn[1]*

[1]Institute of Life Sciences, University of Applied Sciences and Arts Western Switzerland (HES-SO Valais-Wallis), Sion, Switzerland, [2]Empa—Swiss Federal Laboratories for Material Science and Technology, Technology and Society Laboratory, St. Gallen, Switzerland
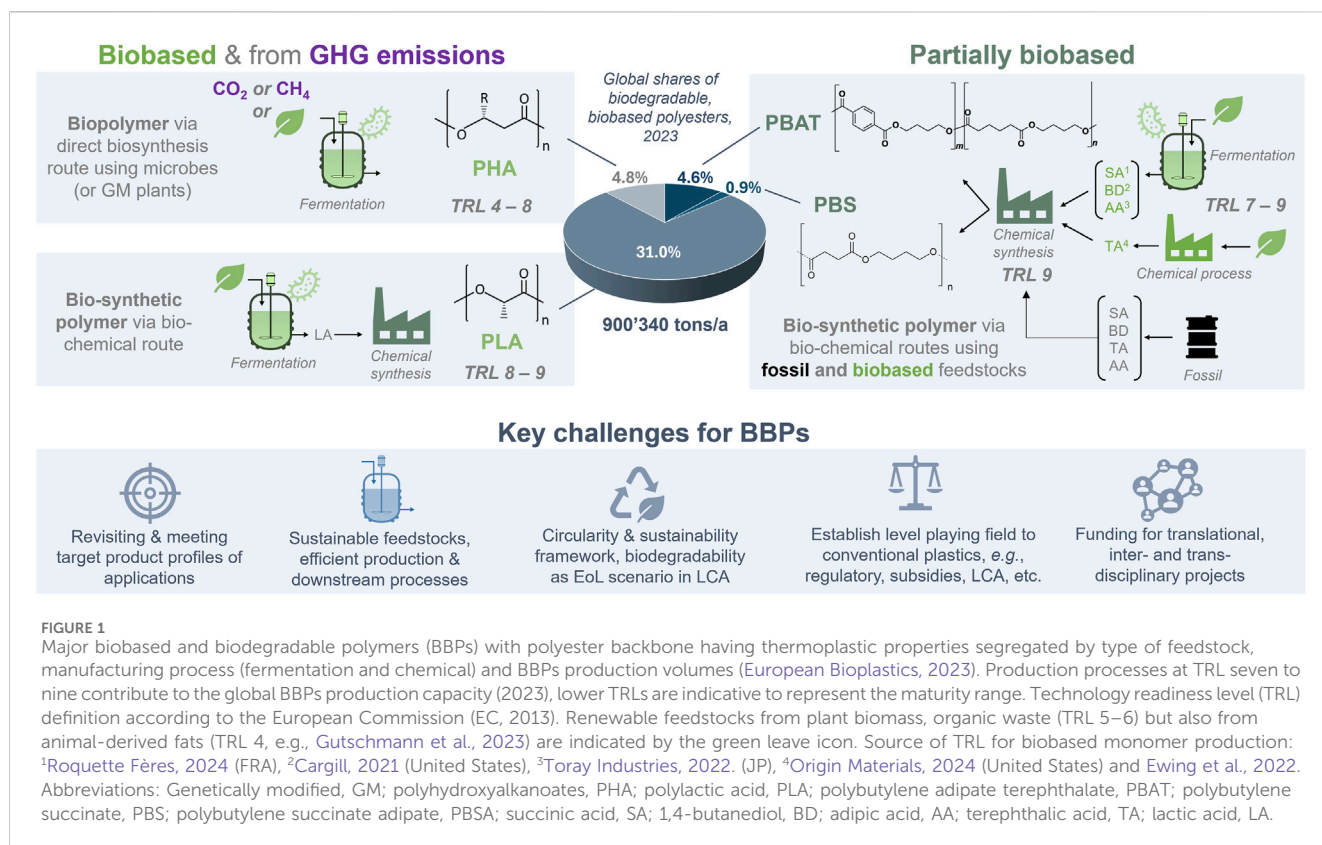
At the International Symposium on Biodegradable Polymers (ISBP2022) in Sion, Switzerland, experts from academia and industry underscored the remarkable progress in biobased and biodegradable polymers (BBPs) since their initial commercialization around 50 years ago. Despite significant advancements, the technology readiness level (TRL), market adoption, and industrialization of BBPs is not yet competitive to conventional plastics. In this perspective, we summarize the challenges and requirements for advancing the development and industrialization of BBPs, drawing insights from international experts coming from academia and industry, who had participated in the survey and podium discussion during the ISBP2022. In fact, BBPs grapple with persistent and emerging challenges throughout the value chain. These challenges can be grouped into four areas and involve i) the pursuit of sustainable feedstocks together with efficient production and downstream processes as well as recycling technologies and infrastructure; ii) meeting or revisiting product requirements by industry, markets, and consumers; iii) navigating a non-level playing field in their sustainability assessment (LCA) compared to conventional plastics; and iv) struggling with underdeveloped and partially biased policy and financial frameworks as well as lacking clear definitions, terminologies and communication.

1 Introduction to biobased and biodegradable polymers (BBPs)

Conventional, fossil-based plastics have historically been designed for durability and toughness affording long lasting products, which are, however, embedded in a linear economy framework. While the non-degradability of conventional plastics is desirable in the production and use phase, it has brought about issues at the end-of-life (EoL), that are the limited recyclability and environmental pollution by persistent micro- and nanoparticles. A significant body of evidence suggests adverse effects of microplastics on humans and animal health, biodiversity, and soil quality, as well as their contribution to climate change (WWFthe Ellen MacArthur Foundation and BCG, 2020; Marfell et al.,

FIGURE 1
Major biobased and biodegradable polymers (BBPs) with polyester backbone having thermoplastic properties segregated by type of feedstock, manufacturing process (fermentation and chemical) and BBPs production volumes (European Bioplastics, 2023). Production processes at TRL seven to nine contribute to the global BBPs production capacity (2023), lower TRLs are indicative to represent the maturity range. Technology readiness level (TRL) definition according to the European Commission (EC, 2013). Renewable feedstocks from plant biomass, organic waste (TRL 5–6) but also from animal-derived fats (TRL 4, e.g., Gutschmann et al., 2023) are indicated by the green leave icon. Source of TRL for biobased monomer production: [1]Roquette Fères, 2024 (FRA), [2]Cargill, 2021 (United States), [3]Toray Industries, 2022. (JP), [4]Origin Materials, 2024 (United States) and Ewing et al., 2022. Abbreviations: Genetically modified, GM; polyhydroxyalkanoates, PHA; polylactic acid, PLA; polybutylene adipate terephthalate, PBAT; polybutylene succinate, PBS; polybutylene succinate adipate, PBSA; succinic acid, SA; 1,4-butanediol, BD; adipic acid, AA; terephthalic acid, TA; lactic acid, LA.
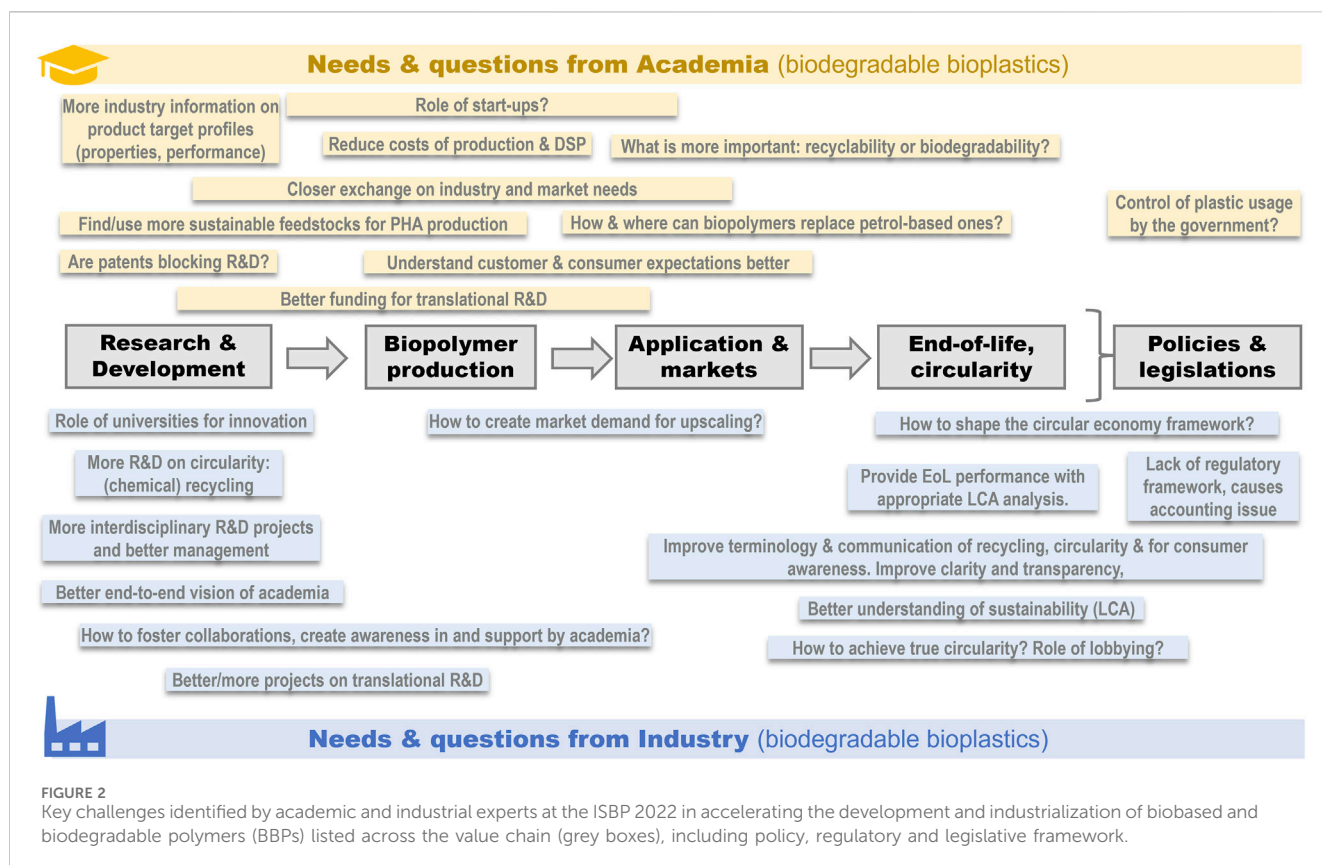
2024). Furthermore, global, fossil-based plastic production is responsible for at least 4.5% of greenhouse gas (GHG) emissions (Cabernard et al., 2022).

Consequently, much effort has been invested into the research and development of BBPs to raise their technology readiness level (TRL) as sustainable alternatives to conventional, non-biodegradable plastics. Biodegradability is important for applications having an intended use or likely fate of ending up in the natural and engineered (e.g., wastewater treatment, industrial composting) environments, such as cosmetics and agricultural formulations (e.g., seed coatings and mulch films), protective films for laundry and detergent pods, gras trimmer lines, seedling pods, fishing gear, food packaging, e.g., coffee capsules, tea bags, fruit and vegetable sticker, etc. But also, for products that experience significant abrasion during use, such as shoe soles, tires, artificial turf, protective coatings and paints, etc. (Bertling et al., 2018; Bertling et al., 2021). Biodegradation of BBP-based products at their EoL avoids the formation of persistent microplastics and results in biomass, biogenic CO_2 or methane (CH_4). In addition, organic recycling via industrial composting and anaerobic digestion can valorise the biogenic carbon in BBPs in the form of methane and compost for energy recovery, chemical and biogenic feedstock. Organic recycling is particularly useful for post-consumer waste containing significant organic loadings (e.g., food residues), and are thus difficult to recycle mechanically and likely entering and contaminating organic waste streams with non-biodegradable (micro) plastics (European Commission, 2022). Importantly, BBPs are also mechanically and chemically recyclable (Kumar R. et al., 2023). Moreover, the biodegradability of BBPs can be leveraged for creating a circular material and bioeconomy via a technical recycling loop employing biotechnological and chemical recycling (see, e.g.,

reviews by García-Depraect et al., 2021; von Vacano et al., 2023). Finally, BBPs show on average 20%–30% and up to 40%–50% lower carbon footprints (cradle-to-gate) as compared to conventional, fossil-based plastics (RCI, 2024; Vom Berg and Carus, 2024).

BBPs had created already some significant waves during the 1970ies to 1990ies, "fuelled" by the oil crisis, and then during 2000–2010, due to significant performance improvements in polymer properties and production processes. The biodegradable polyesters PLA (polylactic acid), PHAs (polyhydroxyalkanoates), and PBAT (polybutylene adipate-co-terephthalate) have achieved to date the highest market traction and production volumes (Figure 1). While PHA is a natural, microbial biopolyester produced via fermentation (e.g., by Kaneka, Danimer Scientific, BluePHA, RWDC Industries) (Koller and Mukherjee, 2022), production of PLA is achieved via the bio-chemical route employing fermentative lactic acid production with a subsequent chemical polymerization (e.g., by Total-Energies and Corbion, 2022, NatureWorks; Commerer, 2024; Teixeira et al., 2023). PBAT is produced by BASF through chemical synthesis from biobased and petrochemical feedstocks.

Despite their increase in technology readiness level (TRL) together with their environmental as well as circularity advantages, the market adoption of BBPs (excluding polysaccharides) remain at low levels with a share of production capacity of only about 0.2% (ca. 900 t/a) in 2023 compared to the global plastics market (European Bioplastics, 2023). PLA holds the largest share (75%) of the global BBP production volume (Figure 1) and exhibits the highest market adoption with key applications in 3D-printing, FDA-approved medical implants and devices (Tyler et al., 2016), fibres (carpet, textiles), mulch films, food packaging, etc. (Fiori, 2014). Importantly, whilst PLA is only certified for industrial

FIGURE 2
Key challenges identified by academic and industrial experts at the ISBP 2022 in accelerating the development and industrialization of biobased and biodegradable polymers (BBPs) listed across the value chain (grey boxes), including policy, regulatory and legislative framework.

composting conditions, its biocompatibility in humans has been demonstrated *in vivo* for medical implants (Da Silva et al., 2018). While PHAs are widely biodegradable in natural and engineered environments including some medical applications (sutures made of poly (4-hydroxybutyrate)), PBAT biodegrades in soil and under home and industrial composting conditions. Polybutylene succinate (PBS) only biodegrades under industrial composting conditions, whereas its co-polymer with adipic acid (PBSA) shows similar biodegradability to PBAT (for overview see Nova Institute, 2021).

In the last decade BBPs have gained further momentum through the increased environmental awareness of consumers, customers, and industry as well as by policy and governmental bodies. On the other hand, successful applications and industrialization of BBPs are still hindered by several key challenges that require solutions to yield economically viable BBPs and BBPs-based products as sustainable alternatives to conventional plastics. The identification and elaboration of these key challenges in accelerating the development and industrialization of BBPs have been discussed by leading experts from academia and industry during the International Symposium on Biopolymers (ISBP2022) in Sion, Switzerland (see HES-SO YouTube channel, 2022).

2 Key challenges for the advancement and industrialization of BBPs

Figure 2 lists the various challenges across the BBP value chain that have been identified by experts during ISBP2022 and will be discussed in more detail as follows.

2.1 Meeting the target product properties (TPPs) and managing expectations

One key challenge for BBPs lies in achieving the TPPs demanded by industry, customers, and consumers as well as regulatory bodies. Meeting these TPPs is critical to trigger market demand and market adoption. However, corporates may need to revisit and most likely re-define their product requirements through the lenses of sustainability and with the knowledge of the associated recycling and other EoL challenges. Expectations of corporates are frequently to obtain "drop-in" solutions that are biobased and radically change the EoL properties but maintain all other features of the "conventional" plastics (price, availability, stability, processibility, user performance, etc.). In case of PLA, some successful polymer processing developments for challenging application formats have been made (Fiori, 2014), including foamed PLA as recently reported by Sulzer (Commerer, 2024). Similarly, to enhance the toughness of PBAT, a blend with PLA was shown to yield satisfactory properties for various film applications (e.g., ecovio® by BASF). Similarly, Danimer Scientific is blending PHA with PLA or other short-chain length (scl-) PHAs to improve biodegradability and processibility (Plastics Technology Online, 2024; Commerer, 2021). Developments in formulation, processing and (co-) polymer composition will expand the applicability and product portfolio of BBPs and thereby boosting their market adoption (Park et al., 2024).

While ensuring biodegradation through microorganisms constitutes an important EoL feature, the hydrolytic stability during processing and application is often compromised.

Consequently, adaptation and developments in formulations, compounding, and processing conditions are often required. In fact, process-induced degradation can have a significant effect on BBPs, e.g., PLA (Velghe et al., 2023) and PHA (Yeo et al., 2018). Contrary, higher stability requirements during processing and use, negatively affect the biodegradability (for example, see: Mochizuki and Hirami, 1997). For instance, impact modifiers and other additives enforcing the polymer network can impair the accessibility of enzymes and microorganisms and, thereby, the effectiveness of polymer biodegradation (i.e., rate and/or extent). Further research is needed to build knowledge on the structure-function relationship of various PHA types linked to TTPs, e.g., tensile strength, and elongation at break (Choi et al., 2020). Medium-chain-length (mcl-)PHAs have a broader property and application range than scl-PHAs (Li et al., 2016) but only a couple are at pre-commercial scale TRL 6 (Bioplastech, IRL; TerraVerdae, CAN; Bioextrax, SWE). A production platform affording tailored PHAs (e.g., mcl-PHA) at 10—200 g is in dire need for lab-scale testing experiments. Availability of test material at kg scale is key at a second stage, to conduct industrial application trials. A first coordinated step in this direction has been initiated for PHAs by the GO!PHA organization (online sample shop) and few industrial compounders, such as Helian Polymers (NL).

2.2 Advancing and scaling of BBP production

2.2.1 Producing BBPs from alternative and more sustainable feedstocks

Whilst PLA, PBAT, and PBS are synthesized via chemical polymerization from their respective (fossil or biobased) monomers, PHAs are produced intracellularly by microorganisms, microalgae, and in transgenic plants (Koller and Mukherjee, 2022). Commercially available PLA and PHAs, as well as the biobased monomers for PBAT and PBS, are produced via microbial fermentation using primarily first-generation feedstocks, i.e., sugars and oils from crops (Figure 1). BBP production processes utilizing more sustainable feedstocks represent another challenge. In case of solid and liquid organic waste streams, the typically heterogenous nature and (seasonal and regional) variations in composition require the development of efficient (and flexible) pre-treatment and fermentation processes for both monomers (Mancini et al., 2020; Bibra et al., 2022; Song et al., 2022) and biopolymers (Molina-Peñate et al., 2022; Kumar V. et al., 2023). Concomitantly, metabolic engineering strategies (Wang et al., 2023) and/or use of microbial mixed cultures (Pagliano et al., 2021) have been developed at lab-scale to enhance the capacity of microbial PHA producers and to synergistically utilize recalcitrant and complex organic waste streams more efficiently.

Adopting and developing process strategies to handle complex and varying feedstock compositions is essential in yielding constant polymer (e.g., PHA) quality as well as appropriate productivity (Wang et al., 2021). Also, establishing cost effective supply chains of novel feedstocks is typically achieved through the economy of scale. Bioprocesses using alternative, more sustainable feedstocks such as organic waste streams and greenhouse gas (GHG) emissions are at a lower maturity level, however, spreading from first proof-of-concept (TRL 3) and small-scale laboratory prototypes (TRL 4) to larger

scale pilots (TRL 5 & 6) as well as to demo systems (TRL 7) and first-of-a-kind (FOAK) facility (TRL 8). Commercial scale (TRL 9) is reached only if volumes and quality meet customer demand. (Note, the authors adopted the TRL definition recommended by the European Commission, 2013) Importantly, due to lack of publicly available process data, it remains difficult to conclude on the actual TRL and if such BBPs production processes are operated in an environment of pre-commercial scale (as required for TRL 7) or if manufacturing issues have been solved to reach TRL 8. Notable examples of startup companies demonstrating TRL five to six for the fermentative production of scl-PHA from waste streams are Paques Biomaterials (NL) using municipal wastewater (and sludge), PlantSwitch (United States) and Venvirotech (ESP) using agricultural waste. Newlight Technologies (United States) announced to have advanced to a FOAK in 2019 with thousands of tons of PHA per annum using methane rich emission gases from industrial digestors (Bioplastics Magazine, 2020). In 2015, the company reported a production volume of 45 t/a, a scaling factor of about two orders of magnitude (Bioplastics News, 2015). Mango Materials (United States) employs a similar technology for PHA production from raw biogas and is close to demo system scale (TRL 7) with 5 t/a (Tullo, 2019). All the above companies produce scl-PHAs, which have a limited application range (see Section 2.1).

2.2.2 Fermentation and downstream processes

Fermentation enables the direct biosynthesis of PHAs and monomers for BBP production from various biobased feedstocks (Figure 1), but current BBP production costs are 2–10 times higher as compared to the chemical production of conventional, non-biodegradable plastics. Besides cost reduction through sustainable feedstock supply and pre-treatment (see Section 2.2.1), advancement of fermentation technologies, production strains, and more efficient DSP methods are needed to afford high quality PHAs and monomers at competitive costs. The main process challenges, particularly for PHAs, are summarized below.

- Increase of bioprocess productivity towards the chemical industry's performance metrics (i.e., 100 g/l/h (Lange, 2021)) by advancing and scaling continuous fermentation, for example, which also affords tailored, high quality PHAs as compared to fed-batch processes (Zinn et al., 2004; Hanik et al., 2019; Dong et al., 2023). Realizing high cell density of 100 g/l in continuous fermentation, which is half of what has been reported for fed-batch (Arikawa et al., 2018), together with a growth rate of 0.5 h^{-1} and 80% PHA content, for example, would yield a >20 fold higher productivity (of 40 g/l/h) compared to the state-of-the-art in continuous PHA production (Koller, 2018). Such bioprocess metrics would also simplify the DSP of PHAs, reduce waste, and enable direct processing of PHA-biomass (see Collet et al., 2022).
- Energy-efficient fermenters with high mass transfer rates (e.g., k_La), gas recycling, etc. Advance and scale aerobic (hydrogen-oxidizing) fermentation systems (>TRL 5) for direct conversion of CO_2 (Miyahara et al., 2022; Lambauer et al., 2023) with higher productivity.
- High carbon yields (≥90%) also for alternative feedstocks. C-yield of ~99% in commercial scl-co-mcl-PHA production from palm oil is possible (personal industry communication).

- Optimal DSP methods depend on the type of PHA, and monomer used in BBP production. Reduce DSP cost contribution from ≥50% (Pérez-Rivero et al., 2019; Zytner et al., 2023) to 20%–40% of total production costs (Straathof, 2011). Depending on the methods used, scl-PHA can be recovered and purified today at costs of 1.1—5 €/kg PHA (De Koning et al., 1997; López-Abelairas et al., 2015). Solvent-free recovery of scl-PHA granules (Latex) may be 50% cheaper (Bioextrax, 2023); yet, efficient and sustainable solvent-based DSP methods are typically needed for mcl-PHAs (Hahn et al., 2024).
- Reduce waste and valorise residual cell biomass for additional revenue streams (e.g., Pesante and Frisont, 2023)

2.3 More value-chain overarching collaborations through inter- and transdisciplinary projects

To develop and scale technical solutions for the maturation of the BBP value chain (Figure 2), interdisciplinary and transdisciplinary projects are needed, including experts in material and process engineering, environmental sciences, biotechnology, regulatory affairs, marketing, and related fields. While academia often lacks the technical information for polymer processing and application properties (i.e., TPPs), the industry frequently lacks the in-depth research and development capabilities/capacities at the interdisciplinary level. Therefore, translational R&D projects based on pre-competitive collaborations between academia and industry will help to better define technical targets and facilitates communication across the value chain, including policymakers, and consumers.

2.4 A none-level playing field for BBPs vs. conventional plastics

2.4.1 Learning curve effect: it takes R&D, capital investments and time

Growing market shares and competitiveness depends on the learning curve (or experience curve) effect, that is, learning-related cost advantages are achieved by companies through increasing R&D and capital investments (Liebermann, 1984; Lieberman, 1989). Interestingly, the initial market demand of PLA was artificially hyped by producers, which then led to disappointment by customers and a drop in demand due to insufficient functionality and performance (Befort, 2021). PLA capacities grew from 70′000 t/a in 2003 to about 459′000 t/a in 2022 with an average market price of about US$1.6—$2.3 per kg (Jem and Tan, 2020; Teixeira et al., 2023). According to the Jem's law (Jem and Tan, 2020), the PLA demand has been doubling about every 3–4 years since 2007 and is likely to exceed the current production capacity making it less cost competitive to conventional plastics (<1–4 € per kg). This mismatch of demand and supply as well as struggling to meet TPPs is, however, normal for early-stage products, as they require further developments, optimization and growth across the value chain to profit from the learning curve and economy-of-scale effect. PHAs, PBAT and PBS are in a similar learning curve dilemma. In comparison, efficiency gains in oil supply and plastic production resulted in significant cost reduction of 19%–37% per doubling of the polyethylene (PE) production volumes (Simon, 2009). This resulted in market prices of 2.5–4 € per kg in the 1970ies and to around 1 €/kg PE by 2020 (Statista, 2023). A simple comparison reveals that BBPs stand today at a similar product maturity level as PE in 1970ies (not adjusting for currency inflation). Therefore, the challenge for the BBP value chain to become competitive is to either rapidly lower the production costs or to create a framework allowing to accept these costs and/or to temporarily buffer them until sufficient maturity is reached. Besides production costs, the product environmental footprint has gained significance as both policy and economic factor (Damiani et al., 2022). To accelerate the defossilization and transformation of the plastics industry, it is thus imperative to create a funding and policy framework that shortens the learning curve of BBPs by funding of inter- and transdisciplinary R&D as well as sector coupling and scaling projects, enabling the creation of alternative business models together with capital investments, incentives, standards, etc.

2.4.2 Developing a policy framework that promotes innovation and scaling of sustainable technologies and business models is key to achieve defossilization and circularity

Fermentation technologies can help transitioning from a fossil-based, linear industry and society to a circular bioeconomy (Ewing et al., 2022). Despite the many policy developments, such as the European Green Deal, the EUs Circular Economy Action Plan and Plastic Strategy, the Single-Use Plastic (SUP) directive, and the European regulatory framework on Plastic Packaging Waste Regulation (PPWR), there remains still "an urgent need for clarity, predictability, and confidence in Europe and its industrial policy" (The Antwerp Declaration for European Industrial Deal Summit, 2024).

For example, while current LCA methods are sufficiently developed to provide valuable insights into the sustainability and circularity of different products and technologies, continuous improvements in data quality, methodological consistency, and incorporation of more circular economy metrics are necessary to enhance the robustness, comparability, and reliability of LCAs. "Poor data and outdated methods sabotage the decarbonization efforts of the chemical industry" (Oberschelp et al., 2023). Existing LCA studies do not address environmental or human health impacts of neither non-biodegradable nor biodegradable (micro) plastics (Jiao et al., 2024). Biodegradation as EoL in natural and engineered environments is poorly or not quantifiable in current LCAs. Establishing a level-playing field for both BBPs and conventional plastics/polymers (Miller, 2022; Vom Berg and Carus, 2024) is therefore crucial to all stakeholders across the value chain, including policymakers, standardization, and certification bodies. Such advancements in cradle-to-grave and cradle-to-cradle LCAs will also create higher confidence for decision-making processes, avoid green washing, establish coherent terminology as well as transparent communication to consumers and for corporate sustainability reporting, for example,.

Harmonizing definitions, bans, and targets as well as financing mechanisms also at global scale will help to shorten the learning curve effect and to accelerate scaling of plastic pollution and climate

change mitigation strategies (WEF World Economic Forum, Insight Report, 2024). According to SUP directive, the current EU definition on natural polymers would ban products made of PBAT, PLA, PBS and modified PHAs, for example, thereby strongly restricting their applications. On the other hand, the PPWR will enforce from 2033 that compostable packaging be mandatory for tea/coffee bags and capsules as well as for sticky labels attached to fruits and vegetables. Also, harmonization of waste recycling targets is needed together with developing the infrastructures to enable collection, sorting and recycling of BBPs present in mixed waste streams, for example. PLA is compatible with existing polyester (PET) waste streams if its fraction stays below 1% (Total-Energies and Corbion, 2022). Therefore, the handling of small BBP waste streams currently hinders market introduction from an EoL point of view and must normally reach sufficient volumes, so that their identification, sorting, and processing is technically and economically feasible (Kumar R. et al., 2023).

Although governmental funding and private investments in clean tech and sustainable products is having its share, subsidies for fossil fuels had a global record high of seven trillion US dollars in 2022 (IMF Blog, 2023). The fossil fuel and oil industry also receive financial compensations (Timperley, 2021). While individual oil and plastics companies have received various subsidies from three million to US$1.8 billion within defined periods till about 2021 (Steenblik, 2021), the bioplastics industry does not receive such incentives as of today and the manufacturers and value chain members must solely carry their financial responsibilities (Green dot Bioplastics, 2024). On the other hand, bioplastics have been listed as "green investments" by the EU's Taxonomy Climate Delegate Act (European Bioplastics, 2022). Moreover, carbon taxation (ETC) and the EU's Carbon Border Adjustment Mechanism (CBAM) have the aim to put a fair price on the carbon emitted during the production of carbon intensive goods, which in turn should benefit BBPs having a lower carbon footprint during production. The price of emission allowances in the EU is fluctuating and had decreased from 100 € to less than 60 € per metric ton of CO_2 (Statista, 2024). The current carbon taxation levels (0.06 € per ton) do not confer a financial advantage, as the significant price gap between conventional plastics and current BBPs (with 20% to one magnitude higher production costs) cannot be bridged.

3 Conclusion

Overall, it becomes apparent that the key needs and questions for academia and industry are complementary and spread over the entire BBPs value chain (Figure 2). BBPs are still at the early learning curve towards maturity, facing challenges in accomplishing the fit-for-purpose status, efficient production, purification and processing with proven viability and superior sustainability as well as resolving feedstock utilization and supply chain challenges. BBPs are facing a non-level playing field compared to the well-established oil and plastics industry in terms of underdeveloped LCA methods, policies, funding, and incentives, for example. Consequently, it is essential to consolidate academic and industry efforts in inter- and

transdisciplinary projects to overcome these value chain overarching challenges.

Data availability statement

The datasets presented in this study can be found in online repositories. The names of the repository/repositories and accession number(s) can be found in the article/Supplementary Material.

Author contributions

Funding

Acknowledgments

Conflict of interest

The authors declare that the research was conducted in the absence of any commercial or financial relationships that could be construed as a potential conflict of interest.

Publisher's note

All claims expressed in this article are solely those of the authors and do not necessarily represent those of their affiliated

organizations, or those of the publisher, the editors and the reviewers. Any product that may be evaluated in this article, or claim that may be made by its manufacturer, is not guaranteed or endorsed by the publisher.

References

Arikawa, H., and Matsumoto, K. Evaluation of gene expression cassettes and production of poly(3-hydroxybutyrate-co-3-hydroxyhexanoate) with a fine modulated monomer composition by using it in Cupriavidus necator. *Microb Cell Fact* 15, 184 (2016). doi:10.1186/s12934-016-0583-7

Befort, N. (2021). The promises of drop-in vs. functional innovations: the case of bioplastics. *Ecol. Econ.* 181, 106886. doi:10.1016/j.ecolecon.2020.106886

Bioplastics News (2015). Vinmar Signs Polyhydroxyalkanoates (PHA) Deal with Newlight Technologies Available at: https://bioplasticsnews.com/2015/07/29/vinmar-signs-polyhydroxyalkanoates-pha-offtake-deal-with-newlight-technologies/ (Accessed on May 23, 2024)

Bioextrax, (2023). Available at: https://bioextrax.com/wp-content/uploads/2023/03/bioextrax-230316-final-draft.pdf (Accessed on June 20, 2024)

Bertling, J., Bertling, R., and Hamann, L. (2018). *Kunststoffe in der Umwelt: Mikro-und Markoplastic. Ursachen, Mengen, Umweltschicksale, Wirkungen, Lösungsansätze, Empfehlungen. Kurzfassung der Konsortialstudie, Fraunhofer-Institu für Umwelt-, Sicherheits-und Energietechnik UMSICHT (Hersg.).*

Bertling, J, Zimmermann, T., and Rödig, L. (2021) "*Kunststoffe in der Umwelt: Emissionen in landwirtschaftlich genutzte Böden, Oberhausen*," Fraunhofer UMSICHT, 220.

Bibra, M., Samanta, D., Sharma, N. K., Singh, G., Johnson, G. R., and Sani, R. K. (2022). Food waste to bioethanol: opportunities and challenges. *Fermentation* 9 (1), 8. doi:10.3390/fermentation9010008

Bioplastics Magazine (2020). Newlight Technol. opens new commercial-scale AirCarbon Prod. Facil. 25. Available at: https://www.bioplasticsmagazine.com/en/news/meldungen/20200925-Newlight-Technologies-opens-new-commercial-scale-AirCarbon-production-facility.php.

Cabernard, L., Pfister, S., Oberschelp, C., and Hellweg, S. (2022). Growing environmental footprint of plastics driven by coal combustion. *Nat. Sustain.* 5 (2), 139–148. doi:10.1038/s41893-021-00807-2

Cargill and HELM partner to build (2021). $300M commercial-scale, renewable BDO facility, first in the US, to meet growing customer demand. Available at: https://www.cargill.com/2021/cargill-and-helm-partner-to-build-$300m-facility (Accessed on May 15, 2024).

Choi, S. Y., Cho, I. J., Lee, Y., Kim, Y. J., Kim, K. J., and Lee, S. Y. (2020). Microbial polyhydroxyalkanoates and nonnatural polyesters. *Adv. Mater.* 32 (35), 1907138. doi:10.1002/adma.201907138

Collet, C., Vaidya, A. A., Gaugler, M., West, M., and Lloyd-Jones, G. (2022). Extrusion of PHA-containing bacterial biomass and the fate of endotoxins: a cost-reducing platform for applications in molding, coating and 3D printing. *Mater. Today Commun.* 33, 104162. doi:10.1016/j.mtcomm.2022.104162

Commerer, S. (2024) "PLA foaming, properties and applications,". Winterthur, Switzerland: Sulzer White Paper. Available at: https://www.sulzer.com/-/media/files/products/polymer_production_technology/casestudies/pla_foaming_properties_and_applications_a10652_en_web.pdf.

Damiani, M., Ferrara, N., and Ardente, F. (2022) *Understanding product environmental footprint and organisation environmental footprint methods, Eur 31236 en.* Luxembourg: Publications Office of the European Union. doi:10.2760/11564,JRC129907

Da Silva, D., Kaduri, M., Poley, M., Adir, O., Krinsky, N., Shainsky-Roitman, J., et al. (2018). Biocompatibility, biodegradation and excretion of polylactic acid (PLA) in medical implants and theranostic systems. *Chem. Eng. J.* 340, 9–14. doi:10.1016/j.cej.2018.01.010

De Koning, G. J. M., Kellerhals, M., Van Meurs, C., and Witholt, B. (1997). A process for the recovery of poly(hydroxyalkanoates) from Pseudomonads Part 2: process development and economic evaluation. *Bioprocess Eng.* 17, 15–21. doi:10.1007/s004490050346

Dong, Y., Zhang, Y., Liu, D., and Chen, Z. (2023). Strain and process engineering toward continuous industrial fermentation. *Front. Chem. Sci. Eng.* 17 (10), 1336–1353. doi:10.1007/s11705-022-2284-6

European Commission (2013). Annex G. Technology Readiness Level (TRL) Available at: https://ec.europa.eu/research/participants/data/ref/h2020/wp/2014_2015/annexes/h2020-wp1415-annex-g-trl_en.pdf (Accessed on January 12, 2024)

European Bioplastics (2022). "Why the EU's Taxonomy Climate Delegated Act correctly lists bio-based plastics as "green investments". Available at: https://www.european-bioplastics.org/why-the-eus-taxonomy-climate-delegated-act-correctly-lists-bio-based-plastics-as-green-investments/(Accessed on January 12, 2024).

European Bioplastics (2023). Market and development update 2023. Available at: https://www.european-bioplastics.org/bioplastics-market-development-update-2023-2/(Accessed on January 12, 2024).

European Commission (2022). The EU's policy framework on the sourcing, labelling and use of biobased plastics, and the use of biodegradable and compostable plastics. Available at: https://environment.ec.europa.eu/topics/plastics/biobased-biodegradable-and-compostable-plastics_en (Accessed January 12, 2024).

Ewing, T. A., Nouse, N., van Lint, M., van Haveren, J., Hugenholtz, J., and van Es, D. S. (2022). Fermentation for the production of biobased chemicals in a circular economy: a perspective for the period 2022–2050. *Green Chem.* 24 (17), 6373–6405. doi:10.1039/d1gc04758b

Fiori, S. (2014). "In poly(lactic acid) science and technology: processing, properties," in *Additives and applications*. Editors A. Jiménez, M. Peltzer, and R. Rusecaite (Hong Kong, China: The Royal Society of Chemistry), 315–333.

García-Depraect, O., Bordel, S., Lebrero, R., Santos-Beneit, F., Börner, R. A., Börner, T., et al. (2021). Inspired by nature: microbial production, degradation and valorization of biodegradable bioplastics for life-cycle-engineered products. *Biotechnol. Adv.* 53, 107772. doi:10.1016/j.biotechadv.2021.107772

Green dot Biolastics (2024). What growth in bioplastics industry means for investors and the economy. Available at: https://www.greendotbioplastics.com/growth-bioplastics-industry-means-investors-economy/(Accessed January 12, 2024).

Gutschmann, B., Maldonado Simões, M., Schiewe, T., Schröter, E. S., Münzberg, M., Neubauer, P., et al. (2023). Continuous feeding strategy for polyhydroxyalkanoate production from solid waste animal fat at laboratory-and pilot-scale. *Microb. Biotechnol.* 16 (2), 295–306. doi:10.1111/1751-7915.14104

Hahn, T., Alzate, M. O., Leonhardt, S., Tamang, P., and Zibek, S. (2024). Current trends in medium-chain-length polyhydroxyalkanoates: microbial production, purification, and characterization. *Eng. Life Sci.* 2300211. doi:10.1002/elsc.202300211

Hanik, N., Utsunomia, C., Arai, S., Matsumoto, K. I., and Zinn, M. (2019). Influence of unusual co-substrates on the biosynthesis of medium-chain-length polyhydroxyalkanoates produced in multistage chemostat. *Front. Bioeng. Biotechnol.* 7, 301. doi:10.3389/fbioe.2019.00301

HES-SO YouTube channel (2022). Biopolymers: the challenges towards their acceptance and implementation, podium discussion ISBP2022. Available at: https://www.youtube.com/watch?v=aisqQM404Lg.

IMF Blog (2023). Fossil fuel subsidies surged to record $7 trillion. Available at: https://www.imf.org/en/Blogs/Articles/2023/08/24/fossil-fuel-subsidies-surged-to-record-7-trillion (Accessed on December 13, 2023).

Jem, K. J., and Tan, B. (2020). The development and challenges of poly(lactic acid) and poly (glycolic acid). *Adv. Industrial Eng. Polym. Res.* 3 (2), 60–70. doi:10.1016/j.aiepr.2020.01.002

Jiao, H., Ali, S. S., Alsharbaty, M. H. M., Elsamahy, T., Abdelkarim, E., Schagerl, M., et al. (2024). A critical review on plastic waste life cycle assessment and management: challenges, research gaps, and future perspectives. *Ecotoxicol. Environ. Saf.* 271, 115942. doi:10.1016/j.ecoenv.2024.115942

Koller, M. (2018). A Review on Established and Emerging Fermentation Schemes for Microbial Production of Polyhydroxyalkanoate (PHA) Biopolyesters. *Fermentation* 2, 30. doi:10.3390/fermentation4020030

Koller, M., and Mukherjee, A. (2022). A new wave of industrialization of PHA biopolyesters. *Bioengineering* 9 (2), 74. doi:10.3390/bioengineering9020074

Kumar, R., Sadeghi, K., Jang, J., and Seo, J. (2023a). Mechanical, chemical, and bio-recycling of biodegradable plastics: a review. *Sci. Total Environ.* 882, 163446. doi:10.1016/j.scitotenv.2023.163446

Kumar, V., Lakkaboyana, S. K., Tsouko, E., Maina, S., Pandey, M., Umesh, M., et al. (2023b). Commercialization potential of agro-based polyhydroxyalkanoates biorefinery: a technical perspective on advances and critical barriers. *Int. J. Biol. Macromol.* 234, 123733. doi:10.1016/j.ijbiomac.2023.123733

Lambauer, V., Permann, A., Petrášek, Z., Subotić, V., Hochenauer, C., Kratzer, R., et al. (2023). Automatic control of chemolithotrophic cultivation of *Cupriavidus necator*: optimization of oxygen supply for enhanced bioplastic production. *Fermentation* 9 (7), 619. doi:10.3390/fermentation9070619

Lange, J. P. (2021). Performance metrics for sustainable catalysis in industry. *Nat. Catal.* 4 (3), 186–192. doi:10.1038/s41929-021-00585-2

Li, Z., Yang, J., and Loh, X. J. (2016). Polyhydroxyalkanoates: opening doors for a sustainable future. *NPG Asia Mater.* 8 (4), e265. doi:10.1038/am.2016.48

Lieberman, M. B. (1984). The learning curve and pricing in the chemical processing industries. *RAND J. Econ.* 15 (2), 213–228. doi:10.2307/2555676

Lieberman, M. B. (1989). The learning curve, technology barriers to entry, and competitive survival in the chemical processing industries. *Strategic Manag. J.* 10 (5), 431–447. doi:10.1002/smj.4250100504

López-Abelairas, M., García-Torreiro, M., Lú-Chau, T., Lema, J. M., and Steinbüchel, A. (2015). Comparison of several methods for the separation of poly(3-hydroxybutyrate) from *Cupriavidus necator* H16 cultures. *Biochem. Eng. J.* 93, 250–259. doi:10.1016/j.bej.2014.10.018

Mancini, E., Mansouri, S. S., Gernaey, K. V., Luo, J., and Pinelo, M. (2020). From second generation feed-stocks to innovative fermentation and downstream techniques for succinic acid production. *Crit. Rev. Environ. Sci. Technol.* 50 (18), 1829–1873. doi:10.1080/10643389.2019.1670530

Marfella, R., Prattichizzo, F., Sardu, C., Fulgenzi, G., Graciotti, L., Spadoni, T., et al. (2024). Microplastics and nanoplastics in atheromas and cardiovascular events. *N. Engl. J. Med.* 390 (10), 900–910. doi:10.1056/nejmoa2309822

Miller, S. A. (2022). The capabilities and deficiencies of life cycle assessment to address the plastic problem. *Front. Sustain.* 3, 1007060. doi:10.3389/frsus.2022.1007060

Miyahara, Y., Wang, C. T., Ishii-Hyakutake, M., and Tsuge, T. (2022). Continuous supply of non-combustible gas mixture for safe autotrophic culture to produce polyhydroxyalkanoate by hydrogen-oxidizing bacteria. *Bioengineering* 9 (10), 586. doi:10.3390/bioengineering9100586

Mochizuki, M., and Hirami, M. (1997). Structural effects on the biodegradation of aliphatic polyesters. *Polym. Adv. Technol.* 8 (4), 203–209. doi:10.1002/(sici)1099-1581(199704)8:4<203::aid-pat627>3.3.co;2-v

Molina-Peñate, E., Artola, A., and Sánchez, A. (2022). Organic municipal waste as feedstock for biorefineries: bioconversion technologies integration and challenges. *Rev. Environ. Sci. Bio/Technology* 21 (1), 247–267. doi:10.1007/s11157-021-09605-w

Nova Institute (2021). Biodegradable polymers in various environments. Available at: https://renewable-carbon.eu/publications/product/biodegradable-polymers-in-various-environments-according-to-established-standards-and-certification-schemes-graphic-pdf/(Accessed on May 3, 2024).

Oberschelp, C., Hellweg, S., Bradford, E., Pfister, S., Huo, J., and Wang, Z. (2023). Poor data and outdated methods sabotage the decarbonization efforts of the chemical industry. ChemRxiv. doi:10.26434/chemrxiv-2023-8c86t

Origine Materials (2024). Available at: https://www.originmaterials.com/products/terephthalic-acid-pta.

Park, H., He, H., Yan, X., Liu, X., Scrutton, N. S., and Chen, G. Q. (2024). PHA is not just a bioplastic!. *Biotech. Advan.*, 108320. doi:10.1016/j.biotechadv.2024.108320

Pagliano, G., Galletti, P., Samorì, C., Zaghini, A., and Torri, C. (2021). Recovery of polyhydroxyalkanoates from single and mixed microbial cultures: a review. *Front. Bioeng. Biotechnol.* 9, 624021. doi:10.3389/fbioe.2021.624021

Pérez-Rivero, C., López-Gómez, J. P., and Roy, I. (2019). A sustainable approach for the downstream processing of bacterial polyhydroxyalkanoates: state-of-the-art and latest developments. *Biochem. Eng. J.* 150, 107283. doi:10.1016/j.bej.2019.107283

Pesante, G., and Frison, N. (2023). Recovery of bio-based products from PHA-rich biomass obtained from biowaste: a review. *Bioresour. Technol. Rep.* 21, 101345. doi:10.1016/j.biteb.2023.101345

Plastics Technology Online (2024). Why are they blending biopolymers? Available at: https://www.ptonline.com/blog/post/why-are-they-blending-biopolymers.

Plastics Today (2021). Danimer scientific scoops up novomer. Available at: https://www.plasticstoday.com/business/danimer-scientific-scoops-up-novomer.

RCI, Renewable Carbon Initiative (2024). News letter, 23.2. Available at: https://renewable-carbon.eu/news/products-made-from-crude-oil-have-a-significantly-higher-co2-footprint-than-previously-assumed/.

Roquette Fères, biobased succinic acid (2024). *Roquette Fères, biobased succinic acid.* Available at: https://www.roquette.com/industries/selected-products/industry-performance-materials-biosuccinum.

Simon, T. (2009) "*Master thesis: experience curve in the world polym xer industry*," Netherlands: Utrecht University. Available at: https://studenttheses.uu.nl/bitstream/handle/20.500.12932/3869/MSc%20Thesis%20Tristan%20Simon%203072657%20public.pdf?sequence=2 (Accessed on September 23, 2023).

Song, L., Yang, D., Liu, R., Liu, S., Dai, L., and Dai, X. (2022). Microbial production of lactic acid from food waste: latest advances, limits, and perspectives. *Bioresour. Technol.* 345, 126052. doi:10.1016/j.biortech.2021.126052

Statista (2023). *Global price of high-density polyethylene 2017-2022.* Publ. by Statista Res. Dep. Available at: https://www.statista.com/statistics/1171074/price-high-density-polyethylene-forecast-globally/(Accessed February 24, 2024).

Statista (2024). Daily European union emission trading system (EU-ETS) carbon pricing from 2022 to 2024. Available at: https://www.statista.com/statistics/1322214/carbon-prices-european-union-emission-trading-scheme/(Accessed on February 12, 2024).

Steenblik, R. (2021). *Subsidies and plastic production – an exploration.* Int. Inst. Sustain. Dev. (IIISD). Available at: https://snis.ch/wp-content/uploads/2020/01/2019_Littoz-Monnet_Working-Paper-6.pdf.pdf (Accessed on January 12, 2024).

Straathof, A. J. J. (2011). The proportion of downstream costs in fermentative production processes. In *Comprehensive biotechnology* 2nd Edn, Editor. M. Murray (Sierra Leone, West Africa: Elsevier), 2, 811–814. doi:10.1016/b978-0-08-088504-9.00492-x

Toray Industries (2022). Toray invents 100% bio-based adipic acid from sugars derived from inedible biomass, scaling up for application to eco-friendly Nylon 66 Available at: https://www.toray.com/global/news/details/20220818103248.html (Accessed on July 3, 2024).

Teixeira, L. V., Bomtempo, J. V., Oroski, F. D. A., and Coutinho, P. L. D. A. (2023). The diffusion of bioplastics: what can we learn from poly (lactic acid)? *Sustainability* 15 (6), 4699. doi:10.3390/su15064699

The Antwerp Declaration for European Industrial Deal (2024). European industry Summit: a business case for Europe. Available at: https://antwerp-declaration.eu/.

Timperley, J. (2021). Why fossil fuel subsidies are so hard to kill. *Nature* 598, 403–405. doi:10.1038/d41586-021-02847-2

Total-Energies and Corbion (2022). PLA does not endanger PET recycling. Available at: https://www.totalenergies-corbion.com/news/pla-does-not-endanger-pet-recycling/.

Tullo, A. (2019). PHA: a biopolymer whose time has finally come. *Chem. Eng. News.* Available at: https://cen.acs.org/business/biobased-chemicals/PHA-biopolymer-whose-time-finally/97/i35 (Accessed on May 15, 2024).

Tyler, B., Gullotti, D., Mangraviti, A., Utsuki, T., and Brem, H. (2016). Polylactic acid (PLA) controlled delivery carriers for biomedical applications. *Advanced Drug Delivery Reviews* 107, 163–175. doi:10.1016/j.addr.2016.06.018

Velghe, I., Buffel, B., Vandeginste, V., Thielemans, W., and Desplentere, F. (2023). Review on the degradation of poly(lactic acid) during melt processing. *Polymers* 15 (9), 2047. doi:10.3390/polym15092047

Vom Berg, C., and Carus, M. (2024). Non-level playing field for renewable materials vs. fossil in life cycle assessments. Critical aspects of the JRC Plastics LCA methodology and its policy implications. *Renew. Carbon News.*

von Vacano, B., Mangold, H., Vandermeulen, G. W., Battagliarin, G., Hofmann, M., Bean, J., et al. (2023). Sustainable design of structural and functional polymers for a circular economy. *Angew. Chem. Int. Ed.* 62 (12), e202210823. doi:10.1002/anie.202210823

Wang, J., Liu, S., Huang, J., Cui, R., Xu, Y., and Song, Z. (2023). Genetic engineering strategies for sustainable polyhydroxyalkanoate (PHA) production from carbon-rich wastes. *Environ. Technol. Innovation* 30, 103069. doi:10.1016/j.eti.2023.103069

Wang, J., Liu, S., Huang, J., and Qu, Z. (2021). A review on polyhydroxyalkanoate production from agricultural waste Biomass: development, advances, circular approach, and challenges. *Bioresour. Technol.* 342, 126008. doi:10.1016/j.biortech.2021.126008

WEF World Economic Forum, Insight Report (2024). *Circular industry solutions a Glob. plastics treaty.* Available at: https://www.weforum.org/publications/circular-industry-solutions-for-a-global-plastics-treaty/.

WWF the Ellen MacArthur Foundation and BCG (2020). *The business case for a UN treaty on plastic pollution.*

Yeo, J. C. C., Muiruri, J. K., Thitsartarn, W., Li, Z., and He, C. (2018). Recent advances in the development of biodegradable PHB-based toughening materials: approaches, advantages and applications. *Mater. Sci. Eng. C* 92, 1092–1116. doi:10.1016/j.msec.2017.11.006

Zinn, M., Witholt, B., and Egli, T. (2004). Dual nutrient limited growth: models, experimental observations, and applications. *J. Biotechnol.* 113 (1-3), 263–279. doi:10.1016/j.jbiotec.2004.03.030

Zytner, P., Kumar, D., Elsayed, A., Mohanty, A. K., Ramarao, B., and Misra, M. (2023). *A review on cost-effective polyhydroxyalkanoate (PHA) production through the use of lignocellulosic biomass.* Ontario, Canada: RSC.

Frontiers in
Bioengineering and Biotechnology

Accelerates the development of therapies, devices, and technologies to improve our lives

A multidisciplinary journal that accelerates the development of biological therapies, devices, processes and technologies to improve our lives by bridging the gap between discoveries and their application.

Discover the latest Research Topics

See more →

frontiers in
Bioengineering
and Biotechnology

frontiers | Research Topics